

FINAL REPORT, 2017-2019
GEOHERMAL HEAT RECOVERY COMPLEX: LARGE-SCALE, DEEP DIRECT-USE
SYSTEM IN A LOW-TEMPERATURE SEDIMENTARY BASIN

U.S. Department of Energy award number: DE-EE0008106

Sponsoring program office: U.S. Department of Energy, Energy Efficiency & Renewable Energy

Name of recipient: Illinois State Geological Survey, University of Illinois

Name of PI: Yu-Feng Lin, PhD, PG

Project title: Geothermal Heat Recovery Complex: Large-Scale, Deep Direct-Use System in a Low-Temperature Sedimentary Basin

Consortium/team members (*denotes student participant):

University of Illinois – Yu-Feng Lin (PI), Andrew Stumpf (Co-PI), Scott Frailey (Co-PI), Roland Okwen, Yongqi Lu, Tim Stark, James Damico, Scott Elrick, John Nelson, Damon Garner, Fang Yang, Hafiz Salih, Wenfeng Fu, Zhaowang Lin*, Jiale Lin*, Chris Korose

U.S. Army Construction Engineering Research Laboratory – Frank Holcomb* (also affiliated with the University of Illinois at Urbana-Champaign)

University of Wisconsin-Madison – Jim Tinjum, Lauren Thomas*

Trimeric Corporation – Ray McKaskle, Kevin Fisher, Austyn Vance

MEP Associates, LLC – Jeff Urlaub

Loudon Technical Services, LLC – Jim Kirksey

Andrews, Hammock, Powell, Incorporated – Chuck Hammock

Federal support acknowledgement: This material is based on work supported by the U.S. Department of Energy's Office of Energy Efficiency and Renewable Energy (EERE), under the Geothermal Technologies Office Award Number DE-EE0008106.

Federal support disclaimer: This report was prepared as an account of work sponsored by an agency of the United States Government. Neither the United States Government nor any agency thereof, nor any of their employees, makes any warranty, express or implied, or assumes any legal liability or responsibility for the accuracy, completeness, or usefulness of any information, apparatus, product, or process disclosed, or represents that its use would not infringe privately owned rights. Reference herein to any specific commercial product, process, or service by trade name, trademark, manufacturer, or otherwise does not necessarily constitute or imply its endorsement, recommendation, or favoring by the United States Government or any agency thereof. The views and opinions of the authors expressed herein do not necessarily state or reflect those of the United States Government or any agency thereof.

Suggested citation: Lin, Y.F., A. Stumpf, S. Frailey, R. Okwen, Y. Lu, F. Holcomb, J. Tinjum, T. Stark, J. Damico, S. Elrick, K. Fisher, W. Fu, D. Garner, C. Hammock, J. Kirksey, C. Korose, J. Lin, Z. Lin, R. McKaskle, J. Nelson, H. Salih, L. Thomas, J. Urlaub, A. Vance, and F. Yang. 2020. “Geothermal Heat Recovery Complex: Large-Scale, Deep Direct-Use System in a Low-Temperature Sedimentary Basin.” Champaign, IL: Illinois State Geological Survey. DOE-DE-EE0008106 Final Report.

A handwritten signature in blue ink that reads "Yu Feng Lin". The signature is written in a cursive, flowing style.

Yu-Feng F. Lin, March 6, 2020

TABLE OF CONTENTS

EXECUTIVE SUMMARY	13
1. INTRODUCTION.....	15
2. APPROACHES.....	20
2.1 <i>Geologic and Geocellular Modeling.....</i>	20
2.2 <i>Reservoir and Wellbore Modeling</i>	27
2.3 <i>Surface Infrastructure Modeling.....</i>	38
2.4 <i>Analyses of Life Cycle Cost and Levelized Cost of Heat</i>	44
3. DISCUSSION: DDU Feasibility Funding Opportunity Criteria.....	51
3.1 <i>Criterion 1 – Geothermal Resource Assessment.....</i>	51
3.2 <i>Criterion 2 – Regulatory Compliance Plan</i>	56
3.3 <i>Criterion 3 – End-Use Load (and framework used to determine) Market Transformation Plan</i>	58
3.4 <i>Criterion 4 – Technical Description of the Proposed Deep Direct-Use Technology</i>	65
3.5 <i>Criterion 5 – Costs and Benefits Methodology.....</i>	77
CONCLUSIONS	81
REFERENCES.....	84
Appendix A – Comparison of Actual Accomplishments with Goals and Objectives.....	96
Appendix B – Formulas and Calculations	99
B1. <i>Geologic and Geocellular Modeling</i>	99
B2. <i>Fluid Flow Modeling.....</i>	102
B3. <i>Surface Infrastructure Modeling – EBS Data Tables.....</i>	104
B4. <i>Review of Software for LCCA Spreadsheet Tool.....</i>	106
B5. <i>LCCA Equations.....</i>	107
B6. <i>Environmental Life Cycle Assessment of a Deep Direct-use Geothermal System in Champaign, Illinois</i>	108
Appendix C – Subcontractor Reports.....	122
C1. <i>Well Design Report</i>	122
C2. <i>Assessment of Water Chemistry Impacts on Equipment Design and Costs</i>	134
C3. <i>DDU GES Infrastructure Design</i>	138
C4. <i>Assessment of Water Chemistry, Heat Distribution Losses, and DDU System Sizing & Costs</i>	163

<i>C5. Piping and Instrumentation Diagrams (P&IDs); Case 1 and Case 2.....</i>	<i>180</i>
<i>C6. Commercialization for Military Applications</i>	<i>192</i>
Appendix D – Products Developed Under Award and Submissions to the Geothermal Data Repository (GDR)	215
<i>D1. Products Developed Under Award</i>	<i>215</i>
<i>D2. Submissions to the Geothermal Data Repository (GDR).....</i>	<i>216</i>
Appendix E – F&S and U of IL Campus Support	220

LIST OF FIGURES

Figure 1. Location of the study site within the Illinois Basin (ILB) in east-central Illinois. The University of Illinois at Urbana-Champaign (U of IL) is denoted by the green box.....	16
Figure 2. Schematic diagram of the doublet well system designed for the deep direct-use (DDU) geothermal system at the U of IL campus.....	17
Figure 3. Flow chart illustrating workflow for the feasibility study.	19
Figure 4. Stratigraphic column of geologic formations at the U of IL. Stratigraphy primarily based on Nelson (in press).	21
Figure 5. Gamma ray and neutron porosity logs from CCS1 well at the IBDP showing the base of the Eau Claire Formation, the MSS, the Argenta Formation, and Precambrian basement.....	23
Figure 6. ILB thermal gradient based on a DTS log in well CCS1 for the IBDP.	24
Figure 7. Geocellular static models for the MSS were constructed using Schlumberger Limited Petrel© software and analyzed in ArcGIS©. Structure contour maps are shown of (a) top surface elevation and (b) thickness. (Contours are in feet; 1 foot = 0.305 m).	25
Figure 8. Distribution of (a) porosity and (b) permeability in the MSS model constructed using Petrel© software.....	27
Figure 9. Temperature change (after 50 years) at the mid-perforation of the extraction vs. well spacing between the injection and extraction wells.	32
Figure 10. Impacts of varying rate of extraction and injection on temperature distribution after 50 years. The warm colors (red to yellow) represent lower temperatures (near injection well), and cooler colors (green and blue) represent higher temperatures	32
Figure 11. Effect of seasonal changes in temperature for “Heating Only” and “Heating and Cooling” scenarios over 50 years	33
Figure 12. Wellbore modeling geometry and boundary conditions for (a) axisymmetric wellbore model and (b) wellbore components.....	34
Figure 13. Temperature profiles along the center line of extraction well for different flow rates and wellbore insulation techniques.....	36
Figure 14. Temperature profiles along the center line of extraction well for different formation heat capacities.	36
Figure 15. Temperature profiles along the center line of the extraction wellbore for different tubing radius, (a) in the extraction wellbore and (b) in the injection wellbore.	38
Figure 16. Temperature profiles for different flow rates in the injection wellbore. The initial injection temperature (T_{inj}) was 21°C (70°F).....	38
Figure 17. Existing and planned ARFs along the southern part of the ACES Legacy Corridor. Red circles denote existing ARFs and yellow boxes denote ARFs currently under construction or planned for relocation.	39
Figure 18. Average monthly fuel consumption at the ARF (based on FY2015 through FY2017).....	43
Figure 19. Schematic diagram summarizing the four stages of the LCA.....	45
Figure 20. Flow diagram representing the scope of the LCA, including the components that comprise the well design and operation of the GES at the U of IL.	46
Figure 21. The location of military installations in the ILB evaluated in this feasibility study.	49
Figure 22. Location of the study site in the ILB. The pink box delineates the extent of geologic, geocellular, and reservoir models that were completed; an area covering 93 km ² (36 square miles).....	52
Figure 23. Estimated degree days in Champaign-Urbana for the period FY2015 through FY2017.....	60
Figure 25. Hourly heat load (Q^h) demands of the six ARFs sorted from high to low levels.	61
Figure 26. Cumulative heating load demand vs. heat supply capacity.	63

Figure 27. Case 1 Process Flow Diagram (1M = 1 unit of mass flow).	65
Figure 28. Case 2 Process Flow Diagram (1M and 2M = 1 unit and 2 units of mass flow, respectively).66	
Figure 29. The “virtual” routes for the pipes carrying the geothermal fluids and clean water	69
Figure 30. Conceptual diagrams of three types of trenches (Note that the marked pipe diameters include insulation and approximate values for only illustrative purpose).	72
Figure 31. Case 1 – Sensitivity of Capital Costs versus Total Heating Demand.	76
Figure 32. Case 2 – Sensitivity of Capital Costs versus Total Heating Demand.	76
Figure 33. Impact comparison of the four life cycle stages, showing significant GWP associated with the operation of the DDU GES.	79

LIST OF TABLES

Table 1. <i>Depths and Thicknesses of the Geologic Formations</i>	22
Table 2. <i>Thermophysical and Hydraulic Properties of Geologic Formations</i>	26
Table 3. <i>Simulation Parameters to Evaluate Sensitivity of the Doublet Well System to Extract Geothermal Energy from the LMSS</i>	29
Table 4. <i>Finite Element Modeling Parameters</i>	29
Table 5. <i>Pressure and Temperature Changes after 50 Years of Operating GES</i>	31
Table 6. <i>Season Duration and Input Data – Simulating Effects of Ambient Temperature Changes</i>	31
Table 7. <i>Material Properties of Wellbore Components</i>	35
Table 8. <i>Thermal Conductivities of Different Insulation Scenarios and Wellbore Parameters</i>	35
Table 9. <i>Seasonal Surface Injection Temperatures</i>	35
Table 10. <i>Average Fuel Consumption at the ARF between FY2015 and FY2017</i>	42
Table 11. <i>Energy Consumption at the ARFs</i>	46
Table 12. <i>Military Installation and Energy Characteristics</i>	49
Table 13. <i>Parameters for Calculating the Geothermal Energy Resource in the MSS</i>	54
Table 14. <i>Parameters for GIS-Based Estimate of Geothermal Energy Resource in the MSS</i>	56
Table 15. <i>Peak Heating Load Demands from Degree Days Approach and Hourly Load Analysis</i>	62
Table 16. <i>Length and Sizing Information of Main and Branch Hydronic Piping Systems</i>	70
Table 17. <i>Estimated Costs of Main and Branch Hydronic Piping Systems</i>	71
Table 18. <i>Estimated Costs of Trench Excavation and Backfilling</i>	72
Table 19. <i>Estimated Capital Costs for the Surface Infrastructure</i>	74
Table 20. <i>Case 1: Sensitivity of Capital and Operating Cost of Heat vs. Total Heat Demand</i>	75
Table 21. <i>Case 2: Sensitivity of Capital and Operating Cost vs. Total Heat Demand</i>	76
Table 22. <i>Summary of Initial Conditions for Cases 1 and 2</i>	77
Table 23. <i>LCCA and LCOH Results</i>	78
Table 24. <i>Emissions Associated with Current Heating Operations at the ARFs</i>	80

List of Acronyms and Abbreviations

°C	degrees Celsius
°F	degrees Fahrenheit
ACES	College of Agricultural, Consumer and Environmental Sciences
AEWRS	Army Energy Water and Energy Reporting System
AFB	U.S. Air Force Base
AH&P	Andrews, Hammock and Powell, Incorporated
AHU	air handling unit
ARF	agricultural research facility at U of IL along the southern part of the ACES Legacy Corridor in the South Farms
ATES	Aquifer Thermal Energy Storage
BHT	bottomhole temperature
BHP	bottomhole pressure
BLCC	Building Life Cycle Cost
BTES	Borehole Thermal Energy Storage
C-T front	cold temperature front
CFCs	chlorofluorocarbons
CHP	Combined Heat and Power
CO ₂	carbon dioxide
DDU	deep direct-use
DoD	U.S. Department of Defense
DSB	discounted simple payback
DPB	discounted payback
DTS	distributed temperature sensing
EBS	U of IL Energy Billing System
EGS	enhanced geothermal system
ERDC-CERL	Engineer Research and Development Center - Construction Engineering Research Laboratory
ES ²	Energy Security & Sustainability
ESP	electric submersible pump
F&S	Facilities & Services at U of IL
FY	fiscal year
GDR	Geothermal Data Repository
GES	geothermal energy system
GeoHRC	Geothermal Heat Recovery Complex
GEOPHIRES	GEoThermal Energy for Production of Heat and Electricity (IR) Economically Stimulated
GHG	greenhouse gases
GHX	ground loop heat exchanger
GTO	Geothermal Technologies Office
GWP	global warming potential
HDD	horizontal directional drilling
HDPE	high-density polyethylene
HVAC	heating, ventilation, and air conditioning
IBDP	Illinois Basin – Decatur Project
iCAP	Illinois Climate Action Plan

IEPA	Illinois Environmental Protection Agency
IDPH	Illinois Department of Public Health
ILARNG	Illinois Army National Guard
ILB	Illinois Basin
ISGS	Illinois State Geological Survey
ISRL	Imported Swine Research Laboratory
K	degrees Kelvin
LCA	life cycle assessment
LCCA	life cycle cost analysis
LCOE	levelized cost of electricity
LCOH	levelized cost of heat
LMSS	Lower Mt. Simon Sandstone
LPG	liquefied petroleum gas (propane)
LT	low-temperature
MSS	Mt. Simon Sandstone
NEPA	National Environmental Policy Act
NG	natural gas
NIST	National Institute of Standards and Technology
NPV	net present value
NREL	National Renewable Energy Laboratory
NSWC	U.S. Naval Surface Warfare Center
NWS	National Weather Service
OD	outer diameter
O&M	operation and maintenance
OOIP	original oil in place
P&IDs	pipng and instrumentation diagrams
PFE	plate and frame heat exchanger
PNNL	Pacific Northwest National Laboratory
PPA	Purchased "Power" (Thermal) Agreement (PPA)
PRL	Physiology Research Laboratory
PVC	polyvinyl chloride
ROI	return on investment, ratio of net profit to cost of investment
SIR	savings to investment ratio
SPS	St. Peter Sandstone
TDS	total dissolved solids
TSS	total suspended solids
UCSD	Urbana and Champaign Sanitary District
UIC	Underground Injection Control
U of IL	University of Illinois at Urbana-Champaign
US	United States
USDOE	U.S. Department of Energy
USDW	Underground Source of Drinking Water
USEPA	United States Environmental Protection Agency
USGS	United States Geological Survey
VAV	variable air volume
VFDs	variable frequency drives
VLT	very low temperature

VOC

volatile organic compound

List of units

\$/ft	U.S dollars per foot
\$/kWh	U.S. dollars per kilowatt-hour
\$/MWh	U.S. dollars per megawatt-hour
\$/MMBtu	U.S. dollars per million British Thermal Units
\$/yd ³	U.S. dollars per cubic yards
bbl/d	barrel per day
Btuth/ft ³ ·°C	British Thermal Unit per cubic foot-°C
Btu/h·ft·°F	British Thermal Unit per hour-foot-°F
Btu/h-ft-K	British Thermal Unit per hour-foot-K
Btu/h·ft ³	British Thermal Unit per hour-square foot
Btu/lb·°F	British Thermal Unit per pound-°F
Btu/lb·K	British Thermal Unit per pound-K
ft	feet
ft ²	square feet
ft lbf	foot pound-force
ft/s	feet per second
g/cm ³	grams per cubic centimeter
ha	hectare
inch/h/ft ² ·°F	inch per hour per square foot-°F
J/kg·°C	joules per kilogram-°C
J/kg·K	joules per kilogram-K
J/m ³ ·K	joule per cubic meter-K
kh	permeability-thickness
kg/m ³	kilograms per cubic meter
kJ/kg·K	kilojoules per kilogram-K
kPa	kilopascals
km ²	square kilometer
m	meters
m/s	meters per second
m ³ /d	cubic meters per day
mD	millidarcy
MJ/m ³ ·K	megajoule per cubic meter-K
MMBtu	million British Thermal Units
MMBtu/hr	million British Thermal Units per hour
MMBtu/yr	million British Thermal Units per year
MWh	megawatts per hour
N/m ³	newtons per cubic meter
ppm	parts per million
Pa	pascals
psig	pounds per square inch gauge
psi/ft	pounds per square inch per foot
W/m	watts per meter
W/m ³	watts per cubic meter
W/m·°C	watts per meter-°C
W/m·K	watts per meter-K

Nomenclature

A = reservoir area

α_F ($1.54 \times 10^{-5} \text{ 1/}^\circ\text{C}$) = the coefficient of thermal expansion of K-feldspar.

α_Q = coefficient of thermal expansion of quartz ($4.98 \times 10^{-5} \text{ 1/}^\circ\text{C}$)

C_p or C_t = specific heat capacity of geologic materials

C_{pf} = specific heat capacity of fluid ($\text{J}/(\text{kg}\cdot^\circ\text{C})$)

C_{pF} = specific heat capacity of K-feldspar ($628 \text{ J}/(\text{kg}\cdot^\circ\text{C})$)

C_{pQ} = specific heat capacity of quartz ($740 \text{ J}/(\text{kg}\cdot^\circ\text{C})$)

C_{pT_1} = specific heat capacity at 20°C

C_{pnT_1} = normalized specific heat capacity at 20°C

C_{pnT_2} = normalized specific heat capacity at reservoir temperature

C_{ps} = specific heat capacity ($\text{J}/(\text{kg}\cdot^\circ\text{C})$) of the matrix in porous media

CU = conductivity unit (in Robertson, 1988)

C_w = specific heat of the geothermal fluid

D = depth in feet and meters

D_H = characteristic length (in meters) (e.g., the diameter of circular channels).

D_i = degree day on the i -th day.

D_{\max} and D_{ave} = highest and average degree day temperatures, respectively, for one year.

DPB = year where cumulative cash flow (Savings – Costs) is positive

E_1 = 7,994 MMBtu/year (Case 1)

E_2 to E_{50} are calculated using the discount rate (d) and NG escalation rate (e)

F = volume force (N/m^3)

h = average reservoir thickness

h^y = total hours in a year

kf = thermal conductivity ($\text{W}/(\text{m}\cdot^\circ\text{C})$) of fluid in porous media

KFel = % of K-feldspar in the rock

ks = thermal conductivity ($\text{W}/(\text{m}\cdot^\circ\text{C})$) of matrix in porous media

p = pressure (in Pa)

ρ_t = density of geologic materials (bulk)

ρ_f = fluid density (kg/m^3)

ρ_s = density (kg/m^3) of the matrix in porous media

ρ_w = density of geothermal fluid

Q_1 = 7,994 MMBtu/year (Case 1)

Q_2 to Q_{50} = calculated using the discount rate (d) and NG escalation rate (e)

Q = heat source (or sink) (W/m^3)

Q_b^m and Q_b^h = monthly and hourly base heating load for domestic water use, respectively, for the entire year. The value of 732 is the monthly hours averaged over June to September.

Q^h = hourly heat load

Q_{max}^h = hourly peak load

Q_j^m = monthly heat use in j^{th} month

Qtz = % of quartz in rock

Q^y = total heating demand for a year

Re = Reynolds number

S = slope constant (0.157 CU/% for sandstone)

T = temperature in $^\circ\text{C}$ or $^\circ\text{F}$

$T_{i,j}$ = hourly ambient temperature of i^{th} hour in j^{th} month

T_{inj} = injection temperature

t_{\max}^i and t_{\min}^i = highest and lowest ambient temperatures, respectively, on that day

T_{res} and T_0 = average reservoir & reference temperatures (calculated in absolute values [i.e., K]).

τ = viscous stress (Pa) calculated using the following expression for Newtonian fluids

u = flow velocity (m/s).

μ = fluid dynamic viscosity (Pa·s).

V = reservoir volume.

γ = solidity of rock equal to 1 – porosity.

λ_F = pore fluid thermal conductivity intercept at $\gamma^2 = 0$.

λ_S = solid rock thermal conductivity intercept at $\gamma^2 = 0$.

Unit Conversions

1 bbl = 42 U.S. gallons = 0.159 m³

1 bbl/d = 0.16 m³/d

1 cm² = 1.01 × 10¹¹ mD

1 CU = 1 × 10⁻³ cal/cm·s·°C = 0.4184 W/m·K

1 exajoule = 1 × 10¹⁸ joules = 0.9478 Quads = 9.5 × 10⁸ MMBtu = 2.8 × 10⁸ MWh

1 °F = 9/5 × °C + 32

1 ft = 0.305 m

1 ft/s = 0.305 m/s

1 g/cm³ = 1000 kg/m³

1 inch = 0.0254 m

1 J/cm³·K = 1 MJ m³·K

1 J/cm³ = 1000 kJ/m³

1 J/cm³·K = 1 MJm³·K

1 J/kg·K = 2.39 × 10⁻⁴ Btu/lb·°F

1 J/m³·°C = 0.015 Btu_{th}/ft³·°C

1 J/m³·K = 0.015 Btu_{th}/ft³·K

1 kJ/kg·K = 0.239 Btu/lb·K

1 km = 0.62 miles

1 m³/s = 5.43 × 10⁵ bbl/d

1 MJ = 947.8 Btu

1 N/m³ = 0.74 ft lbf

1 Pa = 1.45 × 10⁻⁴ psi

1 bbl = 5.62 ft³ = 0.16 m³

1 W/m = 0.58 Btu/h-ft

1 W/m³ = 0.097 Btu/h·ft³

1 W/m·°C = 0.58 Btu/h-ft-K

1 W/m·K = 6.934 inch/h/ft²·°F

EXECUTIVE SUMMARY

This feasibility study is the first assessment of geothermal resources in the Illinois Basin (ILB). The breadth of previous, geologic-based research in the ILB supported this thorough determination of geothermal resources in the Mt. Simon Sandstone (MSS) and the techno-economics of establishing a geothermal energy system (GES) at the University of Illinois at Urbana-Champaign (U of IL). An integrated, multi-disciplinary scientific and engineering approach allowed simulations for both the belowground and aboveground components of the GES that would meet the required baseload of 2 MMBtu/hr at the end-user agricultural research facilities (ARFs). This assessment contributes to the broader discussion surrounding the U of IL's goal to achieve net-zero carbon emissions by 2050. Furthermore, a rigorous evaluation of the ILB's geological, hydrological, and thermal frameworks facilitated a broader assessment of the feasibility of applying deep direct-use (DDU) technologies at facilities (e.g., military installations, hospitals, and school campuses) in other geographical areas in the ILB, and in other sedimentary basins in midcontinent of the US.

The objective of this study is to determine the feasibility of using a DDU GES to extract heat from low-temperature (30°–90°C; 90°–190°F) geothermal resources in the ILB to condition ARFs at the U of IL. To assess the potential geothermal resources in the ILB, the prolific, water-bearing MSS formation was the focus of this study. From a geothermal energy resource perspective, *in-situ* temperature and fluid volume are the key parameters involved in calculating geothermal resources. The top of the MSS at the U of IL is ~1,750 m (5,745 ft) below the ground. A detailed analysis using thermal gradients based on formation-specific temperature with ILB bottomhole temperatures (BHT) yielded MSS estimates of 44°–46°C (111°–115°F). In addition, a compilation of archival geothermal fluid chemistry established the salinity of MSS geothermal fluids to be >200,000 ppm (seawater ~35,000 ppm).

While the *Geothermal Resource Assessment* is a necessity, this study emphasizes the importance of the mass flow rate of extracted fluids and minimizing heat losses. Based on the flow properties of the MSS, the proposed GES can readily meet the baseload heating requirement of 2 MMBtu/hr using a doublet (two well) design with separate extraction and injection wells constructed in the Lower Mt. Simon Sandstone (LMSS). However, all sources of heat loss will reduce delivered thermal energy. This study provides solutions that will minimize heat losses in the subsurface and aboveground. The proximity of the wells to the GES is an important factor in minimizing heat loss at the surface. Heat losses between geologic formations and the ground surface are a consequence of extraction, but will be minimal, primarily because of the high velocity of fluid extraction required to meet the heat demands of the ARFs.

Geologic and geocellular models formed the basis of the flow modeling (geothermal reservoir simulations) that estimated fluid extraction rates. Combined with wellbore and surface pipe flow models, estimates of deliverable geothermal energy for numerous combinations of extraction depths and well designs were completed. Results of the flow modeling indicated an expected temperature loss of <0.56°C (<1°F) in the extraction wellbore and an expected temperature loss of 0.78°–7.22°C (1.4°–13.0°F) along the surface pipeline. The amount of heat loss depends on the

type of insulation and annular fluids in the wellbore and whether the surface pipe is buried and/or insulated.

The capacity of the GES scenarios designed in this feasibility study were compared with the required energy loads for the existing heated- and cooled-water systems at the ARFs. As part of the work to design a technically feasible GES, specific components of the existing ARF energy systems (including the heating, ventilation, and air conditioning [HVAC] and configuration of hot- and cold-water systems) were studied in terms of their compatibility with the temperature and flow rates available from the LMSS. This study includes two scenarios of the GES that estimate efficiency and associated costs, including wellbore designs, well drilling, and well completion costs. Energy usage and source type are key operational issues regularly discussed by facility managers at the U of IL, and this study contributes to their ongoing analyses and goals to meet long-term energy delivery and usage targets.

An essential outcome of this study was identifying the value of the geothermal resources. An economic valuation was made comparing extraction depth with well costs and well locations. Deeper wells require higher capital expenditures. Additionally, GES operating costs increase as the geothermal fluid is lifted from greater depths, at higher flow rates, and as procedures for handling higher-salinity geothermal fluids become necessary. The estimated total capital cost (including the construction of extraction and injection wells and water pipeline) range from \$11.2 to \$26.1 million for Case 1 (80% of thermal load supplied with DDU) and \$11.8 to \$27.5 million for Case 2 (80% of thermal load supplied with DDU and 20% peak load supplied from heat pump and gas furnace). The levelized cost of heat (LCOH) ranged from \$46.3 to \$58.0 MMBtu/hr for Case 1 and \$41.1 to \$50.9 MMBtu/hr for Case 2. Construction capital costs and LCOH estimates varied with flow rate, which is dependent on the required ARFs' heating load. Total costs for constructing and operating the DDU GES ranged from \$11,421,732 to \$27,093,926 for Case 1 and \$12,050,868 to \$28,596,473 for Case 2. From the Life Cycle Cost Analysis (LCCA), the Net Present Value (NPV) and Savings to Investment Ratio (SIR) were negative \$18,914,538 and 0.23 for Case 1 and negative \$20,323,093 and 0.27 for Case 2.

This feasibility study identified the key components of the fully-integrated DDU technology that can be implemented, both technically and economically. The results and information from this study provides end-users and policy makers with guidance for additional research on the specific components of DDU technology such that its widespread use can provide an uninterrupted energy source, increase resilience from extreme weather conditions, reduce U.S. dependency on fossil fuels, and reduce greenhouse gas (GHG) emissions. The site-specific part of this study gives U of IL administrators a realistic and pragmatic assessment of the financial resources necessary to add a DDU GES in the MSS to the campus' energy portfolio.

1. INTRODUCTION

The objective of this feasibility study is to provide a preliminary evaluation of the technical and economic viability of developing a DDU technology for a GES, referred to as the “Geothermal Heat Recovery Complex: Large-Scale, Deep Direct-Use System in a Low-Temperature Sedimentary Basin” at the U of IL campus (Figure 1). Thermal energy would be obtained from geothermal fluid extracted from the MSS and delivered through an aboveground infrastructure to six ARFs along the Agricultural, Consumer and Environmental Sciences (ACES) Legacy Corridor (University of Illinois, 2018e). The geothermal energy is extracted via a doublet (two well) system (Figure 2) completed in the LMSS. The proposed DDU GES application at the U of IL will support a secure, long-term supply of heating that will reduce GHG emissions and simultaneously increase energy security and improve energy resiliency.

This feasibility study was funded by a grant from the U.S. Department of Energy (USDOE) Geothermal Technologies Office (GTO) as part of a program to promote the wider use of low-temperature (<90°C; <190°F) geothermal resources in large-scale, fully integrated DDU GES outside of the U.S. western states, including applications in low-temperature sedimentary basins. Hydrothermal or enhanced geothermal system (EGS) resources used for direct-use applications are generally shallower than those same resources used for power generation purposes, but are significantly deeper than ground source heat pumps. Recently completed studies by the National Renewable Energy Laboratory (NREL) (Mullane et al., 2016; Akar and Turchi, 2016) and the U.S. Geological Survey (USGS) (Williams et al., 2015) report that the available energy from low-temperature geothermal resources (30°–90°C; 90°–190°F) are substantial and could supply a significant portion of the U.S. heating demand. Low-temperature sedimentary basins in the U.S., like the ILB, hold quite large thermal energy resources (Porro et al., 2011) that have yet to be utilized.

While the proposed DDU GES was designed to primarily meet the average annual heating load of the ARFs, a scenario was presented where the entire heating load (even during peak energy use) was met by way of adding a heat pump. The addition of innovative equipment and technologies has been shown to improve efficiency, reduce cost, and increase the overall utility of the GES (Fleuchaus et al., 2018). One technology the DOE has recently begun to promote is Underground Thermal Energy Storage (UTES) (USDOE, 2019a), which includes these sister technologies, (1) Aquifer Thermal Energy Storage (ATES), (2) Borehole Thermal Energy Storage (BTES), and (3) Reservoir Thermal Energy Storage (RTES), and (4) Underground Thermal Battery (UTB) (e.g., Hesaraki et al., 2015).

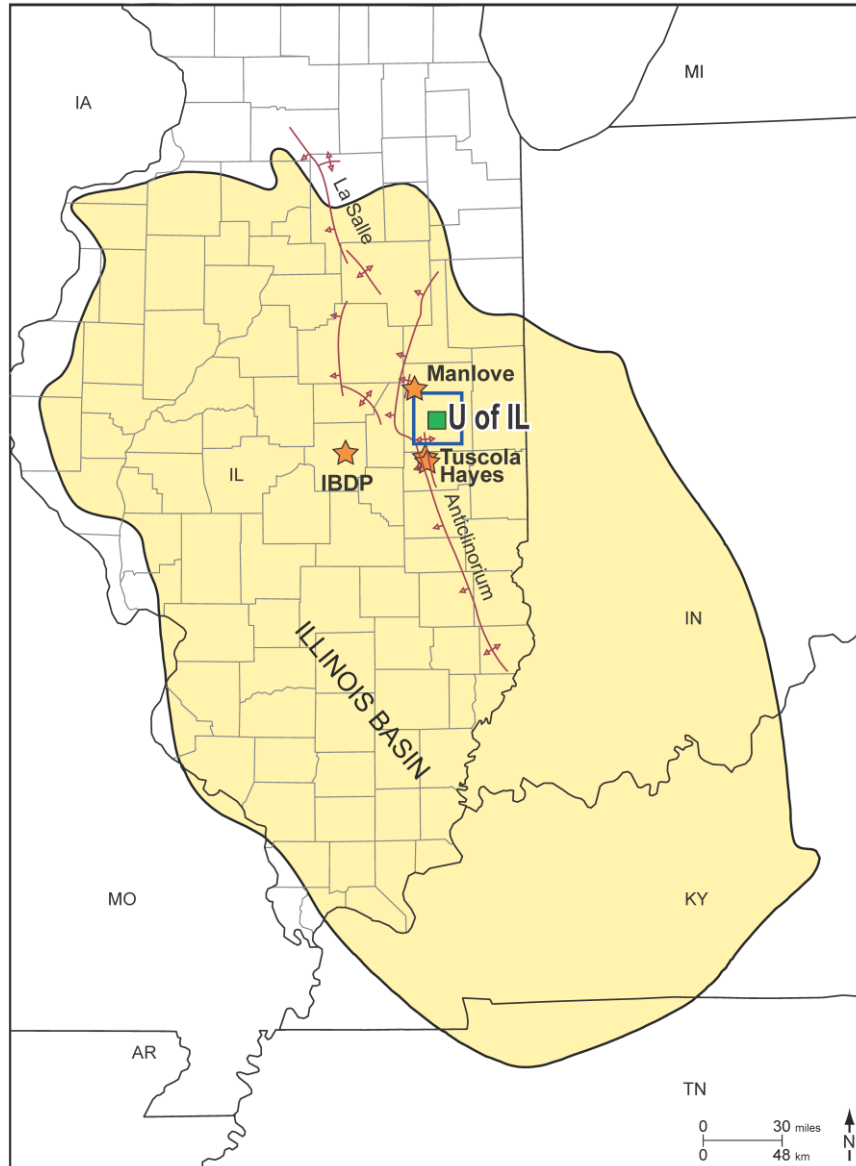


Figure 1. Location of the study site within the Illinois Basin (ILB) in east-central Illinois. The University of Illinois at Urbana-Champaign (U of IL) is denoted by the green box. The ILB is a low-temperature (30°–90°C; 90°–190°F) sedimentary basin (cf., Akar and Turchi, 2016; Williams et al., 2015) covering a ~155,000 km² (~60,000 square mile) area (Buschbach and Kolata, 1990); the basin’s extent is delineated by yellow shading. The 93 km² (36 square mile) area where the geologic, geocellular, and geothermal reservoir modeling were conducted is outlined by the blue box. Also, denoted by the orange stars are the Manlove and Tuscola gas storage fields, the Illinois Basin–Decatur Project (IBDP), and the Hayes oil field. The major structural lineaments in the region are traced by the red lines.

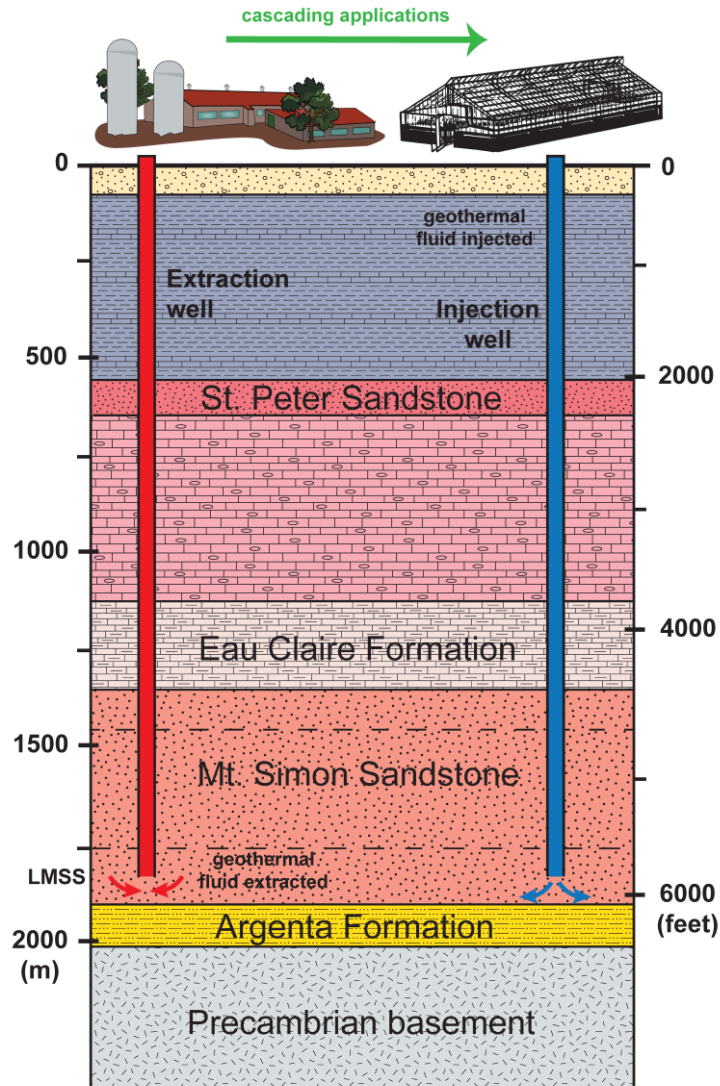


Figure 2. Schematic diagram of the doublet well system designed for the deep direct-use (DDU) geothermal system at the U of IL campus. The extraction wellbore is designed to deliver 954 m³/d (6,000 bbl/d) of geothermal fluid (44°–46°C; 111°–115°F) from a screened interval between 1,860 m and 1,905 m (6,100 ft and 6,250 ft). In order to inject the same amount of fluid extracted, the injection zone was established between 1,890 and 1,935 m (6,200 ft and 6,350 ft). Different injection depths were considered, but the hydraulic conditions in other parts of the MSS were not adequate to achieve the required injection rate. See Appendix C1 for more details about the design of the extraction and injection wellbores.

Successfully extracting geothermal energy from deep geologic formations relies not only on the *in-situ* fluid temperatures, but also on the adequate flow of fluid to meet end-user heat demands, which requires thick, highly permeable and porous, laterally extensive geologic formations. Unlike many “prospective” or “potential” EGS resource targets that initially, or prior to stimulation, lack the flow rates necessary to meet end-user demands (Mullane et al., 2016), most sedimentary basins contain rocks with very high porosity and permeability that contain sufficient volumes of geothermal fluid to meet the flow rates of large, district-scale GES (Limberger et al., 2018). Also, sedimentary basins are regionally continuous and often contain thick carbonate and sandstone

aquifers, but many of the deepest sedimentary basins in the US midcontinent (>2 km; >1.2 miles) have relatively low thermal gradients (<25°C; <77°F). The thermal gradient for the ILB, where this study was undertaken, averages 16.5°C/km (0.9°F/100 ft). However, deep geothermal reservoirs in the Basin and Range Province of the Western U.S. have sufficiently high temperatures (150°–200°C [300°–400°F] at 2–4 km [6,560–13,120 feet] deep) and good permeability for power generation (Allis et al., 2016).

To evaluate the feasibility of a DDU GES along the ACES Legacy Corridor (University of Illinois, 2018) for large-scale agricultural research and production applications, a multidisciplinary research team with expertise across the geology and engineering disciplines was assembled. Specifically, experts in geologic modeling, geothermal modeling, wellbore modeling, mechanical/chemical engineering, and techno-economic analyses formed five Task Groups responsible for various components of the study, presented in the workflow shown in Figure 3. Throughout the study, extensive, in-house geology and geochemistry databases that the U of IL maintains at the Illinois State Geological Survey (ISGS) were used to develop the models and simulations that informed the GES design. The team engaged campus end-users and officials to obtain critical information about the current and future energy loads for the ARFs and the long-term development plan for the ACES Legacy Corridor. Together with the modeling data, the team completed a *Geothermal Resource Assessment* of the MSS and the ILB and developed the *End-Use Load Market Transformation Plan*. Furthermore, interactions with campus end-users and officials assisted the team in identifying additional uses for the thermal energy, including cascading applications to further optimize GES energy efficiency and favorable project economics. The team also sought input from potential ILB end-users at military installations, educational campuses, communities, and industries to determine the potential market demand and address challenges to commercializing the DDU technology. The U.S. Environmental Protection Agency (USEPA) and Illinois Environmental Protection Agency (IEPA) were contacted to develop the *Regulatory Compliance Plan*.

An important consideration in designing the GES was limiting heat losses during extraction and injection along the entire stratigraphic column (vertically within wellbores) and, generally, horizontally across the surface infrastructure. The development of a site-specific model allowed for the assessment of multiple scenarios with different well locations, design capacities, fluid handling equipment, heat exchangers, and supplemental heat sources. To demonstrate the technical feasibility of the DDU technology, it was necessary to identify designs with higher energy efficiency to improve the economics of the GES. This work included evaluating enhancements to the existing ARF heating systems, expanding the sensitivity analysis to provide a range of LCOH values versus total heat demand, and determining how to reduce the operating and maintenance costs (O&M) of the DDU GES.

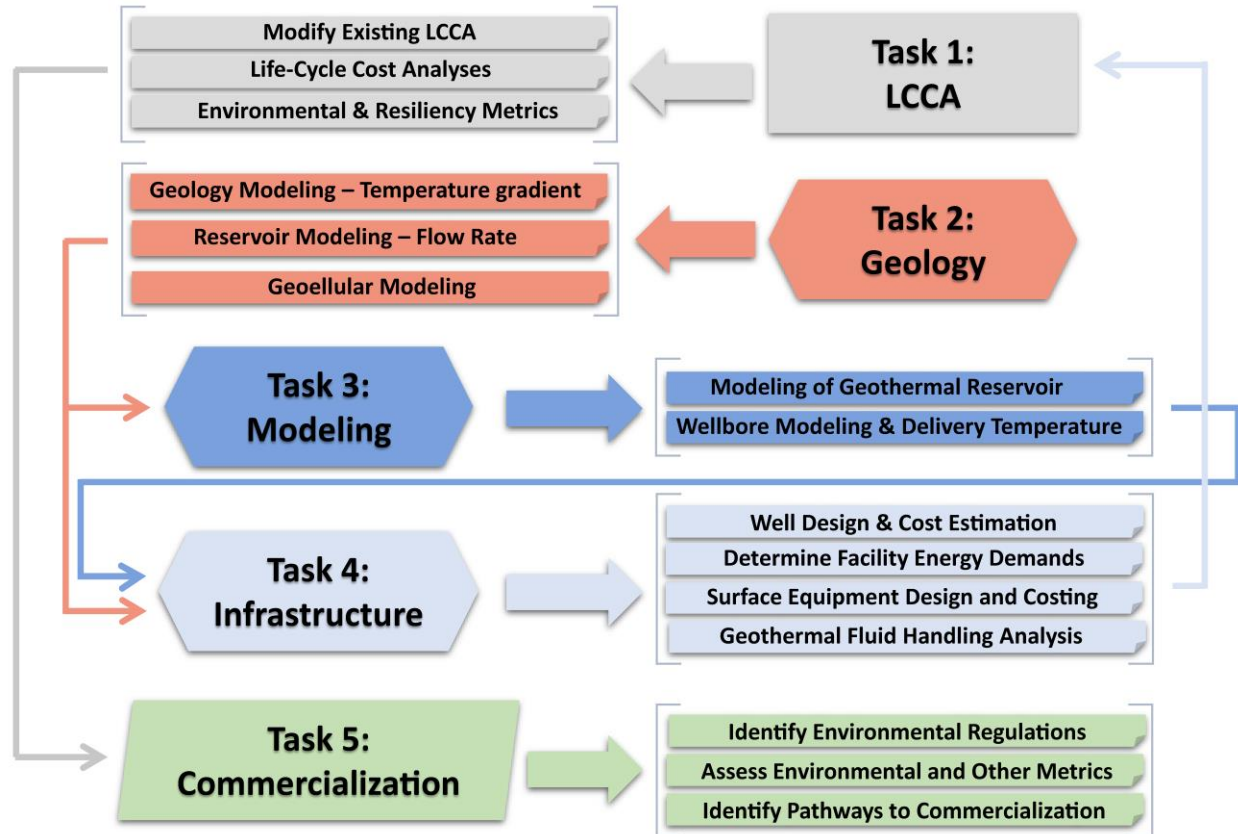


Figure 3. Flow chart illustrating workflow for the feasibility study.

While the U of IL has a specific and keen interest in using the proposed DDU technology to provide a reliable supply of heat and reduce GHG emissions in support of the campus-wide, net-zero 2050 target, they are cognizant of the capital costs involved in building large-scale energy systems where several competing energy sources are available. By combining technical feasibility with project economics, the team made an objective and rigorous assessment of the selected scenarios. The team developed specialized Life Cycle Assessment (LCA) and Life Cycle Cost Analysis (LCCA) spreadsheet tools to evaluate and assess the economics and environmental impacts over the life of the DDU GES. Through the development of the techno-economic feasibility model, several DDU GES scenarios were identified that met or exceeded economic, regulatory, and marketing criteria. This study will reduce challenges to the widespread use of DDU GES in the U.S. midcontinent as well as other geographical areas with known, low-temperature geothermal resources that have similar hydraulic and thermodynamic conditions.

2. APPROACHES

2.1 Geologic and Geocellular Modeling

In order to identify and fully understand the effects of far-field geologic features and processes on temperature distribution as a consequence of geothermal fluid extraction and injection via a doublet well system, an analysis and characterization of *in-situ* geological architecture and inherent hydraulic, thermal, and mechanical properties was conducted. This analysis provided a basis for geothermal reservoir modeling and the *Geothermal Resource Assessment*. Two geologic formations were initially studied for their geothermal resources: the St. Peter Sandstone (SPS) and MSS. Both formations are found in the subsurface at the U of IL and contain porous, permeable, and relatively thick sandstones. The SPS and MSS have no known hydrocarbon or mineral resources; however, in some areas, they are used for the storage of natural gas (NG) and carbon dioxide (CO₂). Additionally, the formations are relatively widespread in the ILB. Geologic and geocellular modeling were used to estimate (1) subsurface temperatures, (2) *in-situ* geothermal fluid volumes, and (3) extraction rates (i.e., meters per day [m³/d] or barrels per day [bbl/d]).

2.1.1 Geologic Modeling

To develop a conceptual geologic model for the study area, subsurface contour maps of SPS and MSS gross thickness, structure, and porosity available to the ISGS were reviewed. Data from geologic and petrophysical logs, wellbore tests, and regional geology maps provided the basis for generating structure contour maps, facilitating construction of the SPS and MSS geologic models.

A stratigraphic column representing the geology at the U of IL was developed that included primary rock properties and structure of geologic formations from the recent Quaternary glacial deposits down to the Precambrian bedrock, referred to as the “basement” (Figure 4). Also included were formation tops, bottoms, and thicknesses (Table 1). Much of this information was obtained from existing reports and maps of the ILB, including a new ISGS report by Nelson (in press) that describes in detail the bedrock geology in Champaign County – the county where the U of IL is located. The report contains structure contour maps for the top of the Devonian rocks and Pennsylvanian Colchester coal, which are key strata used in ILB studies for determining the depths to deeper formations. A major geologic structure, known as the La Salle Anticlinorium, crosses the ILB to the southwest of the U of IL (Figure 1). The anticlinorium has subparallel anticlines, domes, monoclines, and synclines along a northwest-southeast trend (Buschbach and Bond, 1974; Nelson, 1995; 2010). In Champaign County, the structures in the bedrock are masked by Quaternary glacial deposits averaging 51 m (167 ft) in thickness (Stumpf and Dey, 2012), and are therefore only recognized by geophysical imaging and test drilling (Stumpf and Ismail, 2013).

After reviewing the geologic and structure data for the SPS and MSS, it was determined that gross thickness, structure, porosity, and temperature were relatively constant for most formations across the study area; therefore, it was not necessary to make contour maps of these data. However, there was some variation on the bedrock surface and top surfaces of the Pennsylvanian Colchester coal, New Albany Shale, and Galena (Kimmswick) Limestone in the area being reviewed that warranted making structure contour maps. These maps were uploaded to the Geothermal Data Repository (GDR) (Nelson, 2018).

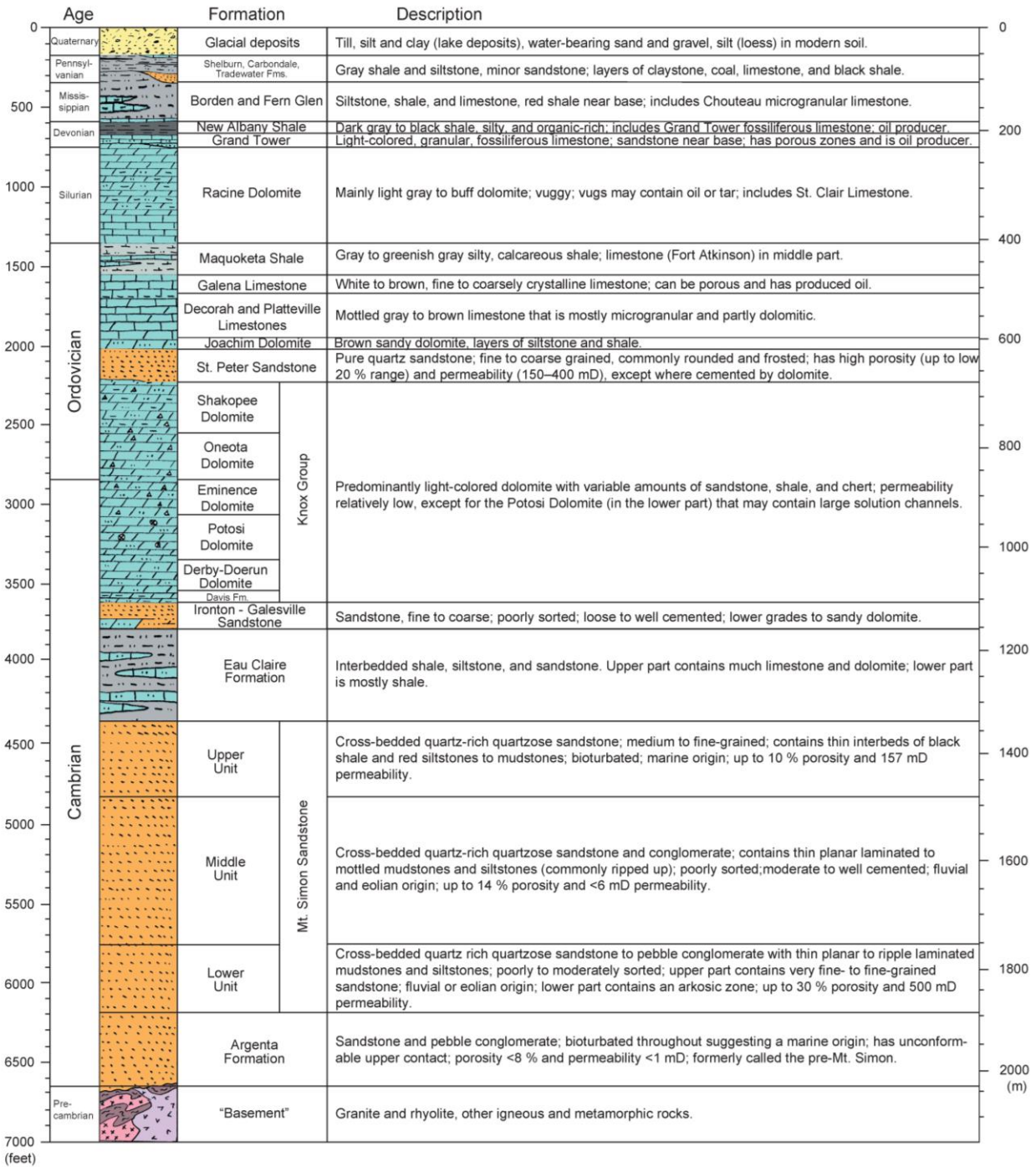


Figure 4. Stratigraphic column of geologic formations at the U of IL. Stratigraphy primarily based on Nelson (in press).

Table 1. Depths and Thicknesses of the Geologic Formations

Geologic Formation	Top (m, bgs)	Thickness (m)	Bottom (m, bgs)	Description of Geologic Materials
Soil	0	2	2	Loess, silt and fine sand
Quaternary (fine)	2	25	26	Till, fine sand, lake sediment
Quaternary (coarse)	26	25	51	Glacial outwash, mostly sand w/ gravel
Pennsylvanian	51	53	104	Shale, siltstone, sandstone, coal beds
Mississippian	104	78	183	Largely siltstone; Chouteau Limestone at base
New Albany	183	24	207	Dark colored, hard shale
Grand Tower (Devonian)	207	24	231	Limestone, commonly sandstone at base
Silurian	231	180	411	Vuggy dolomite, lower part limestone; shows of oil likely
Maquoketa (Ordovician)	411	61	472	Shale; limestone in middle
Kimmswick	472	39	510	Limestone
Decorah and Platteville	510	82	593	Limestone, thin shale layers
Joachim	593	19	612	Dolomite and sandstone, shale layers
St. Peter (SPS)	612	59	671	Pure quartz sandstone, water bearing
Knox Group	671	427	1098	Dominantly dolomite, partly sandy and cherty
Ironton	1098	53	1151	Pure quartz sandstone, water bearing
Eau Claire	1151	183	1334	Shale, sandstone, and limestone; shale increasing downward
Mt. Simon (upper)	1334	139	1473	Sandstone with mudstones, arkose wacke to quartz arenite, well cemented, high porosity
Mt. Simon (middle)	1473	277	1750	Sandstone and conglomerate, quartz arenite to wacke with thin interbeds of mudstone and clay
Mt. Simon (lower) (LMSS)	1750	137	1887	Sandstone, subarkose to arkose wacke, water bearing, good reservoir
Argenta	1887	146	2033	Sandstone, sublithic arenite to quartz arenite, well cemented
Precambrian	2033	>100		Maroon-colored porphyritic rhyolite over diorite and granite

2.1.2 Reservoir Characterization

The hydraulic, thermal, and mechanical properties of the geologic formations were compiled from existing ISGS datasets and publications in the public domain to determine geothermal energy resources and extraction and injection rates. Geologic field and laboratory data and general petrophysical relationships based on previous studies of the ILB (e.g., Figure 5) were used to undertake the subsurface characterization and provided baseline information for the geologic and geocellular models. This information was compiled into a project database (the references to these data were uploaded to the GDR [Damico et al., 2018; University of Illinois, 2018a; b; c]).

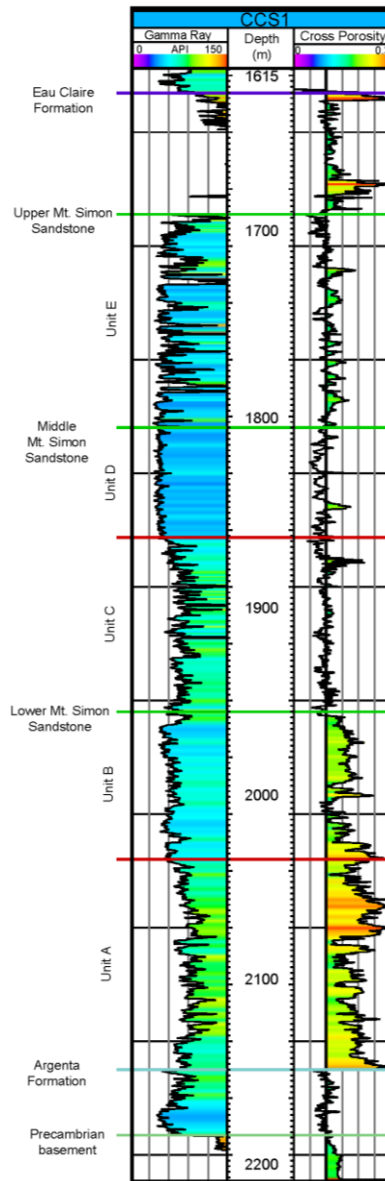


Figure 5. Gamma ray and neutron porosity logs from CCS1 well at the IBDP showing the base of the Eau Claire Formation, the MSS, the Argenta Formation, and Precambrian basement. The MSS is divided into three major units: the Lower, Middle, and Upper. The MSS is further divided into Units A through E. Increasing gamma ray intensity is indicated from green to blue. Porosities greater than 10% on the neutron porosity log are indicated by the green and red shading (after Freiburg et al., 2014).

The thermal gradient (from ground surface to the Precambrian basement) for the study area was developed primarily from a continuous log of distributed temperature sensing (DTS) measurements taken in CCS1 (i.e., CO₂ injection well) for the IBDP (Schlumberger Carbon Services, 2012). The DTS log supported the development of formation-specific thermal gradients, which were integral for estimating temperatures of the SPS and MSS (Figure 6). The gradients were increased or decreased depending on the change in formation thickness projected from the IBDP to the U of IL. The thermal gradients were then calibrated to regional BHT measurements

taken at specific depths to infer SPS and MSS temperatures (The subsurface temperature profile was uploaded to the GDR [Lin et al., 2018]).

Implementing the procedure described above was found to be necessary given an initial review of the BHTs. Numerous inconsistencies were found between the reported temperatures and depths. Also, many of the BHT records lacked sufficient information regarding activities performed prior to taking the temperature measurements (i.e., immediately after drilling [prior to thermal equilibration], under static conditions, or under flowing conditions). Having a full understanding of these activities is critical for identifying measurements that are impacted by heating from the drilling operation or pumping of fluids. Consequently, these BHTs are not suitable calibrations for thermal gradients. Furthermore, there is a high degree of confidence the DTS log best represents the *in-situ*, subsurface thermal conditions in the ILB because the measurements were taken over a month after the borehole was drilled, and a month before CO₂ injection started. The estimated temperature ranges are 28°–29°C (82°–84°F) for the SPS and 44°–46°C (111°–115°F) for the LMSS (Figure 6). Because the estimated temperatures in the SPS would be too low for directly heating the ARFs, no further work was undertaken to assess geothermal resources in the formation.

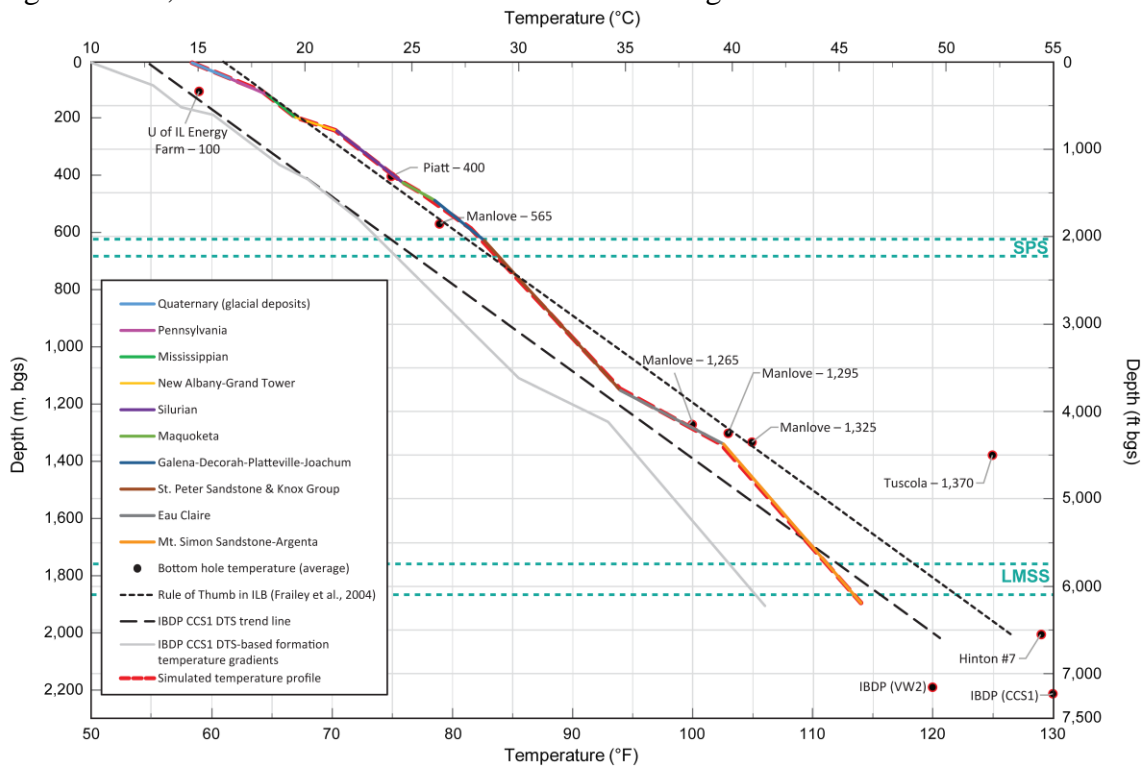


Figure 6. ILB thermal gradient based on a DTS log in well CCS1 for the IBDP. The formation-specific temperature gradients for the IBDP (solid gray line) was moved up the y-axis to intersect representative BHTs at various depths in wells located closer to the U of IL. Specifically, BHTs were measured in wells at the Manlove and Tuscola NG storage fields, at Hayes oil field in Piatt County (Piatt – 400), for the IBDP, and in a geothermal well at the U of IL Energy Farm (ISGS-Energy Farm – 100). The temperatures in the geothermal well are reported in McDaniel et al. (2018b).

2.1.3 Geocellular Modeling

Information pertaining to the heterogeneity and distribution of reservoirs and caprocks and the geostatistical analysis performed for reservoir characterization informed the geocellular models of the SPS and MSS (Figure 7). The geocellular models were populated with thermal, hydraulic, and mechanical properties (Table 2) that were required for subsequent geothermal reservoir modeling. Petrel© and ArcGIS® software were used to build the geocellular models. Preliminary models were constructed (e.g., Stumpf et al., 2018) and then reviewed by additional ISGS geologists and experts from other universities to confirm that both the geologic model and reservoir characterization were adequately representative of the geology and stratigraphic framework. These consultations were conducted in the Earth Systems Visualization Laboratory at the ISGS, where the geologic model and results of the reservoir characterization were presented in 3-dimensions for group discussion. For the final version of the models, files (in “csv” format) containing grid points for the top surfaces of the SPS and MSS were uploaded to the GDR; spreadsheets with input parameters for the geocellular model were also uploaded to the GDR (Damico, 2019a; b).

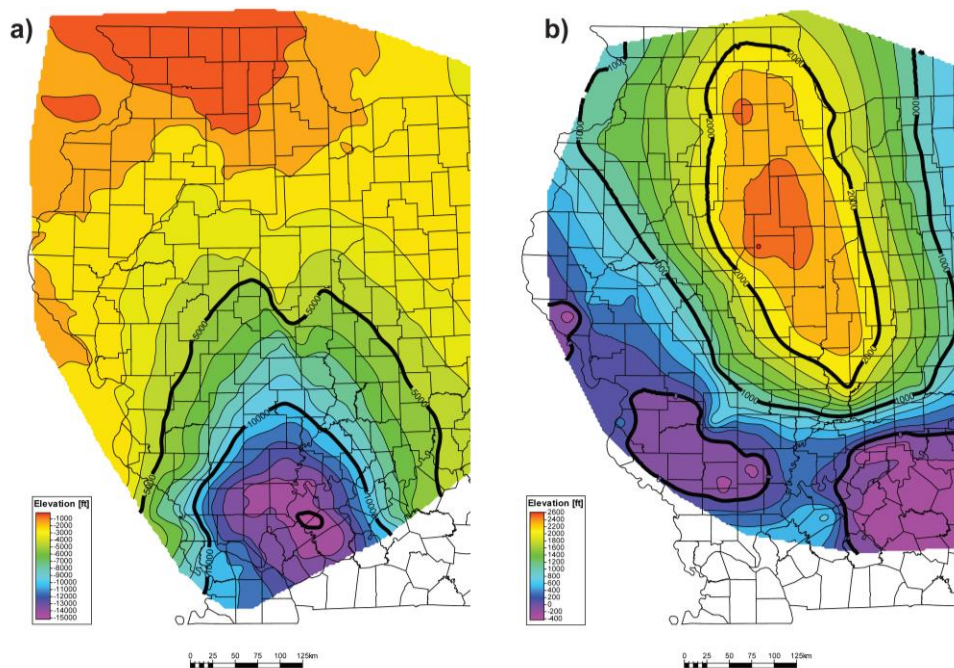


Figure 7. Geocellular static models for the MSS were constructed using Schlumberger Limited Petrel© software and analyzed in ArcGIS®. Structure contour maps are shown of (a) top surface elevation and (b) thickness. (Contours are in feet; 1 foot = 0.305 m).

The SPS and MSS geocellular models represent a $9.7 \text{ km} \times 9.7 \text{ km}$ (6 miles \times 6 miles) area centered on the U of IL (Figure 8). The models were made sufficiently large such that cones of temperature depression associated with extracting and injecting the geothermal fluid would not overlap. Each of the model layers were calibrated with published average thermophysical and hydraulic properties (e.g., Waples and Waples, 2004). The thermal conductivity, specific heat capacity, and thermal expansion coefficient were determined from calculations provided in Appendix B-1.

Table 2. Thermophysical and Hydraulic Properties of Geologic Formations

Geologic Formation	Density (g/cm ³)	Porosity (%)	Permeability (mD)	Thermal Conductivity (W/m·K)	Heat Capacity (J/kg·K)
Soil	1.09	40	40–60	1.57	2760
Quaternary (fine)	2.40	25	2	2.21	1048
Quaternary (coarse)	1.64	38	9000	2.31	3322
Pennsylvanian	2.48	12	5	1.84	1010
Mississippian	2.66	15	10	3.50	820
New Albany	2.54	20	0.01	2.25	879
Grand Tower (Devonian)	2.71	14	12	2.60	921
Silurian	2.80	12	1	4.50	879
Maquoketa (Ordovician)	2.54	20	0.01	3.39	863
Galena	2.71	14	10	2.60	921
Decorah and Platteville	2.71	14	10	2.60	921
Joachim	2.70	13	2	4.20	900
St. Peter (SPS)	2.67	17	163	3.30	825
Knox Group	2.71	7	4	2.60	921
Ironton	2.67	5	0.4	3.50	820
Eau Claire	2.60	6	0.65	1.84	795
Mt. Simon (upper unit)	2.67	10	157	5.16	730
Mt. Simon (middle unit)	2.67	8	3.3	5.71	740
Mt. Simon (lower unit) - LMSS	2.67	16	110	4.15	725
Argenta	2.67	7	0.85	3.50	820
Precambrian (rhyolite)	2.45	7	0.07	3.00	960
Precambrian (granodiorite)	2.72	0	0.001	2.60	1090
Precambrian (granite)	2.60	1	0.001	3.22	960

The top of the MSS model coincides with the Eau Claire Formation. The bottom of the model extends 91 m (300 ft) into the Precambrian basement. Which is subdivided into three subzones (Figure 8; Table 2). Also represented in the model are three units of the MSS and the Argenta Formation. Porosity and permeability were distributed using histograms of well log data for the MSS and Argenta Formation. The permeability of the MSS was determined from core analyses for the IBDP (Freiburg et al., 2014) and Manlove and Tuscola NG storage fields (e.g., Morse and Leetaru, 2003). In the MSS model, permeability averages 99.6 mD ($9.83 \times 10^{-10} \text{ cm}^2$); however, the property has quite a large range: between 0.0005 mD and 1,480 mD ($4.93 \times 10^{-15} \text{ cm}^2$ and $1.46 \times 10^{-8} \text{ cm}^2$). The average porosity is 15.1%, with a range between 0.554% and 31.4%. The Precambrian basement and Eau Claire Formation were assigned constant values for porosity and permeability, with values published in Eckstein et al. (1983) and McDaniel et al. (2018).

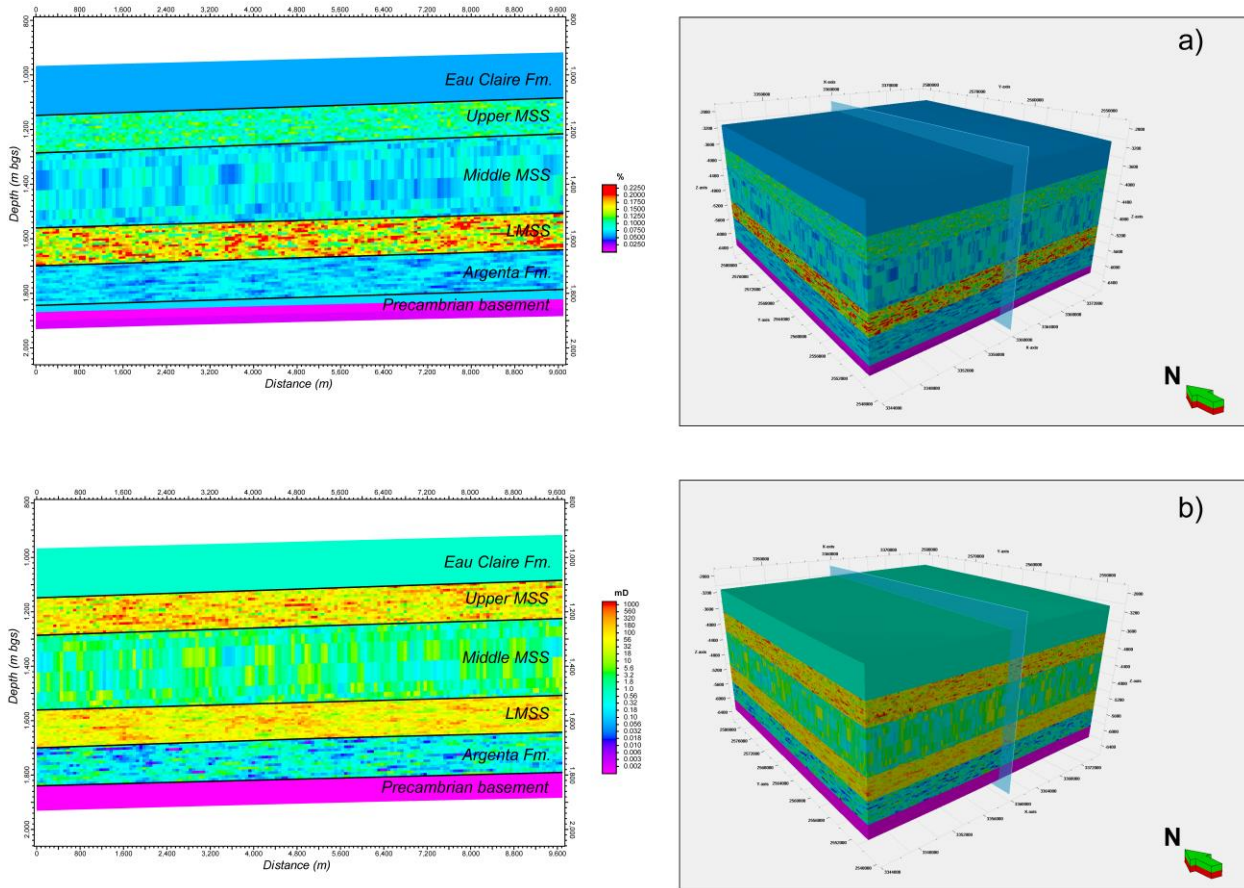


Figure 8. Distribution of (a) porosity and (b) permeability in the MSS model constructed using Petrel© software. The model x and y grid-cell dimensions were set to 61.0 m × 61.0 m (200 ft × 200 ft). The average model thickness is 552 m (1,810 ft). The MSS model includes 62 layers, resulting in an average layer thickness of 13 m (42 ft).

As aforementioned, because the estimated SPS temperature range indicated that the temperature of its geothermal fluid would not be sufficient to meet ARFs’ heating demands, only the MSS was modeled for the *Geothermal Resource Assessment*. The final MSS model was used in geothermal reservoir and wellbore modeling that simulated geothermal fluid extraction, injection, and heat exchange in the extraction and injection wellbores.

2.2 Reservoir and Wellbore Modeling

Reservoir and wellbore models simulated geothermal fluid extraction from the MSS via a doublet well system in order to assess its ability to accommodate flow rates sufficient to meet ARFs’ heating demands. The geologic and geocellular models of the MSS were the foundation for building a geothermal reservoir model. Geothermal, hydraulic, and mechanical properties in the geocellular model were inputted into the reservoir model for accurate geologic representation (Section 2.1). The geothermal reservoir model simulated formation temperature changes over 50 years of DDU GES operation. Simulation results established the maximum flow rates at which geothermal fluid could be extracted from the MSS and injected back into the LMSS as well as the

minimum distance between the extraction and injection wells. Together, these results helped design the doublet well system.

Wellbore modeling estimated the amount of thermal heat that could be delivered to the ARFs by simulating temperature changes (i.e., heat loss or gain) along the wellbores during extraction and injection. Temperature change was estimated as an effect of the thermal properties of wellbore materials, insulation methods, and extraction rates. Eight scenarios were derived from the simulations.

Simulation results were subsequently used for other project activities – specifically, developing designs for the wellbores and surface infrastructure and identifying regulatory implications of the well design. The wellbore simulations informed the (1) placement of wells, (2) size and grade of tubulars, (3) type of cement and annulus fluids used in the wellbore, (4) wellhead design compatible with MSS geothermal fluid composition, and (5) regulatory compliance plan.

2.2.1 Geothermal Reservoir Modeling

Geothermal reservoir simulations evaluated the sensitivity of reservoir temperature to variations in extraction and injection rate, well spacing, geothermal fluid temperature during injection, and seasonal, ambient temperature at the ground surface.

The simulations estimated the maximum extraction rate to ensure that enough thermal energy could be delivered to the ARFs and meet their heating demands. The extraction rate required to supply the 2 MMBtu/hr baseload heating is 954 m³/d (6,000 bbl/d). This is also the targeted extraction rate to maintain temperature change in the GES (ΔT) at 11°C (20°F) (i.e., inflow and outflow temperatures of 43°C [110°F] and 32°C [90°F], respectively). The simulations also estimated the maximum injection rate at which extracted geothermal fluid could be injected into the LMSS at pressures less than formation parting pressure (Table 3). The bottomhole pressure (BHP) of the simulated injection rate was constrained at 90% of the fracture pressure gradient of the MSS based on the LMSS fracture gradient at the IBDP site (15.8 kPa/m [0.72 psi/ft]) (Leetaru et al., 2009). The BHP at the extraction well was held constant at 100 psia.

The simulations also inferred the impacts of seasonal, ambient temperature changes at the ground surface on subsurface temperature and pressure (i.e., the temperature of injected geothermal fluid). These specific simulations included a year-round, heating-only scenario as well as a scenario that simulated cooling during summertime and heating during fall, spring, and winter (Table 3). The effects of seasonal temperature changes on the temperature at the ground surface were also simulated in a scenario where the direction of fluid flow is reversed during summertime to meet cooling demand.

The following assumptions were made in all scenarios: (1) a constant temperature boundary condition at the bottom, confining layer of the MSS (i.e., Precambrian basement), (2) a laterally continuous MSS (i.e., infinite hydraulic boundary conditions), (3) an MSS at hydrostatic equilibrium with adjacent formations (lower and upper confining units), and (4) all extracted

geothermal fluid is injected into the LMSS at the same depth of extraction. Lastly, all scenarios were simulated for a period of 50 years, equivalent to or greater than the proposed life span of the DDU GES.

Table 3. Simulation Parameters to Evaluate Sensitivity of the Doublet Well System to Extract Geothermal Energy from the LMSS

Sensitivity Parameters	Range or Limit	Description
Extraction	BHP at datum (top of model, 100 psi) and	Unconstrained fluid extraction. Assumption: spatial variation in extraction rate is minimal.
Injection	BHP 90% of fracture gradient (0.90×0.71psi/ft = 0.68 psi/ft).	Brine injection (salinity 200,000 ppm). Unconstrained injection rate. Assumption: spatial variation in injection rate is minimal.
Well spacing	0.16–3.2 km 0.10 –2.0 miles	Vary spacing of extraction and injection wells between 0.5–2 miles. Using most likely fluid extraction rate (6,000 stb/d). It is assumed that all the brine produced is injected into the MSS.
Extraction rate	5,000 –10,000 bbl/d	Vary extraction rate. Injection rate must be equal to extraction rate to ensure steady state.
Return temperature	10–32°C 50–90°F	Vary temperature of fluid prior to injection into the MSS.
Seasonal Temperature	Heating only or Heating and Cooling	Vary fluid injection temperature to mimic changes in surface temperature during winter, spring, summer, and fall (Table 4).

Table 4. Finite Element Modeling Parameters

Model Structure	Fluid Type	Tubing	Annulus space	Casing	Grout	Geologic Formations
Horizontal number of elements	20 elements across fluid	2	7	2	7	40
Vertical mesh size and number	1.5 m (5 ft) vertical element height/1,236 elements in vertical direction 1.5 m (5 ft) × 1,236 = 6,180 feet deep model					

Maximum Extraction and Injection Rates:

Reservoir modeling predicted maximum extraction and injection rates of 3,339 m³/d (21,000 bbl/d) and 1,431 m³/d (9,000 bbl/d), both of which exceed the flow rate required to meet ARFs’ baseload heating demand. The maximum injection rate is lower than the maximum extraction rate because the pressure difference between the injection well and the reservoir is lower compared to the pressure difference between the extraction well and the reservoir.

Well Spacing and Extraction Rate:

The simulation results showed a direct, positive relationship between the maximum pressure change and well spacing; however, there was no clear correlation between the minimum pressure

change and well spacing (Table 5, rows 3 to 6). Variability in the minimum pressure change may be attributable to differences in the permeability-thickness (kH) product at the extraction well as its location changes between scenarios. Separately, a direct relationship between extraction rate and pressure change was observed (Table 5, rows 7 to 9).

As anticipated, reservoir modeling predicted lower reservoir temperatures near the injection well and no temperature change within the vicinity of the extraction well, when the extraction and injection wells were used for 50 years and spaced 0.8 km (≥ 0.5 mile) apart. Due to the lower reservoir temperature near the injection well, a cold-temperature (C-T) front formed that over time moves closer to the extraction well. When the two wells were located < 0.8 km (< 0.5 mile) apart, the C-T front reached the extraction well *before* 50 years (Figure 9). As well spacing increased, the distance between the C-T front and the extraction well increased (Figure 10). When well spacing was ≥ 0.8 km (≥ 0.5 miles), temperature change at the extraction well remained within 0.6°C (1°F) after 50 years of extraction and injection because the C-T front did not breakthrough. To avoid extracting geothermal fluids at temperatures less than 43°C (109°F) (as a result of C-T front breakthrough at the extraction well), the two wells were spaced 2.4 km (1.5 miles) apart in subsequent simulations (i.e., the injection temperature and seasonal temperature change scenarios) (Table 5).

Injection Temperature:

Injection temperature decreased the temperature near the injection well and a C-T front that propagated towards the extraction well over time developed. Before C-T front breakthrough at the extraction well, the temperature of extracted geothermal fluid was unaffected when injection temperature was varied; temperature decreased at the injection well (at the center grid cell of the perforated interval of the injection well) as injection temperature also increased, while temperature change at the extraction well remained constant (Table 5, rows 10 to 14). Only *after* C-T front breakthrough did the temperature of extracted geothermal fluid decrease.

Pressure change decreased at the injection well (at the center grid cell of the perforated interval of the injection well) as injection temperature increased (Table 5, rows 10 to 14), which may be because the viscosity of water decreases with increasing temperature. This result was observed while simulating a constant extraction rate of $954\text{ m}^3/\text{d}$ (6,000 bbl/d).

Seasonal Changes:

Seasonal, ambient temperature at the ground surface caused injection temperature to decrease and caused cyclical temperature changes at the injection well. For the “Heating Only” scenario, temperature at the injection well (the grid cell at the center of the perforated interval of the injection well) decreased by $23^{\circ}\text{--}29^{\circ}\text{C}$ ($42^{\circ}\text{--}52^{\circ}\text{F}$). For the “Heating and Cooling” scenario, temperature at the injection well decreased by $\sim 25^{\circ}\text{--}30^{\circ}\text{C}$ ($\sim 46^{\circ}\text{--}54^{\circ}\text{F}$) (Figure 11).

For the “Heating Only” scenario, temperature at the extraction well remained constant (Figure 11, bottom left). For the “Heating and Cooling” scenario, temperatures at the extraction well changed cyclically (up to 1.7°C [3.0°F]) (Figure 11, bottom right). The temperature change at the extraction

well for the “Heating and Cooling” scenario is most likely a result of injecting geothermal fluid during the summer season at 60°C (140°F), which is warmer than the formation fluid (45.6°C; 114.0°F) (Table 6).

Seasonal changes in extraction and injection rates for the “Heating Only” and “Heating and Cooling” scenarios (Table 5) caused cyclical pressure changes near the extraction and injection wells, especially for the “Heating and Cooling” scenario (Figure 11). The large fluctuations in pressure at the extraction and injection wells for the “Heating and Cooling” scenario are most likely due to reversing the direction of fluid flow (i.e., wells switched from extraction to injection and vice versa) to provide cooler fluid during the summer.

Table 5. Pressure and Temperature Changes after 50 Years of Operating GES

Scenario	Case	Pressure change (Δp)		Temperature change (ΔT)	
		Δp_{\min} (psi)	Δp_{\max} (psi)	ΔT_{\min} (°F)	ΔT_{\max} (°F)
Extraction Injection	Extraction well	-1,181	0	-1.10	1.73
	Injection well	0	643	-54.42	0.54
Well Spacing	0.5 mile	-271	325	-53.43	0.31
	1.0 mile	-431	356	-53.52	0.96
	1.5 miles	-258	371	-53.56	0.58
	2.0 miles	-319	381	-53.59	0.58
Extraction Rate	5,000 bbl/d	-215	306	-53.38	0.48
	6,000 bbl/d	-258	371	-53.77	0.58
	10,000 bbl/d	-461	624	-54.37	0.96
Injection Temperature	50 °F	-258	413	-63.67	0.58
	60 °F	-258	371	-53.56	0.58
	70 °F	-258	338	-43.47	0.58
	80 °F	-258	311	-33.43	0.58
	90 °F	-258	290	-23.38	0.58
Seasonal Temperature Changes	Heating	-258	353	-48.05	0.58
	Heating and Cooling	-249	351	-52.42	4.49

Table 6. Season Duration and Input Data – Simulating Effects of Ambient Temperature Changes

Season	Period	Heating scenario		Heating and cooling scenario	
		T_{inj} (°F)	T_{ext} (°F)	T_{inj} (°F)	T_{ext} (°F)
Winter	December – April	50	114	50	114
Spring	May – June	70	114	70	114
Summer	July – August	90	114	140*	90
Fall	September – November	70	114	70	114

Note: *Extraction rate = 3,000 bbl/d; 6,000 bbl/d for other cases. T_{inj} and T_{ext} are injection and extraction temperatures.

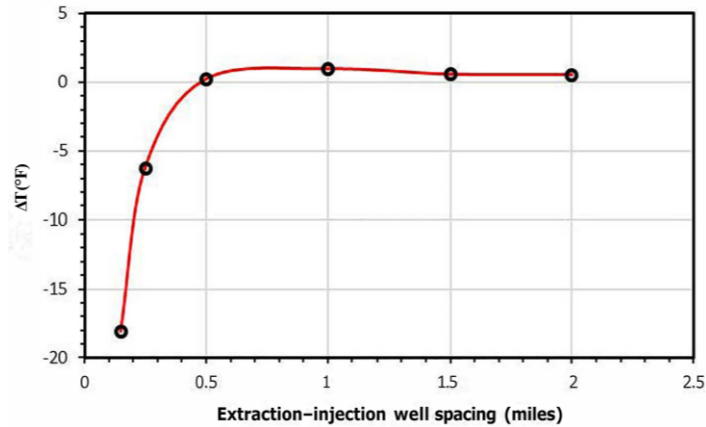


Figure 9. Temperature change (after 50 years) at the mid-perforation of the extraction vs. well spacing between the injection and extraction wells. The temperature change at the extraction well is within 0.6°C (1°F) when well spacing is ≥ 0.8 km (≥ 0.5 miles).

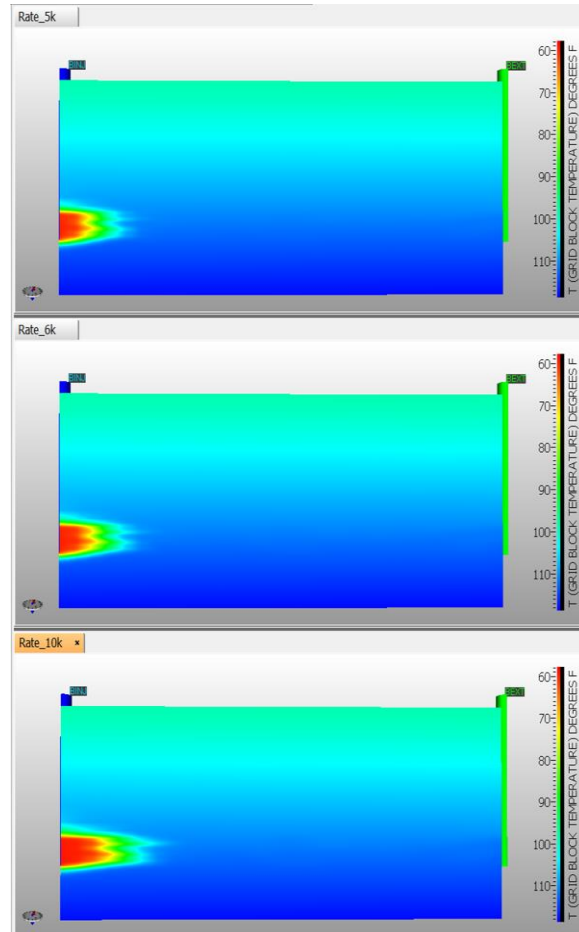


Figure 10. Impacts of varying rate of extraction and injection on temperature distribution after 50 years. The warm colors (red to yellow) represent lower temperatures (near injection well), and cooler colors (green and blue) represent higher temperatures. Overall, the C-T front moves further from the injection well as extraction rate increases (upper = $795\text{ m}^3/\text{d}$ [$5,000\text{ bbl}/\text{d}$], middle = $954\text{ m}^3/\text{d}$ [$6,000\text{ bbl}/\text{d}$], and lower = $1,590\text{ m}^3/\text{d}$ [$10,000\text{ bbl}/\text{d}$]). X-scale: 2.4 km (1.5 miles) and Y-scale: 552 m (1,810 ft).

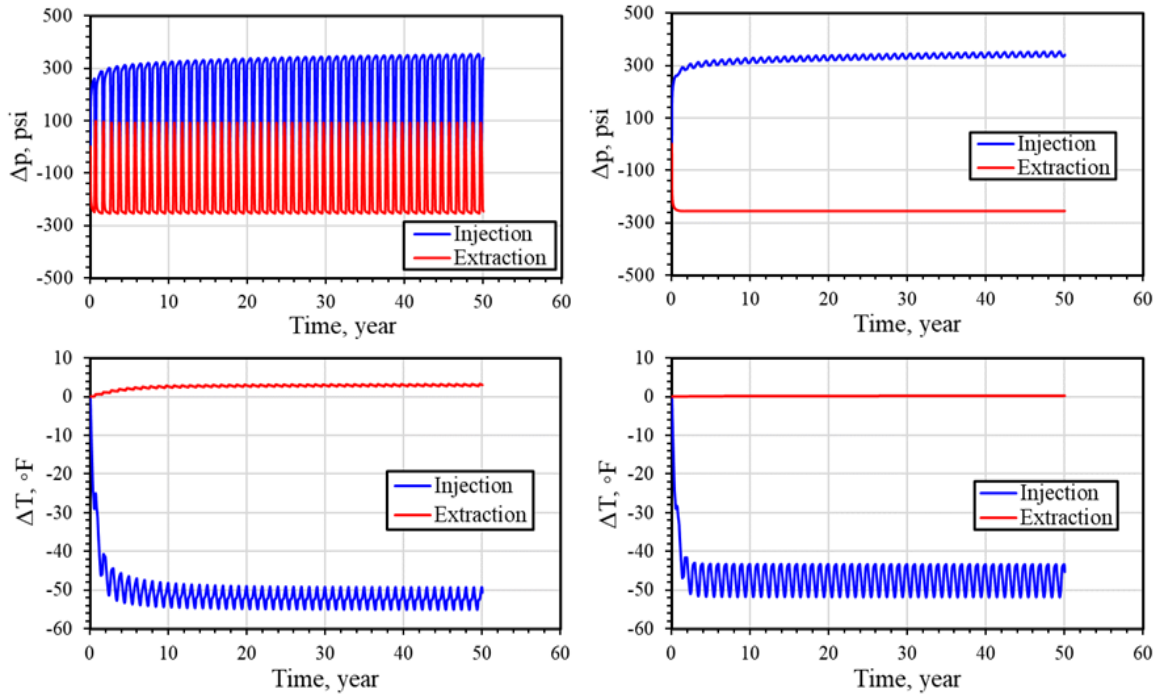


Figure 11. Effect of seasonal changes in temperature for “Heating Only” and “Heating and Cooling” scenarios over 50 years. Temperature changes at the extraction well are relatively small. Pressure changes at the extraction and injection wells are relatively large ($\sim 2,068$ kPa or ~ 300 psi), and cyclical for the “Heating and Cooling” scenario due to reversing the flow direction in the summer season (i.e., wells switched from extraction to injection and vice versa).

2.2.2 Wellbore Modeling

Average reservoir and thermophysical properties of the MSS and overlying geologic formations were used to perform wellbore simulations to assess the sensitivity of heat transfer (temperature changes) to geothermal fluid temperature and flow rate in the vertical extraction and injection wells. Temperature changes from the surface to the bottom of the LMSS were estimated based on the thermal conductivity of the geologic formations belowground surrounding the wellbore (Table 2). To estimate temperature change in the extraction well, a range of formation temperatures were used in conjunction with varying thermal conductivity values. This allowed the delivered geothermal fluid temperature (to the DDU GES) to be estimated as a function of volumetric flow rate. To estimate temperature changes in the injection well, a range of surface temperatures were evaluated, which were based on temperatures immediately downstream from the surface facility (outflow). Temperature changes between the surface and subsurface resulting from heat gained from geologic formations above the MSS determined the temperature of delivered geothermal fluid into the LMSS. The modeling results determined the spacing between the extraction and injection wells so that the extraction well could extract geothermal fluid at the initial MSS temperature.

The numerical radial wellbore model for the ARFs includes 16 different geologic formations (Figure 12). The model dimensions around the extraction wellbore are 1,883.6 m (6,180 ft) high and 50.3 m (165 ft) in diameter. Vertically, the wellbore model includes the geologic formations

from the ground surface down to the Argenta Formation. A large finite element mesh was used to minimize boundary effects (i.e., the effect of system operations on boundary temperature remained constant) in simulations. COMSOL® Multiphysics software (v. 5.3) was used to perform wellbore simulations.

Wellbore modeling and sensitivity analyses were performed to evaluate temperature losses due to: (1) extraction from the LMSS, (2) changes in the rate of extraction, and (3) alternative materials for wellbore insulation (Tables 7 and 8). Following sensitivity analyses, additional analyses were run that varied (1) extraction and injection rates, (2) fluid injection temperatures (Table 9), and (3) casing dimensions to examine the effects of these input parameters on extraction and injection temperatures. In addition, wellbore modeling was performed to determine the time required for fluid flow in the DDU GES to reach hydrostatic equilibrium and to determine how changes in the Reynolds number (R_e) (i.e., transition from laminar to turbulent flow) impacts heat transfer.

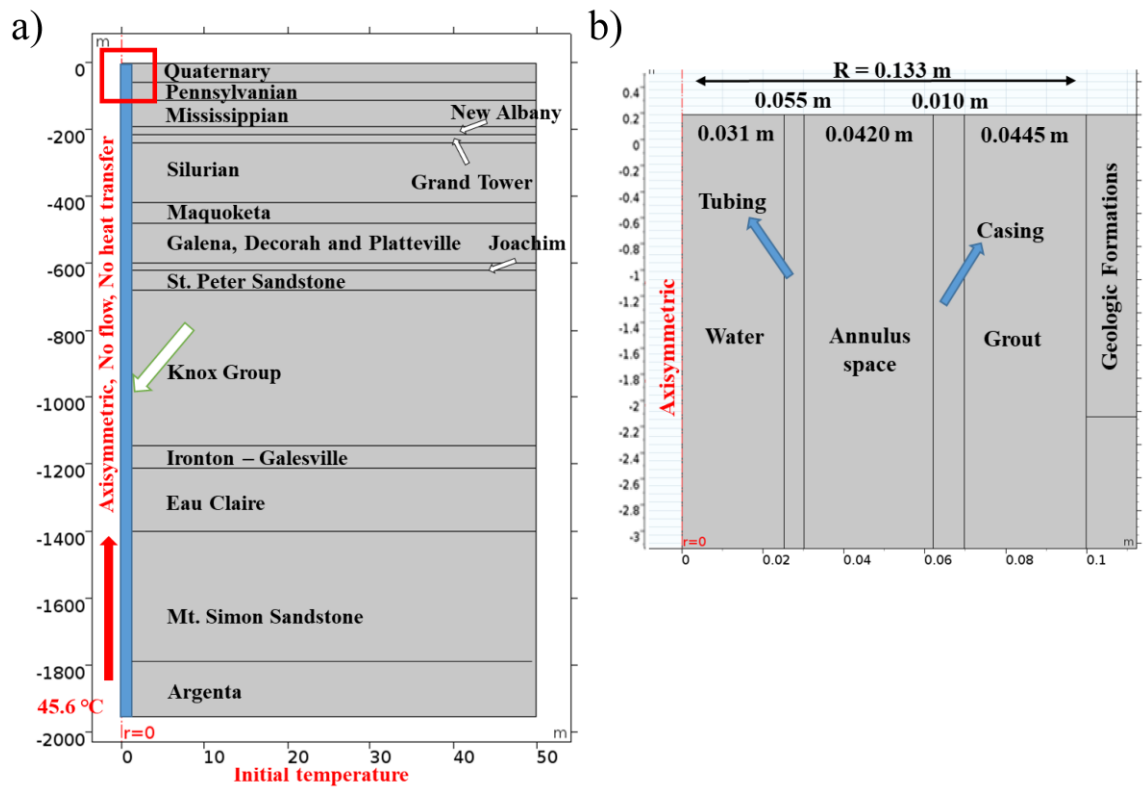


Figure 12. Wellbore modeling geometry and boundary conditions for (a) axisymmetric wellbore model and (b) wellbore components.

Table 7. Material Properties of Wellbore Components

Thermophysical Properties	Tubing and Casing	Grout	Annulus Fluid
	Carbon Steel (API N80 grade)	Type I Portland Cement (ASTM C150)	Potassium Formate (weight concentration =75%)
Thermal Conductivity (W/m·K)	55	0.80	0.38
Density (kg/m ³)	7850	1498 (surface to 1829 m [6000 ft]) 1893 (1829 m [6000 ft] to bottom)	1522
Specific Heat Capacity (J/kg·K)	510	2000	1380

Table 8. Thermal Conductivities of Different Insulation Scenarios and Wellbore Parameters

Insulation Scenario	Grout	Annulus Fluid	Carbon Steel Tubing OD = 0.073 m Casing: OD= 0.178 m (W/m · K)
	Type I Portland Cement (ASTM C150) (W/m · K)	Potassium Formate B – wt. % = 75) (W/m · K)	
Baseline (No insulation)	0.80 (Allen and Philippacopoulos, 1999)	0.38 (CABOT, 2019)	55 (National Physical Laboratory, 2017)
Extraction Well (Silicate foam around tubing)	0.80	0.104 (Penberthy and Bayless, 1974)	55
Insulated Tubing (2-layer tubing vacuum sealed)	0.80	0.38	0.06 (Sliwa and Kruszewski, 2017)

Table 9. Seasonal Surface Injection Temperatures

	Winter	Spring	Summer	Fall
Temperature (°F)	50	70	90	70
Time period (months)	5	2	2	3

Numerical Analysis Results

Extraction Well Results

Wellbore modeling results for extraction rate, wellbore insulation, and heat capacity sensitivity simulations are presented in Figures 13 and 14. The wellbore modeling predicted an increased

temperature change along the wellbore as a consequence of lower extraction rates. This increase in temperature change is most likely because lower extraction rates provide more time for heat transfer (via conduction) between the wellbore and surrounding geologic formations, since the extracted geothermal fluid spends more time in the wellbore. Overall, modeling results suggest that temperature change along the wellbore can be reduced to $<0.6^{\circ}\text{C}$ ($<1^{\circ}\text{F}$) by insulating the wellbore or increasing the extraction rate.

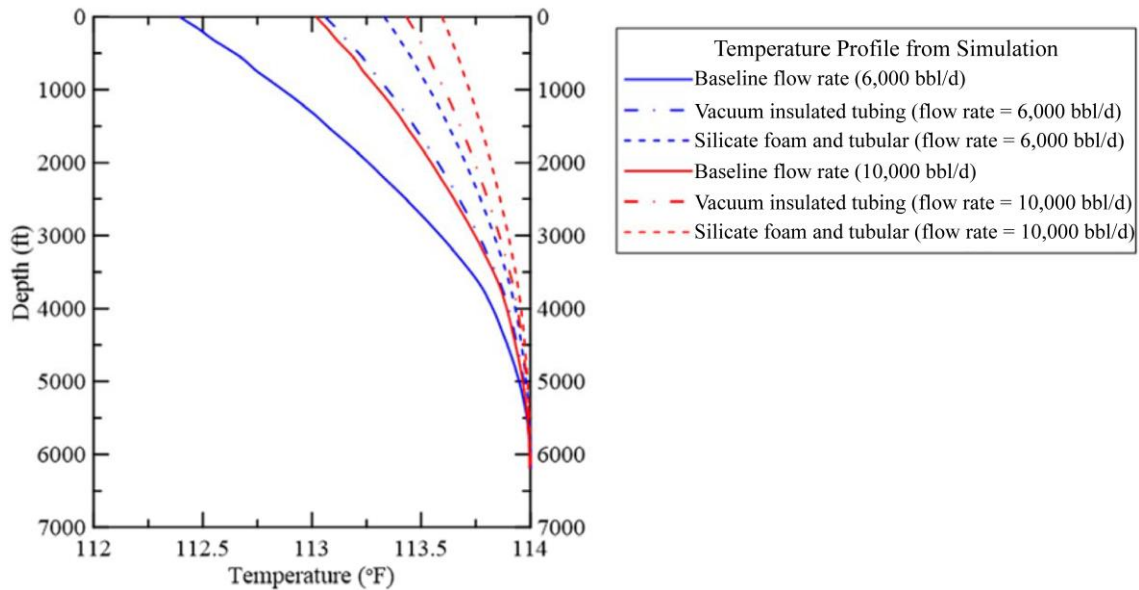


Figure 13. Temperature profiles along the center line of extraction well for different flow rates and wellbore insulation techniques.

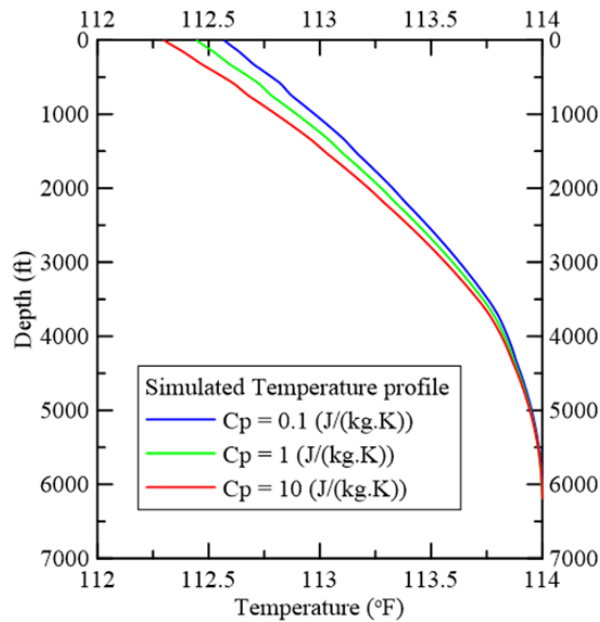


Figure 14. Temperature profiles along the center line of extraction well for different formation heat capacities.

Silicate foam and vacuum-insulated tubing were both simulated, and the results indicated that silicate foam placed around the tubing would be a better insulator. However, the difference in temperature change between the two insulation methods was not significant (i.e., less than 0.3°C [0.5°F]), and therefore either method could be used to insulate the wellbore. Lastly, the temperature change in the wellbore was not significantly and not impacted by variations in heat capacity of the adjacent formations, especially at higher formation temperatures (greater depths) (Figure 14).

Injection Well Results

The wellbore modeling results are presented in Figures 15 and 16 for different wellbore tubing radii and varying geothermal fluid injection rates. At a constant injection rate, the change in tubing radius correlates positively with temperature change (i.e., temperature change increased with increasing tubing size). The temperature change increased with increasing tubing radius because the surface area of contact for heat transfer between geothermal fluid, wellbore, and surrounding geologic formations increases with tubing radius. However, the temperature change for the three tubing sizes simulated were essentially the same in the injection well (Figure 15).

The temperature change at the bottom of the injection wellbore increased with decreasing flow rate (Figure 16). The decrease in temperature at shallower depths during low injection rates is most likely because formation temperatures are less than the temperature of injected geothermal fluid, therefore causing heat from the geothermal fluid to be lost by conduction and convection (Figure 16). Nonetheless, the geothermal fluid gained more heat at lower rates and greater depths as formation temperature became higher than the temperature of the injected geothermal fluid.

2.3 Surface Infrastructure Modeling

To design the DDU GES infrastructure, design parameters and infrastructure components necessary to meet ARFs' heating demand were assessed. This work included determining the well design (i.e., wellbore size, casing and cement, and tubing), geothermal fluid handling procedures required for the surface infrastructure (i.e., surface pumps, chemical additives, corrosion inhibitors, and temporary fluid storage), and its heating system (i.e., heat pumps, heat exchangers, supplementary heat sources). Two DDU GES configurations (Case 1 and Case 2) were developed, and the designs were modeled and assessed based on their capacity to deliver thermal energy (ability to meet ARFs' heating demand). Additionally, capital expenditures and the costs of regular and periodic operation and maintenance (O&M) were assessed for each case.

2.3.1 Energy End-Users

Heating loads were assessed for six ARFs, which included three existing facilities – (1) the Energy Farm, (2) Poultry Farm, and (3) Beef & Sheep Research Field Laboratory – and three planned facilities – (1) the Feed Technology Center, (2) Imported Swine Research Laboratory (ISRL), and (3) Dairy Cattle Research Unit (known widely as the Dairy Farm). The Feed Technology Center is currently under construction and relocation of the ISRL and Dairy Farm is planned within the next 5–10 years. The ARFs support student teaching, basic and applied research, and agriculture production. A map of the existing and planned ARFs is shown in Figure 17. The descriptions of the ARFs are provided below, and were uploaded to the GDR [University of Illinois, 2019a].

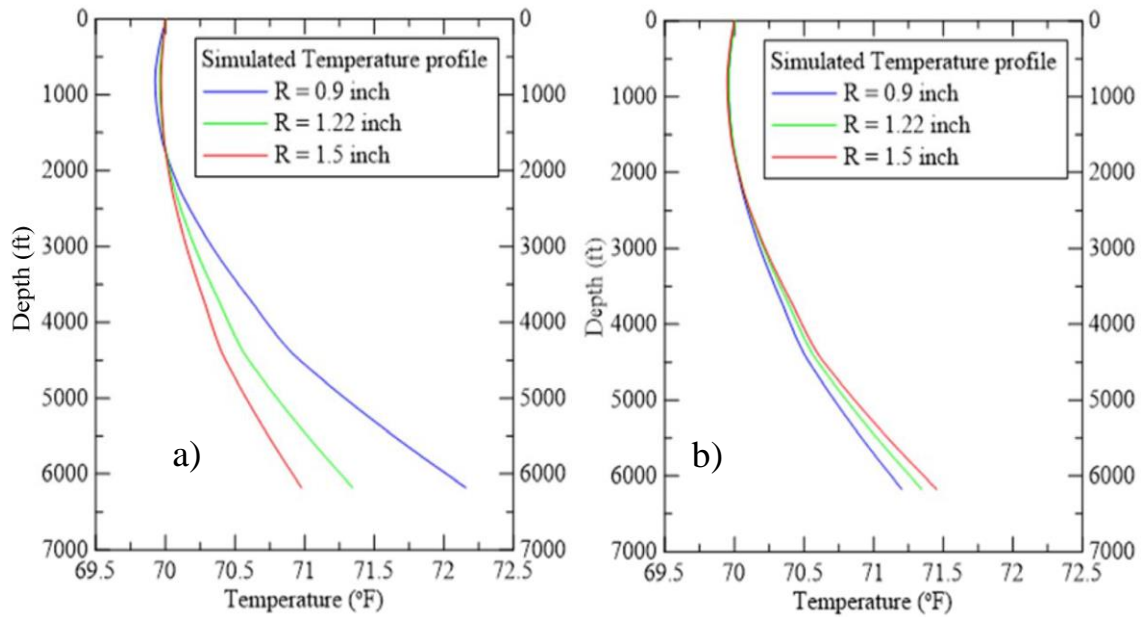


Figure 15. Temperature profiles along the center line of the extraction wellbore for different tubing radius, (a) in the extraction wellbore and (b) in the injection wellbore.

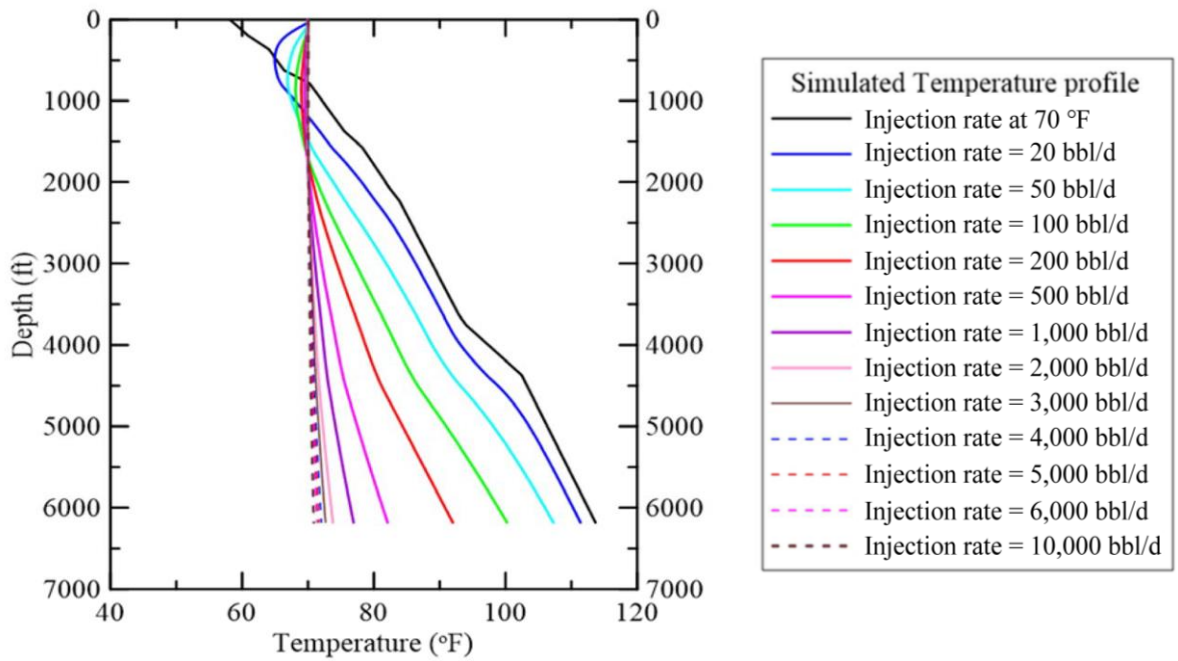


Figure 16. Temperature profiles for different flow rates in the injection wellbore. The initial injection temperature (T_{inj}) was 21°C (70°F).

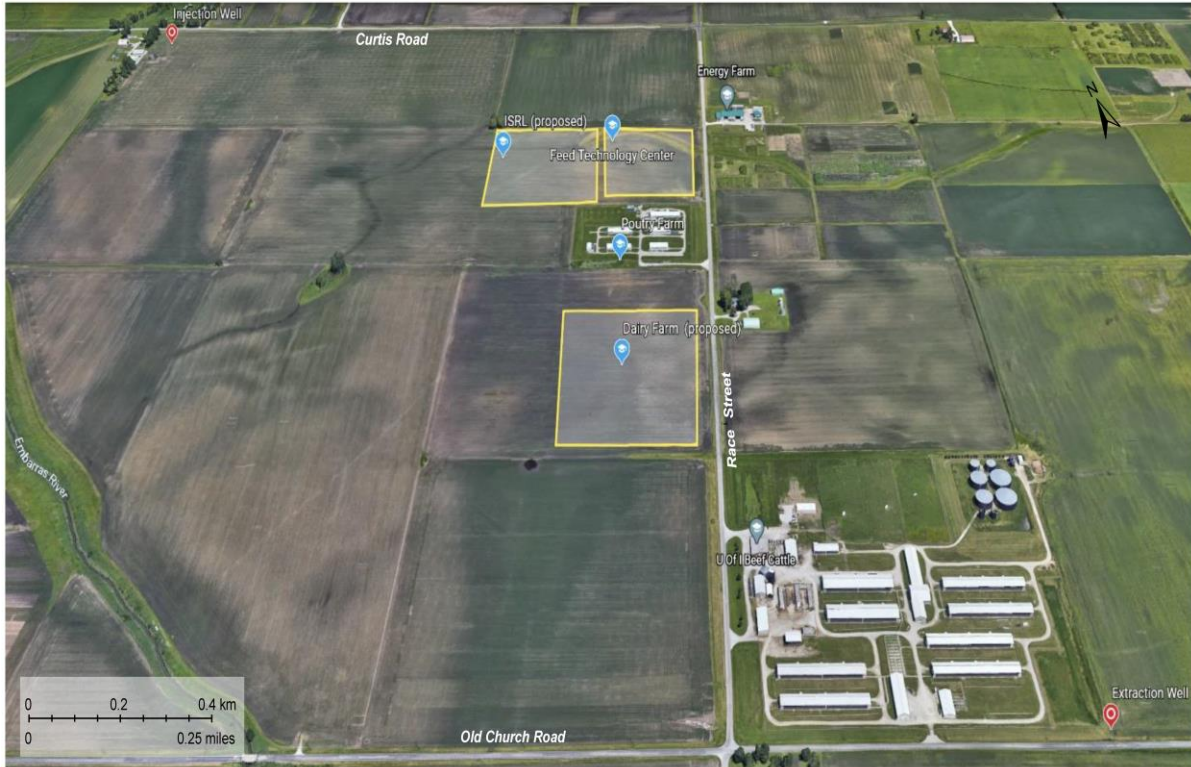


Figure 17. Existing and planned ARFs along the southern part of the ACES Legacy Corridor. Red circles denote existing ARFs and yellow boxes denote ARFs currently under construction or planned for relocation.

General descriptions of these ARFs are as follows:

- **The Energy Farm** occupies 130 ha (320 acres) and includes research plots established as “living laboratories”. The Energy Farm largely supports the research and production of biofuel crops. The Energy Farm has a 1,115 m² (12,000 ft²) facility that includes office space, sample processing laboratories, and equipment storage. The farm also maintains several facilities tailored to grow and work with tall-growing biofuel crops, including a 195 m² (2,100 ft²) crop breeding greenhouse with 6-m-high (20 ft) ceilings and two growth chambers for crops that require day-length control to initiate flowering. These facilities require thermal energy for space heating to promote crop growth. To heat the crop breeding greenhouse, the farm installed a 198 kW (675,000 Btu/hr) state-of-the-art Heizomat biomass heat facility that combusts 60 tons of biomass per year.
- **The Beef & Sheep Research Field Laboratory** is a state-of-the-art bovine facility covering 4 ha (10 acres) used for livestock research operations. The primary research at this ARF is to run experiments to test applied nutrition techniques for raising feedlot and breeding cattle. Eight cattle barns and one sheep barn have the capacity to house 1,000 beef cattle and 100 sheep on slotted floors. Outside of calving season, the cow herd grazes on 73 ha (180 acres) of mixed grass pasture located northwest of the ARF. The metabolism barn has 12 cattle stalls. The metabolism barn and the office building require heating and air conditioning year-round. In addition, heating is needed in two working barns for cattle handling. Furthermore, the large cattle and sheep barns are heated when the ambient

temperature is at or below -3.9°C (25°F).

- The **Poultry Research Farm** researches poultry nutrition, gut health, production and environmental management, immunology, and ovarian cancer. The farm has six pole barns providing $\sim 2,322\text{ m}^2$ ($25,000\text{ ft}^2$) of space for a breeding birds, growing birds, cage laying, hatchery/brooder, and laboratory space for more specialized, intensive research. About 12,000 chickens are currently being raised at the farm. Most of the ARF's space is maintained at a temperature of $\sim 24^{\circ}\text{C}$ ($\sim 75^{\circ}\text{F}$), while the remaining space, depending on its function(s), requires different heating demands. More specifically, the feed mixing room is maintained at $\sim 21^{\circ}\text{C}$ (70°F), while the battery cages for chicks are kept at 32°C (90°F), primarily by using electric heaters. The walk-in egg incubators heat a 3-week hatchery to 37.5°C (99.5°F). The facility for growing birds operates from April to September and is maintained at 32°C (90°F).
- The **ISRL** where swine research is undertaken is a process-based facility with breeding, gestation, farrowing, nursing, growing, and finishing rooms with a capacity to house 120 sows. Current research focuses on the biomedical applications where pigs are used to model human health and medical care. Most of the ISRL is kept at $23^{\circ}\text{--}24^{\circ}\text{C}$ ($73^{\circ}\text{--}75^{\circ}\text{F}$). However, the nursing area is kept warmer, 32°C (90°F) for the first week of breeding, and then the temperature is decreased by $0.28^{\circ}\text{C}/\text{day}$ ($0.5^{\circ}\text{F}/\text{day}$) down to 24°C (75°F). NG-fired heaters are used to heat the ARF in the winter, and is cooled with air-water evaporative cooling cells in the summer. NG-fired heaters are used to heat the ARF in the winter and it is cooled with air-water evaporative cooling cells in the summer.
- The **Dairy Farm** is located south of the campus center and provides healthy animals an infrastructure required by researchers to conduct studies on genetics, nutrition, physiology, immunology, and management. The farm is considered a confinement facility; however, developing heifers have access to dirt exercise lots. There are ~ 180 mature, lactating cows and 150 replacement heifers. The cows are milked in a double 12 parallel parlor, which is the major energy user and is equipped with an NG-fired heater and a supplementary NG boiler for supplying $1.51\text{ m}^3/\text{d}$ (400 gallons/d) of hot water at 77°C (170°F). The hot water is delivered to a hydronic space heating system (operated only in the winter) and washing and sterilizing system used daily, year-round. The milking parlor is equipped with two refrigeration units to maintain the milk tanks at 3.3°C (38°F), and provide indoor cooling for cows and staffers in the summer. Cool clean water is used in a plate and frame cooler to lower the temperature of hot milk from 39°C to 16°C (102°F to 60°F). Except for the calf barns where NG-fired heaters are operated, the other barns require no heat. High-milk-yielding cows held in close proximity generate enough heat to maintain the room temperature at 5°C (40°F). The barns housing cows in the summer are cooled with a tunnel ventilation system.
- The **Feed Mill**, which, when relocated in by the end of 2020, will be known as the **Feed Technology Center**, produces custom livestock and poultry feed for essential campus

animal research and production applications. The operation produces 3,175 tonnes (7,000,000 lbs) of dry product, manufactured in small quantities. A pellet mill uses steam from a NG-fired water-tube boiler to maintain a pressure of 138 kPa (20 psi) for grain pelletizing. An outdoor grain dryer with a heating capacity of 4 MMBtu/hr circulates hot air at 60°C (140°F). The new facility will include a high-throughput storage, processing, mixing, extruding, bagging, and delivery system that will have an expanded capability to deliver ~7,257 tonnes (16 million lbs) of specialized, small-batch products.

2.3.2 Well Design and Geothermal Fluid Handling

Through geothermal reservoir modeling, wellbore modeling, and ARF heating load analysis, it was determined that the doublet well system would be constructed in the LMSS (Figure 2 and Appendix C1). The well designs were based on typical oilfield installations and CO₂ storage wells (e.g., Malkewicz et al., 2015). The extraction and injection wells were designed to circulate geothermal fluid at the required flow rate: ~954 m³/d (~6,000 bbl/d).

Wellbore and tubular sizing (i.e., casing and tubing), casing metallurgy, and wellbore insulation materials were determined, and strongly influenced subsurface temperature changes from reservoir pressure and thermal gradients, flow rate (extraction and injection), and fluid composition.

Geothermal fluid handling procedures were developed to safely and efficiently extract, circulate, and inject the geothermal fluid. Data on geothermal fluid composition (including TDS, main elemental constituents, salinity, and total suspended solids [TSS]) was reviewed to characterize MSS geothermal fluid and predict the possibility of scaling, fouling, corrosion, and blockage (the references to the data were uploaded to the GDR [University of Illinois, 2018d]). This was done to evaluate the compatibility of the geothermal fluid with GES infrastructure and was crucial to identify which chemical additives (e.g., corrosion inhibitors) will be needed to prevent such possibilities (cf. Kaplan et al., 2017). The infrastructure components requiring corrosion protection (i.e., heat exchangers, piping, surge tank, and heat pumps) were identified. A low-cost fluid treatment plan using scale inhibitor was assessed.

Determining geothermal fluid handling procedures also entailed identifying a piping system that would minimize heat loss as geothermal fluid is transported from the extraction well to the ARFs. Heat transfer modeling estimated temperature change along the pipeline using a spreadsheet calculation tool. Three piping systems were modeled: (1) an insulated, aboveground pipe, (2) a buried, insulated pipe, and (3) a buried, uninsulated pipe. Heat loss and temperature change per unit length of pipe were estimated for a range of subsurface conditions. The modeling for buried, pipe showed minimal temperature changes in terms of heat loss that informed the well design.

Equipment was identified to circulate geothermal fluid through the GES, while at the same time maintain the injection wellhead pressure. Equipment to circulate geothermal fluid through the GES that, while at the same time, maintains the injection wellhead pressure was identified. This work considered the type and size of a downhole submersible pump and tubulars in the extraction well. An electric submersible pump (ESP) was selected for the extraction well and was sized to

accommodate the 954 m³/d (6,000 bbl/d) flow rate. The surface pump chosen for the injection well met the required flow rate, power requirements, and pressure differentials.

2.3.3 End-User Heating Demand

Estimating ARFs' heating and cooling demands, conducting end-use load analysis, and assessing the capacity of the DDU GES required the retrieval and review of historical fuel consumption data from three past fiscal years (FY), FY2015 to FY2017; information that is held in the U of IL Energy Billing System (EBS) (University of Illinois, 2019b). The Energy Farm uses liquified propane gas (LPG) for space heating and hot water. The ISRL uses NG and LPG for heating. All other ARFs use NG as their sole heating source. Both Table 10 and Figure 18 provide a summary of the monthly consumption of NG and LPG for each ARF.

Table 10. Average Fuel Consumption at the ARF between FY2015 and FY2017

Fuel Consumption (MMBtu)	Energy Farm (LPG)	Beef & Sheep Rs. Field Lab (NG)	Poultry Farm (NG)	ISRL (NG and LPG)	Dairy Farm (NG)	Feed Mill (NG)	Total
July	2.76	4.07	17.42	28.10	19.67	65.33	137.35
Aug	0.75	4.04	22.98	23.23	18.87	84.33	154.20
Sept	17.53	4.05	20.38	91.13	19.33	73.60	226.03
Oct	94.54	13.50	19.27	144.68	32.67	68.83	373.50
Nov	240.65	73.16	83.02	364.00	109.67	122.10	992.59
Dec	349.56	128.40	156.28	679.44	202.43	181.63	1,697.75
Jan	402.57	158.35	118.73	746.07	187.63	162.63	1,775.99
Feb	340.08	391.48	115.56	638.94	152.77	125.63	1,764.45
March	253.56	306.67	96.52	614.09	110.83	159.37	1,541.03
April	111.65	96.03	88.52	282.87	60.83	152.03	791.92
May	48.75	20.06	58.44	195.59	34.73	77.80	435.38
June	2.01	5.60	20.77	37.31	23.77	47.20	136.65
Yearly total	1,864.39	1,205.40	817.90	3,845.44	973.20	1,320.50	10,026.84
Fuel consumption during the non-heating season, June to September (4 months).							
Monthly Average	5.76	4.44	20.39	44.94	20.41	67.62	163.56
Hourly Average (per hour)	0.01	0.01	0.03	0.06	0.03	0.09	0.22
Fuel consumption during the heating season, October to May (8 months).							
Monthly Average	230.17	148.45	92.04	458.21	111.45	131.25	1,171.58
Hourly Average (per hour)	0.32	0.20	0.13	0.63	0.15	0.18	1.60

The monthly data was averaged over the three-year period, FY2015 to FY2017. The ISRL was the ARF requiring the most thermal energy, consuming ~38% of the total energy used by the ARFs.

The Poultry Farm and Dairy Farm used the least amount of energy, consuming <10% of total energy used. These ARFs required less energy because the heated area at the Poultry Farm is smaller and the relatively lower heating demand (i.e., lower temperatures) required at the Dairy Farm. NG or LPG consumption, mainly for space heating, is highly correlative with the seasonal ambient temperature. At each ARF, the highest NG and LPG consumption is during the period October to May, with peak heating between December and March. (Detailed climate data with high sampling frequency were archived in the characterization database and uploaded to the GDR [Lin, 2018]).

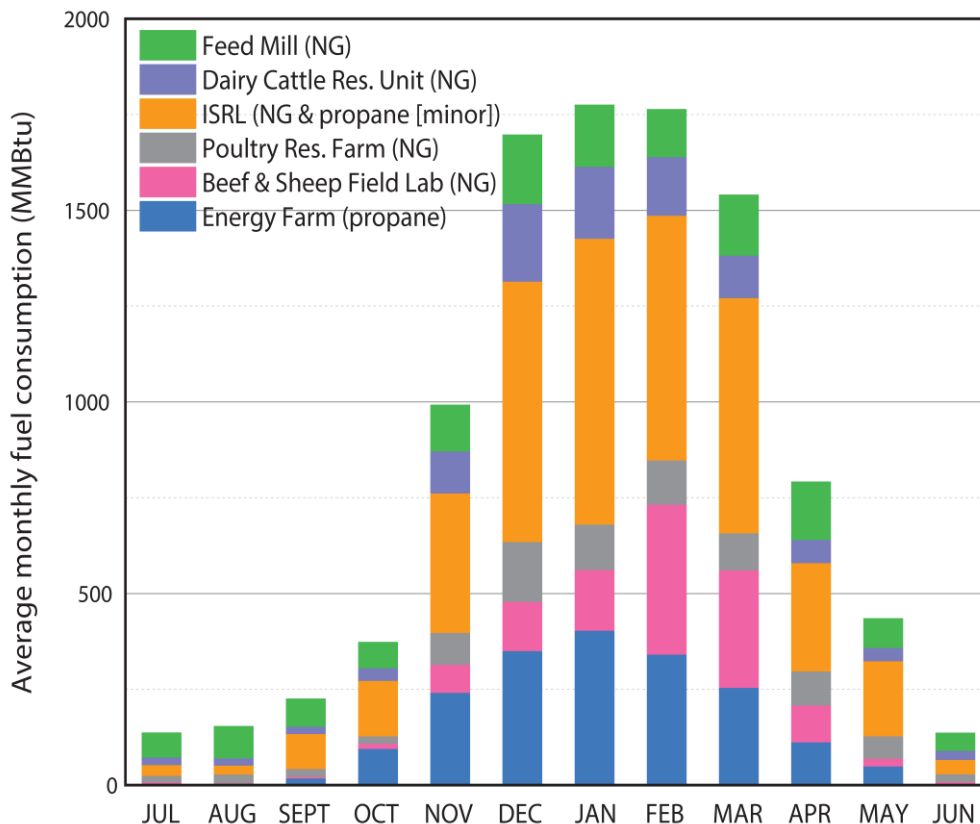


Figure 18. Average monthly fuel consumption at the ARF (based on FY2015 through FY2017).

2.3.4 GES Assessment

The GES Assessment used process simulation modeling to estimate the heat and material balance and energy efficiency of the DDU GES in Case 1 and Case 2. Case 1 was simulated to understand the capacity of a standalone DDU GES: Case 1 only supplied the 2 MMBtu/hr baseload (~80% of total annual heating demand) and did not use any supplemental heat sources to cover peak load demand. Case 2 also supplied the 2 MMBtu/hr baseload *but* included an electrical heat pump and used the existing, NG-fired heaters at the ARFs to provide supplemental energy to cover peak load demand (<2 MMBtu/hr). Together, the electrical heat pump and NG-fired heaters supplied the remaining 20% of total annual heating demand.

The GES Assessment used fluid flow simulations of the “virtual” piping (and trenching) network (developed from GIS, design blueprints, and other building-level information) linking the extraction well, ARFs, and injection well to size the main pipeline and the branch pipelines, determine trenching requirements, and estimate construction costs for installing the pipelines and trenches (See Section 3.4.2.2). The simulations of the piping network included the (1) distance between the two wells, (2) location of existing utilities, and (3) topography at the ground surface.

The results of the GES Assessment demonstrated its energy efficiency, and returned data that was used to size and estimate the cost of major surface facility equipment (i.e., heat exchanger, heat pump, surface pump, surge tank; these costs constituted the capital expenditures for the surface facility equipment. In addition, annual O&M costs were estimated, which accounted for the amount and cost of the electricity needed to run the entire DDU GES, the cost of supplemental heating, chemical treatment, and ongoing, required maintenance (Section 3.4.3).

A potential cascading application using spent geothermal fluids to preheat domestic water was incorporated into the GES system (Section 3.4). A sensitivity analysis assessed the cost of heat versus heating demand to assess the effect of the GES scale (Section 3.4.3).

2.4 Analyses of Life Cycle Cost and Levelized Cost of Heat

Techno-economic analyses were conducted for Case 1 and Case 2 by evaluating the technological feasibility and project economics of each case. Economic criteria (i.e., LCOH, NPV, ROI, SIR) and project risk (i.e., of deployment and implementation) were included in the techno-economic analyses. The *Geothermal Resource Assessment* and the ARF energy demand assessment were integrated to estimate the lifecycle costs and benefits of the DDU GES. Following the GES Assessment, a direct implementation plan was determined and potential challenges to commercializing the DDU technology were identified. A market transformation plan was developed to expand the use of the DDU technology outside of the ILB to other sedimentary basins with similar end-user demand. (See Appendix C6).

2.4.1 Cost Estimates, Project Economics, Techno-Economics, and LCA Spreadsheet Tool Development

Cost Estimates and Project Economics

Costs were estimated for Case 1 and Case 2, including the price of goods and installation labor. Capital and O&M costs were calculated based on information from local vendors that were validated against similar projects that ISGS staff have previously managed and participated in. Project economics were evaluated through Life Cycle Cost Analysis (LCCA) using economic metrics (i.e., LCOH, NPV, ROI, SIR) to compare the economic feasibility of each case. The LCCA tool evaluated project economics by quantifying cash flows (positive or negative) from constructing, operating, and maintaining the DDU GES, as well as any other costs or revenues that may be incurred or realized. Cash flows over time were converted to present dollar values (i.e., NPV) to compare Case 1 and Case 2.

LCOH is an economic parameter used to compare energy systems that produce heat as the primary output. LCOH was computed using discounted cash flows and dividing the discounted costs by the discounted heat (energy) produced over the lifetime of the DDU GES. (Units of LCOH are \$/MMBtu or \$/MWh.)

The criteria for the selection of LCCA and LCOH tools used for this project were as follows: existing, recommended, and freely available. The tools reviewed were Cornell’s GEOPHIRES and the National Institute of Standards and Technology’s (NIST) Building Life Cycle Cost (BLCC) Programs. GEOPHIRES and BLCC were found equally capable to meet the needs of this project.

Environmental Life Cycle Assessment (LCA)

The environmental impacts and benefits of the DDU GES were determined using a Life Cycle Analysis (LCA) tool. LCA measures the potential environmental impacts of products or processes over their life cycle, from “cradle” (where the raw materials are sourced) to “grave” (end of economic life). For this project, an LCA spreadsheet tool analyzed the environmental impacts and/or benefits of the proposed DDU GES, including raw material extraction, materials processing, manufacture, distribution, use, disposal, and recycling. The LCA comprises four life cycle stages of proposed DDU GES (Figure 19).

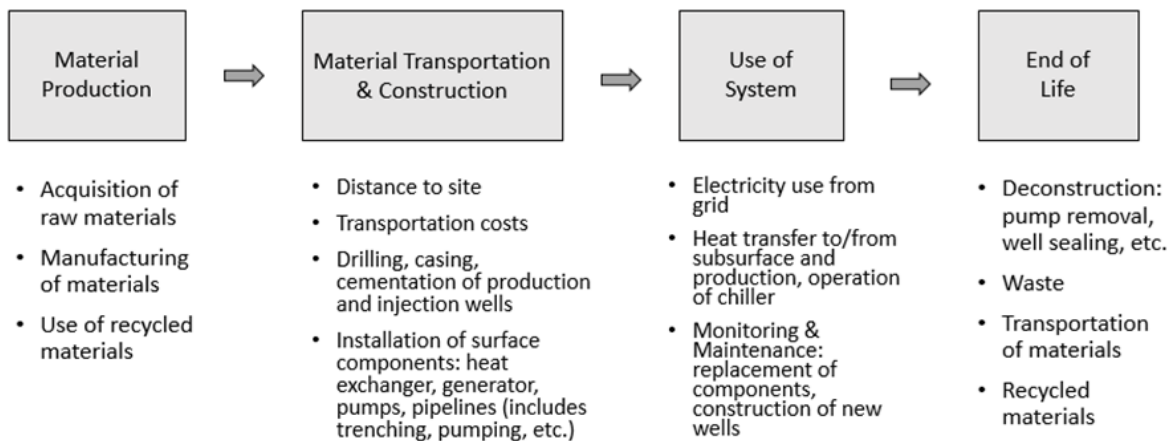


Figure 19. Schematic diagram summarizing the four stages of the LCA.

Energy consumption data for the ARFs, informed by the end-user energy demand assessment (Section 2.3.4), was used to inform the LCA (Table 11). Additionally, the infrastructure components of the proposed extraction and injection well designs were investigated in detail, as material acquisition and well installation are shown to constitute a significant portion of the environmental impacts of a DDU GES (Thomas et al., 2020). An inventory flow diagram illustrating the scope of the LCA is shown in Figure 20. Using the flow diagram, the impacts of individual DDU GES components were inventoried using SimaPro® (v 8.5.2).

Table 11. Energy Consumption at the ARFs

Fuel Consumption (MMBtu)	Energy Farm (LPG)	Beef and Sheep Res. Field Lab (NG)	Poultry Farm (NG)	ISRL (NG, LPG)	Dairy Farm (NG)	Feed Mill (NG)	Total
Total Annual Heating	2,140	1,006	791	3,348	1,009	1,158	9,452
Average Hourly Heating (per hour)	0.24	0.11	0.09	0.38	0.12	0.13	1.07
Total Winter Season Heating	1,852	959	648	2,995	929	929	8,312
Winter Season Heating (per hour)	0.42	0.22	0.15	0.68	0.21	0.21	1.89
Maximum Monthly Heating	365	322	173	770	197	197	2,024
Average for Month of Max. Heating (per hour)	0.49	0.45	0.23	1.03	0.26	0.26	2.72

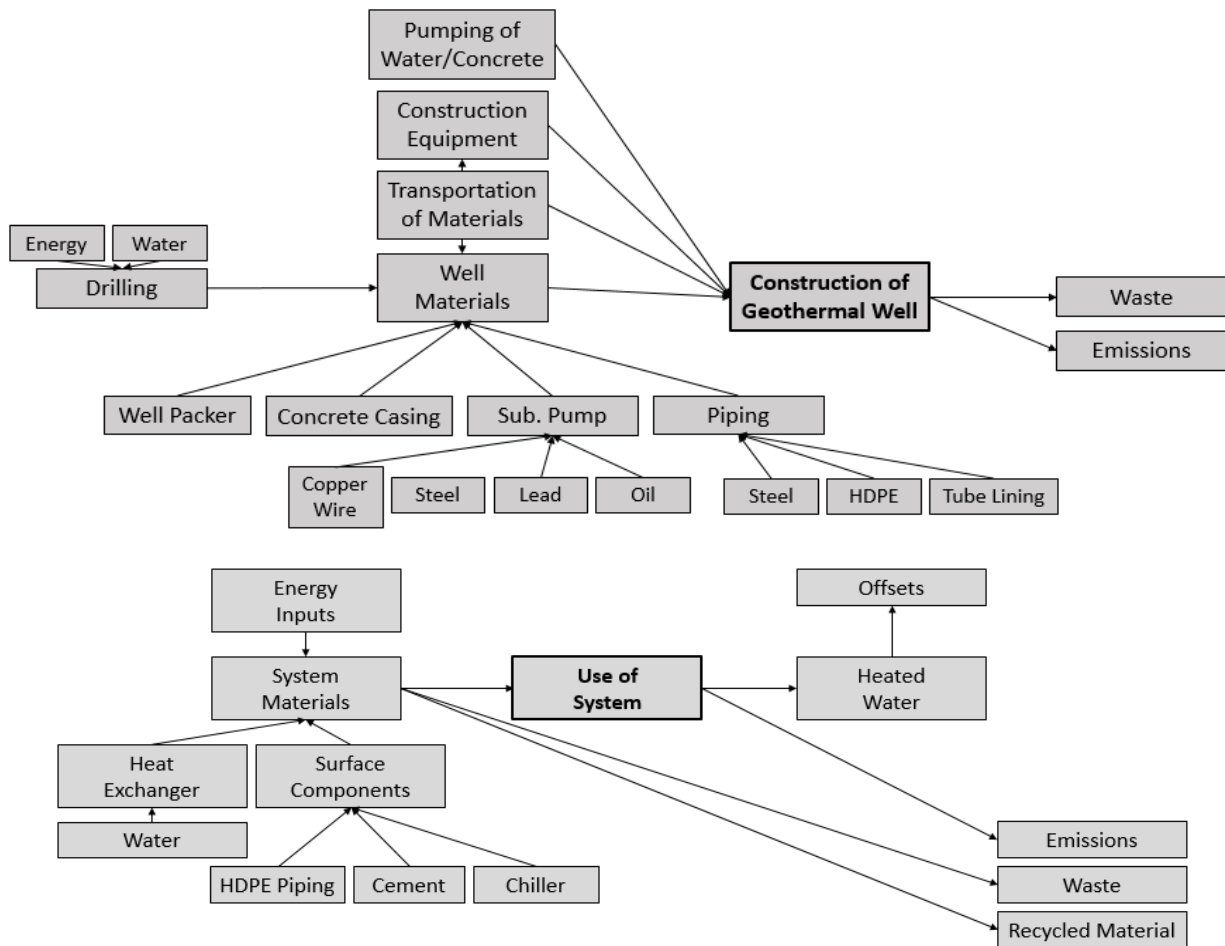


Figure 20. Flow diagram representing the scope of the LCA, including the components that comprise the well design and operation of the GES at the U of IL.

The five environmental impacts evaluated using the spreadsheet tool included: (1) ozone depletion, (2) global warming potential (GWP), (3) smog, (4) acidification, (5), eutrophication, and (6) fossil fuel depletion. Ozone depletion measures chlorofluorocarbons (CFCs) levels, which are ozone-depleting substances. High concentrations of CFCs lead to more harmful UV radiation reaching the ground surface, has negative human health risks, and poses threats to terrestrial and aquatic ecosystems (Solomon, 1999). GWP is a measure of atmospheric CO₂ levels, which absorbs sunlight and solar radiation, leading to elevated global temperatures (Eckaus, 1992). Smog is a measure of O₃ – reaction of NO_x and volatile organic compounds (VOCs) in the atmosphere – that has associated human health risks and poor air quality. Acidification relates to SO₂ concentrations, an acidifying compound with potential groundwater and surface water impacts that threaten soil and aquatic organisms. Eutrophication quantifies nitrogen levels; eutrophication causes dense plant growth and, consequently, animal death in aquatic bodies due to a lack of oxygen. This issue is particularly important in areas like Illinois that have significant agriculture markets because fertilizer collects in surface water runoff and deposits nitrogen in surrounding lakes, rivers, and streams. Finally, fossil fuel depletion is measured in terms of MJ surplus: the total, additional future cost to global society as a result of producing one unit of resource (cf. Ponsioen, 2013). These five impact categories provide guidance to DDU GES end-users and the U of IL as to the system’s environmental sustainability.

2.4.2 Market Demand and Transformation

The energy demand for the ARFs application has been detailed in Section 2.3.3. This section will focus on military applications. A market transformation plan was completed that included a target market, competitors, and distribution channels to identify challenges to commercialization. Estimates (including necessary assumptions) of the impact on end-user energy consumption for this project were made.

The majority of military installations are similar in size and function to small cities or large university campuses; however, unique differences may exist depending on the mission of the installation. A few examples follow:

- Installations with industrial operations, such as arsenals or depots, have higher energy demands related to the production-focused mission.
- Training installations generally have facilities that are spatially separated, requiring the usage and maintenance of large tracts of land for training and large, on-base residential complexes housing soldiers and their families.
- Some installations may have force projection missions that require a combination of these attributes (i.e., large tracts of land and on-base residential complexes), along with airfields or access to railways, in order to mobilize and transport equipment and personnel.

Since passage of the Energy Policy Act of 2005 (U.S. Congress, 2005), there have been multiple energy and sustainability objectives and requirements put forth by federal and military installations. The objectives, regulations, policies, and directives were instituted to address energy efficiency, renewable energy, net zero energy and water, fossil fuel energy reductions, energy security, and, most recently, energy resilience. (A number of citations referencing these programs

are included in Appendix A of the Army Energy Security & Sustainability (ES²) Strategy [U.S. Department of the Army, 2015]).

The U.S. Department of Defense (DoD) defines energy resilience as “[t]he ability to avoid, prepare for, minimize, adapt to, and recover from anticipated and unanticipated energy disruptions in order to ensure energy availability and reliability sufficient to provide for mission assurance and readiness, including task critical assets and other mission essential operations related to readiness, and to execute or rapidly reestablish mission essential requirements” (U.S. Congress, 2017, p. 1858). The US Army published its own policy related to resilience in Army Directive 2017-07: Installation Energy and Water Security Policy (U.S. Department of Defense, 2017). The policy establishing the requirement that the Army prioritize energy and water security to ensure the continuous availability of high-quality power and water resources to sustain critical missions for a minimum of 14 days. Consequently, a renewable energy source such as DDU GES (installed locally at each installation) would 1) improve energy security; 2) less susceptible to extreme weather or aboveground disruptions; and 3) increase resilience, all of which are attractive to the DoD and U.S. Army.

All the military installations (including fixed facilities and Illinois Army National Guard [ILARNG] units) within the ILB were assessed for DDU GES applications. A list was compiled for military installations (including fixed facilities and ILARNG units) in the ILB where the DDU GES may be applicable, and they are shown on the map in (Figure 21). To identify those military installations that could be compatible with DDU GES, the following criteria were used: (1) availability of land, (2) energy load requirement, and (3) availability of energy usage data. The ILARNG units were excluded from this analysis because of their limited land availability and lower energy consumption. It was recognized that constructing the extraction and injection wells would require more land area than currently available. However, additional land could be acquired to site the GES. Furthermore, there was limited access to energy use data at ILB ILARNG units. After applying these criteria, three ILB installations were identified for further study: Rock Island Arsenal (IL), Fort Campbell (KY), and Fort Knox (KY).

For security reasons, the installations in this analysis are referred to as Installation 1, Installation 2, and Installation 3 when energy and other site-specific data (not generally available to the public) are presented. Information about the sites and energy usage are shown in Table 12.

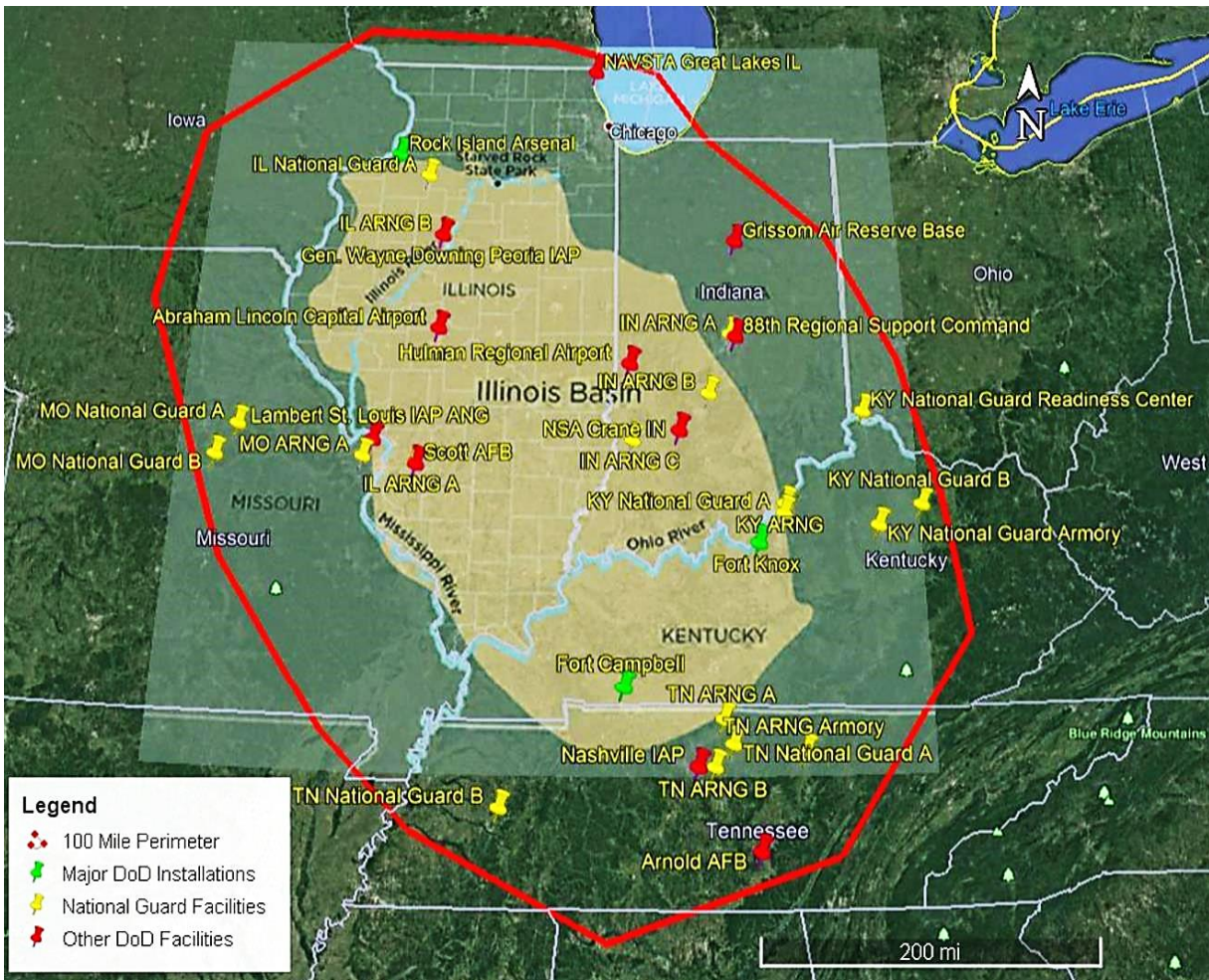


Figure 21. The location of military installations in the ILB evaluated in this feasibility study.

Table 12. Military Installation and Energy Characteristics

Installation 1	16,987,000 Gross Square Footage (Buildings)				
Commodity	Annual Amount	Annual (K\$)	Annual MMBtu	Unit Cost	Units
Electricity (MWh)	248,648	17,216		\$ 0.069	/kWh
Nat Gas (Kcf)	641,869	1,836	661,766.94	\$ 2.77	/MMBtu
Fuel Oil (K gallons)	48	104	6,594.35	\$ 15.77	/MMBtu
Propane (K gallons)	9	10	897.89	\$ 11.18	/MMBtu
Total Annual		\$ 19,166	668,361.29		
Installation 2	5,592,000 Gross Square Footage (Buildings)				
Commodity	Annual Amount	Annual (K\$)	Annual MMBtu	Unit Cost	Units
Electricity (MWh)	56,352	2,952		\$ 0.052	/kWh
Nat Gas (Kcf)	194,862	814	200,902.48	\$ 4.05	/MMBtu
Coal (short ton)	6,167	798	151,596.76	\$ 5.27	/MMBtu

Total Annual		\$ 4,564	352,499.24		
Installation 3	11,611,000 Gross Square Footage (Buildings)				
Commodity	Annual Amount	Annual (K\$)	Annual MMBtu	Unit Cost	Units
Electricity (MWh)	68,085	5,976		\$ 0.088	/kWh
Nat Gas (Kcf)	728,858	2,354	751,452.60	\$ 3.13	/MMBtu
Total Annual		\$ 8,330	751,452.60		

These military installations have required, annual heating loads of 668,361 MMBtu, 352,499 MMBtu, and 751,452 MMBtu, respectively. Andrews, Hammock and Powell, Incorporated (AH&P) estimate that an annual thermal load of ~1,624,242 therms, or 162,385 MMBtu, would need to be provided by the DDU GES located in the ILB in order to have a 10-year payback (Appendix C6). The heating load requirement for the ARFS is almost half of the annual heating load of the smallest military installation identified, and a little <25% of the annual heating load of the largest military installation in the ILB. The heating load requirement for the ARFs is almost half of the annual heating load of the smallest military installation identified, and a little <25% of the annual heating load of the largest military installation in the ILB. This size of the GES would benefit the military installations from energy security and, potentially, energy resilience standpoints. Any sustainability components of the GES would also facilitate other military goals and requirements to reduce dependence on fossil fuels and reduce GHG emissions.

Based on findings from the feasibility study, commercialization strategies for the DDU GES in the ILB should focus on large end-users with the greatest energy requirements, that could take advantage of the full GES capacity, including its unique application in addressing energy security, resilience, and sustainability goals and requirements. The feasibility of implementation and commercialization should be based on a holistic analysis of all these factors, instead of only focusing on single attributes (e.g., economics).

3. DISCUSSION: DDU Feasibility Funding Opportunity Criteria

The information in this section is provided in response to DOE’s request to address the following criteria outlined in the DDU Feasibility Funding Opportunity:

1. *Geothermal Resource Assessment*. Present results of the geologic modeling and determine the available thermal energy based upon the modeled flow rate and extracted geothermal fluid temperature for the proposed life of the GES.
2. *Regulatory Compliance Plan*. Describe how the project would address the relevant federal, state, and local environmental regulations governing the characterization and utilization of the geothermal resources at the ARFs prior to completion of the GES.
3. *End-Use Load (and Framework Used to Determine) Market Transformation Plan*. Provide a preliminary estimate of the impact(s) the project will have on energy consumption for the proposed activities, and include the assumptions used in calculating those preliminary impacts. Clearly state the proposed geographical and or structural boundaries of the end-use load under consideration. Describe how the innovative DDU applications are used for heating floor space at the ARFs and the associated, cascading thermal applications. Also include the modeling results from determining the individual and cumulative energy loads for the ARFs.
4. *Technical Description of Proposed DDU Technology(s)*. Specify the type and location of extraction and injection wells and the system design for the DDU GES at the U of IL. Emphasize any innovative approaches used. Describe how the design and modeling of the geothermal wells impact the resource over time; how spent geothermal fluids will be utilized; and how piping, infrastructure, and other methods of thermal exchange and heat transport impact the project economics.
5. *Costs and Benefits Methodology*. Specify how project costs and benefits were assessed to determine the project business case and describe the financial viability of the proposed GES. Provide the resulting metrics used in the techno-economic analysis.

3.1 Criterion 1 – Geothermal Resource Assessment

The *Geothermal Resource Assessment* for the MSS was undertaken for both (1) the ARFs at the U of IL and (2) entire ILB based on results from the geologic modeling, including the geological characterization of the subsurface formations (from ground surface into the Precambrian basement), a reassessment of the temperature profile, the geocellular modeling, and geothermal reservoir and wellbore modeling. Together, this work provided a better understanding of the geothermal resource and how best to extract it. Assessing the MSS in terms of its hydraulic and mechanical heterogeneity led to identifying the most productive interval that informed the wellbore design to optimize geothermal fluid extraction and minimize the project cost.

3.1.1 Results of the Geologic, Reservoir, and Wellbore Modeling

The work included a thorough analyses of existing hydraulic, thermal, and mechanical properties of the MSS in the ILB (Figure 22). The thermal, hydraulic, and petrophysical data (Table 2) were drawn from the literature—either measurements from the ILB (Leetaru, 2014; Freiburg et al., 2016; Panno et al., 2013; Anovitz et al., 2018; Ritzi et al., 2018) or from data for similar geologic materials (Freeze and Cherry, 1979; Morrow et al., 2017; Robertson, 1988; Schön, 2015; Waples and Waples, 2004; Walker et al., 2015). Geothermal-specific properties such as thermal conductivity, specific heat capacity, and thermal expansion coefficient were modeled from overall

quartz content and temperature (Appendix B1). The average porosity of 15.1% was used in both assessments.

A high resolution DTS log from the IBDP site (Schlumberger Carbon Services, 2012) was used to determine the thermal gradient at the U of IL (Figure 6). Using this thermal gradient, geothermal fluid temperatures in the LMSS are expected to be between 44°C and 46°C (111°F and 115°F). These temperatures are slightly lower than 49°C and 51°C (119°F and 124°F), estimates made using the ILB “rule of thumb” (1.8°C/100 m or 1°F/100 ft starting at a ground surface temperature of 15°C [60°F]) (Frailey et al., 2004); this thermal gradient was used for the ILB assessment.

Based on the geothermal reservoir and wellbore modeling (Section 2.2), the DDU GES will supply 2 MMBtu/hr, the heating demand of the ARFs, by extracting geothermal fluid at a rate of 954 m³/d (6,000 bbl/d). It is expected there will be a temperature drop of <0.6°C (<1°F) along the wellbore during extraction if a silicate foam insulation is applied to the tubing.

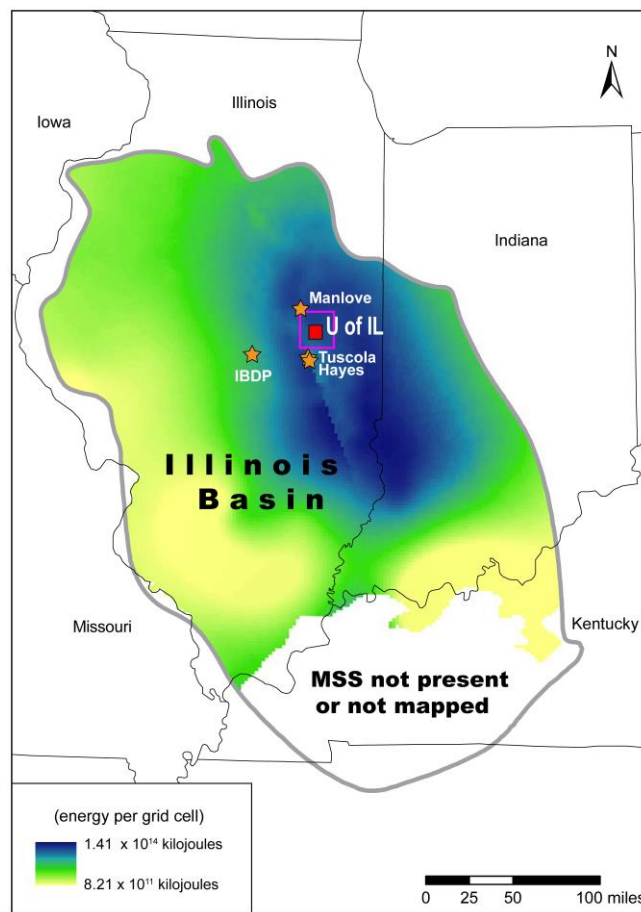


Figure 22. Location of the study site in the ILB. The pink box delineates the extent of geologic, geocellular, and reservoir models that were completed; an area covering 93 km² (36 square miles). Also, the orange stars denote the Manlove and Tuscola natural gas (NG) storage fields, the Illinois Basin–Decatur Project (IBDP), and the Hayes oil field. The geothermal resources available in the MSS is represented by the colored shading.

3.1.2 Available Thermal Energy at the ARFs and ILB

To determine the geothermal resources of the area around the ARFs and the entire ILB, using a GIS to estimate the spatial and thickness parameters of the MSS was required. The geothermal energy stored (Q_{tot}) in a geothermal reservoir can be defined as the amount of extractable heat that can be used to do work. The energy (heat) stored in formation fluids is analogous to original-oil-in-place (OOIP) used in the petroleum industry to estimate hydrocarbon resources. A method proposed by Muffler (1977, 1978), Muffler and Cataldi (1978), and, most recently, used by AGEG (2008) was used to estimate Q_{tot} as follows:

$$Q_{tot} = \int \rho_t C_t (T_{res} - T_0) dV = Ah\rho_t C_t (T_{res} - T_0) \quad (1)$$

where

C_t and ρ_t are the specific heat capacity and density of the formation.

T_{res} and T_0 are average reservoir and reference (absolute) temperatures [e.g., Kelvin or Rankin].

V is the reservoir volume.

A is the reservoir area.

h is the average reservoir thickness.

The reference temperature (T_0) represents the endpoint of the thermodynamic process that will utilize geothermal energy. As such, T_0 was equivalent to standard temperature in this study. Alternatively, T_0 can be equivalent to the reject temperature (Pastor et al., 2010).

The recoverable geothermal energy or resource (i.e., the heat that can be delivered to the surface at the well head, assuming zero temperature loss) is the heat transported by the geothermal fluid in the reservoir pore space. Heat exchange between the geothermal fluid and reservoir rock via convection (Benoit, 1978), conduction (Benoit, 1978), and diffusion (to a lesser extent) is assumed to be insignificant compared to the heat already stored in the geothermal fluid. As a result, the recoverable resource (Q) was calculated as follows:

$$Q = \phi Q_{tot} = Ah\phi\rho_w C_w (T_{res} - T_0) \quad (2)$$

where

C_w is the specific heat of the geothermal fluid.

ρ_w is the density of geothermal fluid.

The density and specific heat capacity of the MSS as reported in the technical literature are 1,040 kg/m³ and 4.18 kJ/kg·K, respectively (Breunig et al., 2013).

Estimating the reservoir volume is very challenging, as it is difficult to accurately define reservoir boundaries (i.e., lateral extent), thickness, and porosity. For this study, the reservoir volume was estimated based on average reservoir properties of the MSS within the ILB (i.e., porosity, and thickness; Freiburg et al., 2014; Buschbach and Kolata, 1990). Although the regional extent of the

MSS extends beyond the ILB boundary (Figure 22), the defined MSS boundary from Buschbach and Kolata (1990) was used to determine the best estimate of the geothermal resource.

Using the Q_{min}/Q_{max}

equations (below) and the average reservoir property constants listed below for **Method 1** (Table 13), a geothermal energy resource estimate was calculated for the ILB and ARFs. The available thermal energy ranges from 2.93×10^2 to 2.94×10^3 exajoules for the ILB and 9.663×10^{-5} to 1.034×10^{-4} exajoules for the ARFs.

$$Q_{max} = PV [m^3] * 1040 [kg/m^3] * 4.18 [kJ/(kg \cdot K)] * (\Delta T_{max}) [K] = \underline{4347.2 * PV * \Delta T_{max} [kJ]} \quad (3)$$

$$Q_{min} = PV [m^3] * 1040 [kg/m^3] * 4.18 [kJ/(kg \cdot K)] * (\Delta T_{min}) [K] = \underline{4347.2 * PV * \Delta T_{min} [kJ]} \quad (4)$$

Table 13. Parameters for Calculating the Geothermal Energy Resource in the MSS

Method 1: Average Reservoir Values (input into static Qmax/Qmin equations)			
Parameter	Value	Unit	Comments
A _{ARF}	3.60 9,324	sq. miles m ²	• MSS extent at ARF.
A _{ILB}	1,576,900,000,000 (1.58 × 10 ¹²) 146,498,809,448 (1.46 × 10 ¹¹)	ft ² m ²	• MSS extent in ILB, grid cell count * cell area. • Comparable with estimate of ~155,000 m ² (~60,000 sq. miles) for ILB area from Buschbach and Kolata (1990).
h _{ARF} h _{ILB}	553 356	m m	• Thickness at ARF. • Average thickness of MSS in ILB.
V _{ARF} V _{ILB}	5,156,172 (5.16 × 10 ⁶) 52,153,576,163,309 (5.22 × 10 ¹³)	m ³ m ³	• Volume of MSS in ILB. • Volume of MSS at ARF.
Porosity	0.151	P	• 15.1 %; average for MSS in ILB.
Porosity Volume PV _{ARF} PV _{ILB}	778,582 (7.79 × 10⁵) 7,875,190,000,660 (7.88 × 10¹²)	m ³ m ³	• PV for ARF • PV for ILB
T _{grad}	((depth-100) / 100) + 62	°F	• Thermal gradient for ILB (rule-of thumb) 1°F/100 ft depth; average temperature 62°F at 100 ft below ground surface.
T _{0_K}	60 288.71	°F K	• 60°F (15°C) ground temperature (T ₀ for standard geothermal resource calculation (e.g., Reed, 1983).
d _{max-ARF} d _{max-ILB}	6,192 15,337	ft ft	• Base depth: deepest MSS in ARF • Base depth: deepest MSS in the ILB.
T _{max_°F-ARF} T _{max_°F-ILB}	114.0 214.4	°F °F	• Maximum temperature at base of MSS at ARF. • Maximum temperature at base of MSS in ILB.
T _{max_K-ARF} T _{max_K-ILB}	319.26 374.48	K K	• Maximum temperature at base of MSS at ARF. • Maximum temperature at base of MSS in ILB.

$\Delta T_{\max\text{-ARF}}$	30.55	K	<ul style="list-style-type: none"> • Temperature difference at ARF. • Temperature difference in ILB.
$\Delta T_{\max\text{-ILB}}$	85.77	K	
$D_{\min\text{-ARF}}$	6,192	ft	<ul style="list-style-type: none"> • Shallowest MSS at ARF. • Shallowest MSS in the ILB.
$D_{\min\text{-ILB}}$	1,443	ft	
$T_{\min\text{-}^\circ\text{F-ARF}}$	111.0	$^\circ\text{F}$	<ul style="list-style-type: none"> • Minimum temperature at top of MSS at ARF. • Minimum temperature at top of MSS in the ILB.
$T_{\min\text{-}^\circ\text{F-ILB}}$	75.4	$^\circ\text{F}$	
$T_{\min\text{-K-ARF}}$	317.04	K	<ul style="list-style-type: none"> • Minimum temperature at top of MSS at ARF. • Minimum temperature at top of MSS in the ILB.
$T_{\min\text{-K-ILB}}$	297.26	K	
$\Delta T_{\min\text{-ARF}}$	28.33	K	<ul style="list-style-type: none"> • Temperature difference at ARF. • Temperature difference in ILB.
$\Delta T_{\min\text{-ILB}}$	8.55	K	
$Q_{\max\text{-ARF}}$	103,401,108,531 (1.034×10^{11})	kJ	1.034×10^{-4} exajoules
$Q_{\min\text{-ARF}}$	96,631,805,190 (9.663×10^{11})	kJ	9.663×10^{-5} exajoules
$Q_{\max\text{-ILB}}$	2,938,131,630,720,000,000 (2.938×10^{18})	kJ	2.94×10^3 exajoules
$Q_{\min\text{-ILB}}$	292,888,252,800,000,000 (2.929×10^{17})	kJ	2.93×10^2 exajoules

An alternative, GIS-based approach considering the spatial variability of volume and thermal properties (**Method 2**) was used to estimate the geothermal resource in the MSS. Gridded geospatial data (i.e., formation thickness isopach maps and depth map-based gradients) (Table 14) were incorporated into the following geothermal resource equation:

$$Q_{\text{map}} = (x \times y) \times h_{\text{isopach}} \times 0.151 \times 1040 \times 4.18 \times \Delta T_{\text{K-MSS}} \times \text{MSS_extent} \quad (5)$$

where

grid cells (x, y) are 3,048 m \times 3,048 m (10,000 ft \times 10,000 ft)

h_{isopach} is thickness of MSS from isopach map for the ILB and area around ARFs

porosity is 0.151

density is 1,040 kg/m³

specific heat capacity is 4.18 kJ/kg·K

ΔT in Kelvin for the MSS in the ILB and at the ARF

MSS_extent is the area covered by MSS (extent of ILB)

For each grid-cell area, the temperature at the base of the MSS ($T_{\max\text{-K}}$) was used to determine the ΔT . The spatial variability of the resource estimate is primarily controlled by the isopach thickness component of the pore volume (PV), although the depth-based temperature component also contributes to the variability. The results from all grid cells in the ILB and area around the ARFs were added together, and the map-based data effectively averaged the Q_{\min}/Q_{\max} end members.

Table 14. Parameters for GIS-Based Estimate of Geothermal Energy Resource in the MSS

Method 2: Spatial distributions and grid calculations (grid-based map data)			
MSS base formation depth grid (depth to top of formation plus formation isopach thickness). 10,000 ft × 10,000 ft grid cells			
Thermal gradient and T ₀ ; same as in Method 1 . Temperature (max) at base of MSS was used in calculation. ΔT _{max-ILB} = 85.77 K ΔT _{max-ARF} = 30.55 K			
Isopach map of MSS, as a grid; volume is roughly the same as in Method 1. Porosity = 0.151 V _{ARF} = 5.16 × 10 ⁶ m ³ V _{ILB} = 5.22 × 10 ¹³ m ³ MSS_extent = area; extent of MSS within ILB.			
Sum_{ILB}	Sum of all grids for MSS in ILB; inputted to estimate available geothermal resource.		
Sum_{ARF}	Sum of all grids for MSS at ARF; inputted to estimate total available geothermal resource.		
Q_{map-ARF}	176,923,514,849,198 (1.769 × 10¹⁴)	kJ	1.32 × 10³ exajoules
Q_{map-ILB}	1,320,606,740,000,000,000 (1.320 × 10¹⁸)	kJ	0.177 exajoules
1 exajoule (EJ) = quintillion kilojoules = 10 ¹⁸ joules 1 EJ = 23.9 megatonnes of oil equivalent (Mtoe)			

Based on this method of using spatial calculations and input map data, a “most likely” estimate for the geothermal energy resource in the MSS for the entire ILB is **1.32 × 10³ exajoules**. This thermal energy resource is **~1.5 times** the amount of energy consumed (fuel and electricity) in the North America region in 2018 (IAEA, 2019), which is equivalent to 216 billion barrels of oil.

3.2 Criterion 2 – Regulatory Compliance Plan

State, federal, and local regulations were considered in designing the injection well and selecting its construction materials to (1) protect underground sources of drinking water (USDWs), (2) maintain temperature and pressure, (3) determine subsurface pumping needs, and (4) minimize project costs. Drilling, construction, and data acquisition costs were estimated as part of the overall project costs.

To determine the requirements for developing a Regulatory Compliance Plan for the DDU GES at U of IL, the IEPA, USEPA, and Champaign County Health Department were contacted. Federal, state, and local environmental regulations governing the characterization and utilization of geothermal resources from the MSS were identified through ongoing communications. The IEPA and USEPA require reporting/permitting of the injection well to dispose of spent geothermal fluid back into the LMSS. Since the geothermal fluid has a TDS concentration exceeding 10,000 mg/L, the salinity upper threshold for potable water under the Safe Drinking Water Act (SDWA) (42 U.S.C. §300f et seq. [1974]), the Illinois Department of Public Health (IDPH) has no regulatory oversight for the DDU GES. The Champaign County Health Department is primarily concerned

with impacts on the potable water supplies from local and regional aquifers, typically found in the shallow Quaternary glacial deposits lying in the uppermost ~150 m (~500 ft). At the ARFs, geothermal fluid would be injected thousands of feet below the lowermost USDW.

The IEPA and USEPA (Region 5) gave two differing and unique directives pertaining to the injection of geothermal fluid:

- 1) USEPA requires well owners or operators submit an Underground Discharge System (Class V) inventory sheet. Under USEPA's directive, no permit for injection is necessary.
- 2) IEPA regulates the injection of geothermal fluid under UIC Class I (non-hazardous). This type of injection well requires a permit. The owner or operator of the well shall submit a permit application to seek further guidance on the siting and construction.

Under USEPA regulations, wells used to dispose of geothermal fluids leaving the DDU GES would fall under UIC Class V (Geothermal Direct Heat Return Flow Wells) (USEPA, 1999). In juxtaposition, the IEPA would regulate the injection under Class I, as the geothermal fluids would be injected below the lowermost formation considered a USDW (IPCB, 2018). Furthermore, Burch et al. (1987), as part of a review of Class V wells in Illinois for the IEPA, suggested that “geothermal wells injecting spent fluid at depths well below USDW would not fall under Class V regulations.”

Because injection wells for DDU GES have yet to be constructed in Illinois, no precedence exists for permitting them. IEPA has the primary enforcement authority (i.e., primacy) for the UIC program in Illinois, including Class I and V wells. Therefore, some uncertainty exists in addressing the UIC regulations. However, IEPA and USEPA consultations were encouraging, and the UIC permitting of similar wells in nearby states (e.g., Arkansas and Missouri) under Class V could be used as precedent for the injection well in Illinois. Additional review of UIC regulations in Kansas and Texas indicate that injection of fluids that are highly saline or contain corrosion inhibiting chemicals would not be permitted under Class V, but perhaps under Class I (e.g., KDHE, 2012; CDM Smith, 2014).

Facilities & Services (F&S) at U of IL was informed by the IEPA that additional requirements are needed to operate the GES. As owner/operator of the Class I injection well, the U of IL is required to obtain 39(i) Certification to operate a waste management facility. The project may also require a National Environmental Policy Act (NEPA) review. Because several NEPA environmental assessments have previously been completed for USDOE-funded projects in the area to study CO₂ storage in the MSS (e.g., USDOE, 2011), and a Federal Highway Administration study was completed for the Curtis Road corridor, along the north side of the ARFs (CCRPC, 2017), there exists a significant body of information to support the preparation of an environmental assessment.

3.3 Criterion 3 – End-Use Load (and framework used to determine) Market Transformation Plan

3.3.1 Market Transformation Plan Framework

In 2010, the U of IL adopted the Illinois Climate Action Plan (iCAP, 2015) that committed the campus to carbon neutrality by 2050. Currently, there is growing consensus that solar and wind energy alone will not meet the 2050 target. Therefore, the results of this feasibility study concerning the installation and operation of a DDU GES are timely with campus' interest in carbon neutrality. As this feasibility study focuses on reducing GHG emissions from the ARFs, the framework for the Market Transformation Plan at the U of IL is demonstrating the technical and financial feasibility of the proposed DDU GES at the U of IL and extrapolating findings and conclusions to urge widespread implementation of the DDU technology in other areas of the ILB. DDU technology can secure a long-term, uninterrupted supply of heating and cooling, increase resilience to extreme weather conditions, reduce U.S. fossil fuel dependency, and offset carbon dioxide equivalent GHG emissions.

U of IL Campus

This study addresses the major issues associated with implementing DDU technology at the U of IL by (1) reducing geologic uncertainty, (2) minimizing drilling risk, (3) optimizing system performance and flexibility with reliable fluid delivery and heat transport, and (4) supporting expertise through established partnerships. An investigation of regulatory requirements for the injection well also addresses regulatory uncertainty (Section 3.2). It is possible that permits for similar wells in surrounding states or states with sedimentary basins where DDU GES projects are proposed could be used as precedent for geothermal injection wells in Illinois.

The U of IL is building a coalition, coordinated by F&S, of corporations, non-profits, and researchers to establish the State of Illinois as a leader in geothermal energy utilization: a renewable energy source that fully or partially replaces fossil fuels. Through the work required to complete this feasibility study and the experiences with new technology, implementation of existing technologies, and support for the various studies of geothermal applications by the members, this coalition will strengthen and advance the design and implementation of DDU technologies in the ILB and other midcontinent sedimentary basins. In addition, several Illinois House Representatives and Senators have been communicating with the project team about the progress of this feasibility study. They provided important information about thermal energy demand and economic development that assisted us in developing a Market Transformation Plan for the ILB. The plan has been in progress since November 2019 under the coordination jointly led by the F&S Director's office, Government Relationship Office, and Illinois Water Resources Center at the U of IL.

ILB and other Midcontinent Sedimentary Basins

For all end-users in the ILB and other low-temperature sedimentary basins, this DDU technology could serve many applications when geothermal fluids can be obtained in sufficient quantities and temperatures to supply or supplement preexisting heating loads. A cascading application for the DDU GES investigated in this feasibility study was preheating of domestic water. The GES could be further optimized by applying supplemental, innovative heat transport and/or thermal storage

technologies to provide space cooling and thermal storage. State-of-the-art technologies, such as UTES, would allow excess energy produced with renewable sources or electricity from the grid during off-peak hours to be stored and accessed later when thermal demands for buildings is greatest. Integrating UTES with heat pump systems could significantly reduce system costs without increasing electricity requirements, with the additional benefit of stabilizing the grid load. In addition, the RTES technology, while not specifically investigated in this feasibility study, would be equivalent to reversing the direction of fluid flow to provide space cooling during the summer season (Section 2.2.1).

While the feasibility of implementing this DDU technology at ILB military installations was not the focus of this study, these facilities could use the GES to increase energy resiliency, improve energy security, and ensure a long-term, reliable supply of heating and cooling for mission critical operations (Section 2.4.2). The Market Transformation could assist decision makers in the DoD and policy makers in Congress with updating and improving technology to meet the Army's energy needs (e.g., National Defense Authorization Act 2021) (Appendix C6).

3.3.2 Geographical and/or Structural Boundaries of the End-Use Load (under consideration)

The ARFs will be the end-users of the thermal energy extracted from the ground, and are located on the U of IL campus along 1.6 km (1 mile) of the ACES Legacy Corridor on Race Street; bounded to the north by Curtis Road and Old Church Street on the south (Figure 17). Three ARFs are currently located along Race Street; the Feed Technology Center is under construction, and relocation of the ISRL and Dairy Farm to the area is being considered.

3.3.3 Modeling Results: Individual and Cumulative Energy Loads for All Proposed End-Uses

End-use heating load was assessed for the six ARFs. Historical, monthly fuel consumption data for each facility was obtained and used along with hourly climate data from a nearby National Weather Service (NWS) station (Willard Airport) to predict the hourly heating load profile (Lin, 2018). The profile of hourly heating loads was necessary to determine peak load demand and determine the design load required of the DDU GES.

Hourly Heating Load

The degree days in FY2015 through FY2017 were estimated and used to correlate energy consumption with the local, ambient temperature. Degree days are typical indicators of energy consumption for space heating and cooling. A nominal temperature of 18°C (65°F) is generally adopted for estimating degree days. If the ambient temperature is below this threshold, heating is considered necessary. The sum of degree days over a month, a season (e.g., winter), or an entire heating season can be used to estimate the amount of heating required for a particular building (Figure 23).

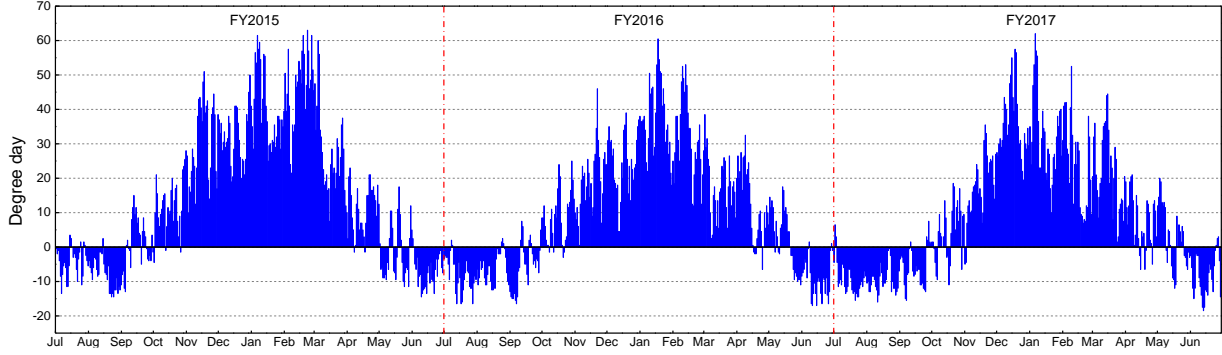


Figure 23. Estimated degree days in Champaign-Urbana for the period FY2015 through FY2017.

As shown in Figure 23, over 90% of the degree days from June to September are negative (i.e., the measured temperature is above the baseline [average annual temperature]), indicating that the heating demand is a minimum during this time period. Positive degree days are primarily recorded from October through May, with maximums in January and February (the coldest months of the year). These degree days are consistent with temporal changes in monthly fuel usage (Figure 23). Accordingly, the heating season starts in October and ends in May.

During the non-heating season, NG or LPG is primarily used to make domestic hot water. However, the heating demand for domestic hot water is assumed to be constant throughout the entire year, and therefore the following equation was used to calculate heating demand during the summer and early fall seasons:

$$Q_b^m = \frac{1}{4}(Q_6^m + Q_7^m + Q_8^m + Q_9^m) \quad (\text{MMBtu/month}) \quad (1)$$

$$Q_b^h = \frac{Q_b^m}{732} \quad (\text{MMBtu/hr}) \quad (2)$$

where

Q_b^m and Q_b^h are monthly and hourly base heating loads for domestic hot water, respectively. The values 6, 7, 8, and 9 represent June, July, August, and September, respectively. The value of 732 is the monthly hours averaged over June to September.

During the heating season, fossil fuels are used for making domestic hot water and to provide space heating. The hourly heating load for conditioning office and laboratory space greatly depends on the ambient temperature. There is a linear relationship between hourly heating load and ambient temperature as it approaches the nominal, average annual air temperature of 18°C (65°F). The amount of energy required for space heating can be determined by subtracting the baseline calculated above for heating domestic water from total energy use. The hourly heating load ($Q_{i,j}^h$) at the i^{th} hour in j^{th} month over the entire year was estimated as follows:

$$Q_{i,j}^h = \begin{cases} Q_b^h & (\text{if } j = 6, 7, 8, 9) \\ \frac{D_{i,j}^h}{\sum_{i=1}^{\text{hours in } j \text{ month}} D_{i,j}^h} \times (Q_j^m - Q_b^m) + Q_b^h & (\text{if } j = 1, 2, 3, 4, 5, 10, 11, 12) \end{cases} \quad (3)$$

$$\text{where } D_{i,j}^h = \begin{cases} 65 - t_{i,j} & (\text{if } T_{i,j} < 65) \\ 0 & (\text{if } T_{i,j} \geq 65) \end{cases} \quad (4)$$

$Q_{i,j}^h$ is hourly heat load at j^{th} month, i^{th} hour.

Q_b^h is hourly base heating load for domestic water use.

$D_{i,j}^h$ temperature approach to 65°F. When the temperature is >65°F, the value is 0.

Q_j^m is the monthly heat use in j^{th} month.

$T_{i,j}$ is the hourly ambient temperature of i^{th} hour in j^{th} month.

Q_b^m is monthly base heating load for domestic water use.

The results of the degree day methodology are displayed in Figure 24 and are sorted from large to small in Figure 25. Heating is required for 5,832 hours annually based on the three-year average from FY2015 through FY2017.

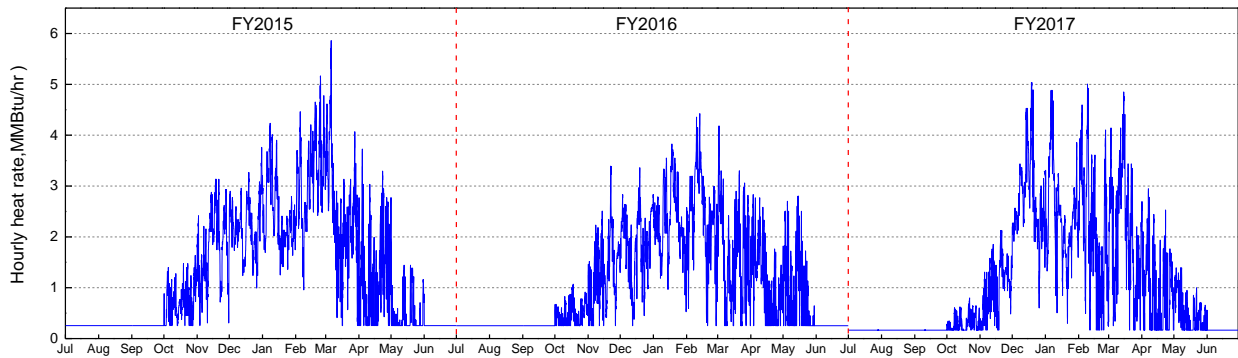


Figure 24. Hourly heat load (Q^h) demands for the six ARFs from FY2015 to FY2017.

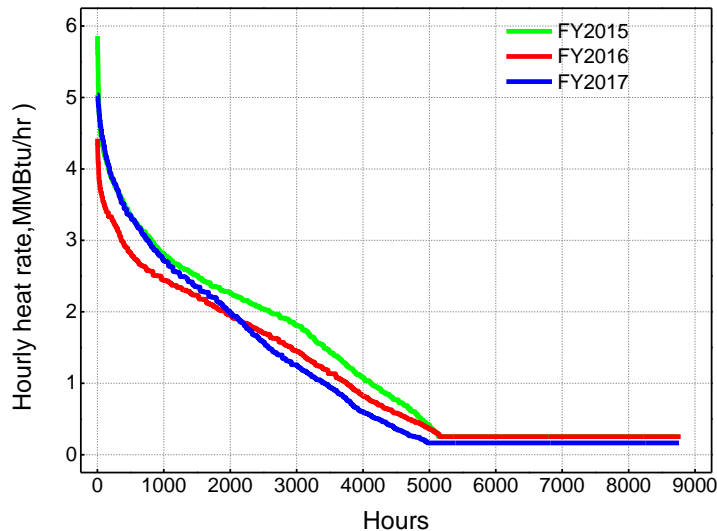


Figure 24. Hourly heat load (Q^h) demands of the six ARFs sorted from high to low levels.

Peak Load

Peak loads were estimated for FY2015, FY2016, and FY2017. The hourly peak load (Q_{max}^h) reached 5.86 MMBtu/hr in FY2015, 4.42 MMBtu/hr in FY2016, and 5.04 MMBtu/hr in FY2017,

with a 3-year average of 5.68 MMBtu/hr (Figure 25). The highest heating loads are only required for a relatively short period of time. To ensure that the peak load was not underestimated, another approach based on degree days was used (cf. Althouse et al., 2017). In this approach, the hourly peak load was estimated as follows:

$$Q_{max}^h = \frac{D_{max}}{D_{ave}} \times \frac{Q^y}{h^y} \quad (5)$$

where

D_{max} and D_{ave} are the highest and average degree day temperatures, respectively, for one year.

Q^y is the total heating demand for a year.

h^y is the total hours in a year.

For comparison purposes, the peak loads estimated from the hourly heating load analysis (Figure 25) are also listed in Table 15. The peak load calculated from the two different methods differ to some extent. The average peak load over the three years and between the two estimation methods amounts to 5.68 MMBtu/hr. Thus, as a conservative estimate, a peak load of 6 MMBtu/hr was adopted for the GES analysis in this feasibility study.

Table 15. Peak Heating Load Demands from Degree Days Approach and Hourly Load Analysis

Year	Maximum degree days (°F)	Average degree days (°F)	Yearly average heating load (MMBtu/hr)	Peak heating load (based on Eq. 5) (MMBtu/hr)	Peak heating load (from Fig. 25) (MMBtu/hr)
FY2017	62.0	9.42	1.06	7.01	5.86
FY2016	60.5	10.44	1.09	6.30	4.42
FY2015	63.0	14.79	1.28	5.45	5.04

3.3.4 Impact(s) the Project Will Have on Energy Consumption (for proposed activities)

The relationship between the cumulative total heating load demand and capacity of the DDU GES is not linear (Figure 26). A heat supply capacity of 2 MMBtu/hr will satisfy at least 80% of the total heating load. The peak load requirement (as high as 6 MMBtu/hr) comprises the remaining balance (20%). For the existing ARFs, the remaining balance of the total heating load should be satisfied using currently-installed heating systems, including NG-fired boilers. As a result, the DDU GES would decrease NG and LPG consumption for domestic hot water production and space heating by at least 80%.

The DDU GES would make ARFs' energy consumption more efficient. The proposed DDU GES can operate at a steady rate (since extremely high heating loads are only required for a short period of time) instead of high turndown (Figure 26). The system design includes equipment to be installed on heat pumps and fans that will increase turndown capacity and reduce the amount of energy consumed by the DDU GES. (Section 3.4 details the technical components of system equipment).

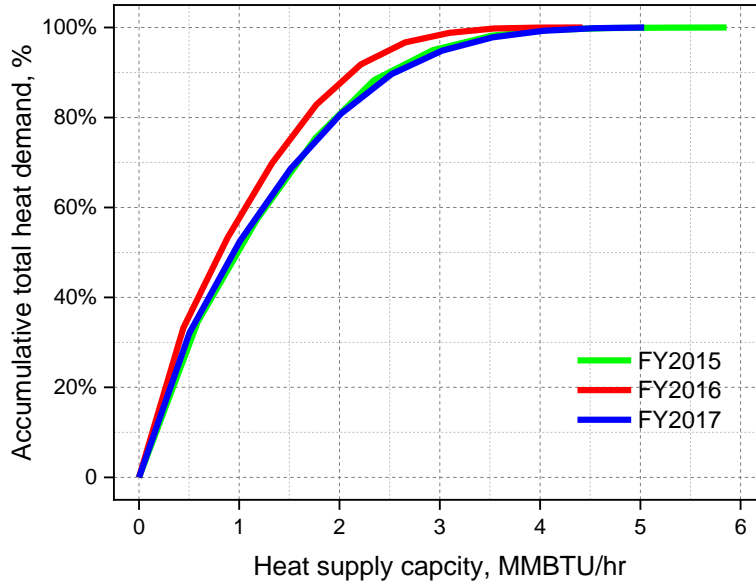


Figure 25. Cumulative heating load demand vs. heat supply capacity.

3.3.5 Capability to Serve Large-Scale Residential, Commercial, or Institutional Developments

While the doublet well DDU GES for this feasibility study was only assessed with regards to the ARFs, up to four additional doublet well systems would be feasible for heating and cooling buildings at other U of IL locations (e.g., South Engineering (Bardeen) Quad, Center for Networked Intelligent Components and Environments, and Research Park).

In order to determine challenges to deployment of the doublet well DDU GES at the ARFs, the following U of IL organizations and divisions were contacted:

- F&S
- ACES
- U of IL Provost

Other use of DDU GES on the U of IL campus are as follows:

- Cooling classrooms and computing facilities
- Preheating water for cold-hot water distribution system
- Heating and cooling dormitories

Within the ILB, 8 major university and 11 community college campuses would have similar DDU GES applications and be strategically located over the portions of the MSS projected to have high flow rate potential to meet energy demands similar to the energy demands of the following campuses:

Universities:

- Illinois State University, Normal, IL

- University of Illinois at Springfield, Springfield, IL
- Southern Illinois University-Edwardsville, Edwardsville, IL
- Southern Illinois University-Carbondale, Carbondale, IL
- Eastern Illinois University, Charleston, IL
- Indiana State University, Terra Haute, IN
- Vincennes University, Vincennes, IN
- Indiana University, Bloomington, IN

Community Colleges:

- Parkland College, Champaign, IL
- Danville Area Community College, Danville, IL
- Heartland Community College, Normal, IL
- Richland Community College, Decatur, IL
- Lincoln Land Community College, Springfield, IL
- Lake Land College, Mattoon, IL
- Kaskaskia College, Centralia, IL
- Wabash Valley College, Mount Carmel, IL
- John A Logan College, Carterville, IL
- Wabash College, Crawfordsville, IN
- Owensboro Community and Technical College, Owensboro, KY

In addition to major university campuses, hospitals in the ILB would have applications for DDU GES. Those with similar energy demands as the ARFs include the following:

- OSF Saint Francis Medical Center, Peoria, IL
- Carle Foundation Hospital, Urbana, IL
- St. John’s Hospital, Springfield, IL
- Memorial Medical Center, Springfield, IL
- Illiana Veteran’s Administration Hospital, Danville, IL
- Good Samaritan Regional Health Center, Mount Vernon, IL
- Greenville Regional Hospital, Greenville, IL
- Union Hospital, Terra Haute, IN
- Terre Haute Regional Hospital, Terra Haute, IN
- Good Samaritan Hospital, Vincennes, IN
- Indiana University Health Bloomington Hospital, Bloomington, IN

While not studied in as much detail as the ARFs, a high-level review of three ILB military installations (Rock Island Arsenal, Fort Campbell, and Fort Knox) was completed. The following was found:

1. DDU GES would improve the military’s energy security and energy resilience for mission critical operations.
2. Partially meeting energy load requirements with geothermal energy would reduce the dependence on fossil fuels and offset GHG emissions.

- Further work to determine the feasibility of the DDU GES should focus on military installations that have the largest energy requirements and set sustainability goals such that they can take full advantage of the GES capacity.
- Implementing and commercializing the DDU technology should be based on a holistic analysis that considers multiple issues rather than *only* project economics.

3.4 Criterion 4 – Technical Description of the Proposed Deep Direct-Use Technology

3.4.1 Deep Direct-Use Heating System for ARFs

There are six ARFs that will utilize heat from the DDU GES, and each facility includes multiple buildings. Three ARFs already have having equipment that provides heat to their buildings. The other three ARFs will have new buildings and no existing heating equipment. Figures 27 and 28 show process flow diagrams for Cases 1 and 2, respectively.

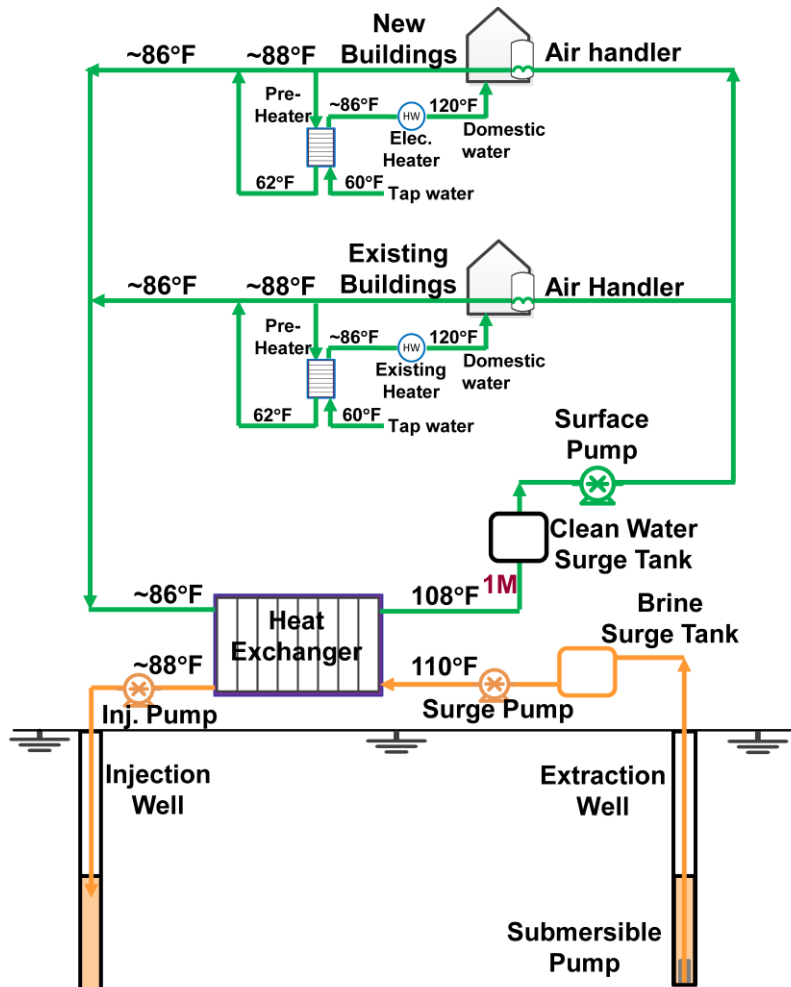


Figure 26. Case 1 Process Flow Diagram (1M = 1 unit of mass flow).

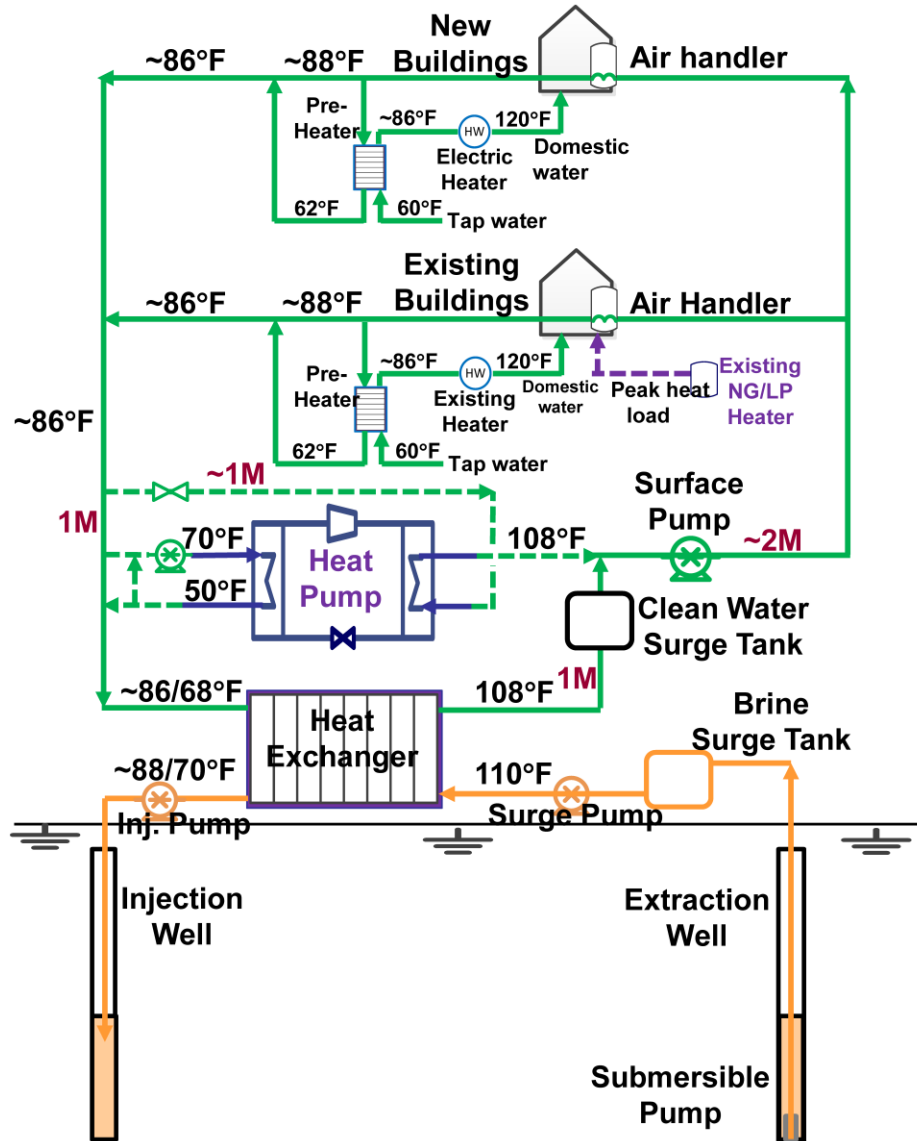


Figure 27. Case 2 Process Flow Diagram (1M and 2M = 1 unit and 2 units of mass flow, respectively).

In both cases, geothermal fluid is extracted from the extraction well using an ESP. Geothermal fluid enters the surge tank that has a residence time of ~10 minutes and operates near atmospheric pressure. The surge pump downstream from the surge tank transports the geothermal fluid to the heat exchanger. The surge pump is a stainless-steel centrifugal pump that increases the pressure to 689 kPa (100 lbs/square inch, gauge pressure [psig]). The heat exchanger transmits the heat from the geothermal fluid to the clean water via indirect (i.e., non-contact) heat transfer.

The heated clean water then enters the clean water surge tank. The clean water surge tank is made of carbon steel and provides up to 12 hours of storage for the heated water. Then, the surface pump—a centrifugal pump with a carbon steel body and stainless-steel internals—pumps the clean water at ~689 kPa (~100 psig) to the ARFs. The heated clean water branches off to each facility and, subsequently, to each building at the facilities. The heated clean water provides warm air to

each building by exchanging heat in an air handler that uses a fan for forced air flow. As a cascading application, after heating the buildings, the cooled clean water is used to provide preheating for domestic hot water production before recirculating to enter the heat exchanger. After providing heat, the geothermal fluid flows 3.2 km (2 miles) through underground piping back to the injection well. At the injection well, a stainless-steel triplex pump will be installed to increase injection pressure to 8,039 kPa (1,166 psig).

For Case 2, during peak loads, a heat pump and the existing heaters at the ARFs are turned on to provide additional heating. The heat pump removes heat from a slip-stream of the cooled clean water and uses it to heat the clean water circulating to the ARFs via a refrigeration loop. When the heat pump is running, the temperature of the clean water entering the heat exchanger drops to 20°C (68°F) and the temperature of the geothermal fluid leaving the heat exchanger drops to 21°C (70°F). (Process modeling using VMGSim® software developed by Virtual Materials Group Incorporated was used to confirm the temperatures shown in the process flow diagrams.)

The DDU GES is most efficient operating at full capacity in both cases; however, most of the time, heating requirements will be less than the full design load. This applies to both Case 1 and Case 2. In order to increase efficiency, variable frequency drives (VFDs) would be installed on all pumps and fans in order to increase the turndown capacity of the equipment and reduce energy consumption. Equipment will be turned off when possible to reduce energy use. The ESP manufacturer recommends turning off the ESP in the extraction well no more than twice a day and a minimum shutdown time of one hour. Each time the ESP is shut down, solids (e.g., scale, fines) may fall back into the pump, and an excessive number of shutdowns could lead to premature failure. After discussing this possibility with the ESP supplier, the clean water surge tank was sized to limit ESP shutdowns to once a day for up to 12 hours and allow the ESP to operate at full design load by storing heated clean water.

Preliminary piping and instrumentation diagrams (P&IDs) for both cases can be found in Appendix C5. The preliminary P&IDs show example controls, pipe sizes and materials, and insulation requirements.

3.4.2 Preliminary DDU GES Design and Project Economics

3.4.2.1 Well Specifications: Type and Location

The district-scale DDU GES in the low-temperature ILB requires drilling and completing two wells. The extraction well would be built to deliver a flow rate of ~954 m³/d (~6,000 bbl/d) of the geothermal fluid from the LMSS at a depth of ~1,920 m (~6,300 ft). The injection well would be constructed to return the rejected fluid back into the LMSS at the same depth as extraction. Each well has different design criteria and constraints that must be met.

Many determining factors influenced the final well design, including flow rate, fluid composition, subsurface conditions, and temperature. The design of the doublet well system is similar to typical GES that utilizes fluids from a deep reservoir. The doublet design should be reviewed and modified as needed to optimize fluid extraction and injection and negate any heat loss. The actual design of

the GES will need to be updated as new information about the subsurface is acquired in order to optimize the actual cost of the equipment at the actual time of construction. The costs presented here are good faith estimates based on current market conditions. Actual market conditions at the time of well construction could either increase or decrease the true cost of the well.

Extraction Well

The extraction well is designed to meet two criteria and must have: (1) casing with a large-enough diameter to lower an ESP that is sized to deliver the required flow rate and (2) ensure cost effective wellbore insulation is used to minimize heat loss. Based on the required flow rate (954 m³/d [6,000 bbl/d]), a pump diameter of 0.14 m (5.6 inches) is required. This pump diameter requires a well extraction casing with a 0.18 m (7.0 inch) outer diameter (OD). Wellbore stability and severe lost circulation issues have been encountered in almost all previously drilled MSS wells, so an intermediate casing or protection string is included in the well design (Appendix C1).

While it might be possible to eliminate the casing string, it is prudent to keep it in the initial design until more local knowledge of the subsurface is gained. The protection string also helps insulate the wellbore and prevent heat loss during extraction. The ESP will be placed at the shallowest depth possible in the well to deliver geothermal fluids as quickly as possible to the surface, preventing significant heat loss. The well casing will be lined with plastic for protection against corrosion. A packer will be used to make it possible to place an insulating fluid in the tubing casing annulus and to protect the casing in the extraction well from the corrosive geothermal fluid. The 0.18 m (7.0 inch) casing placed across the MSS extraction zone will be made of chrome alloy to limit corrosion. The extraction well casing will be cemented all the way to the ground surface. While cementing to the surface is not required in an extraction well, it provides additional insulation. The estimated cost of drilling and completing the extraction well is \$4.3 million.

Injection Well

The injection well is designed to meet the requirements of a UIC Class I injection well. Typically, shallow geothermal applications in Illinois either do not have injection wells (are not permitted under UIC regulations) or the returned water meets USEPA and USDA drinking water requirements. However, MSS geothermal fluid has more TDS than fresh (potable) water, and as a result, the injection well would most likely be permitted as a Class I (Non-Hazardous) injection well. Therefore, all casing strings must be cemented to the surface.

Protective measures will be taken in order to prevent corrosion in the injection well. The casing placed across the injection interval will be made of chrome alloy. The tubular sizes will be 0.14 m (5.5 inches) for the injection casing and 0.07 m (2.9 inches) for the injection tubing. Friction pressure was considered, and while the friction in the injection tubing might be 1,723 kPa (250 psi), higher than the next larger size (0.09 m [3.5 inches]), the cost of additional surface pump horsepower would be less than the cost of constructing a larger wellbore to accommodate the larger tubing size. The estimated cost of drilling and completing the injection well is \$3.8 million.

3.4.2.2 Heat Transport to the ARFs: Piping Systems

Geothermal Fluid and Clean Water Piping Routes

The “virtual” routes of the piping systems to carry geothermal fluid and clean water are illustrated in Figure 29. All pipes, including the pipeline that returns the geothermal fluid from the heat exchanger to the injection well, will be insulated and buried underground. Insulating the pipeline is not necessary from a thermal performance perspective, but is necessary to prevent potential scaling or precipitation due to heat loss.

According to the current site plan, the extraction well (A) would be located on Old Church Road, ~0.4 km (~0.25 miles) east of Race Street. The injection well (C) sits along Curtis Road, ~1.2 km (~0.75 miles) west of Race Street. The two wells are 2.3 km (1.4 miles) apart, which, according to the reservoir simulations, are far enough apart that the C-T front does not reach the extraction well. The wells are sited close to buildings, allowing for convenient access to the electrical grid. A small building at the extraction well will house process and control systems (e.g., heat exchanger, pumps, heat pump [for peak loads], power breaker, and instrumentation and controls). Also, the well is located near the clean water loop to allow immediate heat transfer. Another small building near the injection well will house the injection pump and other instrumentation and control components.

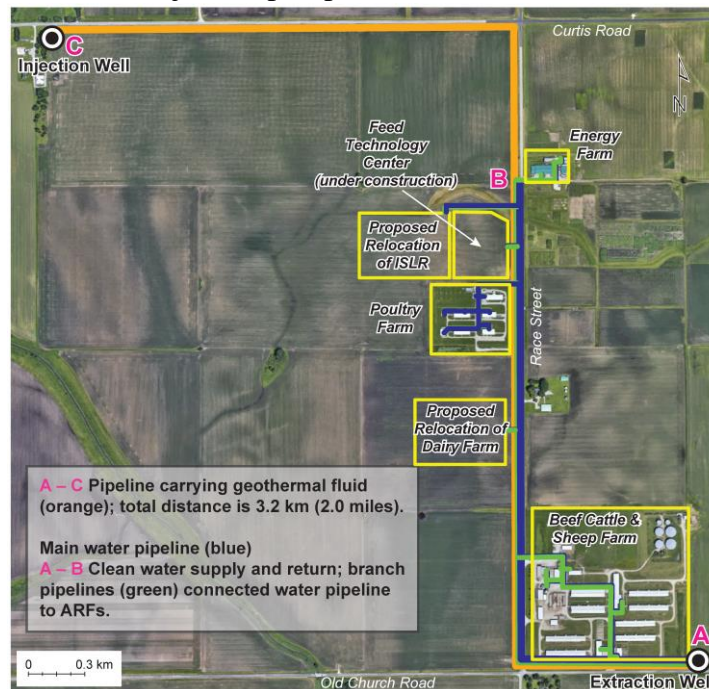


Figure 28. The “virtual” routes for the pipes carrying the geothermal fluids and clean water. The orange line (B) delineates the route of the main pipeline carrying geothermal fluid between the extraction well (A) and injection well (C). The blue and green lines delineate pipes carrying clean water to and from the ARFs.

Three main lines will be constructed for the piping system to (1) transport geothermal fluid, (2) deliver a clean water supply, and (3) return the cooled clean water. The main pipeline transporting geothermal fluid will be 3.2 km (2.0 miles) long, beginning at the extraction well (A), running west along Old Church Road, turning north along Race Street, and then towards the west along Curtis Road, where it eventually reaches the injection well (C) (Figure 29). The main clean water

supply and return pipelines are both 1.6 km (1.0 mile) long from the heat exchanger exit near the extraction well to the end of the clean water pipeline along Race Street near the Energy Farm.

Multiple branch lines will supply heated clean water from the main supply line and return the cooled clean water to the main return line from each ARF. All the ARFs that are to be move will be located along Race Street, and will have easy access to the pipelines carrying clean water. For the Poultry Farm and Beef & Sheep Research Field Laboratory, water piping routes were determined by reviewing the existing NG piping and utility networks. For the Energy Farm, the water pipes would be routed to the two parts of the facility with the highest heating loads: the office building and greenhouses. For the three ARFs that will be relocated, the clean water supply and return lines are assumed to be installed adjacent to the existing NG supply lines. Descriptions of the main and branch pipelines are presented in Table 16.

Table 16. Length and Sizing Information of Main and Branch Hydronic Piping Systems

	Description	Pipe length (ft)	Case 1 Pipe size (inches)	Case 2 Pipe size (inches)
Main lines	Geothermal fluid	10,560	6	6
	Clean water supply	5,280	6	6
	Clean water return	5,280	6	6
Branch lines (water supply and return)	Energy Farm	603 (×2)	2	3
	Beef & Sheep Research Field Laboratory	2,160 (×2)	2	3
	Poultry Research Farm	1579 (×2)	2	2
	ISRL	675 (×2)	3	4
	Dairy Cattle Research Unit	2,377 (×2)	2	3
	Feed Technology Center	299 (×2)	2	2

Pipe Sizing and Costs

The geothermal fluid and clean water pipes were sized to limit the typical fluid velocity to 1.5 m/s (5 ft/s) in order to avoid excessive pressure drop, and ensuring the main lines were kept at ≤345 kPa (≤50 psi) over the entire distribution network. For both Cases 1 and 2, the main geothermal fluid pipeline is 0.15 m (6.0 inches) wide and designed to carry fluids flowing at 954 m³/d (6,000 bbl/d) or higher, with a total pressure drop of 200 kPa (29 psi) over 3.2 km (2 miles).

In Case 1, clean water is delivered through a 0.15 m (6 inches) pipe at flow rates of ~954 m³/d (~6,000 bbl/d), with a total pressure drop of 193 kPa (28 psi) over a distance of 3.2 km (2 miles). The pipeline includes a 1.6 km (1 mile) segment to deliver the clean water and a 1.6 km (1 mile) segment for the return line. In Case 2, the main water loop is designed to deliver clean water at flow rates of 908 m³/d (12,000 bbl/d), with a total pressure drop of 359 kPa (52 psi). Branch lines for each ARF were sized smaller than the main lines because the branch lines accommodate lower flow rates.

High-density polyethylene (HDPE) pipes were chosen over polyvinyl chloride (PVC) pipes. While both are durable and strong for water piping applications, HDPE is more resistant to salt, corrosive fluids, and abrasion from dust and precipitates. Thus, HDPE is better suited to transport high-salinity geothermal fluid (PPI, 2019). All pipes buried underground are insulated and covered with a jacketing layer. Two insulation materials, Foamglas® and Gilsulate®, were assessed and compared with other insulative materials. Based on company quotes, Foamglas insulation costs \$15.06/ft., and a thickness of 0.05 m (2.0 inches) is required for a 0.14 m (5.5 inches) pipe. Gilsulate is estimated to cost \$500/cubic yard, which is equivalent to \$14–\$37/ft of pipe, depending on the number and size of pipes in each trench, assuming that Gilsulate is filled in the trench from 0.05 m [2.0 inches] below the pipes and 0.05 m [2.0 inches] above the pipes). Ultimately, Foamglas insulation was selected because it is less expensive. Based on heat transfer calculations, 0.05 m (2.0 inches) thick insulation is required to limit the temperature change to 0.56°C (1°F) over mile.

Total piping cost includes the piping material, insulation material, fittings and valves, and pipe laying (installation). The prices (\$/ft) of HDPE pipes varying by size and pressure ratings. The prices (\$/ft) of various Foamglas pipes with all-service jacketing were also quoted by vendors. The cost of fittings and valves was assumed to be 5% of the total cost of materials. The cost of pipe installation was estimated using rates reported in the literature, that are corrected for inflation (USDA, 2007). The estimated piping costs are shown in Table 17.

Table 17. Estimated Costs of Main and Branch Hydronic Piping Systems

	Description	Pipe length (ft)	Case 1 (\$)	Case 2 (\$)
Main lines	Geothermal fluid	10,560	297,790	297,790
	Clean water supply	5,280	148,895	148,895
	Clean water return	5,280	148,895	148,895
Branch lines (supply and return)	Energy Farm	603 (×2)	15,840	18,958
	Beef & Sheep Research Field Laboratory	2,160 (×2)	56,755	67,928
	Poultry Research Farm	1579 (×2)	41,488	41,488
	ISRL	675 (×2)	21,225	26,147
	Dairy Cattle Research Unit	2,377 (×2)	62,442	74,735
	Feed Technology Center	299 (×2)	7,847	7,847
Total			801,179	832,685

Trench Sizing and Costs

The piping will be buried in trenches to limit heat loss and interference with surface activities. According to F&S, a 1.5 m (5.0 ft) of clearance from the bottom of the pipe to the ground surface is required for trenching (Figure 30). The maximum, allowable slope for excavation was set at 1:1, based on the local soil properties. Main and branch lines running in parallel will share the same trench, where possible. For trenches accommodating multiple pipes, a horizontal arrangement (instead of vertical stacking) is preferable for convenient repair and maintenance. F&S recommends that pipes in the same trench be separated by 0.6 m (2.0 ft).

Based on the above assumptions, trenching requirements for the main and branch lines were estimated. Three types of trenches were considered. Trench 1 would house the main pipeline that carries the geothermal fluid and clean water supply, as well as the clean water return line that run from the extraction well to the end of the clean water line near the Energy Farm. Trench 2 would house only the main pipeline carrying geothermal fluid from the end of the clean water lines (Location B in Figure 29) to the injection well. Trench 3 would accommodate the clean water supply and return branch lines for each ARF. Conceptual diagrams of the three types of trenches are shown in Figure 30.

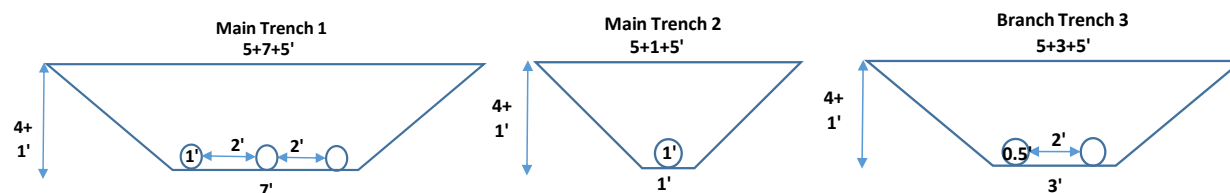


Figure 29. Conceptual diagrams of three types of trenches (Note that the marked pipe diameters include insulation and approximate values for only illustrative purpose).

High-level costs, including those for excavation and backfilling, were estimated for the three types of trenches. Due to their large size, which F&S has limited experience in constructing, the Urbana and Champaign Sanitary District (UCSD), which has experience constructing large-diameter pipelines, was contacted to get additional estimates. Estimates from the USDA for trenching irrigation pipelines (USDA, 2007) were also reviewed. Accordingly, the costs provided by F&S, UCSD, and USDA ranging from \$28 to \$125/ft (Trench 1), \$17 to \$60/ft (Trench 2), and \$23 to \$75/ft (Trench 3). Therefore, \$62.5/ft, \$30.0/ft and \$37.5/ft were considered the best estimates for constructing Trenches 1, 2, and 3, respectively. The total costs for trenching are provided in Table 18. Note, there are no differences in trench sizing or costs between Cases 1 and 2.

Table 18. Estimated Costs of Trench Excavation and Backfilling

	Description	Length (ft)	Excavation and Backfilling Cost (\$)
Trench 1	Pipes (geothermal fluid, water supply & return)	5,280	330,000
Trench 2	Pipe with geothermal fluid	5,280	158,400
Trench 3 (branch water supply and return)	Energy Farm	603	22,609
	Beef & Sheep Research Field Laboratory	2,160	81,007
	Poultry Research Farm	1,579	59,217
	ISRL	675	25,312
	Dairy Cattle Research Unit	2,377	89,125
	Feed Technology Center	299	11,200
Total		18,253	776,870

3.4.3 Estimated Equipment Sizes and Costs and Operating Costs

Equipment sizes, costs, and operating costs for the surface infrastructure were estimated. Equipment costs were estimated using multiple methods. The costs for heat exchanger, clean water

surge tank, surge pump, and surface pump costs were estimated using Aspen Capital Cost Estimator (v. 10). For the fluid surge tank, injection well inlet pump, and heat pump cost estimates, reliable quotes were obtained from several vendors. The air handler, domestic water preheater, and smaller-horsepower pump VFD costs were scaled from catalog pricing of “off-the-shelf” equipment available from a leading national supplier. No spare or replacement equipment were included in the cost estimates. The surface infrastructure equipment specifications, estimates for purchased equipment, and the total installed costs are shown in Table 19. An installation factor of 2 was used to predict the total installed surface facility capital cost based on the total purchased equipment cost.

The total installed cost of the surface facility in Case 1 is \$1,484,000. The total installed cost of the Case 2 surface facility is \$2,048,000. The total costs for piping and trenching reported in Table 19 were rounded to the nearest thousand dollars. Piping and trenching costs were estimated on an installed basis, and were added to the total installed cost of the surface facility equipment in order to calculate the total installed capital cost for each case.

Most of the cost differential between Cases 1 and 2 can be attributed to the inclusion of a heat exchanger (which exchanged more heat in Case 2 requiring a larger heat exchanger), air handler, and heat pump. The heat exchanger chosen contains 316 stainless steel tubes, which will conduct heat from the geothermal fluid. The estimated cost of a heat exchanger with titanium tubes is ~3 times more expensive (See Appendix C4). In addition to the tube bundle(s), heat exchanger also includes an exchanger shell, which is made of carbon steel regardless of tubular material because the clean water will stay on the ARFs’ side of the heat exchanger.

The cost differs significantly for the heat exchangers in Cases 1 and 2 due to the difference in temperature differential being addressed. The heat exchanger was sized to handle a small temperature difference (1.1°C [2.0°F]) between the geothermal fluid exiting the heat exchanger and the clean water entering it. This range was chosen to exchange as much heat as possible with the clean water, but it also increases the size and cost of the heat exchanger. For Case 1, the temperature of the clean water entering the heat exchanger is ~30°C (~86°F) and the temperature of the geothermal fluid leaving the heat exchanger is ~31°C (~88°F). When the heat pump is running in Case 2, the temperature of the clean water entering the heat exchanger is ~20°C (~68°F) and the temperature of the geothermal fluid leaving the heat exchanger is ~21°C (~70°F). The larger temperature difference in Case 2 requires a larger heat exchanger to extract the same amount of energy.

The air handlers for Case 1 were sized to meet the baseload heating requirement for all the ARFs. For Case 1, it was assumed that air handlers in the existing buildings were not in use. New air handlers would be installed for the GES. The air handlers in Case 2 were sized according to the baseload heating requirements of the existing buildings and the peak heating loads for the new buildings. For Case 2, during peak heating, the heaters in the existing buildings would be turned on to provide additional heat through the existing air handlers, and the baseload requirement would be met with new air handlers.

Table 19. Estimated Capital Costs for the Surface Infrastructure

DDU GES Equipment	Specifications			Equipment Costs	
	General Specifications	Case 1	Case 2	Case 1	Case2
Heat Exchanger	316SS tube/CS shell, max. 100 psig	Area =	Area =	\$149,500	\$251,000
		7,018 ft ²	12,759 ft ²		
Surface Pump	Centrifugal, CS, 25/100 psig in/outlet	182 gpm/11 hp	390 gpm/23 hp	\$9,200	\$11,400
Air Handler	20 handlers for six ARFs; 70°F/95°F air inlet/outlet	Total capacity = 2.0 MMBtu/hr (all for baseload heating)	Total capacity = 4.6 MMBtu/hr (peak for new and baseload for existing buildings)	\$61,600	\$124,000
Domestic Water Preheater	21 preheaters; 60–86°F preheating			\$37,700	\$37,700
Heat Pump	Heat duty = 2.3 MMBtu/hr, 86°F/108°F inlet/outlet			n/a	\$116,000
Fluid Surge Tank	3,900 gallons FRP tank, near atmospheric pressure			\$17,600	\$17,600
Clean Water Surge Tank	160,000 gallons CS tank, near atmospheric pressure			\$168,000	\$168,000
Injection Well Inlet Pump	Triplex (piston), 316SS 50 psig/1166 psig inlet/outlet, 169 hp			\$285,800	\$285,800
Surge Tank Pump	Centrifugal, 316SS casing, 5 psig/100 psig inlet/outlet, 14 hp			\$12,400	\$12,400
Total Surface Facility Purchased Equipment Cost (PEC)				\$742,000	\$1,024,000
Total Surface Facility Installed Capital Cost				\$1,484,000	\$2,048,000
Piping Cost (Including Materials, Insulation, and Installation)				\$801,000	\$833,000
Trenching, Excavation, and Backfilling Cost				\$777,000	\$777,000
Total Installed Capital Cost				\$3,062,000	\$3,658,000

Estimated annual operating costs were broken down into (1) electricity use and electricity cost per piece of equipment, (2) chemical treatment, (3) NG use (for NG or LPG heaters in existing buildings), and (4) maintenance costs. The unit cost of electricity used in this study is \$0.08/kWh, based on the current rate at U of IL (University of Illinois, 2019b). Most of the operating cost can be attributed to the electricity required to run the pumps. Reduced electricity use for the pumps because of VFDs was accounted for in the capital and operating cost estimates. The chemical

treatment costs are \$30/gallon, and the cost of NG was estimated to be \$5/MMBtu. The total annual operating cost for Case 1 is \$239,732, and for Case 2 \$272,868 (Table 20).

Sensitivity of the LCOH vs. the Total Heat Demand

The sensitivity analysis on the LCOH versus the total heat demand was assessed based on four fluid flow rates. The base flow rate for Cases 1 and 2 is 954 m³/d (6,000 bbl/d), and the costs are shown in Table 19. The additional flow rates of 1,908 m³/d (12,000 bbl/d), 2,862 m³/d (18,000 bbl/d), and 3,816 m³/d (24,000 bbl/d) were also considered.

The scenario for handling 2,862 m³/d (18,000 bbl/d) of fluid assumed (1) an extraction well pumping at 954 m³/d (6,000 bbl/d), (2) a second extraction well pumping at 1,908 m³/d (12,000 bbl/d), (3) an injection well injecting at 954 m³/d (6,000 bbl/d), and (4) a second injection well injecting at 1,908 m³/d (12,000 bbl/d).

The scenario for handling 3,816 m³/d (24,000 bbl/d) of fluid assumed (1) two extraction wells pumping at 1,908 m³/d (12,000 bbl/d) and (2) two injection wells injecting at 1,908 m³/d (12,000 bbl/d). Following the well capacity estimates (Appendix C1), a maximum flow rate in a single well is 1,908 m³/d (12,000 bbl/d). A flow rate >1,908 m³/d (>12,000 bbl/d) would require additional extraction wells.

The LCOH in \$/MMBtu does not account for the time value of money (Tables 20 and 21), and the equipment cost is not discounted over time. The life of the project was assumed to be 50 years. To calculate the cost of heat, the total capital cost was divided by 50 years to annualize capital costs. To calculate the LCOH, the annual capital cost was added to the annual operating cost and divided by the annual heating load.

The estimated costs of (1) purchasing surface equipment, (2) installation, (3) constructing the extraction and injection well(s), (4) installing the pipelines and distribution piping, (5) total capital and operation costs (Figures 31 and 32), and (6) the heating load for each sensitivity case were determined (Tables 20 and 21).

Table 20. Case 1: Sensitivity of Capital and Operating Cost of Heat vs. Total Heat Demand

Geothermal Fluid Flow Rate bbl/day	Surface Equipment Total Purchased Cost	Surface Equipment Total Installed Cost	Extraction Well Cost*	Injection Well Cost*	Fluid and Water Pipelines Cost	Total Capital Cost	Operating Cost, \$/year	Heat Load, MMBtu/yr	Levelized Cost of Heat (\$/MMBtu)
6,000	\$742,000	\$1,484,000	\$4,300,000	\$3,820,000	\$1,578,000	\$11,182,000	\$239,732	7,994	58.0
12,000	\$1,125,000	\$2,250,000	\$5,100,000	\$4,450,000	\$2,392,000	\$14,192,000	\$479,463	15,988	47.7
18,000	\$1,434,000	\$2,868,000	\$9,400,000	\$8,270,000	\$3,051,000	\$23,589,000	\$719,195	23,982	49.7
24,000	\$1,705,000	\$3,410,000	\$10,200,000	\$8,900,000	\$3,625,000	\$26,135,000	\$958,926	31,976	46.3

* From Kirksey and Lu (2019) and Appendix C1

Table 21. Case 2: Sensitivity of Capital and Operating Cost vs. Total Heat Demand

Geothermal Fluid Flow Rate bbl/day	Surface Equipment Total Purchased Cost	Surface Equipment Total Installed Cost	Extraction Well Cost*	Injection Well Cost*	Fluid and Water Pipelines Cost	Total Capital Cost	Operating Cost, \$/year	Heat Load, MMBtu/yr	Levelized Cost of Heat (\$/MMBtu)
6,000	\$1,024,000	\$2,048,000	\$4,300,000	\$3,820,000	\$1,610,000	\$11,778,000	\$272,868	9,992	50.9
12,000	\$1,552,000	\$3,104,000	\$5,100,000	\$4,450,000	\$2,440,000	\$15,094,000	\$545,737	19,984	42.4
18,000	\$1,980,000	\$3,960,000	\$9,400,000	\$8,270,000	\$3,112,000	\$24,742,000	\$818,605	29,976	43.8
24,000	\$2,353,000	\$4,706,000	\$10,200,000	\$8,900,000	\$3,699,000	\$27,505,000	\$1,091,473	39,968	41.1

* From Kirksey and Lu (2019) and Appendix C1

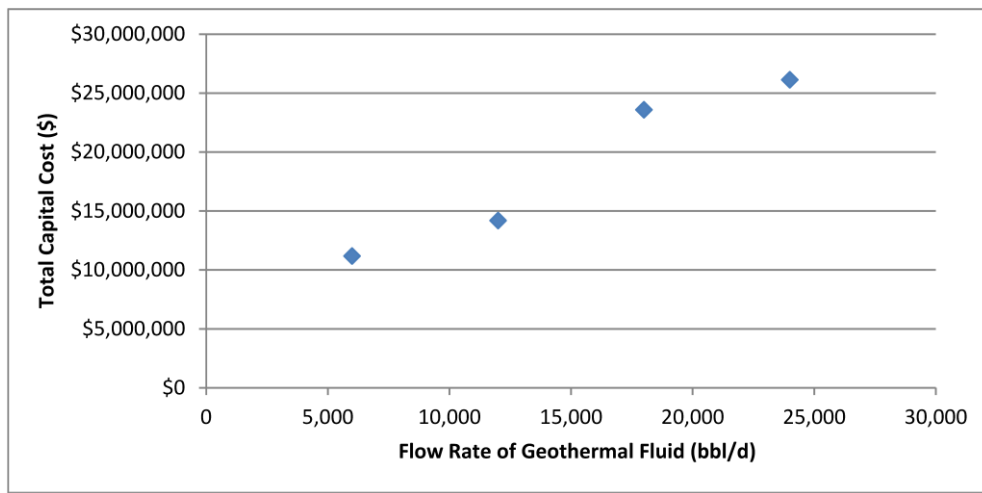


Figure 30. Case 1 – Sensitivity of Capital Costs versus Total Heating Demand.

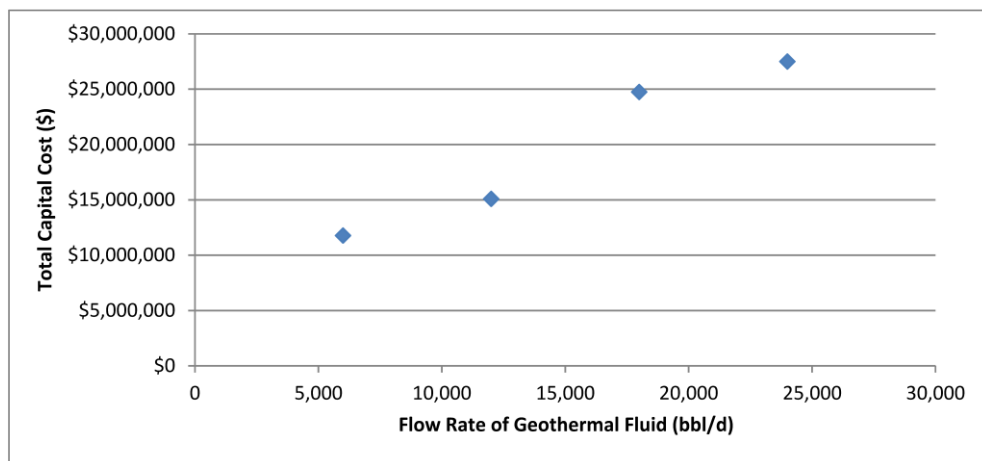


Figure 31. Case 2 – Sensitivity of Capital Costs versus Total Heating Demand.

3.5 Criterion 5 – Costs and Benefits Methodology

3.5.1 Tecno-Economic Analyses: LCCA Metrics and Results

The LCCA of the DDU GES economics included LCOH, NPV, ROI, and SIR. The following describes inputs to the LCCA: (1) geographical boundaries of the end-users (Section 3.3.2), (2) DDU GES surface and subsurface equipment design (Section 3.4.2), (3) estimated surface facility capital costs and annual O&M costs for Cases 1 and 2 (Section 3.4.3), and (4) the results of the sensitivity analysis of LCOH versus total heat demand (Section 3.4.3). The sensitivity analysis calculated preliminary (i.e., without using discount rates or using a present value approach) LCOH values for Cases 1 and 2. The initial capital cost, annual heat output, first year costs, and first year energy savings were also used as inputs (Table 22).

Table 22. Summary of Initial Conditions for Cases 1 and 2

Case	Initial Capital Cost	Annual Heat Output (MMBtu)	First Year Costs				First Year Energy Savings
			Electricity Consumption	NG	O&M	Chemicals	
1	\$11.182	7,994	\$142,703		\$84,539	\$12,490	\$39,970
2	\$11.778	9,992	\$149,042	\$4,247	\$107,090	\$12,490	\$49,960

The LCCA used a present value approach in constant dollars using the USDOE’s 3% value for the real discount rate (excluding general price inflation) and the 2019 U.S. Department of Commerce’s NIST Energy Price Indices (Lavappa and Kneifel, 2019). A 2% escalation factor for non-fuel costs (e.g., maintenance and chemical treatments) was used in the LCCA analysis. The results of the LCCA and LCOH analyses are presented in Table 23.

3.5.2 Project Business Case

The feasibility study demonstrates that there are quantifiable and nonquantifiable benefits to implementing the proposed DDU GES at the U of IL. The quantifiable costs and benefits are illustrated through (1) the results of the LCCA undertaken to assess project economics and (2) the results of the LCA (cf. Thomas et al., 2020). The LCA analysis results emphasize the environmental benefits of the DDU GES and demonstrates its potential to offset ARFs’ emissions within the first 10 years of operation. In terms of nonquantifiable environmental benefits, the GES will support the U of IL’s effort to meet sustainability goals by including geothermal energy in the energy portfolio (as further described in “Environmental Benefits”).

Project Economics

Since the NPV for Case 2 is lower than for Case 1, Case 1 is considered more financially viable option (Table 23). Considering SIR values, (a metric that the federal government and military currently use to evaluate project economics), neither Case 1 or 2 is financially viable (the standard value for financial viability is ≥ 1.25). Considering SIR values and the negative NPV values for Cases 1 and 2, neither GES should be built *if* project economics are the only variable used in the decision-making.

Table 23. LCCA and LCOH Results

	Variable	Case 1	Case 2
Project Capital Costs	C_{Cap}	\$11,182,000	\$11,778,000
Project O&M Costs (includes fuel)	$C_{O\&M}$	\$10,293,528	\$11,746,171
Heat Extracted over 50 years (MMBtu)	Q_{50}	399,700	499,600
Discounted Heat Extracted over 50 years (MMBtu)	Q_d	211,854	264,805
Energy Savings (\$ Value of Heat Extracted)	ES	\$2,560,990	\$3,201,077
Net Present Value	NPV	(\$18,914,538)	(\$20,323,093)
Discounted Payback (years)	DPB	not applicable	not applicable
Return on Investment (ROI)	ROI	(0.8807)	(0.8639)
Savings to Investment Ratio (SIR)	SIR	0.23	0.27
Levelized Cost of Heat (LCOH)¹	LCOH	\$101.37	\$88.84
Project Lifetime	t	50 years	
USDOE Discount Rate²	d	3.0%	
Electricity Escalation Indices³	$Elec_i$	Ranges from 0.99 to 0.88	
Natural Gas Escalation Indices⁴	NG_i	Ranges from 1.03 to 1.54	
Non-Fuel Cost Escalation Rate⁵	e	2.0%	

¹Using the time value of money with all discount and escalation factors, compared to Tables 20 and 21

²Page 1, NIST 85-3273-34 (Lavappa and Kneifel, 2019), USDOE Discount Rate

³Pages 35-36, NIST 85-3273-34 (Table Ca-2: Commercial-Natural Gas) in Lavappa and Kneifel (2019)

⁴Pages 35-36, NIST 85-3273-34 (Table Ca-2: Commercial-Electricity) in Lavappa and Kneifel (2019)

⁵Assumption based on current inflation projections and research

LCOH results highlight one benefit of the proposed DDU GES. The preliminary LCOH values calculated via the sensitivity analysis (Section 3.4.3) were \$58.0/MMBtu for Case 1 and \$50.9/MMBtu for Case 2. These values were converted using a present value approach in constant dollars. For Case 1, the LCOH is \$101.37/MMBtu, whereas for Case 2 the LCOH is \$88.84/MMBtu. The LCOH for Case 2 is lower because a heat pump is used to meet the peak heating requirements. While the LCOH values are relatively high, this is *not* the only metric that should be considered in evaluating the overall feasibility of the proposed DDU GES. The following subsection describes the results of the LCA analysis, which ought to be the key motivating factor for installing the proposed GES at the U of IL.

Environmental Impacts and Benefits

The proposed DDU GES will advance the U of IL effort to meet its 2050 carbon neutrality goal by offsetting carbon emissions from the ARFs that would otherwise be generated following “business as usual” operations. This feasibility study went beyond an evaluation of project economics and examined the environmental impacts of the GES, in terms of carbon emissions, by performing an LCA analysis that calculated the life cycle impacts for each lifecycle stage as well as the overall lifecycle of the proposed GES.

For the material production phase, the use of steel and concrete made to construct the extraction and injection wells leaves a significantly large environmental footprint. Additionally, the diesel fuel used during the material transport and construction phase constitutes a significant environmental impact. Together, the use of concrete, steel, and diesel are the top contributors to the GWP and fossil fuel depletion impacts associated with these two lifecycle phases of the DDU GES. Of the four phases of its lifecycle, operating the GES (i.e., use of system phase) contributes the most to GWP (kg eCO₂). The high levels of emissions resulting from its operation can be attributed to the generation of electricity used to run the pumps, heat exchangers, and other handling equipment. The impacts associated with each lifecycle stage are compared in Figure 33. (Lifecycle totals for each impact category can be found in Appendix B6.)

Emissions from the ARFs were calculated using available emissions data for LPG and NG usage (Table 24). Although there are CO₂ emissions associated with the DDU GES, it can still offset the environmental impacts associated with using fossil fuels at the ARFs (i.e., LPG and NG) in the first 10 years).

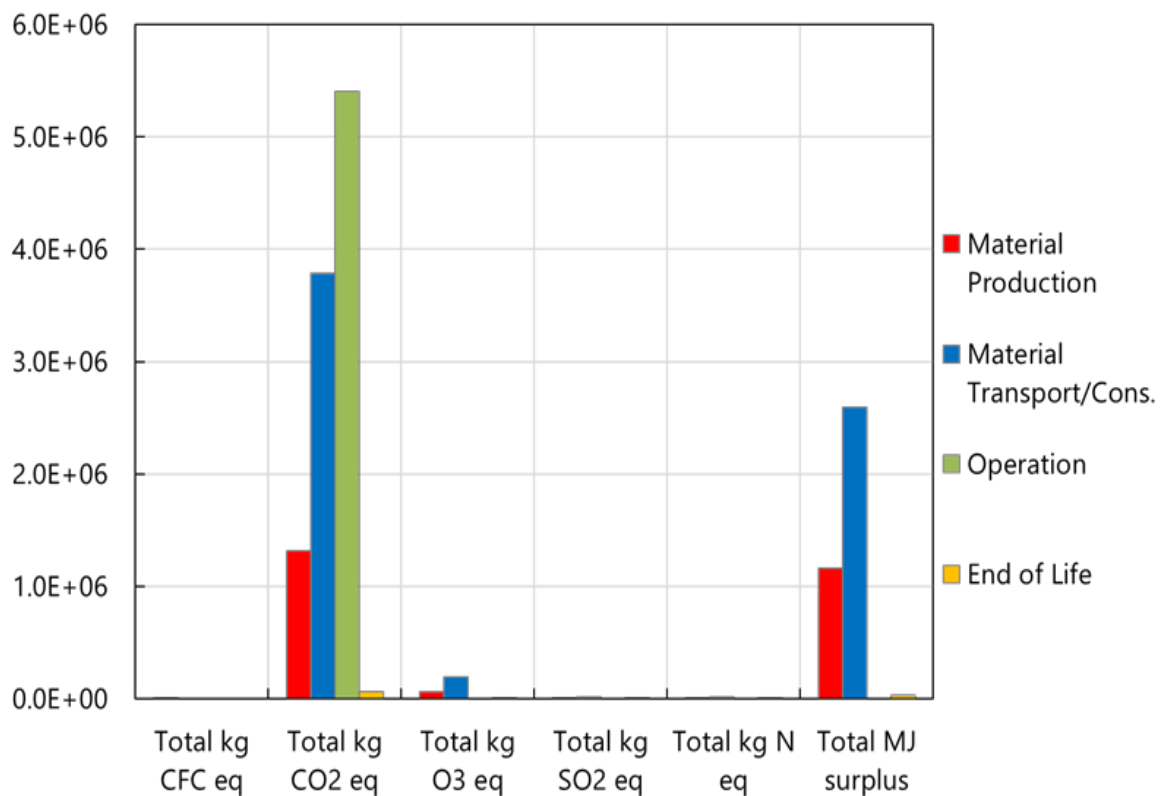


Figure 32. Impact comparison of the four life cycle stages, showing significant GWP associated with the operation of the DDU GES.

Table 24. Emissions Associated with Current Heating Operations at the ARFs

Emissions Sources	
Annual NG Use (MMBtu/yr)	5,638
Emissions from NG (kg CO ₂ /MMBtu)	53.07
Annual Propane Use (MMBtu/yr)	3,814
Emissions from Propane (kg CO ₂ /MMBtu)	63.07
Existing Energy Corridor Emissions (kg CO ₂ /yr)	5.40×10 ⁵
Years until DDU emissions offset	10.02

The proposed DDU GES, considering the current environmental impacts from the ARFs, is a comparable alternative and would improve campus performance in annual energy use, GWP, water consumption, waste production, and annual heat production. Based on the estimated, low-end of GES heat production over the entire lifetime of operation, the GES could produce 2,053% more heat than is currently required by the ARFs. These results show that, despite its environmental impacts, there are tangible benefits that make installing and operating the proposed DDU GES an environmentally sustainable investment that would advance the U of IL towards its sustainability goals.

CONCLUSIONS

The use of a doublet well system for the DDU GES at the U of IL is technically feasible with surface infrastructure designs to meet 80% and 100% of the ARFs' heating requirements through 2050. The use of LMSS 44°–46°C (111°–115°F) geothermal fluid at a flow rate of 954 m³/d (6,000 bbl/d) results in a very small drop in temperature <1.1°C (<2.0°F) in the extraction well and between the different end users. Costs of energy, as determined by the LCOH analysis, are \$46.3 to \$58.0 MMBtu/hr for Case 1 and \$41.1 to \$50.9 MMBtu/hr for Case 2 (Stumpf et al., 2020), or \$101.37 for Case 1 and \$88.84 for Case 2, after including the time value of money and all discount and escalation factors.

In addition to evaluating the technical feasibility, project economics, and LCOH of the proposed DDU GES, this feasibility also examined the environmental impacts of the system associated with each stage of its project lifecycle, over the entire lifetime of the project. Within the first 10 years of operation, the proposed DDU GES will offset carbon emissions from the ARFs currently being emitted by “business as usual” operations. Therefore, results of the LCA analysis ought to be weighed more heavily than the results of the LCCA. Besides being technically feasible, the proposed GES exhibits a plethora of environmental benefits, each of which are detailed in the “Life Cycle Analysis (LCA)” subpoint of this section.

The following conclusions are supportive of the main findings of this feasibility study:

Geology

- A stratigraphic column was established for the ARFs. The top of the LMSS is at 1,750 m (~5,743 ft) and has an average thickness of 553 m (~1,810 ft).
- A database for thermo-hydraulic-mechanical properties was developed for the geologic formations in the ILB. The data informed the geologic and geothermal reservoir modeling efforts for the *Geothermal Resource Assessment* of the study site and the entire ILB. Much of the data was collected during previous USDOE-funded deep drilling projects in the ILB (e.g., IBDP).
- The LMSS has the highest porosity and high permeability.
- A database of major chemistry and TDS of geothermal fluid was compiled for the MSS. The geothermal fluid may exceed 200,000 ppm TDS with TSS of ~3,000 ppm.
- A temperature profile (temperature vs. depth) for the ARFs was established using available high resolution DTS data to estimate the temperature of the LMSS at the U of IL.
- A static geocellular model for the MSS was completed, and this information assisted in developing the DDU GES.
- A static geocellular model and reservoir model for the SPS were completed, but it was determined that without using a heat pump or other source of energy, the temperature of geothermal fluid would likely not be high enough to meet the requirements of the ARFs.

Reservoir and Wellbore Modeling

- The LMSS is the most productive geothermal resource at the U of IL study site. Flow rates up to 3,339 m³/d (21,000 bbl/d) were estimated for the formation, which exceed extraction and injection requirements. Therefore, no hydraulic fracturing in the LMSS is required.
- Scenarios were simulated to account for different well spacings, flow rates, and seasonal temperature changes. The C-T front moving out from injection well did not impact the thermal efficiency of the extraction well over the entire life of GES (50 years).
- The vertical distribution of permeability in the MSS impacts the depth of the completion interval. To maintain a flow rate through the surface infrastructure that meets the heating demand of ARFs, the injection well must be in the high porosity zone (base) of the LMSS.
- The thermal wellbore modeling sensitivity analysis determined the amount of heat loss between the subsurface and the surface. Different thermally-conductive cements, annulus fluids, tubing, and casing were evaluated for various well designs and injection temperatures. Generally, wellbore heat loss was very low, primarily due to the high extraction rates needed to meet heating demand at the ARFs. For the extraction well, results showed that temperature change along the wellbore can be kept at <0.6°C (<1°F) by insulating the wellbore. Silicate foam and vacuum-insulated tubing were both shown to be effective insulation methods for minimizing temperature change along the wellbore. For the injection well, results showed that tubing size did not significantly affect temperature change along the wellbore.

Infrastructure

- Pertinent regulations were identified that implicate constructing the DDU GES. The IEPA would likely require a UIC Class 1 (Non-Hazardous) permit for the injection well. However, no DDU GES injection wells have been permitted in Illinois. Therefore, there is some regulatory uncertainty. IEPA and USEPA consultations were encouraging, and it is possible that permits for similar wells in surrounding states or states with low-temperature sedimentary basins where DDU GES projects are proposed could be used as precedent for geothermal injection wells in Illinois.
- Wellbore designs were developed for the extraction and injection wells. Current and recent MSS drilling in the ILB provided accurate, high-level costs of \$4.3 million and \$3.8 million for the extraction and injection wells, respectively. The well design is similar to typical wells used for oil and gas production and NG and CO₂ storage. The cost of treating geothermal fluid per year is \$12,490 for Cases 1 and 2. The database of geothermal fluid chemistry informed the following decisions:
 - It was decided that scale inhibitors and corrosion-resistant construction materials would be used in the GES to avoid adverse impacts from circulating the high-salinity geothermal fluid through the system. This approach is similar to routine oilfield practices.
 - Based on the potential for scaling and precipitation in the GES, the extraction well casing will be lined with plastic to protect against corrosion and a packer will be used such that an insulating fluid in the tubing casing annulus can be used to protect the extraction well casing against corrosion. The casing across the MSS extraction zone will be made of chrome alloy. For the injection well, the

casing across the injection interval will also be made of chrome alloy. HDPE pipes were chosen over PVC pipes because the latter is better suited to transport high-salinity geothermal fluid.

- The maximum flow rate directly impacted the well design and size of the heat exchanger and other surface equipment. Differences in these parameters were shown to significantly change the total capital cost.
- The historic and current energy consumption data received from the end-users at the ARFs indicated that the current cooling demand at each facility is insignificant.
- A distribution piping network for the geothermal fluid and clean water was developed for the ARFs. The proposed piping network provides the flexibility to meet the required end-user heating demands as well as the heating demands for domestic water preheating and other cascading applications.
- In Case 1, the DDU GES provides 80% of the total annual heating load at a design capacity of 2 MMBtu/hr. In Case 2, the DDU GES provides 80% of the total annual heating load and, during peak heating, a heat pump (for new buildings) and existing NG- or LPG-fired heaters (for existing buildings) provide the remaining 20% of the total annual heating load.
- The LCOH in \$/MMBtu was estimated for the DDU GES. The estimated LCOH ranged from \$46.3 to \$58.0 per MMBtu for Case 1 and from \$41.1 to \$50.9 per MMBtu for Case 2 (without using discount rates or a present value approach).
- Capital and O&M costs were estimated for Case 1 and Case 2: \$11,421,732 to \$27,093,926 and \$12,050,868 to \$28,596,473, respectively (Section 3.4.3).

Life Cycle Cost Analysis (LCCA)

- LCCA related values of NPV, ROI, SIR, and LCOH were determined for two DDU cases. For Case 1, the values are NPV = -\$18,914,538, ROI = -88.1%, SIR = 0.23, and LCOH = \$101.37. For Case 2, the values are NPV = -\$20,323,093, ROI = -86.4%, SIR = 0.27, and LCOH = \$88.34.
- The LCOH of the DDU GES is high; however, results of the LCA analysis prove that the environmental benefits of the proposed DDU GES ought to be weighed more heavily than financial and/or economic metrics (see below).

Life Cycle Analysis (LCA)

- An LCA was performed to quantify the overall environmental impacts and benefits of the DDU GES. The results show that the DDU GES would offset the current GHG emissions from the ARFs within the first 10 years of operation.
- LCA identified the cradle-to-grave environmental impacts associated with the DDU GES. The phases of the project lifecycle that were identified as having the largest environmental impacts include the (1) material production phase, (2) material transport and construction phase (specifically, the use of steel and concrete), and (3) use of system phase.

ILB Military Installations

- An assessment of the applicability of DDU technology at military installations in the ILB was completed. Three military installations in the ILB have heating loads sufficiently large enough to utilize a DDU GES similar to the DDU GES proposed for the ARFs.

REFERENCES

- Akar, S., and C. Turchi. 2016. “Low temperature geothermal resource assessment for membrane distillation desalination in the United States.” *Geothermal Resource Council Transactions* 40: 129–140. <http://pubs.geothermal-library.org/lib/grc/1032317.pdf>.
- Allan, M.L., and A.J. Philippacopoulos. 1999. *Properties and Performance of Cement-Based Grouts for Geothermal Heat Pump Applications*. Upton, NY: Brookhaven National Laboratory. BNL-67006. <https://doi.org/10.2172/751116>.
- Allis, R.G., M. Gwynn, C.L. Hardwick, G. Mines, and J.N. Moore. 2015. “Will stratigraphic reservoirs provide the next big increase in U.S. geothermal power generation.” *Geothermal Resource Council Transactions* 39: 389–398. <https://doi.org/10.2172/1399014>.
- Althouse, A.D., C.H. Turnquist, A.F. Bracciano, D.C. Bracciano, and G.M. Bracciano. 2017. “*Modern Refrigeration and Air Conditioning (20th Edition)*.” Tinley Park, Illinois: The Goodheart-Willcox Company, Incorporated.
- Anovitz, L.M., J.T. Freiburg, M. Wasbrough, D.F.R. Mildner, K.C. Littrell, V. Pipich, and J. Ilavsky. 2018. “The Effects of Burial Diagenesis on Multiscale Porosity in the St. Peter Sandstone: An Imaging, Small-Angle, and Ultra-Small-Angle Neutron Scattering Analysis.” *Marine and Petroleum* 92: 4352–4371. <https://doi.org/10.1016/j.marpetgeo.2017.11.004>.
- American Society of Heating, Refrigerating and Air-Conditioning Engineers (ASHRAE). 2017. “ASHRAE Handbook.” Atlanta, GA: American Society of Heating, Refrigerating and Air Conditioning Engineers Atlanta, 1088 p.
- Australian Geothermal Energy Group (AGEG). 2008. *Geothermal Lexicon for Resources and Reserves Definition and Reporting*. Australian Geothermal Energy Group, Geothermal Code Committee. Accessed November 27, 2019: <http://citeseerx.ist.psu.edu/viewdoc/download?doi=10.1.1.670.9571&rep=rep1&type=pdf>.
- Beckers, K.F., M.Z. Lukawski, T.J. Reber, B.J. Anderson, M.C. Moore, and J.W. Tester. 2013. “Introducing GEOPHIRES v1.0: Software Package for Estimating Levelized Cost of Electricity and/or Heat from Enhanced Geothermal Systems.” Presented at the Thirty-Eighth Workshop on Geothermal Reservoir Engineering Stanford University, Stanford, CA, February 11–13, 2013. <https://pangea.stanford.edu/ERE/pdf/IGAstandard/SGW/2013/Beckers.pdf>.
- Beckers, K.F., and K. McCabe. 2018. *Introducing GEOPHIRES v2.0: Updated Geothermal Techno-Economic Simulation Tool*. Golden, CO: National Renewable Energy Lab. NREL/CP-5500-70856. <https://www.nrel.gov/docs/fy18osti/70856.pdf>.

Beckers, K.F., and K. McCabe. 2019. “GEOPHIRES v2.0: Updated Geothermal Techno-Economic Simulation Tool.” *Geothermal Energy* 7(5). <https://doi.org/10.1186/s40517-019-0119-6>.

Benoit, D. 1978. “The use of shallow and deep temperature gradients in geothermal exploration in northwest Nevada using the Desert Peak thermal anomaly as a model.” *Geothermal Resource Council Transactions* 2(7): 45–46. <http://pubs.geothermal-library.org/lib/grc/1000118.pdf>.

Breunig, H.M., J.T. Birkholzer, A. Borgia, P.N. Price, C.M. Oldenburg, and T.E. McKone. 2013. *Assessment of Brine Management for Geologic Carbon Sequestration*. Berkeley, CA: Lawrence Berkeley National Laboratory. LBNL-6361E. <https://doi.org/10.2172/1166990>.

Burch, S.L., B.R. Hensel, J.S. Nealon, and E.C. Smith. 1987. *An Assessment of Class V Underground Injection in Illinois*. Champaign, IL: Illinois State Water Survey. Contract Report 425. <http://hdl.handle.net/2142/73864>.

Buschbach, T.C., and D.R. Kolata. 1991. “Regional Setting of Illinois Basin.” In Leighton, M.W., D.R. Kolata, D.F. Oltz, and J.J. and Eidel, eds. *Interior Cratonic Basins*. Tulsa, OK: American Association of Petroleum Geologists. Memoir 51. 29–55. <https://pubs.geoscienceworld.org/books/book/1351/chapter/107171640/regional-setting-of-illinois-basin>.

Buschbach, T.C., and D.C. Bond. 1974. *Underground storage of natural gas in Illinois, 1973*. Champaign, IL: Illinois State Geological Survey, Illinois Petroleum 101, 71 p. <http://hdl.handle.net/2142/43186>.

CABOT Corporation. 2019. *Formate Technical Manual*. Alpharetta, GA: Cabot Corporation.

CDM Smith Incorporated, 2014. “Guidance manual for permitting Class I and Class II wells for the injection and disposal of desalination concentrate.” Prepared for the Texas Water Development Board. http://www.twdb.texas.gov/publications/reports/contracted_reports/doc/1004831106_injectionwells.pdf.

Champaign County Regional Planning Commission (CCRPC). 2017. *Curtis Road Corridor Study*. Champaign, IL: Champaign County Regional Planning Commission. Curtis Road Corridor Study Steering Committee. <https://ccrpc.org/wp-content/uploads/2016/10/Curtis-Road-Corridor-Study-120117.pdf>.

Damico, J. 2019a. “Geocellular model of St. Peter Sandstone for University of Illinois at Urbana-Champaign DDU Feasibility Study [data set].” Urbana, IL: University of Illinois. <https://doi.org/10.15121/1495414>.

Damico, J. 2019b. “Geocellular Model of Mt. Simon Sandstone for University of Illinois at Urbana-Champaign DDU feasibility study [data set].” Urbana, IL: University of Illinois. <https://doi.org/10.15121/1495417>.

Damico, J., L.M. Anovitz, J.T. Freiburg, M. Wasbrough, D.F.R. Mildner, K.C. Littrell, V. Pipich, J. Ilavsky, and M.L. Szulczewski. 2018. “University of Illinois Campus Deep Direct-Use Feasibility Study – Porosity and Permeability of Rock Formations [data set].” Urbana, IL: University of Illinois. <https://doi.org/10.15121/1458561>.

Eckaus, R.S. 1992. “Comparing the Effects of Greenhouse Gas Emissions on Global Warming.” *The Energy Journal* 13(1): 25–35.

Eckstein, Y., P.S. Dahl, and C.J. Vitaliano. 1983. “Petrographic and Physical Factors Controlling Thermal Conductivity of Granitic Rocks in Illinois Deep Holes UPH 1, 2, and 3.” *Journal of Geophysical Research* 88(B9): 7381–7385. <https://doi.org/10.1029/JB088iB09p07381>.

Erbs, D.G., S.A. Klein, W.A. Beckman. 1983. “Estimation of degree-days and ambient temperature bin data from monthly-average temperatures.” *ASHRAE Journal* 25(6): 60–65.

Finley, R.J., S.E. Greenberg, S.M. Frailey, I.G. Krapac, H.E. Leetaru, and S. Marsteller. 2011. “The Path to a Successful One-Million Tonne Demonstration of Geological Sequestration: Characterization, Cooperation, and Collaboration.” *Energy Procedia* 4: 4770–4776. <https://doi.org/10.1016/j.egypro.2011.02.441>.

Fleuchaus, P., B. Godschalk, I. Stober, and P. Blum. 2018. “Worldwide Application of Aquifer Thermal Energy Storage – A Review.” *Renewable and Sustainable Energy Reviews* 94: 861–876. <https://doi.org/10.1016/j.rser.2018.06.057>.

Frailey, S.F., J.R. Damico, and H.E. Leetaru. 2011. “Reservoir Characterization of the Mt. Simon Sandstone, Illinois Basin, USA.” *Energy Procedia* 4: 5487–5494. <https://doi.org/10.1016/j.egypro.2011.02.534>.

Frailey, S.M., J.P. Grube, B. Seyler, and R.J. Finley. 2004. “Investigation of Liquid CO₂ Sequestration and EOR in Low Temperature Oil Reservoirs in the Illinois Basin.” Presented at SPE/DOE 14th Symposium on Improved Oil Recovery. Tulsa, OK, April 17–21. Society of Petroleum Engineers. SPE-89342-MS. <https://doi.org/10.2118/89342-MS>.

Freeze, R.A., and J.A. Cherry. 1979. *Groundwater*. Englewood Cliffs, New Jersey: Prentice-Hall Incorporated. http://hydrogeologistswithoutborders.org/wordpress/wp-content/uploads/Freeze_and_Cherry_1979-smaller.pdf.

Freiburg J.T., R.W. Ritzi, and K.S. Kehoe. 2016. Depositional and Diagenetic Controls on Anomalously High Porosity within a Deeply Buried CO₂ Storage Reservoir the Cambrian Mt.

Simon Sandstone, Illinois Basin, USA. *International Journal of Greenhouse Gas Control* 55: 42–54. <https://doi.org/10.1016/j.ijggc.2016.11.005>.

Freiburg, J.T., D.G. Morse, H.E. Leetaru, R.P. Hoss, and Q. Yan. 2014. *A Depositional and Diagenetic Characterization of the Mt. Simon Sandstone at the Illinois Basin – Decatur Project Carbon Capture and Storage Site, Decatur, Illinois, USA*. Champaign, IL: Illinois State Geological Survey. Circular 583. <http://hdl.handle.net/2142/55338>.

Grant, M.A., and P.F. Bixley. 2011. *Geothermal Reservoir Engineering*. Burlington, Massachusetts: Elsevier Incorporated. <https://doi.org/10.1016/B978-0-12-383880-3.10022-8>.

Hesaraki, A., S. Holmberg, and F. Haghighat. 2015. “Seasonal Thermal Energy Storage with Heat Pumps and Low Temperatures in Building Projects—A Comparative Review.” *Renewable and Sustainable Energy Reviews* 43: 1199–1213. <https://doi.org/10.1016/j.rser.2014.12.002>.

Hu, M. 2019. “Cost-Effective Options for the Renovation of an Existing Education Building toward the Nearly Net-Zero Energy Goal—Life-Cycle Cost Analysis.” *Sustainability* 11: 2444. <https://doi.org/10.3390/su11082444>.

International Atomic Energy Agency (IAEA). 2019. “Energy, Electricity and Nuclear Power Estimates for the Period up to 2050.” Vienna, Austria: International Atomic Energy Agency. Reference Data Series No. 1. <https://www.iaea.org/publications/13591/energy-electricity-and-nuclear-power-estimates-for-the-period-up-to-2050>.

Illinois Pollution Control Board (IPCB). 2018. “Environmental Protection (Rule: Title 35, Subtitle G: Waste Disposal, Chapter I: Pollution Control Board, Subchapter D: Underground Injection Control and Underground Storage Tank Programs).” Springfield, IL: Illinois Pollution Control Board. Part 730, Section 730.105 Classification of Injection Wells. <https://pcb.illinois.gov/documents/dsweb/Get/Document-12249/>.

Kabassi, K., and Y.K. Cho. 2012. “BLCC Analysis derived from BIM and energy data of Zero Net Energy Test Home.” In *ICSDC 2011: Integrating Sustainability Practices in the Construction Industry*. Reston, VA: American Society of Civil Engineers, 292–298. <https://doi.org/10.1061/9780784412046>.

Kaplan, R., D. Mamrosh, H.H. Salih, and S.A. Dastgheib. 2017. “Assessment of Desalination Technologies for Treatment of a Highly Saline Brine from a Potential CO₂ Storage Site.” *Desalination* 404: 87–101. <http://dx.doi.org/10.1016/j.desal.2016.11.018>.

KDHE (Kansas Department of Health and Environment), 2012. “Class V underground injection control (UIC) heat pump & air conditioning return flow well requirements.” Topeka, KS: Kansas Department of Health and Environment, Bureau of Water. Procedure #:UICV-3. <http://www.kdheks.gov/uic/download/UICV-3.pdf>.

Kirksey, J., and Y. Lu. 2019. “Extraction/Injection Well Design for Deep Direct Use at University of Illinois at Urbana-Champaign [data set].” Urbana, IL: University of Illinois. <https://doi.org/10.15121/1526474>.

Lavappa, P., and J.D. Kneifel. 2019. *Energy Price Indices and Discount Factors for Life-Cycle Cost Analysis – 2019 Annual Supplement to NIST Handbook 135*. Gaithersburg, MD: National Institute of Standards and Technology. NISTIR 85-3273-34. <https://doi.org/10.6028/NIST.IR.85-3273-3>.

Leetaru, H.E. 2014. “An Evaluation of the Carbon Sequestration Potential of the Cambro-Ordovician Strata of the Illinois and Michigan Basins.” Champaign, IL: Illinois State Geological Survey. DOE-DE-FE0002068 Final Report. <https://doi.org/10.2172/1167490>. <http://hdl.handle.net/2142/95114>.

Leetaru, H.E., S. Frailey, D. Morse, R.J. Finley, J.A. Rupp, J.A. Drahozval, and J.H. McBride. 2009. “Carbon sequestration in the Mt. Simon Sandstone saline reservoir” In Grobe M., Pashin, J.C., and Dodge, R.L., eds. *Carbon Dioxide Sequestration in Geological Media—State of the Science*. Tulsa, OK: American Association of Petroleum Geologists. Studies in Geology 59: 261–277. <https://doi.org/10.1306/13171243St592566>.

Limberger, J., T. Boxem, M. Pluymaekers, D. Bruhn, A. Manzella, P. Calcagno, F. Beekman, S. Cloetingh, and J.-D. van Wees. 2018. “Geothermal energy in deep aquifers: A global assessment of the resource base for direct heat utilization.” *Renewable and Sustainable Energy Reviews*, 82(1), 961–975. <https://doi.org/10.1016/j.rser.2017.09.084>.

Lin, Y.-F. 2017. “Geothermal Heat Recovery Complex: Large-Scale, Deep Direct-Use System in a Low-Temperature Sedimentary Basin.” Presented at 2017 U.S. Department of Energy Geothermal Technologies Project Peer Review. Denver, CO, November 13–15, 2017. https://www.energy.gov/sites/prod/files/2017/12/f46/1_1_DDU_U_of_IL_Geothermal_Heat_Recovery_Presentation.pdf.

Lin, Y.-F. 2018. “University of Illinois Campus Deep Direct-Use Feasibility Study – Long-Term Meteorological Data [data set].” Urbana, IL: University of Illinois. <https://doi.org/10.15121/1458558>.

Lin, Y.-F., E. Mehnert, J. Damico, S. Frailey, H.E. Leetaru, R. Okwen, B. Storsved, A. Valocchi, J. Kirksey. 2018. “University of Illinois Campus Deep Direct-Use Feasibility Study – Subsurface Temperature Profile [data set].” Urbana, IL: University of Illinois. <https://doi.org/10.15121/1458560>.

Malkewicz, N., J. Kirksey, and R. Finley. 2015. “Drilling, Completion, and Data Collection Plans An Assessment of Geological Carbon Sequestration Options in the Illinois Basin: Phase

III. IL, Champaign: Illinois State Geological Survey. DE-FC26-05NT42588 Topical Report 4, 417 p. <https://www.osti.gov/servlets/purl/1222708>.

McDaniel, A., D. Fratta, J.M. Tinjum, and D.J. Hart. 2018a. “Long-Term District-Scale Geothermal Exchange Verified Monitoring with Fiber Optic Distributed Temperature Sensing.” *Geothermics* 72(3): 193–204. <https://doi.org/10.1016/j.geothermics.2017.11.008>.

McDaniel A, J. Tinjum, D.J. Hart, Y-F Lin, A. Stumpf, L. Thomas. 2018b. “Distributed Thermal Response Test to Analyze Thermal Properties in Heterogeneous Lithology.” *Geothermics* 76: 116–124. <https://doi.org/10.1016/j.geothermics.2018.07.003>.

Morrow C.A., J.O. Kaven, D.E. Moore, and D.A. Lockner. 2017. Physical Properties of Sidewall Cores from Decatur, Illinois. Reston, VA: U.S. Geological Survey. Open-File Report 2017-1094. <https://doi.org/10.3133/ofr20171094>.

Morse, D.G., and H.E. Leetaru. 2005. “Reservoir Characterization and Three-Dimensional Models of Mt. Simon Gas Storage Fields in the Illinois Basin.” Champaign, IL: Illinois State Geological Survey. Circular 567. <http://hdl.handle.net/2142/73423>.

Morse, D.G., and H.E. Leetaru. 2003. “Reservoir Characterization & 3D Models of Mt. Simon Gas Storage Fields in the Illinois Basin.” Champaign, IL: Illinois State Geological Survey. DE-FG26-99FT40375 Final Report and ISGS Open File 2003-13, 148 p. <http://library.isgs.illinois.edu/Pubs/pdfs/ofs/2003/ofs2003-13.pdf>.

Muffler, L.P.J. 1977. “1978 USGS Geothermal Resource Assessment.” 1st Workshop on Geothermal Reservoir Engineering, Stanford University, p. 3–8. <https://pangea.stanford.edu/ERE/pdf/IGAstandard/SGW/1977/Muffler.pdf>.

Muffler, L.P.J. 1978. “Assessment of Geothermal Resources of the United States: 1978.” Reston, VA: U.S. Geological Survey. Circular 790. <https://doi.org/10.3133/cir790>.

Muffler, L.P.J., and R. Cataldi. 1978. “Methods for the Regional Assessment of Geothermal Resources.” *Geothermics* 7(2–4): 53–89. [https://doi.org/10.1016/0375-6505\(78\)90002-0](https://doi.org/10.1016/0375-6505(78)90002-0).

Mullane, M., M. Gleason, K. McCabe, M. Mooney, T. Reber, and K.R Young. 2016. “An Estimate of Shallow, Low-Temperature Geothermal Resources of the United States.” *Geothermal Resources Council Transactions* 40: 735–748. <http://pubs.geothermal-library.org/lib/grc/1032389.pdf>.

National Physical Laboratory. 2017. “Kaye and Laby Tables of Physical and Chemical Constants.” Teddington, Middlesex, UK: <https://web.archive.org/web/20190507172955/http://www.kayelaby.npl.co.uk/toc/>.

Nelson, W.J. in press. “Bedrock Geology of Champaign County, Illinois.” Champaign, IL: Illinois State Geological Survey, Bulletin.

Nelson, W.J. 2018. “University of Illinois Campus Deep Direct-Use Feasibility Study – Bedrock Geology ArcGIS Layers [data set].” Urbana, IL: University of Illinois.
<https://doi.org/10.15121/1458548>.

Nelson, W.J. 2010. “Structural features”. In Kolata, D.R. and C.K. Nimz, C.K., eds. *Geology of Illinois*. Champaign, IL: Illinois State Geological Survey, 90–104.

Nelson, W.J. 1995. Structural features in Illinois. Champaign, IL: Illinois State Geological Survey, Bulletin 100. 144 p. and 2 plates. <http://hdl.handle.net/2142/43644>.

Okwen R, S. Frailey, and S. Dastgheib. 2017. “Brine Extraction and Treatment Strategies to Enhance Pressure Management and Control of CO₂ Plumes in Deep Geologic Formations.” Champaign, IL: Illinois State Geological Survey. DOE-DE-FE0026136 Final Technical Report, 349 p. <http://dx.doi.org/10.2172/1363792>.

Panno S.V., K.C. Hackley, R.A. Locke, I.G. Krapac, B. Wimmer, A. Iranmanesh, and W. Kelly. 2013. “Formation Waters from Cambrian-Age Strata, Illinois Basin, USA: Constraints on their Origin and Evolution.” *Geochimica et Cosmochimica Acta* 122: 184–197.
<https://doi.org/10.1016/j.gca.2015.06.013>.

Pastor, M.S., A.D. Fronda, V.S. Lazaro, and N.B. Velasquez. 2010. Resource Assessment of Philippine Geothermal Areas. Presented at World Geothermal Congress 2010, Bali, Indonesia, April 25–29. <https://www.geothermal-energy.org/pdf/IGAstandard/WGC/2010/1616.pdf>.

Penberthy, W.L. Jr. and J.H. Bayless. 1974. “Silicate Foam Wellbore Insulation.” *Journal of Petroleum Technology* 6: 583–588. <https://doi.org/10.2118/4666-PA>.

Peters, M.S., K.D. Timmerhaus, and R.E. West. 2003. “Plant Design and Economics for Chemical Engineers (5th Edition).” New York, New York: McGraw-Hill Education, 988 p.

Plastic Pipe Institute (PPI). 2019. HDPE High-Density Polyethylene Pipe Systems – Meeting the challenges of the 21st century. Irving, TX: Plastic Pipe Institute, 9 p.
https://plasticpipe.org/pdf/high_density_polyethylene_pipe_systems.pdf.

Ponsioen, T. 2013. The Surplus Cost Method. Retrieved from PRÉSustainability:
<https://www.pre-sustainability.com/news/the-surplus-cost-method-introduction>.

Porro, C., A. Esposito, C. Augustine, and B. Roberts. 2011. “An Estimate of the Geothermal Energy Resource in the Major Sedimentary Basins in the United States,” *Geothermal Resources Council Transactions* 36: 1359–1369. <http://pubs.geothermal-library.org/lib/grc/1030408.pdf>.

Reed, M.J. 1983. “Assessment of Low-Temperature Geothermal Resources of the United States —1982.” Alexandria, VA: U.S. Geological Survey, Circular 892. <https://doi.org/10.3133/cir892>.

Ritzi, R.W., R. Ghose, M. Bottomley, A.J.H. Reesink, J. Best, J.T. Freiburg, and N.D. Webb. 2018. “Linking the Local Vertical Variability of Permeability and Porosity to Newly-Interpreted Lithofacies in the Lower Mt. Simon CO₂ Reservoir.” *International Journal of Greenhouse Gas Control* 68: 26–41. <https://doi.org/10.1016/j.ijggc.2017.09.017>.

Robertson, E.C. 1988. “Thermal Properties of Rocks.” Reston, VA: U.S. Geological Survey, Open-File Report 88-441. <https://pubs.usgs.gov/of/1988/0441/report.pdf>.

Schlumberger Carbon Services. 2012. “Deep Well Monitoring and Verification at the Illinois Basin Decatur Project (Slide 12).” Presented at Midwest Geological Sequestration Consortium Annual Meeting, September 18, 2012. http://www.sequestration.org/resources/PAGSept2012Presentations/06-JimKirksey_PAG2012.pdf.

Schön, J.H. 2015. “Thermal properties (Chapter 9).” In *Physical Properties of Rocks – Fundamentals and Principles of Petrophysics. Developments in Petroleum Sciences* 65: 369–414. <http://dx.doi.org/10.1016/b978-0-08-100404-3.00009-3>.

Shonder, J.A., M.A. Martin, H.A. McLain, and P.J. Hughes. 2000. “Comparative Analysis of Life-Cycle Costs of Geothermal Heat Pumps and Three Conventional HVAC Systems.” *American Society of Heating Refrigerating and Air Conditioning Engineers (ASHRAE) Transactions* 106(2): 551–560. https://www.aivc.org/sites/default/files/airbase_12983.pdf.

SIA-384/6. 2010. “Sondes Géothermiques.” Zurich, Switzerland: The Swiss Society of Engineers and Architects

Sliwa T. and M. Kruszewski. 2017. “The Application of Vacuum Insulated Tubing in Deep Borehole Heat Exchangers.” *AGH Drilling, Oil, Gas* 34(2): 597–616. <http://dx.doi.org/10.7494/drill.2017.34.2.597>.

Solomon, S. 1999. “Stratospheric ozone depletion: A review of concepts and history.” *Reviews of Geophysics* 37(3): 275-316.

Stumpf, A., J. Damico, R. Okwen, T. Stark, S. Elrick, W.J. Nelson, Y. Lu, F. Holcomb, J. Tinjum, F. Yang, S. Frailey, and Y-F. Lin. 2018. “Feasibility of a Deep Direct-Use Geothermal System at the University of Illinois at Urbana-Champaign. *Geothermal Resources Council Transactions* 42: 227–248. <https://www.osti.gov/servlets/purl/1462352>.

Stumpf A.J. and W.S. Dey. 2012. “Understanding the Mahomet aquifer: geological, geophysical, and hydrogeological studies in Champaign County and adjacent areas.” Champaign, IL: Illinois State Geological Survey. Draft Contract no. Illinois-American Water 2007-02899, 480 p. <http://hdl.handle.net/2142/95787>.

Stumpf, A.J., S.M. Frailey, R.T. Okwen, Y. Lu, F.H. Holcomb, J.M. Tinjum, and Y-F. Lin. 2020. “Feasibility of Deep Direct-Use for District-Scale Applications in a Low-Temperature Sedimentary Basin.” Presented at the Forty-Fifth Workshop on Geothermal Reservoir Engineering Stanford University, Stanford, CA, February 10–12, 2020. <https://pangea.stanford.edu/ERE/pdf/IGAstandard/SGW/2020/Stumpf.pdf>.

Stumpf, A.J., and A. Ismail. 2013. “High-Resolution Seismic Reflection Profiling: An Aid for Resolving the Pleistocene Stratigraphy of a Buried Valley in Central Illinois, USA.” *Annals of Glaciology* 54(64): 10–20. <https://doi.org/10.3189/2013AoG64A602>.

Thomas, L.K., J.M. Tinjum, and F.H. Holcomb. 2020. “Environmental Life Cycle Assessment of a Deep Direct-use Geothermal System in Champaign, Illinois.” Presented at the Forty-Fifth Workshop on Geothermal Reservoir Engineering Stanford University, Stanford, CA, February 10–12, 2020. <https://pangea.stanford.edu/ERE/pdf/IGAstandard/SGW/2020/Thomas.pdf>

University of Illinois. 2015. “2015 iCAP – Illinois Climate Action Plan: Climate Action Plan for the University of Illinois at Urbana-Champaign.” Urbana, IL: University of Illinois. <https://icap.sustainability.illinois.edu/files/project/2634/2015iCAPweb.pdf>.

University of Illinois. 2018a. “University of Illinois Campus Deep Direct-Use Feasibility Study – Thermal Properties of Geologic Formations in Illinois Basin [data set].” Urbana, IL: University of Illinois. <http://gdr.openei.org/submissions/1060>.

University of Illinois. 2018b. “University of Illinois Campus Deep Direct-Use Feasibility Study – Geological Characterization of the St. Peter Sandstone [data set].” Urbana, IL: University of Illinois. <http://gdr.openei.org/submissions/1056>.

University of Illinois. 2018c. “University of Illinois Campus Deep Direct-Use Feasibility Study – Geological Characterization of the Mt. Simon Sandstone [data set].” Urbana, IL: University of Illinois. <http://gdr.openei.org/submissions/1058>.

University of Illinois. 2018d. “University of Illinois Campus Deep Direct-Use Feasibility Study – Chemistry of Formation Waters [data set].” Urbana, IL: University of Illinois. <http://gdr.openei.org/submissions/1063>.

University of Illinois. 2018e. “The Impact of Place: University of Illinois at Urbana-Champaign Campus Master Plan (August 2018).” Urbana, IL: University of Illinois.

https://www.uocpres.uillinois.edu/UserFiles/Servers/Server_7758/file/UIUC/mastrpln/uiucmp-tech-rpt-20180828.pdf.

University of Illinois. 2019a. “Farm Facilities: Department of Animal Sciences, College of Agricultural, Consumer and Environmental Sciences, University of Illinois at Urbana-Champaign”. <https://ansc.illinois.edu/research-outreach/farm-facilities>.

University of Illinois, 2019b. “Energy Billing System: Facilities & Services, University of Illinois at Urbana-Champaign.” <https://www.fs.illinois.edu/services/utilities-energy/business-operations/energy-billing-system>.

U.S. Department of Agriculture (USDA). 2007. “Irrigation Pipe Cost Estimator (Version 3).” Washington, DC: U.S. Department of Agriculture (USDA), Natural Resources Conservation Service. <https://ipat.sc.egov.usda.gov/>.

U.S. Department of the Army. 2015. “Energy Security & Sustainability (ES²) Strategy.” Washington, DC: U.S. Department of the Army. 2-204FF1C. <https://www.army.mil/e2/c/downloads/394128.pdf>.

U.S. Department of Defense. 2017. “Installation Energy and Water Security Policy.” Washington, DC: U.S. Department of Defense. Secretary of the Army. Army Directive 2017-07. http://www.asaie.army.mil/Public/ES/doc/Army_Directive_2017-07.pdf.

U.S. Department of Energy (USDOE) 2011. *CO₂ Capture from Biofuels Production and Sequestration into the Mt. Simon Sandstone*. Pittsburgh, PA: U.S. Department of Energy, National Energy Technology Laboratory. DOE/EA-1828. https://www.energy.gov/sites/prod/files/nepapub/nepa_documents/RedDont/EA-1828-FEA-2011.pdf.

U.S. Congress. 2017. *National Defense Authorization Act for Fiscal Year 2018 (Public Law 115–91)*. Washington, DC: 115th U.S. Congress. <https://www.congress.gov/115/plaws/publ91/PLAW-115publ91.pdf>.

U.S. Congress. 2005. *Energy Policy Act of 2005 (Public Law 109-58)*. Washington, DC: 109th U.S. Congress. <https://www.congress.gov/bill/109th-congress/house-bill/6/text>.

U.S. Department of Energy (USDOE), 2019a, *Advanced Energy Storage Initiative*. Washington, DC: U.S. Department of Energy, FY2020 Congressional Budget Request. <https://www.energy.gov/sites/prod/files/2019/04/f61/doe-fy2020-budget-volume-3-Part-2.pdf>.

U.S. Department of Energy (USDOE). 2019b. *Federal Energy Management Program, Building Life Cycle Cost Programs*. Washington, DC: U.S. Department of Energy. <https://www.energy.gov/eere/femp/building-life-cycle-cost-programs>.

U.S. Environmental Protection Agency (USEPA). 1999. “Geothermal Direct Heat Return Flow Wells (Volume 18).” *The Class V Underground Injection Control Study*. Washington, DC: U.S. Environmental Protection Agency. https://www.epa.gov/sites/production/files/2015-08/documents/classvstudy_volume18-geothermaldirectheatreturnflow_1.pdf.

Walker, M.D., L.L. Meyer, J.M. Tinjum, and D.J. Hart. 2015. “Thermal Property Measurements of Stratigraphic Units with Modeled Implications for Expected Performance of Vertical Ground Source Heat Pumps.” *Geotechnical and Geological Engineering* 33(2): 223–238. <https://doi.org/10.1007/s10706-015-9847-y>.

Waples D.W., and J.S. Waples. 2004. “A Review and Evaluation of Specific Heat Capacities of Rocks, Minerals, and Subsurface Fluids (Part 1: Minerals and nonporous rocks).” *Natural Resources Research* 13(2): 97–122. <https://doi.org/10.1023/B:NARR.0000032647.41046.e7>.

Williams C.F., J. DeAngelo, and M.J. Reed. 2015. “Revisiting the Assessment of Geothermal Resources <90 °C in the United States.” *Geothermal Resources Council Transactions* 38: 93–98. <http://pubs.geothermal-library.org/lib/grc/1032137.pdf>.

List of Appendices

A. Comparison of Actual Accomplishments with Goals and Objectives

B. Formulas and Calculations

B1: Geologic and Geocellular Modeling

B2: Fluid Flow Modeling

B3: Surface Infrastructure Modeling – EBS Data Tables

B4: Review of Software for LCCA Spreadsheet Tool

B5: LCCA Equations

B6: Environmental Life Cycle Assessment of a Deep Direct-Use Geothermal System in Champaign, Illinois

C. Subcontractor Reports

C1: Well Design Report

C2: Assessment of Water Chemistry Impacts on Equipment Design and Costs

C3: DDU GES Infrastructure Design

C4: Assessment of Water Chemistry, Heat Distribution Losses, and DDU System Sizing & Costs

C5: Piping and Instrumentation Diagrams (P&IDs); Case 1 and Case 2

C6: Commercialization for Military Applications

D. Products Developed Under Award and Submissions to the Geothermal Data Repository (GDR)

D1: Products Developed Under Award

D2: Submissions to the Geothermal Data Repository (GDR)

E. F&S and U of IL Campus Support

Appendix A – Comparison of Actual Accomplishments with Goals and Objectives

Comparison of Actual Accomplishments with Goals and Objectives				
Recipient Name:		The Board of Trustees of the University of Illinois		
Project Title:		Geothermal Heat Recovery Complex: Large-Scale, Deep Direct-Use System in a Low-Temperature Sedimentary Basin		
Task	Task	Subtask	Goals and Objectives	Accomplishments
PM	Project Management	Project Management	<ul style="list-style-type: none"> • Hold regular meetings with project management team, task group leaders, and project advisors • Participate in quarterly meetings with Deep Direct-Use Feasibility Study Technical and Economic Working Group (DDUFSTEWG). 	<ul style="list-style-type: none"> • Held biweekly meetings with project management team. • Held monthly meetings with task group leaders. • Held annual meetings with project advisors. • Participated in quarterly meetings with DDUFSTEWG.
1.0	Life Cycle Cost Analysis (LCCA)	Life Cycle Cost Analysis (LCCA)	<ul style="list-style-type: none"> • Develop a detailed work flow based on an existing model to perform a quantitative, comparative analysis of the construction and operation of a DDU. 	<ul style="list-style-type: none"> • Developed a detailed work flow for the LCCA. • Developed a new spreadsheet-based LCCA tool after assessing the capabilities of GEOPHIRES and NIST’s BLCC tool suite.
2.0	Geology	2.1 Geologic Modeling 2.2 Reservoir Characterization 2.3 Geocellular Modeling	<ul style="list-style-type: none"> • Complete geologic model, reservoir characterization, and geocellular model. • Compile thermal and hydraulic properties for the ILB. • Develop static geocellular models for the SPS and MSS (the geothermal reservoirs). 	<ul style="list-style-type: none"> • Completed geologic model and established a stratigraphic column for the U of IL campus. • Developed database for thermo-hydraulic-mechanical properties of the geologic formations. • Established temperature gradient for the ILB and determined range of fluid temperatures for the SPS and MSS; temperature in SPS too low to meet majority of end-user demands. • Developed static geocellular models for the SPS and MSS.
3.0	Modeling	3.1 Flow Modeling 3.2 Wellbore Modeling	<ul style="list-style-type: none"> • Develop model scenarios for a doublet well system to deliver geothermal heat to the surface facilities. • Conduct sensitivity analysis for each scenario to understand effects of delivered temperature and flow rate. 	<ul style="list-style-type: none"> • Geothermal reservoir simulations were performed from a static geocellular model of the MSS. • Various scenarios were simulated to account for different well spacings, flow rates, and seasonal temperature changes.

			<ul style="list-style-type: none"> • Determine temperature changes between the subsurface and surface and evaluate effects of different wellbore configurations. 	<ul style="list-style-type: none"> • Wellbore modeling was performed to maximize the delivery of the geothermal resource.
4.0	Infrastructure	<p>4.1 Well Design</p> <p>4.2 Geothermal Fluid Handling</p> <p>4.3 Heating and Cooling Demand Analysis</p> <p>4.4 GES Assessment</p>	<ul style="list-style-type: none"> • Design a GES that provides enough heating and cooling to meet end-user demands; evaluate the different infrastructure components. • Determine salinities SPS and MSS geothermal fluids, which will influence design and cost estimates. • Obtain current and historical heating and cooling load data for the agricultural research facilities. • Complete a site energy analysis. • Determine performance, efficiency, and costs of GES alternatives with respect of operating conditions. • Identify and model cascading applications at agricultural research facilities. 	<ul style="list-style-type: none"> • Designs were developed for the extraction and injection wells in the SPS and MSS. • Obtain historical climate data for U of IL campus. • Calculated high-level cost estimates for wells. • Determined cost of heat \$/MMBtu for use of MSS geothermal fluid. • Compiled major chemistry and TDS composition for MSS geothermal fluid that informed 1) potential for scaling and precipitation; 2) cost of treatment, 3) material used for wells; and 4) fluid flow for sizing heat exchanger. • Obtained heating and cooling demand load data; cooling demand not high enough for GES to be economical. • Identified and modeled possible cascading applications. • Developed a “virtual” piping distribution system between the wells and ARFs; assessed multiple configurations. • Performed a sensitivity analysis on the levelized cost of heat vs total heat demand.
5.0	Commercialization	<p>5.1 Techno-Economics</p> <p>5.2 Regulations</p> <p>5.3 Market Demand and Transformation</p>	<ul style="list-style-type: none"> • Develop life-cycle costs assessment (LCCA) spreadsheet tool to estimate whole life costs and benefits, and environmental benefits. • Determine cost estimates and economics for the scenarios. • Determine economic metrics (e.g., present value and rate of return) for the scenarios. • Determine existing regulations for deployment of the proposed DDU technology. • Ascertain a direct plan for implementing the GES. • Identify challenges for commercializing the DDU technology. 	<ul style="list-style-type: none"> • Performed life-cycle analysis (LCA) to quantify the overall environmental impacts and co-benefits of the system. • Simultaneously developed LCCA spreadsheet tool to identify cradle-to-grave environmental impacts associated with the GES, and other DDU technologies with similar attributes. • Performed high-level economic analysis for GES extracting heat from MSS. • Utilized financial metrics to determine the economic viability of the DDU technology.

			<ul style="list-style-type: none"> • Complete a market transformation plan for the DDU technology. 	<ul style="list-style-type: none"> • Evaluated other barriers to implementing the DDU technology, including alternative fuel economics and limited design experience. • Identified programs and incentives that reduce financial burden to develop DDU technology. • Identified all pertinent regulations for constructing the GES. • Identified challenges to implementing the DDU technology in a low-temperature sedimentary basins. • Completed assessment for applicability of DDU technology at military installations and other similar facilities in the ILB.
--	--	--	---	--

Appendix B – Formulas and Calculations

B1. Geologic and Geocellular Modeling

The SPS and MSS geocellular models of the 93 km² (36 square mile) area around the U of IL has x and y grid-cell dimensions were set to 61.0 m by 61.0 m (200 ft by 200 ft). The average model thicknesses for the SPS and MSS were 46.3 m (152 ft) and 552 m (1,810 ft), respectively. The number of layers in the SPS and MSS models were set at 39 and 62, respectively, resulting in an average layer thickness of 1.5 m (5 ft) for the SPS and 13 m (42 ft) for the MSS.

Thermophysical properties, such as thermal conductivity, specific heat capacity, and thermal expansion coefficient were determined from overall quartz content and temperature of the rock. Analyses of thin sections of the MSS and Argenta Formation indicate that the lithologies are dominated by quartz and K-feldspars (Freiburg et al., 2014). Assuming a binary system of quartz and K-feldspar, quartz content in the formations was distributed using histograms of the percentage of quartz calculated from geochemical logs. The thermal conductivity (λ) for the MSS and Argenta Formation was derived using the following equation from Robertson (1988):

$$\lambda = (\lambda_{Ff} + \gamma^2[(\lambda_S + Q_{tz} * S) - \lambda_{Ff}]) \times 0.418 \text{ (W/m}\cdot\text{K)/1CU} \quad (\text{B1.1})$$

where

γ = solidity of rock equal to 1 – porosity.

λ_{Ff} = pore fluid thermal conductivity intercept at $\gamma^2 = 0$.

λ_S = solid rock thermal conductivity intercept at $\gamma^2 = 0$.

Q_{tz} = % of quartz in rock.

S = the slope constant (0.157 CU/% for sandstone).

CU = conductivity unit.

The specific heat capacity was calculated using methods developed by Waples and Waples (2004). The specific heat capacity was calculated from the proportion of quartz and K-feldspar (measured at 20 °C [68 °F]) using the following equation:

$$C_p = C_p Q_{Qtz} + C_{pF} K_{Fel} \quad (\text{B1.2})$$

where

C_p = specific heat capacity of the rock.

$C_p Q$ = specific heat capacity of quartz (740 J/kg·°C).

Q_{tz} = % of quartz in rock.

C_{pF} = specific heat capacity of K-feldspar (628 J/kg·°C)

K_{Fel} = % of K-feldspar in rock.

Because specific heat capacity is highly dependent on temperature, the value was adjusted (from measurements in Waples and Waples (2004) conducted at 20 °C [68 °F] that account for the ambient reservoir temperature) first by calculating the normalized specific heat capacity (C_{pn}):

$$C_{pn} = 8.95 \times 10^{-10}T^3 - 2.13 \times 10^{-6}T^2 + 0.00172T + 0.716$$

(B1.3)

where

T = the temperature in °C.

C_{pn} was then calculated for the reservoir temperature and 20 °C (68 °F), and further it was used to find the specific heat capacity at reservoir temperature (C_pT_2) using the following equation:

$$C_pT_2 = C_pT_1 \times C_{pnT_2}/C_{pnT_1}$$

(B1.4)

where

C_pT_1 = the specific heat capacity at 20 °C.

C_{pnT_2} = the normalized specific heat capacity at reservoir temperature.

C_{pnT_1} = the normalized specific heat capacity at 20 °C.

In Figures 9a and b, the resulting distribution of thermal conductivity and specific heat capacity is shown. The coefficient of thermal expansion (α) is determined from the mineral content, so a simple mixed model was used as follows:

$$\alpha = \alpha_Q Q_{tz} + \alpha_F K_{FeI}$$

(B1.5)

where

α_Q = the coefficient of thermal expansion of quartz (4.98×10^{-5} 1/°C).

α_F (1.54×10^{-5} 1/°C) = the coefficient of thermal expansion of K-feldspar.

The temperature (T in °C) was calculated from the thermal gradient described earlier:

$$T = [(0.0063D + 74.4892) - 32] \times 5/9$$

(B1.6)

where

D = depth in m.

Salinity of the geothermal fluid was estimated by using a regression model of salinity with depth derived from the geochemistry for the IBDP. Table B1.1 contains the statistics for properties within the geocellular model.

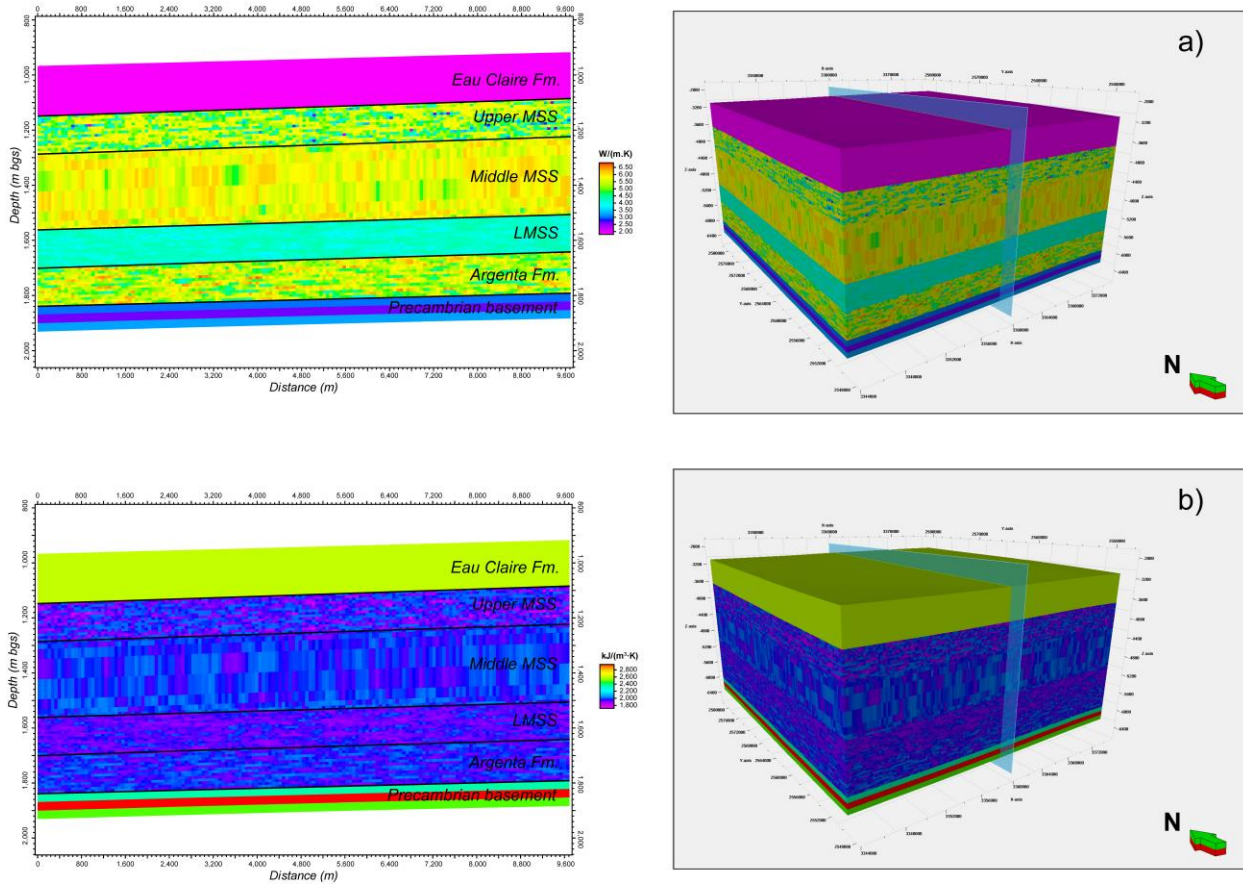


Figure B1.1. Distribution of (a) thermal conductivity and (b) specific heat capacity in the MSS model constructed using Petrel© software. The model x and y grid-cell dimensions were set to 61.0 m × 61.0 m (200 ft × 200 ft). The average model thickness was 552 m (1,810 ft). The MSS model included 62 layers resulting in an average layer thickness of 13 m (42 ft).

Table B1.1. Statistical Analysis of the Thermo-Hydraulic-Mechanical Properties of the MSS and Argenta Formation from the Geocellular Model

	Porosity	Permeability ($\times 10^{-12}$ cm ²) [mD]	λ (W/m·°C)	Cp (J/[kg·°C])	α ($\times 10^{-5}$ 1/°C)	Temperature (°C)	Salinity (ppm)
Min.	0.0402	0.0197 [0.002]	1.80	643	1.77	38.4	50,200
Max.	0.2373	12,800 [1,300]	6.83	762	4.75	47.2	150,000
Mean	0.1077	772 [78.2]	4.97	730	3.92	43.3	106,000
Std Dev.	0.0446	1,420[144]	0.76	15.7	0.425	2.57	29,500

B2. Fluid Flow Modeling

Because conduction and convection are the predominant heat transfer mechanisms between geothermal fluids and wellbore and adjacent formations the Navier-Stokes heat conduction and heat convection equations (described below) were applied in COMSOL to model fluid flow and heat transfer. The Navier-Stokes equations for conservation of momentum (Equation 1) and the continuity for conservation of mass (Equation 2) were used to characterize fluid flow in wellbores:

$$\rho_f \frac{\partial u}{\partial t} + \rho_f (u \cdot \nabla) u = \nabla \cdot [-pI + \tau] + F \quad (1)$$

$$\frac{\partial \rho_f}{\partial t} + \nabla \cdot (\rho_f u) = 0$$

where

ρ_f = fluid density (kg/m³).

u = flow rate (m/s).

p = pressure (in Pa).

F = the volume force (N/m³).

τ = the viscous stress (Pa) (calculated using the following expression for Newtonian fluids).

$$\tau = \mu (\nabla u + (\nabla u)^T) - \frac{2}{3} \mu (\nabla \cdot u) I \quad (2)$$

where

μ = the fluid dynamic viscosity (Pa·s).

Because the extracted geothermal fluid (brine) is less compressible than the surrounding geologic materials, the density is assumed to remain constant as the temperature and pressure changes (i.e., incompressible). This assumption simplifies Equation 2 to:

$$\rho_f \nabla \cdot u = 0 \quad (3)$$

The R_e , which is the ratio of inertial forces to viscous forces, predetermines the type of fluid flow in the wellbore:

$$R_e = \frac{\rho_f u D_H}{\mu} \quad (4)$$

where

D_H is the characteristic length (m) (e.g., the diameter of circular channels).

The critical Reynolds Number (R_e) above which fluid flow regime changes from laminar to transitional and, eventually changes to fully-turbulent flow is 2,000. During operation of the DDU

GES, the required flow rate is typically high enough for fluid flow regime to be turbulent (e.g., the R_e reaches ~225,900 for a flow rate of 3.67 m/s [12.04 ft/s] within a tube with a diameter of 0.06 m [2.44 in]).

Heat Transfer Modeling

Heat transfer occurs in fluid, solid, and porous media in the form of thermal conduction and convection. The general heat conduction and convection equations used in COMSOL are:

$$(\rho C_p)_{eq} \frac{\partial T}{\partial t} + \rho_f C_{pf} \mathbf{u} \cdot \nabla T + \nabla \cdot (-k_{eq} \nabla T) = Q \quad (5)$$

where

T = temperature ($^{\circ}C$).

C_{pf} = specific heat capacity of fluid ($J/(kg \cdot ^{\circ}C)$).

Q = heat source (or sink) (W/m^3).

$(\rho C_p)_{eq}$ and k_{eq} are the equivalent volumetric heat capacity ($J/(m^3 \cdot ^{\circ}C)$) and the equivalent thermal conductivity ($W/(m \cdot ^{\circ}C)$) for porous media, which were calculated as:

$$(\rho C_p)_{eq} = (1-\varepsilon)\rho_s C_{ps} + \varepsilon\rho_f C_{pf} \quad (6)$$

$$k_{eq} = (1-\varepsilon)k_s + \varepsilon k_f \quad (7)$$

where

ρ_s = density (kg/m^3) of matrix in porous media.

C_{ps} = specific heat capacity ($J/(kg \cdot ^{\circ}C)$) of matrix in porous media..

k_s = thermal conductivity ($W/m \cdot ^{\circ}C$) of matrix in porous media.

k_f = thermal conductivity ($W/m \cdot ^{\circ}C$) of fluid in porous media.

For heat transfer from the geothermal fluid, the porosity (ε) is unity (1). For heat transfer in solid materials, the porosity is zero (0) and the heat convection term reduces to zero (0).

B3. Surface Infrastructure Modeling – EBS Data Tables

Table B3.1. Monthly Fuel Consumption at ARFs (FY2015 to FY2017)*

	Fuel Consumption (MMBtu)	Energy Farm (LPG)	Beef & Sheep Rs. Field Lab (NG)	Poultry Farm (NG)	ISRL (NG and LPG)	Dairy Farm (NG)	Feed Mill (NG)	Total
FY2017 (July 2016 to June 2017)	July	0.00	3.89	16.68	20.60	16.90	18.40	76.46
	Aug	0.00	3.91	12.23	15.50	16.10	73.40	121.14
	Sept	478.24	4.55	20.01	62.66	17.40	70.60	653.46
	Oct	0.00	6.77	17.79	79.40	19.80	20.60	144.36
	Nov	172.65	26.93	31.13	230.80	87.90	109.50	658.91
	Dec	359.59	158.51	173.09	769.82	282.30	196.50	1,939.80
	Jan	379.09	135.11	111.56	718.41	198.40	179.90	1,722.46
	Feb	210.15	225.22	96.50	524.64	144.70	156.50	1,357.70
	March	168.55	321.56	133.90	551.13	122.00	159.20	1,456.33
	April	0.00	91.80	102.10	200.10	41.60	127.60	563.20
May	104.13	23.04	50.80	148.60	42.70	12.60	381.87	
June	159.39	4.49	13.40	38.60	32.50	4.70	253.07	
FY2016 (July 2015 to June 2016)	July	0.00	4.66	11.12	27.90	21.70	106.60	171.98
	Aug	0.00	5.11	27.80	22.40	21.70	104.40	181.41
	Sept	63.93	3.99	11.12	138.32	16.70	95.80	329.86
	Oct	102.76	22.09	17.79	125.60	28.40	87.30	383.93
	Nov	102.76	76.93	121.20	371.70	104.90	128.70	906.18
	Dec	0.00	111.99	162.34	579.30	150.50	180.50	1,184.63
	Jan	-29.69	153.31	112.30	786.20	178.40	186.60	1,387.12
	Feb	0.00	397.98	117.86	663.30	139.20	148.90	1,467.24
	March	952.52	161.56	50.04	656.26	82.40	143.00	2,045.78
	April	0.00	59.83	73.39	298.50	75.10	194.40	701.22
May	97.14	18.38	88.95	336.07	32.70	102.80	676.03	
June	0.00	4.61	25.57	26.40	19.30	33.00	108.88	
FY2015 (July 2014 to June 2015)	July	0.00	3.67	24.46	35.80	20.40	71.00	155.33
	Aug	331.54	3.11	28.91	31.80	18.80	75.20	489.36
	Sept	0.00	3.63	30.02	72.40	23.90	54.40	184.35
	Oct	91.59	11.65	22.24	229.05	49.80	98.60	502.93
	Nov	0.00	115.62	96.74	489.50	136.20	128.10	966.15
	Dec	414.97	114.71	133.43	689.20	174.50	167.90	1,694.71
	Jan	54.59	186.64	132.32	733.60	186.10	121.40	1,414.65
	Feb	406.72	551.24	132.32	728.87	174.40	71.50	2,065.04
	March	503.45	436.88	105.63	634.88	128.10	175.90	1,984.84
	April	0.00	136.44	90.06	350.00	65.80	134.10	776.41
	May	308.30	18.75	35.58	102.10	28.80	118.00	611.53
	June	160.84	7.69	23.35	46.93	19.50	103.90	362.20

* Data from U of IL EBS.

The amount of LPG delivered to the Energy Farm each month is not the actual LPG consumed in a month. Therefore, the LPG data was converted into energy consumption data using the daily degree days, which are closely correlated to heating (and cooling) demand and used to predict heat consumption (cf. Erbs et al., 1983). The daily degree day (D_i) on a specific date was calculated as:

$$D_i = 65 - \frac{t_{max}^i + t_{min}^i}{2} \quad (1)$$

where

D_i = the degree day on the i -th day.

t_{max}^i and t_{min}^i = the highest and lowest ambient temperatures, respectively, on that day.

The larger values for D_i , colder the weather, and higher fuel consumption. When $D_i < 0$, it is assumed the heating system is turned off. Based on the degree days, the monthly heat consumption in the j -th month of an FY (Q_j^e) was estimated as:

$$Q_j^e = \left(\sum_{j=1}^{12} Q_j^e \right) \times \frac{\sum_{i=1}^{\text{days in } j \text{ month}} d_i}{\sum_{i=1}^{\text{days in FY}} d_i} \quad (2)$$

$$\text{where: } d_i = \begin{cases} D_i & (\text{if } D_i > 0) \\ 0 & (\text{if } D_i \leq 0) \end{cases} \quad (3)$$

Using the above approximation, the estimated monthly fuel consumption at the Energy Farm is shown in Table B3.2.

Table B3.2. Monthly Fuel Consumption at ARFs (FY2015 to FY2017)
(Estimated from delivered LPG data)

Fuel Consumption (MMBtu)	Energy Farm (LP)	Beef & Sheep Rs. Field Lab (NG)	Poultry Farm (NG)	ISRL (NG and LP)	Dairy Farm (NG)	Feed Mill (NG)	Total	
FY2017 (July 2016 - June 2017)	July	4.15	3.89	16.68	20.60	16.90	18.40	80.61
	Aug	0.00	3.91	12.23	15.50	16.10	73.40	121.14
	Sept	7.21	4.55	20.01	62.66	17.40	70.60	182.43
	Oct	79.95	6.77	17.79	79.40	19.80	20.60	224.31
	Nov	236.80	26.93	31.13	230.80	87.90	109.50	723.06
	Dec	486.70	158.51	173.09	769.82	282.30	196.50	2,066.91
	Jan	442.79	135.11	111.56	718.41	198.40	179.90	1,786.17
	Feb	297.09	225.22	96.50	524.64	144.70	156.50	1,444.64
	March	298.18	321.56	133.90	551.13	122.00	159.20	1,585.97
	April	107.69	91.80	102.10	200.10	41.60	127.60	670.90
	May	68.59	23.04	50.80	148.60	42.70	12.60	346.33
June	2.62	4.49	13.40	38.60	32.50	4.70	96.31	
FY2016 (July 2015 - June 2016)	July	0.67	4.66	11.12	27.90	21.70	106.60	172.65
	Aug	1.33	5.11	27.80	22.40	21.70	104.40	182.74
	Sept	7.20	3.99	11.12	138.32	16.70	95.80	273.13
	Oct	73.86	22.09	17.79	125.60	28.40	87.30	355.03
	Nov	152.78	76.93	121.20	371.70	104.90	128.70	956.20
	Dec	199.97	111.99	162.34	579.30	150.50	180.50	1,384.60
	Jan	313.29	153.31	112.30	786.20	178.40	186.60	1,730.10
	Feb	247.16	397.98	117.86	663.30	139.20	148.90	1,714.40
	March	145.58	161.56	50.04	656.26	82.40	143.00	1,238.84
	April	104.52	59.83	73.39	298.50	75.10	194.40	805.74
	May	42.39	18.38	88.95	336.07	32.70	102.80	621.29
June	0.67	4.61	25.57	26.40	19.30	33.00	109.55	
FY2015 (July 2014 - June 2015)	July	3.45	3.67	24.46	35.80	20.40	71.00	158.79
	Aug	0.91	3.11	28.91	31.80	18.80	75.20	158.73
	Sept	38.18	3.63	30.02	72.40	23.90	54.40	222.53
	Oct	129.82	11.65	22.24	229.05	49.80	98.60	541.16
	Nov	332.36	115.62	96.74	489.50	136.20	128.10	1,298.51
	Dec	362.00	114.71	133.43	689.20	174.50	167.90	1,641.73
	Jan	451.64	186.64	132.32	733.60	186.10	121.40	1,811.69
	Feb	476.00	551.24	132.32	728.87	174.40	71.50	2,134.32
	March	316.91	436.88	105.63	634.88	128.10	175.90	1,798.30
	April	122.73	136.44	90.06	350.00	65.80	134.10	899.13
	May	35.27	18.75	35.58	102.10	28.80	118.00	338.50
June	2.73	7.69	23.35	46.93	19.50	103.90	204.09	

B4. Review of Software for LCCA Spreadsheet Tool

One of the first tools evaluated used to carry out this work was the geothermal techno-economic simulation tool, GEOPHIRES (GEothermal Energy for Production of Heat and electricity (IR) Economically Simulated) versions 1.0 and 2.0 (Beckers et al., 2013; 2018). (Version 1.0 of the software was programmed in 2014 at Cornell University by the lead researcher of the studies.) Below is a summary of GEOPHIRES capabilities (Beckers and McCabe, 2019):

“GEOPIRES is a computer code to perform techno-economic simulations of geothermal energy systems. For a given set of input parameters, the tool simulates the subsurface reservoir, wellbore, and surface plant either by using built-in or external user-provided models. The simulated output includes the reservoir production temperature and instantaneous and lifetime surface plant heat and/or electricity production. Combined with capital and O&M cost correlations, GEOPIRES applies levelized cost models to estimate the overall required investment and levelized cost of electricity and/or heat (LCOE and LCOH). Possible end-use configurations are direct-use heat (e.g., for district heating or an industrial process), electricity, and cogeneration or combined heat and power (CHP). Ground-source heat pumps are not considered.”

National Institute of Standards and Technology’s (NIST) Building Life Cycle Cost (BLCC) Programs has been used for computational support for the analysis of capital investments in buildings (e.g., Hu, 2019). The BLCC programs includes the Energy Escalation Rate Calculator, Handbook 135, and the Annual Supplement to Handbook 135 (USDOE, 2019). BLCC is used to conduct economic analyses by evaluating the relative cost effectiveness of alternative buildings and building-related systems or components. Calculations of comparative economic measures including net savings, SIR, adjusted internal rate of return (AIRR), and years to payback can be made. Typically, BLCC is used to evaluate alternative designs that have higher initial costs, but lower operating costs over the project life than the lowest-initial-cost design. It is especially useful for evaluating the costs and benefits of energy and water conservation and renewable energy projects (USDOE, 2019b). BLCC has been used for energy projects that included geothermal heat pumps (Shonder et al., 2000; Kabassi and Cho, 2012).

B5. LCCA Equations

The equations used to calculate the values in Table B3.2 include:

$$Q_{50} = 50 \text{ years} * 7,994 \text{ MMBtu/year} = 399,700 \text{ MMBtu (Case 1)} \quad (1)$$

$$Q_d = \sum_{t=1}^{50} \frac{Q_t}{(1+i)^t}, \quad (2)$$

where

$Q_1 = 7,994 \text{ MMBtu/year (Case 1)}$.

Q_2 to Q_{50} are calculated using the discount rate (d) and NG escalation rate (e).

$$ES = \sum_{t=1}^{50} \frac{Q_t}{(1+i)^t} * E_t, \quad (3)$$

where:

$E_1 = 7,994 \text{ MMBtu/year (Case 1)}$.

E_2 to E_{50} are calculated using the discount rate (d) and NG escalation rate (e).

$$NPV = ES - C_{Cap} - C_{O\&M} \quad (4)$$

where

DPB = the year where cumulative cash flow (Savings – Costs) is positive. The value for both Case 1 and Case 2 is not applicable because cash flow is negative at the end of the 50th year.

$$ROI = [ES - (C_{Cap} + C_{O\&M})] / (C_{Cap} + C_{O\&M}) \quad (5)$$

$$SIR = ES / (C_{Cap} + C_{O\&M}) \quad (6)$$

$$LCOH = \frac{C_{Cap} + \sum_{t=1}^{50} \frac{C_{O\&M}}{(1+i)^t}}{\sum_{t=1}^{50} \frac{Q_t}{(1+i)^t}} \quad (7)$$

B6. Environmental Life Cycle Assessment of a Deep Direct-use Geothermal System in Champaign, Illinois

Lauren K. Thomas¹, James M. Tinjum² and Franklin H. Holcomb³

¹Invenergy LLC, Chicago, IL 60606, USA

² Department of Civil and Environmental Engineering, University of Wisconsin, Madison, WI 53706, USA

³ Office of Technical Directors, U.S. Army Corps of Engineers, ERDC-CERL, Champaign, IL 61822, USA

Email: LThomas@invenergyllc.com

Keywords: Environmental Life Cycle Assessment, Deep Direct-Use, Geothermal, Global Warming Potential

Abstract

The feasibility of implementing a deep direct-use (DDU) geothermal energy system (GES) was assessed as the primary thermal energy source in agricultural research facilities (ARF) at the University of Illinois at Urbana-Champaign (U of IL) campus. This district-scale heating and cooling source will exploit the Illinois Basin (ILB), a low-temperature sedimentary basin with multiple potential sources of geothermal energy, including the Mt. Simon Sandstone (MSS). DDU GES are believed to provide lower-emission alternatives compared to traditional heating and cooling methods; however, low-temperature, high-salinity DDU heat sources are less frequently utilized. The primary objective of this project is to investigate the feasibility of implementing a DDU GES at the U of IL. Several system characteristics are investigated, including the deployment and performance of the DDU GES, well-design alternatives, challenges to GES commercialization, levelized cost of heat, and life cycle environmental impacts. The work in this paper focuses on an environmental life cycle assessment (LCA) to quantify the overall environmental impacts and co-benefits of the system. The LCA was performed using a spreadsheet tool that was simultaneously developed to provide insight into the cradle-to-grave environmental impacts associated with the proposed geothermal system, as well as other DDU systems with similar objectives. This tool allows for a more in-depth analysis of the feasibility of DDU GES with respect to the overall environmental impacts of the system. The impact categories that were evaluated within this LCA tool are ozone depletion, global warming potential (GWP), smog, acidification, eutrophication, and fossil fuel depletion. As an example of the environmental LCA results, with respect to the GWP category, if the ARF were heated through the use of the proposed DDU system, the GWP emissions associated with the use of traditional fuels such as propane and natural gas could be offset in approximately 10 years of operation.

1. Introduction

A recent initiative of the Department of Energy (DOE) seeks to enable the widespread use of lower-temperature geothermal resources that are shallower than conventional hydrothermal sources, but deeper than geothermal heat pump and other traditional direct-use systems (USDOE 2018). These geothermal resources are believed to bring valuable returns on investment in the near-term. Typical DDU GES utilize a flow of geothermal fluid that is capable of providing heating and cooling to buildings. The overall

objective of this study is to determine the feasibility of designing a district-scale geothermal heating system for the ARF campus using a DDU technology.

As part of this effort, a Life Cycle Assessment (LCA) spreadsheet tool was developed to analyze potential environmental benefits of a DDU GES. The LCA spreadsheet tool is a unique contribution to the project that provides further insight into the cradle-to-grave environmental impacts associated with the GES system over the operating life time, as well as other DDU GES with similar objectives. The tool allows for a more in-depth analysis of the feasibility of DDU GES with respect to the overall environmental impacts. For the U of IL assessment, a doublet (two-well) system is evaluated, which is connected to aboveground mechanical system to supply heating to the ARF. The additional of new equipment are assessed for the technical and economic feasibility. The results from this study will also allow geothermal resources from the entirety of the ILB to be assessed and allow the DDU technology to be extended to additional areas of the ILB and other low-temperature sedimentary basins with similar characteristics.

2. BACKGROUND

2.1 *Direct-Use Geothermal Energy*

The direct use of geothermal energy refers to the thermal utilization of geothermal heat in residential, commercial, and industrial facilities that have an inherent need for a reliable supply of heat. Most applications of DDU technologies require geothermal fluids with low-to-moderate temperatures, which are typically found at depths shallower than resources used for traditional high-temperature power generation methods. DDU technologies has the potential to increase the distribution of geothermal energy in areas with lower heat flow that rely on traditional, high-emission sources of heat. According to data reported by the U.S. Energy Information Administration, the total thermal energy from 0 to 260°C used in 2008 was 33.5 EJ, which is approximately one-third of the entire U.S. demand (Fox et al. 2011). Space heating and water heating, which have end-use temperatures ranging from 40 to 60°C, are responsible for 38% of the total thermal energy demand below 260°C. Utilizing geothermal direct-use through the implementation of DDU projects would offer a relatively sustainable and low-emission alternative to the conventional heat sources supplied by fossil fuels (USDOE 2018).

The concept is to use warm and/or hot water from a subsurface aquifer formation and deliver that heat to a surface application. Once the heat is utilized on the surface, the cooler water is returned to the aquifer through an injection well, where it is mixed with the warmer/hotter water in the aquifer and eventually reused. The temperature of the aquifer can decrease over time due to the recycling of used water through the system. The thermal drawdown rate is dependent on a number of factors, including aquifer size and extraction/injection water temperatures.

2.2 *Illinois Basin*

The MSS has potential as a geothermal energy source based on pre-initial temperatures and flow rates of fluids. The geothermal energy extracted from this formation within the ILB could, theoretically, be used to heat the ARF located at the Energy Farm on the U of IL. A schematic map of the assessment area within the ILB is provided as Figure B6.1. In Champaign County, the bedrock surface is masked by Quaternary glacial deposits, ranging in thickness from 40–120 m. Pennsylvanian through Cambrian sedimentary rocks lie below, with a thickness of ~1,982 m (~6,500 ft) Precambrian igneous rocks underlie the sedimentary bedrock (Stumpf et al. 2018). A detailed stratigraphy of the ILB can be found in Damico et al. (2020). A test borehole was completed in the study area in 2016 to determine the geothermal gradient in the shallow subsurface. This borehole identified multiple geologic formations in the Quaternary glacial deposits and Pennsylvanian strata, including the Glasford Formation and Herrin Coal that have a thermogeology that significantly impact heat transport (McDaniel et al. 2018).

Numerous studies by the Illinois State Geological Survey have been completed to characterize the deep geologic formations. The MSS is found at depths of 1,334 to 1,887 m. Based on bottomhole temperatures from well logs, formation water temperature of the MSS ranged from 44–46°C (111–115°F) (Stumpf et al. 2018, 2020).

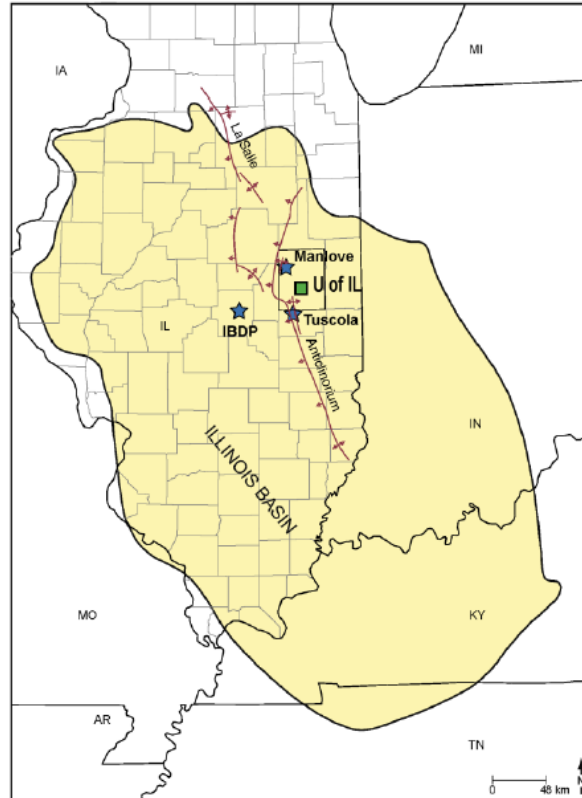


Figure B6.1: Location of the assessment site within the ILB, shaded in yellow. The study site is denoted by the green box labeled U of IL.

2.3 Life Cycle Assessments

Life Cycle Assessment (LCA) is a technique for assessing the potential environmental aspects and potential aspects associated with a product or service by compiling an inventory of relevant inputs and outputs, evaluating the potential environmental impacts associated with those inputs and outputs, and interpreting the results of the inventory and impact phases in relation to the study objectives (ISO 2006). Several LCAs have been performed on a variety of products and services, such as wind farms, recycled concrete aggregate, and other geothermal systems.

An LCA of the Glacier Hills Wind Park in south-central Wisconsin was performed in order to highlight the significant areas of energy consumption and emissions associated with wind energy development (Rajaei and Tinjum 2013). A quantitative analysis of the life cycle emissions and environmental impact associated with wind development from construction through operation revealed that transportation of large components from overseas led to significant consumption of fossil fuels, responsible for nearly a quarter of the total greenhouse gas emissions due to transportation. Energy payback time and total equivalent grams of eCO₂ per kWh were also calculated over the lifetime of the wind farm. LCA methodology was also applied to a non-conventional deep insulated single-hole ground source heat pump in order to compare its impacts with conventional heating, ventilation, and cooling methods. The results of the LCA show that top contributors to CO₂ equivalent emissions are heat-exchanger operation, borehole drilling, and circulation pump operation. The sustainability of construction with recycled materials was also evaluated using LCA methodology (Lee 2010). This work involved developing a rating system called the Building Environmentally and Economically Sustainable Transportation-Infrastructure-Highways (BE²ST-in-Highways™). This system compares the environmental and economic life cycle impacts between different construction material methods. Furthermore, this paper developed an AMOEBA graph to compare the impacts between various construction material alternatives and how they reach certain sustainability goals. A similar concept was applied in this LCA methodology for the DDU GES, which is referred to as a spider diagram herein.

3. METHODS AND MATERIALS

3.1 University of Illinois Urbana-Champaign Field Site

The U of IL is a large academic campus with energy needs served by the central Abbott Power Plant, which provides electricity and heat in the form of steam to more than 250 buildings. Currently, there is no significant use of geothermal on the campus, although there are geologic formations below the campus that have been identified as potential sources of low-temperature (<50 °C) geothermal energy (Stumpf et al. 2018). The ARF was analyzed as the end users for the ILB geothermal resource. The study

area is located on a 90 km² area around the U of IL. There will be six facilities in the ARF in which space heating and pre-heating of domestic water will be used; the Energy Farm, Beef and Sheep Research Laboratory, Poultry Farm, Imported Swine Research Laboratory (ISRL), Dairy Farm, and Feed Mill were analyzed. The heat usage of these facilities varied between buildings as well as seasonally, with annual totals ranging between approximately 791 and 3,348 MMBtu (F&S 2017). A summary of the heat usage for these facilities can be found in Table B6.1.

Table B6.1. Energy consumption at the ARF on the U of IL. Fuel type is specified for each location, and varies between propane, natural gas (NG), or combination of the two at specific locations.

ARF Heat Consumption	Energy Farm (Propane)	Beef and Sheep Field Laboratory (NG)	Poultry Farm (NG)	ISRL (NG, Propane)	Dairy Farm (NG)	Feed Mill (NG)	Total
Yearly Total (MMBtu)	2,140	1,006	791	3,348	1,009	1,158	9,452
Annual Avg. Rate (MMBtu/hr)	0.24	0.11	0.09	0.38	0.12	0.13	1.07
Winter 6-month Total (MMBtu/hr)	1,852	959	648	2,995	929	929	8,312
Winter Avg. Rate (MMBtu/hr)	0.42	0.22	0.15	0.68	0.21	0.21	1.89
Maximum Monthly Rate (MMBtu/mo)	365	322	173	770	197	197	2,024
Maximum Monthly Avg. Rate (MMBtu/hr)	0.49	0.45	0.23	1.03	0.26	0.26	2.72

3.2 DDU GES Design

The system will be comprised of both subsurface and surface components. The subsurface components are designed to exploit the geothermal resource in the ILB by using extraction and injection wells equipped with submersible pumps. A concept diagram of the subsurface components GES are shown in Figure B6.2. The surface equipment includes heat exchangers and possibly a heat pump, as well as a piping system to transport the geothermal fluid to the ARF.

Figure B6.3 illustrates well designs for the extraction and injection wells. Both wells will be drilled to reach the MSS, with both the extraction and injection wells drilled to a depth of 1981 m (6,500 ft). The extraction well is screened between 1860–1905 m (6,100–6,250 feet) and the injection zone is from 1,890–1,935 m (6,200–6,350 ft). The extraction well contains three casings, a surface casing, an intermediate casing, and a long-string casing. The injection well is designed slightly different, and is comprised of a surface, intermediate, and casing. A more detailed breakdown of the individual well components and materials are described in the following sections. The extraction and injection wells will be located at the margins of the study area, located ~1.5 miles apart (Stumpf et al. 2020). High-density polyethylene (HDPE) pipes will be laid underground to transport the heated supply water to the facilities, and a return line will be placed to discharge the cooler water away from the facilities.

3.3 Methodology

An LCA was performed to assess the environmental impacts associated with the project, including raw material extraction, materials processing, manufacture, distribution, use, disposal, and recycling. The goal of this assessment is to quantify the environmental impacts of the project in order to provide information to assist in evaluating design alternatives. The framework of this LCA is based on four life cycle stages: material production, material transport and construction, use of system, and end of life. The material production stage involves the acquisition of raw materials and manufacturing of materials. Material transport and construction includes a number of parameters including the distance to the project site, the methods used to transport materials, the installation of the extraction and injection wells, as well as the installation of certain surface components (e.g., heat exchangers, generators, pumps, and pipelines). The use of system stage involves the use of electricity, heat transfer to and from the subsurface, operation of a chiller, as well as other operation and maintenance activities. Finally, the end of life stage is focused on the deconstruction and sealing of the extraction and injection wells, well sealing, waste, and transportation of waste. Figure B6.4 shows a schematic of the four life cycle stages.

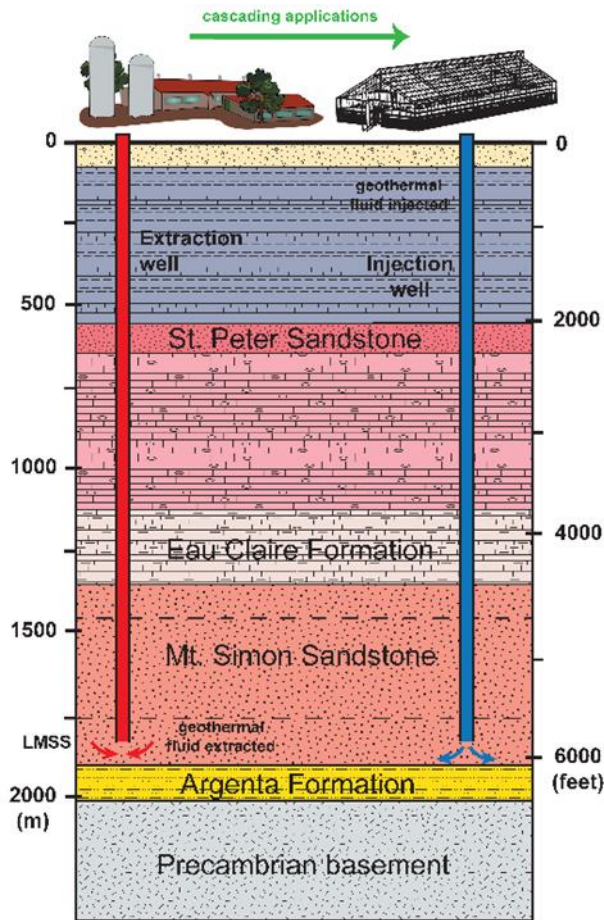


Figure B6.2: Conceptual diagram of the proposed doublet well system for the DDU GES (Stumpf et al. 2020)

The goal and scope and system boundary of the LCA was structured to focus on the materials and processes that have the largest environmental impacts. Because material acquisition and installation of the wells typically comprise a significant portion of the environmental impacts of the system, the components of the extraction and injection wells were investigated in detail. An inventory flow diagram showing a breakdown of the scope of the construction and use of the geothermal system is conveyed as Figure B6.5 (next page).

The inventory of impacts for the LCA spreadsheet tool was collected using SimaPro version 8.5.2 and TRACI version 2.1 Impact Assessment Methodology. SimaPro is a professional LCA tool used to collect, analyze, and monitor the sustainability performance of a product or service. SimaPro measures the environmental impact of products across all life cycle stages, as well as assists with identifying hotspots in the supply chain, from raw material extraction to manufacturing, distribution, use, and disposal. Using the scope diagrams in Figure B6.5, an inventory of individual component impacts was gathered within SimaPro.

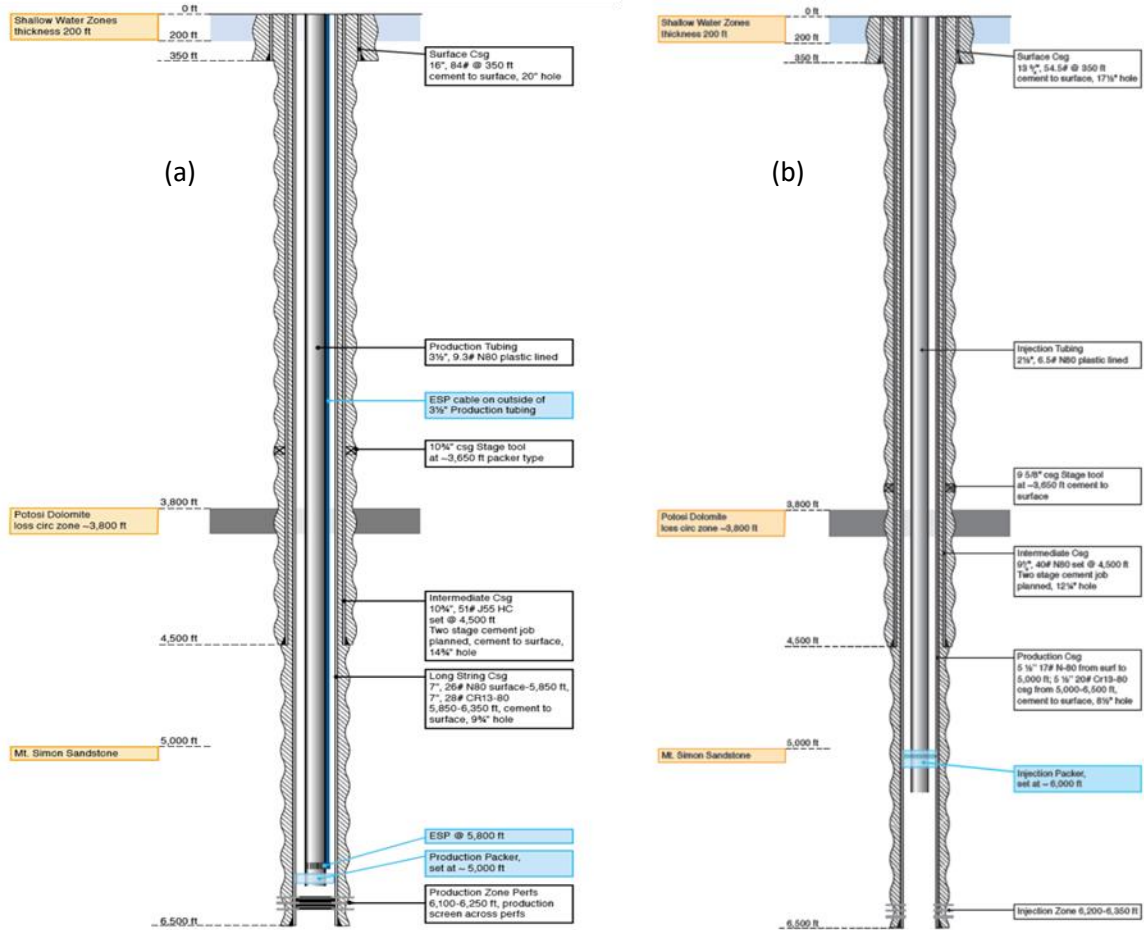


Figure B6.3: Detailed designs for extraction (a) and injection (b) wells (From Kirksey and Lu 2019).

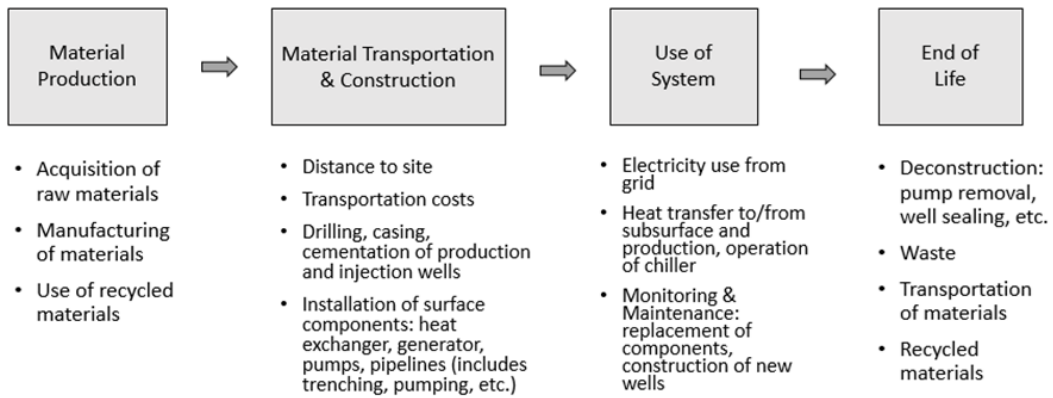


Figure B6.4: Schematic diagram summarizing the four stages of the LCA.

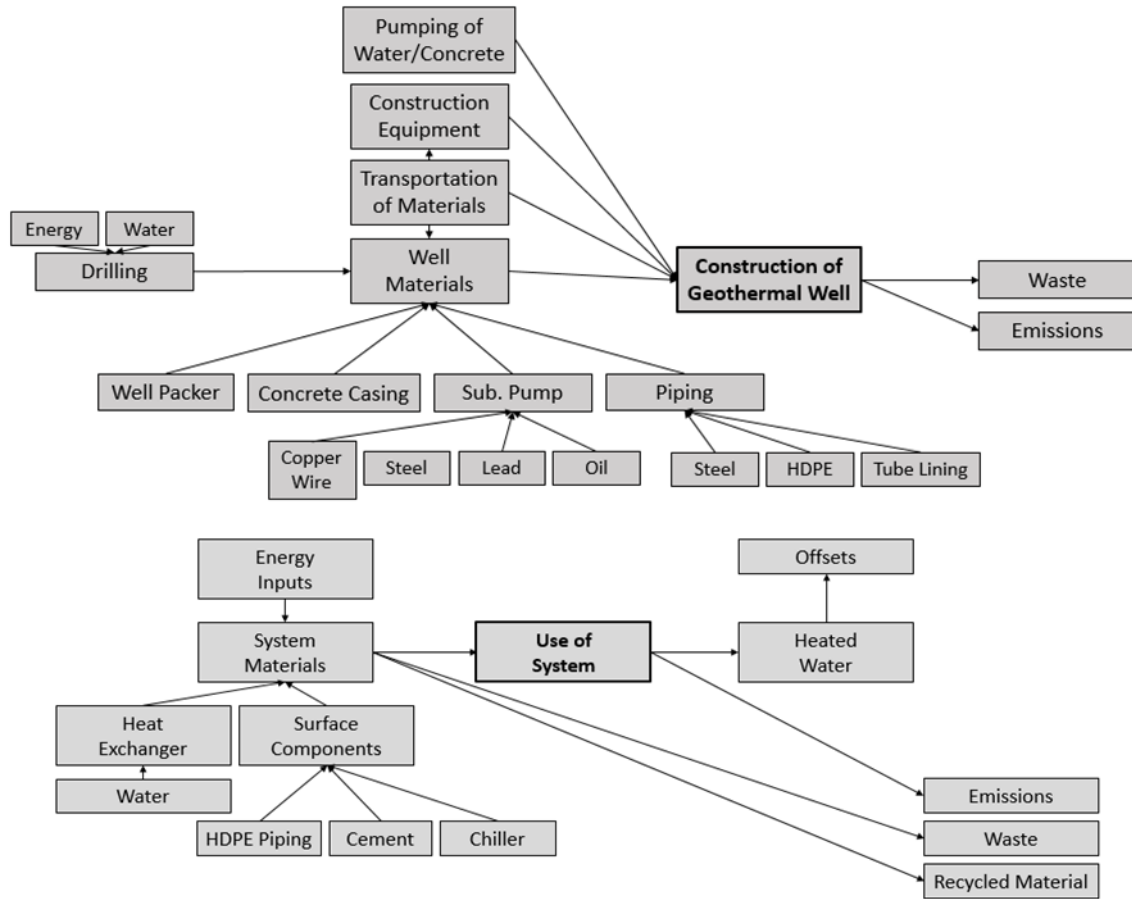


Figure B6.5: Flow diagram representing the scope of the LCA, including the components that comprise the well design and operation of the GES at the U of IL.

The impact categories that are evaluated within this LCA tool are ozone depletion, GWP, smog, acidification, eutrophication, and fossil fuel depletion. Ozone depletion measures the levels of chlorofluorocarbons (CFCs), which are ozone-depleting substances. High concentrations of CFCs lead to more harmful UV radiation reaching the Earth’s surface and has negative human health risks as well as poses threats to terrestrial and aquatic ecosystems (Solomon 1999). GWP is a measure of CO₂ levels in the atmosphere, which absorbs sunlight and solar radiation, leading to elevated global temperatures (Eckaus, 1992). Smog is a measure of O₃, which is a reaction of NO_x and VOCs in the atmosphere and has associated human health risks and reductions in air quality. Acidification relates to SO₂ concentrations, which is an acidifying compound with potential groundwater and surface water impacts, including threats to soil and aquatic organisms. Eutrophication quantifies levels of nitrogen, which is a limiting nutrient. Eutrophication causes dense growth of plant life and death of animal life in aquatic bodies due to a lack of oxygen. This issue is particularly important in areas with significant agriculture markets, as fertilizer collects in surface water runoff and deposits nitrogen in surrounding lakes, rivers, and streams (Harris et al. 2017). Lastly, fossil fuel depletion is measured in terms of MJ surplus, which is defined as the total additional future cost to the global society due to the production of one unit of resource. It is related to future global production, specifically resource extraction cost and recycling rate (Ponsioen 2013). These impact categories are meant to guide a user in evaluation of the overall environmental impacts of a product or service.

The life cycle impacts for the proposed GES were compiled for each of the impact categories. Each individual impact was queried from the SimaPro database as one unit so that the spreadsheet user can adjust the values for the materials accordance to the specific design analyzed. Tables showing the unit impacts for the proposed geothermal system within the ILB can be found in Tables B6.2 and B6.3.

Table B6.2. Inventory table showing the unit impacts of the material production phase of the GES, with the impact values compiled using SimaPro software.

Lifecycle Stage, Components & Processes		Impact Categories					
Material Production		Impact Inventory					
	SimaPro Process and Unit	Total kg CFC eq	Total kg CO ₂ eq	Total kg O ₃ eq	Total kg SO ₂ eq	Total kg N eq	Total MJ surplus
Injection Well (IW)							
Casing 1 (surface)	1 kg Steel, unalloyed (RoW) steel production, converter, unalloyed Alloc Def, U	9.76E-08	1.82E+00	8.99E-02	7.36E-03	6.23E-03	7.45E-01
Casing 2 (int.)	1 kg Steel, unalloyed (RoW) steel production, converter, unalloyed Alloc Def, U	9.76E-08	1.82E+00	8.99E-02	7.36E-03	6.23E-03	7.45E-01
Casing 3 (prod.)	1 kg Steel, unalloyed (RoW) steel production, converter, unalloyed Alloc Def, U	9.76E-08	1.82E+00	8.99E-02	7.36E-03	6.23E-03	7.45E-01
Concrete 1 (surface)	1 m ³ Concrete, normal (RoW) market for Alloc Def, U	1.85E-05	2.24E+02	1.38E+01	7.22E-01	2.68E-01	1.69E+02
Concrete 2 (int.)	1 m ³ Concrete, normal (RoW) market for Alloc Def, U	1.85E-05	2.24E+02	1.38E+01	7.22E-01	2.68E-01	1.69E+02
Concrete 3 (prod.)	1 m ³ Concrete, normal (RoW) market for Alloc Def, U	1.85E-05	2.24E+02	1.38E+01	7.22E-01	2.68E-01	1.69E+02
Tubing	1 kg Steel, unalloyed (RoW) steel production, converter, unalloyed Alloc Def, U	9.76E-08	1.82E+00	8.99E-02	7.36E-03	6.23E-03	7.45E-01
Tube lining	1 kg Tetrafluoroethylene (GLO) market for Alloc Def, U	9.42E-03	3.23E+02	6.41E-01	1.03E-01	4.66E-02	1.77E+01
Injection packer insulation	1 kg Polymer foaming (RoW) processing Alloc Def, U	4.73E-08	9.51E-01	6.90E-02	5.43E-03	3.27E-03	5.01E-01
Drilling (prod. of fuel)	1 kg Diesel, low-sulfur (RoW) production	9.20E-07	5.76E-01	4.60E-02	5.53E-03	1.83E-03	8.15E+00
Drilling (water)	1 kg Tap water (RoW) tap water production, underground water without treatment	1.96E-11	3.07E-04	1.58E-05	1.55E-06	1.28E-06	2.04E-04
Production Well (PW)							
Casing 1 (surface)	1 kg Steel, unalloyed (RoW) steel production, converter, unalloyed Alloc Def, U	9.76E-08	1.82E+00	8.99E-02	7.36E-03	6.23E-03	7.45E-01
Casing 2 (int.)	1 kg Steel, unalloyed (RoW) steel production, converter, unalloyed Alloc Def, U	9.76E-08	1.82E+00	8.99E-02	7.36E-03	6.23E-03	7.45E-01
Casing 3 (long string)	1 kg Steel, unalloyed (RoW) steel production, converter, unalloyed Alloc Def, U	9.76E-08	1.82E+00	8.99E-02	7.36E-03	6.23E-03	7.45E-01
Concrete 1 (surface)	1 m ³ Concrete, normal (RoW) market for Alloc Def, U	1.85E-05	2.24E+02	1.38E+01	7.22E-01	2.68E-01	1.69E+02
Concrete 2 (int.)	1 m ³ Concrete, normal (RoW) market for Alloc Def, U	1.85E-05	2.24E+02	1.38E+01	7.22E-01	2.68E-01	1.69E+02
Concrete 3 (long string)	1 m ³ Concrete, normal (RoW) market for Alloc Def, U	1.85E-05	2.24E+02	1.38E+01	7.22E-01	2.68E-01	1.69E+02
Tubing	1 kg Steel, unalloyed (RoW) steel production, converter, unalloyed Alloc Def, U	9.76E-08	1.82E+00	8.99E-02	7.36E-03	6.23E-03	7.45E-01
Tube lining	1 kg Tetrafluoroethylene (GLO) market for Alloc Def, U	9.42E-03	3.23E+02	6.41E-01	1.03E-01	4.66E-02	1.77E+01
Production packer insulation	Polymer foaming (RoW) processing Alloc Def, U	4.73E-08	9.51E-01	6.90E-02	5.43E-03	3.27E-03	5.01E-01
Drilling (prod. of fuel)	1 kg Diesel, low-sulfur (RoW) production	9.20E-07	5.76E-01	4.60E-02	5.53E-03	1.83E-03	8.15E+00
Drilling (water)	1 kg Tap water (RoW) tap water production, underground water without treatment	1.96E-11	3.07E-04	1.58E-05	1.55E-06	1.28E-06	2.04E-04
Submersible Pump							
Copper wire	1 kg Copper wire, technology mix, consumption mix, at plant, cross section 1 mm ² EU-15 S	1.11E-07	7.89E-01	3.89E-02	3.60E-03	2.41E-04	7.48E-01
Steel	1 kg Steel, low-alloyed (GLO) market for	1.12E-07	1.64E+00	1.02E-01	8.08E-03	1.23E-02	1.04E+00
Lead	1 kg Lead (GLO) market for Alloc Def, U	1.27E-07	1.36E+00	1.38E-01	1.90E-02	1.30E-02	1.40E+00
Lubricant oil	1 kg Lubricating oil (RER) production Alloc Def, U	1.26E-06	1.00E+00	6.98E-02	8.27E-03	4.09E-03	1.11E+01
Chiller							
Refrigerant	1 kg Refrigerant R134a (RoW) production Alloc Def, U	1.04E-02	1.03E+02	7.87E-01	8.98E-02	2.44E-02	1.53E+01
Steel	1 kg Steel, low-alloyed (GLO) market for	1.12E-07	1.64E+00	1.02E-01	8.08E-03	1.23E-02	1.04E+00
Aluminum							
Copper	1 kg Copper wire, technology mix, consumption mix, at plant, cross section 1 mm ² EU-15 S	1.11E-07	7.89E-01	3.89E-02	3.60E-03	2.41E-04	7.48E-01
Surface Components							
Heat Exchanger	1 kg Steel, unalloyed (RoW) steel production, converter, unalloyed Alloc Def, U	9.76E-08	1.82E+00	8.99E-02	7.36E-03	6.23E-03	7.45E-01
HDPE	1 kg HDPE pipes E	0.00E+00	2.48E+00	1.12E-01	9.46E-03	2.16E-04	1.11E+01

To compare the proposed GES with an existing system that also produces thermal energy, a spider diagram template was created. The methodology of this spider diagram is like that of the AMOEBA graph presented in the previous background section (Lee 2010). This diagram allows the user to compare two systems based on five categories: energy use, global warming potential, water consumption, waste production, and annual heat production. The user can also weight the importance of performance improvement for each of the five categories using a point system. In the assessment, the GES was compared against the current usage at the U of IL. Information was gathered using three main sources: the U of IL Combined College Energy Report, the Illinois Climate Action Plan, and the Energy Corridor Energy Usage Report. More information on these sources can be found in Thomas (2019).

4. RESULTS

The inventories of unit impacts shown in Tables B6.2 and B6.3 were used to calculate the life cycle impacts of the proposed GES. Overall, one of the components of the project with a significantly large impact is the material production of the two wells, specifically regarding the use of steel and concrete. These impacts could change noticeably depending on the selected inventory from the database in SimaPro® and should be adjusted if more information about the raw material sourcing is known for the specific project. A table showing the overall lifecycle totals for each impact category is below in Table B6.4.

Table B6.3. Inventory table showing the unit impacts of the construction, use of system, and end of life phases of the GES, with impact values compiled using SimaPro software.

Material Transport & Construction		Total kg CFC eq	Total kg CO ₂ eq	Total kg O ₃ eq	Total kg SO ₂ eq	Total kg N eq	Total MJ surplus
Transportation of Materials	SimaPro Process and Unit						
Transport of concrete	1 tkm Transport, freight, lorry >32 metric ton, EURO5 (GLO) market for Alloc Def, U	2.30E-08	9.13E-02	7.14E-03	3.43E-04	9.74E-05	2.04E-01
Transport of steel	1 tkm Transport, freight, lorry >32 metric ton, EURO5 (GLO) market for Alloc Def, U	2.30E-08	9.13E-02	7.14E-03	3.43E-04	9.74E-05	2.04E-01
Transport of construction equip.	1 tkm Transport, freight, lorry >32 metric ton, EURO5 (GLO) market for Alloc Def, U	2.30E-08	9.13E-02	7.14E-03	3.43E-04	9.74E-05	2.04E-01
Construction of Wells	SimaPro Process and Unit						
Drilling IW (comb. of fuel)	1 m Deep well, drilled, for geothermal power (RoW) deep well drilling, for deep geothermal power Alloc Def, U	2.51E-04	3.92E+03	2.04E+02	1.89E+01	1.67E+01	2.67E+03
Pumping cement IW (comb. of fuel)	1 hr Machine operation, diesel, <18.64 kW, generators (GLO) machine operation, diesel, <18.64 kW, generators Alloc Def, U	1.06E-06	4.37E+00	7.25E-01	2.57E-02	4.13E-03	9.35E+00
Pumping water IW (comb. of fuel)	1 hr Machine operation, diesel, <18.64 kW, generators (GLO) machine operation, diesel, <18.64 kW, generators Alloc Def, U	1.06E-06	4.37E+00	7.25E-01	2.57E-02	4.13E-03	9.35E+00
Drilling PW (comb. of fuel)	1 m Deep well, drilled, for geothermal power (RoW) deep well drilling, for deep geothermal power Alloc Def, U	2.51E-04	3.92E+03	2.04E+02	1.89E+01	1.67E+01	2.67E+03
Pumping cement PW (comb. of fuel)	1 hr Machine operation, diesel, <18.64 kW, generators (GLO) machine operation, diesel, <18.64 kW, generators Alloc Def, U	1.06E-06	4.37E+00	7.25E-01	2.57E-02	4.13E-03	9.35E+00
Pumping water PW (comb. of fuel)	1 hr Machine operation, diesel, <18.64 kW, generators (GLO) machine operation, diesel, <18.64 kW, generators Alloc Def, U	1.06E-06	4.37E+00	7.25E-01	2.57E-02	4.13E-03	9.35E+00
Trenching	SimaPro Process and Unit						
Excavating	1 hr Excavator, technology mix, 100 kW, Construction GLO	4.39E-12	2.00E-03	2.00E-04	9.49E-06	5.40E-07	4.02E-03
Use of System							
Operation of Wells	SimaPro Process and Unit						
Electricity for pumps	1 kWh from Ameren		6.23E-01				
Operation of chiller	1 kWh from Ameren		6.23E-01				
Operation of heat exchanger	1 kWh from Ameren		6.23E-01				
Maintenance	Maintenance, heat and power co-generation unit, 160kW electrical (GLO) market for Alloc Def, U	2.69E-03	3.98E+03	2.07E+03	2.28E+02	1.33E+02	2.22E+04
End of Life							
Deconstruction	SimaPro Process and Unit						
Pump removal	1 hr Machine operation, diesel, <18.64 kW, generators (GLO) machine operation, diesel, <18.64 kW, generators Alloc Def, U	1.06E-06	4.37E+00	7.25E-01	2.57E-02	4.13E-03	9.35E+00
Surface equip. removal	1 hr Machine operation, diesel, <18.64 kW, generators (GLO) machine operation, diesel, <18.64 kW, generators Alloc Def, U	1.06E-06	4.37E+00	7.25E-01	2.57E-02	4.13E-03	9.35E+00
Sealing IW	1 m ³ Concrete, sole plate and foundation (RoW) concrete production, for civil engineering, with cement CEM I Alloc Def, U	1.80E-05	3.55E+02	1.63E+01	9.15E-01	3.66E-01	1.68E+02
Sealing PW	1 m ³ Concrete, sole plate and foundation (RoW) concrete production, for civil engineering, with cement CEM I Alloc Def, U	1.80E-05	3.55E+02	1.63E+01	9.15E-01	3.66E-01	1.68E+02
Waste	1 kg_48 Recycling of concrete, asphalt and other mineral products, DK	0.00E+00	4.81E-03	2.37E-04	2.54E-05	7.42E-07	7.98E-03
Transport of waste	1 tkm Transport, freight, lorry 3.5-7.5 metric ton, EURO3 (RoW) transport, freight, lorry 3.5-7.5 metric ton, EURO3	1.20E-07	5.22E-01	7.55E-02	3.01E-03	7.20E-04	1.08E+00

As seen in Table B6.4, operation of the system contributes the most to GWP (kg eCO₂) of the four phases of the life cycle. This is also seen in Figure B6.6, where the stages are compared. The high emissions associated with operation are likely attributed to the electricity used to run the pumps, heat exchangers, etc. Altering the design of the GES to implement instrumentation with lower electricity use would assist in decreasing the GWP associated with operating the system.

Table B6.4. Impact totals for each lifecycle stage as well as total lifecycle impacts for the GES.

Stages	Total kg CFC eq	Total kg eCO ₂	Total kg eO ₃	Total kg eSO ₂	Total kg eN	Total energy surplus (MJ)
Material Production	1.25E+01	1.32E+06	6.28E+04	5.12E+03	4.02E+03	1.16E+06
Material Transport/Cons.	2.46E-01	3.78E+06	1.98E+05	1.82E+04	1.60E+04	2.60E+06
Operation	0.00E+00	5.41E+06	0.00E+00	0.00E+00	0.00E+00	0.00E+00
End of Life	3.36E-03	6.53E+04	3.03E+03	1.69E+02	6.74E+01	3.13E+04
TOTAL	1.28E+01	1.06E+07	2.64E+05	2.35E+04	2.01E+04	3.79E+06

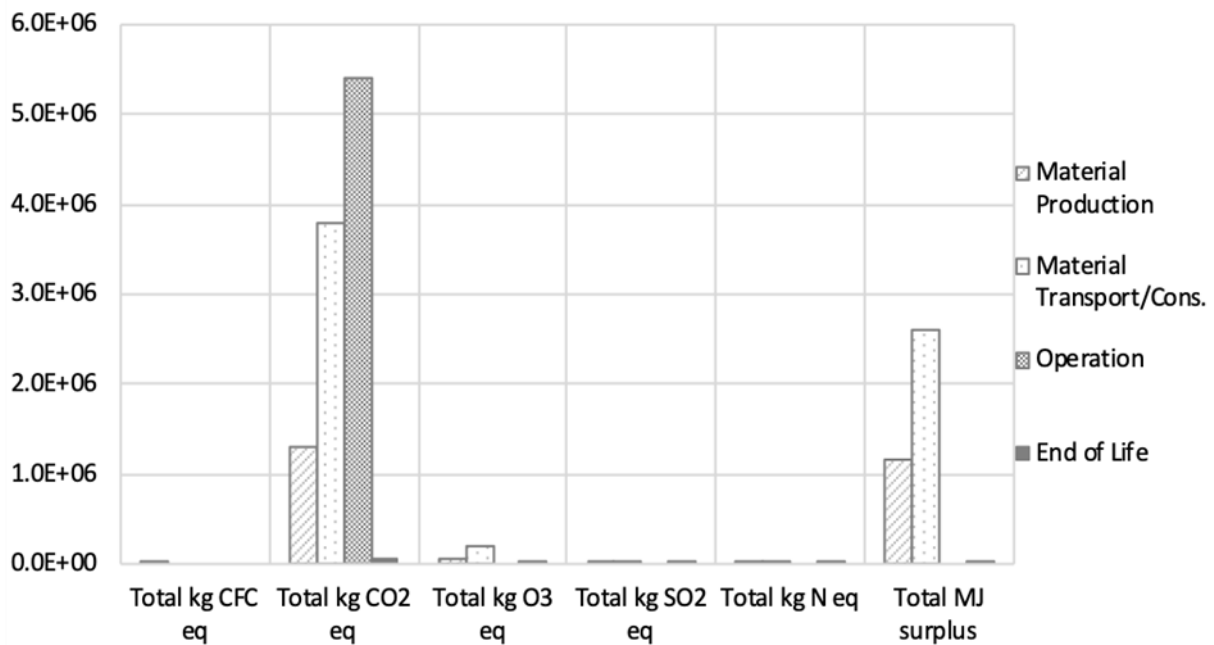


Figure B6.6: Impact comparison of the four life cycle stages, showing significant GWP associated with the operation of the DDU GES.

Figure B6.6 also shows the high impacts associated with the material production and material transport and construction phases; i.e., the GWP and fossil fuel depletion impacts. When investigating those impacts further, concrete and steel are the top contributors to these impacts. Figure B6.7 shows the significant CO₂ emissions associated with the use of steel, totaling to an order of magnitude higher than the other materials. The use of diesel, primarily during the material transport and construction phase of the project, is the primary contributor to the fossil fuel depletion associated with the project.

The depth of the extraction and injection wells requires a significant amount of steel for the well casings, with the deepest casing reaching a depth of 1,981 m. This is likely the explanation for why the steel impacts are higher than the concrete impacts. In many LCAs of geothermal systems, concrete is commonly the top contributor to the overall GWP of the system. This is because concrete has an embodied energy of 12.5 MJ per kilogram, whereas steel has 10.5 MJ per kilogram (Hsu 2010). The amount of steel is higher than that of a low-temperature geothermal exchange system.

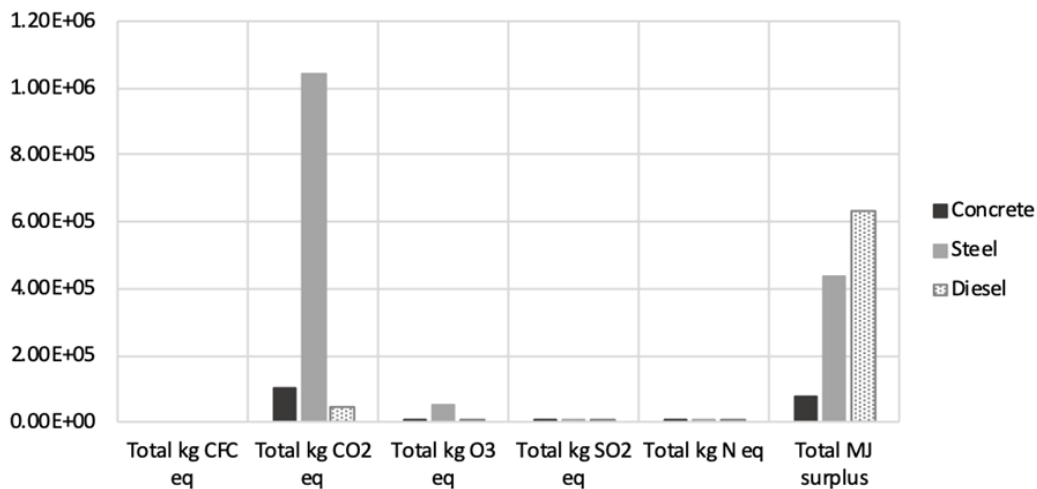


Figure B6.7: Impacts associated with the use of concrete, steel, and diesel for the DDU project in the ILB. These materials comprise the top contributors to the overall environmental impacts of the project.

While there are significant CO₂ emissions associated with the DDU GES system, it still has the potential to offset the environmental impacts associated with the alternative heat option. Currently, the Energy Corridor on the U of IL campus receives energy supply from a combination of propane and natural gas. Using available emissions data for propane and natural gas, the carbon dioxide emissions associated with heating the Energy Corridor were calculated (EIA, 2016). This information is presented in Table B6.5.

Table B6.5. Emissions associated with existing heating operations for the buildings along the Energy Corridor.

Energy Corridor Emissions	
Annual NG Use (MMBtu/yr)	5638
Emissions from NG (kg CO ₂ /MMBtu)	53.07
Annual Propane Use (MMBtu/yr)	3814
Emissions from Propane (kg CO ₂ /MMBtu)	63.07
Existing Energy Corridor Emissions (kg CO ₂ /yr)	5.40E+05
Years until DDU emissions offset	10.02

Table B6.5 shows that the annual emissions associated with the heating of the six buildings along the Energy Corridor total to 539,758 kg CO₂ per year. As stated in Table B6.1, the Beef and Sheep Laboratory, Poultry Farm, Dairy Farm, and Feed Mill are heated using natural gas, the Energy Farm is fueled by propane, and the Swine Farm utilizes a combination of natural gas and propane. If these facilities were instead heated using the proposed deep direct-use system, the emissions associated with the use of traditional fuels could be offset in approximately 10 years of operation.

The DDU GES system can also be compared to the operations of the Abbott Power Plant, which is the central power plant that serves the university campus. Using available data collected at the Abbott Power Plant, the heat production and associated emissions were calculated. This information is presented in Tables B6.6 and B6.7.

Table B6.6. Heat production data at the Abbott Power Plant on the UIUC campus.

Abbott Power Plant Production	
Hourly Steam Production (lb/hr)	8.00E+05
Annual Steam Production (lb/yr)	7.01E+09
% Steam Used	0.60
Heat in 1 lb of 100 C Steam (Btu/lb)	1112
Hourly Heat Production (MMBtu/hr)	8.90E+02
Daily Heat Production (MMBtu/day)	2.14E+04
Annual Heat Production (MMBtu/yr)	7.79E+06

Table B6.7. Calculated CO₂ emissions associated with the use of steam on the UIUC campus.

Abbot Power Plant Emissions	
Co-generated steam emissions, 2016 (kg CO ₂)	112714860
Annual Steam Production at capacity (lb/yr)	4.20E+09
Emissions from Steam (kg CO ₂ /lb)	0.0268

As shown in Table B6.7, approximately 0.0268 kg of CO₂ are emitted per pound of steam used on the UIUC campus, assuming conservatively that only 60% of the total steam produced is used for energy (Lowe 2011). With this information, it is possible to compare the emissions associated with Abbott Power Plant to the emissions associated with the proposed DDU alternative. The CO₂ emissions related to operation of the DDU GES total 5.41E+06 kg CO₂ equivalent. As a result, it will take an estimated 24 years for the DDU emissions to offset the emissions of the Abbott Power Plant alternative. Table B6.8 summarizes this information below. However, one must note that it would be very cost prohibitive to extend steam lines to the ARF, the costs and LCA impacts for which were not accounted for in this LCA.

Table B6.8. CO₂ emissions offset by the proposed system on the UIUC campus to replace the existing Abbott Power Plant.

Facility Steam Usage & DDU Offsets	
Annual Steam Usage (lb/yr)	8,500,000
Annual CO ₂ emissions offset by DDU (kg)	2.28E+05
Years until DDU emissions offset	23.7

Performance of the proposed GES was also compared to the current impacts for the ARF using a Spider diagram. The results show that the GES is a comparable alternative to help improve campus performance in annual energy use, global warming potential, water consumption, waste production, and especially in annual heat production. Using the estimated low end of heat production estimated for the GES, the DDU technology could produce 2,053% more heat than what is currently being used by the ARF. That equates to heating 14 buildings at maximum monthly energy usage. If the analysis was done using the estimated high-end of the GES heat production, the number of possible buildings heated would increase to a total of 23 buildings. These results show that while there are still notable impacts associated with GES like the DDU technology assessed in this study, there are still tangible benefits that should be considered. Table B6.9 shows the criteria categories and the associated points assigned to that target performance. Table B6.10 shows the performance calculation for each of the five categories, and Figure B6.8 shows the resulting Spider diagram.

Table B6.9. Points assigned for each of the criteria with respect to the desired performance.

Criteria	Target Improvement	Points
Energy Use (MMBtu)	20%	1
	35%	2
GWP (kg eCO ₂)	50%	1
	70%	2
Water Consumption (kg)	50%	1
	70%	2
Waste Production (kg)	50%	1
	70%	2
Annual Heat Production (MMBtu)	50%	1
	100%	2

Table B6.10. Performance comparison of the ARF to the proposed GES.

Criteria	Reference	Strategy	Performance	Points
Annual Energy Use (MMBtu)	9.5E+03	7.0E+03	25%	1
GWP (kg eCO ₂)	1.1E+08	1.1E+07	91%	2
Water Consumption (kg)	8.0E+06	2.5E+05	97%	2
Waste Production (kg)	1.0E+04	9.0E+02	91%	2
Annual Heat Production (MMBtu)	1.6E+04	3.5E+05	2053%	2

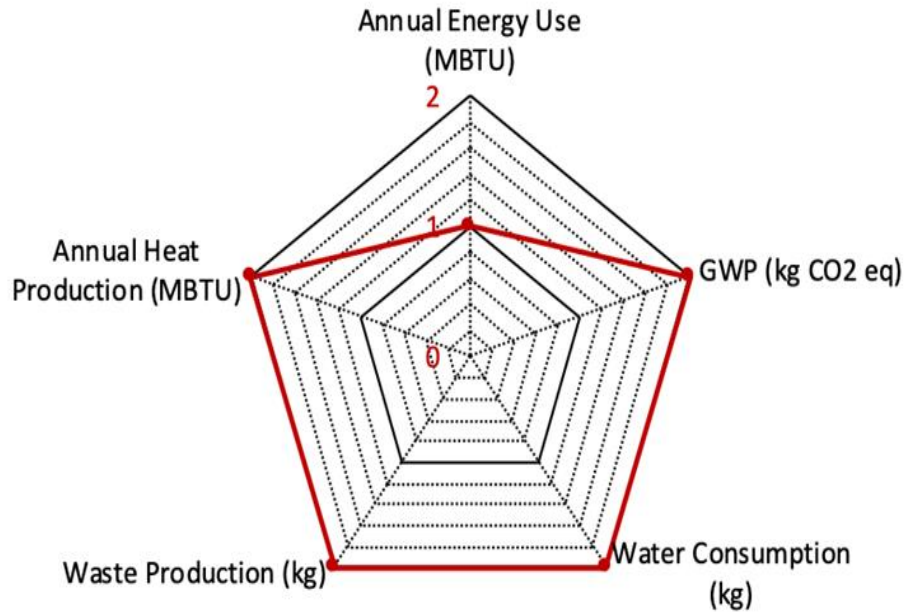


Figure B6.8. Spider diagram showing how the proposed DDU GES would improve the overall waste production, water consumption, global warming potential, annual energy use, and annual heat production at the ARF.

The LCA results presented above can serve as a procedure to represent other DDU GES using the spreadsheet tool that was developed simultaneously to produce these results. Because a significant portion of the GES at the U of IL is still in the feasibility stage and design parameters are subject to change, it is suggested that the inputs presented here are reviewed as designs are updated.

5. CONCLUSION

DDU GES are low-emission heat source alternatives that have the potential to increase the distribution of geothermal energy usage in areas with lower geothermal gradients that rely on traditional, high-emission fossil fuel sources of heating. While these GES are often considered truly sustainable energy sources, further investigation into the environmental performance of the system reveal that there are quantifiable impacts associated with various components of DDU technologies throughout the operation. A number of the high-impact components of DDU GES come from the electricity required to power external supplements to the system. Sourcing the electricity used for these components from low-emission sources could assist in reducing the environmental impacts of the system. Furthermore, carefully considering the amount of raw material used to construct the system could reduce any unnecessary impacts from material sourcing and transport. In the case of the proposed GES for the U of IL, this assessment shows that the GES can serve as promising alternative source to replace heating provided by propane or natural gas. To truly quantify the total environmental impacts associated with a DDU GES, a full design of the system is required. Once the design is completed, using the developed LCA spreadsheet tool would assist the implementation team with understanding the benefits and drawbacks of moving forward with this type of GES. Furthermore, using the tool while finalizing the design of the system could provide further insight into areas of the system that produce emissions that could be managed or minimized.

Acknowledgments:

Federal support acknowledgement: This material is based on work supported by the U.S. Department of Energy’s Office of Energy Efficiency and Renewable Energy (EERE), under the Geothermal Technologies Office Award Number DE-EE0008106.

Federal support disclaimer: This report was prepared as an account of work sponsored by an agency of the United States Government. Neither the United States Government nor any agency thereof, nor any of their employees, makes any warranty, express or implied, or assumes any legal liability or responsibility for the accuracy, completeness, or usefulness of any information, apparatus, product, or process disclosed, or represents that its use would not infringe privately owned rights. Reference herein to any specific commercial product, process, or service by trade name, trademark, manufacturer, or otherwise does not necessarily constitute or imply its endorsement, recommendation, or favoring by the United States Government or any agency thereof. The views and opinions of the authors expressed herein do not necessarily state or reflect those of the United States Government or any agency thereof.

References

- Damico, J.R., Monson, C., Stumpf, A.J., and Okwen, R.T.: Implementation of a Stepwise Procedure for Thermal Gradient Estimations in a Geocellular Modeling Framework for the Low-Temperature Illinois Basin, Proceedings, 45th Workshop on Geothermal Reservoir Engineering, Stanford University, Stanford, CA (2020).
- University of Illinois at Urbana-Champaign Facilities & Services (F&S), University of Illinois. (2017). *Energy Billing System (EBS) Data*.
- U.S. Department of Energy (USDOE). U.S. Department of Energy *Geothermal Technologies Office*. Retrieved from Energy.gov: <https://www.energy.gov/eere/geothermal/low-temperature-deep-direct-use-program-draft-white-paper> (2018).
- Hsu, S. *Life Cycle Assessment of Materials and Construction in Commercial Structures: Variability and Limitations*. Massachusetts Institute of Technology. Retrieved from <http://web.mit.edu/cron/project/concrete-sustainability-hub/Literature%20Review/Building%20Energy/Thesis/Libby%20Hsu%20Thesis.pdf> (2010).
- ISO. *Life Cycle Assessment - Principles and Framework*. Retrieved from International Organization for Standardization: <https://www.iso.org/obp/ui/#iso:std:iso:14040:en>. (2006).
- Kirksey, J, and Y. Lu. "Extraction/Injection Well Design for Deep Direct Use at University of Illinois at Urbana-Champaign [data set]." Urbana, IL: University of Illinois. <https://doi.org/10.15121/1526474>. (2019)
- Lee, J. C. *Evaluating the Sustainability of Construction with Recycled Materials*. Dissertation, University of Wisconsin-Madison. (2010).
- Lowe, R. Combined heat and power considered as a virtual steam cycle heat pump. *Energy Policy*, 39(9), 5528-5534. Retrieved from <https://doi.org/10.1016/j.enpol.2011.05.007>. (2011, September).
- McDaniel, A., Tinjum, J., Hart, D., Lin, Y. F., Stumpf, A., & Thomas, L. Distributed Thermal Response Test to Analyze Thermal Properties in Heterogeneous Lithology. *Geothermics*, 76 (2018), 116-124.
- Ponsioen, T. *The Surplus Cost Method*. Retrieved from PRéSustainability: <https://www.pre-sustainability.com/news/the-surplus-cost-method-introduction>. (2013, March 15).
- Rajaei, M., & Tinjum, J. M. Life Cycle Assessment of Energy Balance and Emissions of a Wind Energy Plant. *Geotechnical and Geological Engineering*. doi:10.1007/s10706-013-9637-3. (2013).
- Solomon, S. (1999, August). Stratospheric ozone depletion: A review of concepts and history. *Reviews of Geophysics*, 37(3), 275-316. d
- Stumpf, A., Damico, J., Okwen, R., Stark, T., Elrick, S., Nelson, W. J., and Lin, Y.-F. Feasibility of a Deep Direct-Use Geothermal System at the University of Illinois Urbana-Champaign. *Geothermal Resources Council Transactions*. (2018).
- Stumpf, A.J., Frailey, S.M., Okwen, R.T., Lu, Y., Holcomb, F.H., Tinjum, J.M., and Lin, Y.-F.: Feasibility of Deep Direct-Use for District-Scale Applications in a Low-Temperature Sedimentary Basin, *Proceedings*, 45th Workshop on Geothermal Reservoir Engineering, Stanford University, Stanford, CA (2020).
- Thomas, L. *District-Scale Geothermal Exchange Performance Evaluation using Thermodynamic and Environmental Analysis*. Thesis, University of Wisconsin-Madison. (2019).

Appendix C – Subcontractor Reports
C1. Well Design Report

Well Design Report

GeoHRC: Large-Scale, Deep Direct-Use System in a Low-Temperature Sedimentary Basin

Prepared by

Loudon Technical Services LLC
Jim Kirksey

August 5, 2019



Well Design Discussion

The large scale Deep Direct Use (DDU) geothermal project in the low temperature environment of the Illinois Basin requires drilling and completing two wells. One well would be the extraction well and would be built to deliver a flow rate of approximately 6,000 barrels per day (bpd) of brine

from the LMSS at a depth of approximately 6,300 ft. The injection well would be constructed to return the extracted brine into the LMSS at a depth of approximately 6,300 ft. Each well has different design criteria that must be met.

The extraction well is designed to meet two criteria, a casing large enough to accommodate an electric submersible pump (ESP) sized to deliver the required flow rate and then how to cost effectively insulate the wellbore to minimize heat loss so that the geothermal fluid reaches the surface at a temperature as close to the bottom hole temperature as possible. The first criteria to be met is designing a well capable of delivering a flow rate of 6,000 bpd. The flow rate defines downhole pump size as well as the tubular sizes. Based on the 6,000-bpd flow rate, a pump diameter of 5.625 inches will be required. This pump diameter will require an extraction well casing of 7-inch OD.

Wellbore stability and severe lost circulation issues have been encountered in almost all offset wells, so an intermediate casing or protection string is included in this well design. While it might be possible to eliminate this casing string, it is prudent to leave it in the initial design until more local knowledge is gained. This string also helps insulate the wellbore to prevent heat loss during extraction. The ESP will be placed deep into the well to deliver warm fluids to the surface as quickly as possible again to prevent heat loss from the extracted geothermal fluid. The extraction well string will be plastic lined for corrosion protection. A packer will be employed to make it possible to place an insulating fluid in the tubing casing annulus and to protect the extraction well casing from the corrosive brine fluid. The seven-inch casing across the MSS extraction zone will be a chrome alloy to protect the casing from corrosion. The extraction well casing will be cemented to surface. While cementing to surface is not required in an extraction well the insulation benefit of the of cemented casing is important.

The injection well is designed to meet the requirements of a Class I injection well. Shallow geothermal applications typically do not require this as the returned water meets USEPA and USDA drinking water requirements. The brine extracted from the MSS has a high TDS content and as a result the injection well will be required to be permitted as a Class I injection well. As a result, all casing strings must be cemented to surface. For reasons discussed above a protection casing string will be employed. The injection casing across the injection interval will be a chrome alloy. The tubular sizes will be 5½ inches for the injection casing and 2⅞-inch for the injection tubing. Friction pressure was considered and while the friction in the 2⅞-inch tubing might be higher by 250 psi over the next larger size, 3½ inches, the cost of additional surface pump horsepower would be more economical than constructing a larger wellbore to accommodate the larger 3½-inch tubing.

Extraction Well

The final well diagram for the extraction well is shown below in Figure C1.1.

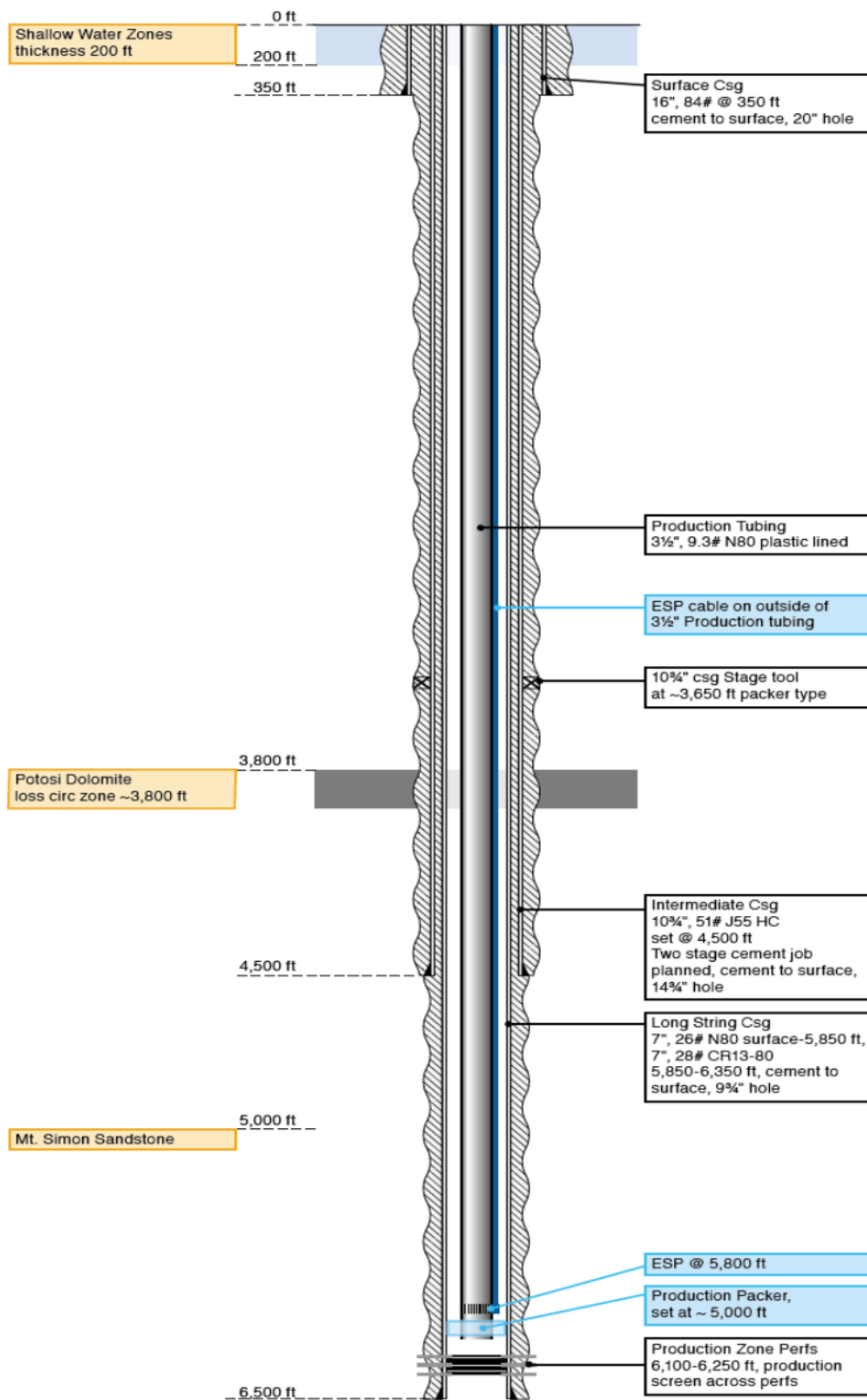


Figure C1.1. Extraction Well Diagram Extraction Well Details

The above discussion illustrates that the well design is integrated into many determining factors. Flow rates, fluid composition, subsurface conditions, and temperature are all factors that influence the final well design. The well designs that are presented here are intended to demonstrate what a typical DDU project in a deep reservoir might look like. They should be reviewed and modified as needed to optimize well design for a specific project. A primary function of creating the well design is to obtain a relative cost for each type of well. These well designs provide a glimpse into the well cost of a DDU project. Some adjustment and optimization might lower the costs presented here by a small fraction but as a starting point for an experimental project the cost numbers are sound. A discussion in the costing section of each well will detail a few of these options.

The costs presented here are good faith estimates based on current market conditions. Actual market conditions at the time of well construction could increase or decrease the real cost. The extraction well will be drilled into the LMSS at a depth of $\pm 6,500$ feet. The casing and corresponding hole sizes are shown below in Table C1.1. The drilling operation should take approximately 55 days.

Table C1.1. Casing and Hole Detail

String-Depth	Size in	Hole size in	Inner Dia.	Weight #/ft	Grade
Surface 0-350 ft	16	20	15.01	84	J-55
Int. 0-4500 ft	10 3/4	14 3/4	9.65	51	J-55 HC
Extr. 0-5850	7	9 3/4	6.276	26	N-80
Extr. 5850-6500 ft	7	9 3/4	6.184	28	Cr13-80

All casing strings will be cemented to surface. Two stage cementing technique will be employed on the intermediate casing string and on the extraction string if required. The well cement and properties are shown below in Table C1.2.

Table C1.2. Cementing Detail

String Depth	Type	Density ppg	Yield Cu ft/sk	K Btu/hr ft. ² °F
Surface 0-300 ft	Class A	15.6	1.18	.73
Int Lead 3650-0	Cmt/poz	12.5	1.85	.54
Int Tail 4500-3650 ft	Class A	15.6	1.18	.73
Extr. Lead 5500-0 ft	LiteCRETE	11.5	1.73	.3
Extr. Tail 6500-5500 ft	Class A	15.6	1.18	.73

The well will be drilled using a freshwater mud system on all strings. A severe lost circulation zone is expected to be encountered in the Potosi section of the Knox at approximately 3,500-3,800 feet. The section may require setting cement plugs and/or drilling with a loss of returns to the intermediate casing point. A packer type cementing stage collar will be used to ensure cement can be placed along the length of the wellbore. The long string casing will be cemented to surface with the lead cement designed to have a low thermal conductivity.

The well will be completed in the LMSS at a to be determined interval. For costing purposes, a 150-foot interval was considered. Tubing conveyed perforating is recommended for this length of interval. Production testing is budgeted prior to final completion. Final completion will consist of a 4½ inch internal screen to be deployed across the perforated interval to mitigate expected sand production. If during testing the sand production is found to be less than expected, the screen could be eliminated. A production packer will be set above the extraction interval to facilitate the placement of insulating fluid in the tubing casing annulus and for protection of the extraction string casing from corrosion. The 5.625-inch ESP will be run on 3½-inch plastic lined 9.3#/ft N-80 tubing with tailpipe below the pump latching into the production packer. The ESP is 102 stages requiring 405 horsepower. The estimated kVA is 502 at 480 volts and 60 HZ. The pump will require a surface power station and controller. Downhole pressure and temperature during extraction can be observed and recorded with the controller. The plastic lining of the 3½-inch extraction tubing will provide protection from corrosion from the heavy brine at a lower cost than chrome alloys.

The insulating annular fluid will be a viscous brine-based fluid that is designed to reduce the thermal conductivity by 30% over a base brine fluid. Flow loop testing suggests a thermal conductivity range of 0.2 Btu/hr·ft·°F. This compares to a base brine thermal conductivity of approximately 0.3 Btu/hr·ft·°F for a non-viscous brine. Other insulating options exist but at higher cost. These are discussed in the discussion on well costs.

Extraction Well Cost

The estimated cost of drilling and completing the extraction well is \$4.3 million. The detail of this cost is shown below in Table B1.3. The cost of \$4.3 million is considerable for a well depth of 6,500 ft. To achieve the desired flow rate of 6,000 bpd a pump diameter of 5.625'' is required. This requires the use of 7-inch casing so immediately the larger pipe and hole sizes increase the cost. The intermediate casing adds cost as well. Due to the severity of the potential loss zone in the Potosi formation however it is prudent to include it. Eliminating this casing string and the associated cost of cementing would reduce well cost by approximately \$400,000 however if the lost circulation is severe the intervention cost could quickly rise into the hundreds of thousand dollars. The worst outcome could be that the well could not be drilled to the target depth. If the injection well was to be drilled first and local geology confirmed, then a fact-based decision could be made as to whether the intermediate casing could be removed. The Potosi formation and the associated severe lost circulation was encountered at all the wells in the IBDP and ICCS projects located some 35–40 miles to the west. About 35–40 miles south, a disposal well into this formation has injected over one trillion gallons of wastewater with no surface pressure.

A few tens of thousand dollars could be saved by not cementing the extraction casing to surface, but the insulation value of the cement justifies the additional cost of cementing to surface. The use of the plastic lined extraction tubing is a savings of approximately \$180,000 over the use of chrome alloy tubing. If sand production is less than expected the extraction screen might be eliminated with a savings approaching \$100,000.

For insulation purposes a silicate fluid could be placed in the annular space between the extraction tubing and the extraction casing. This material would add approximately \$60,000 to the cost of the well but would have a thermal conductivity of ± 0.28 Btu/hr·ft·°F. Vacuum insulated tubing (VIT) could be used to further lower the thermal conductivity to approximately 0.0069 Btu/hr·ft·°F but at an additional cost of \$400,000. A dual wall insulated tubing could be used to lower the thermal conductivity to approximately 0.0347 Btu/hr·ft would increase well costs by approximately \$225,000.

A surface pump control box at a cost of \$20,000 is included in the cost estimate. The well cost includes a contingency of 7.5% for tangible costs and a 5% contingency for intangible costs. An overhead cost of 7.5% is also included for project management.

Table C1.3. Extraction Well Cost Estimate

Illinois DDU Geothermal Mt. Simon Producing Well						
AUTHORIZATION FOR EXPENDITURES - Est Cost						
In US \$						
Operator:	TBD	Project Type :	DDU Geothermal			
Contract Area:		Well Name :	Mt. Simon Producer # 1			
Contract Area #:		Well Type :	Brine producer			
Prepared by	JMK	Platform/Tripod :		AFE #:	1	
		Field/Structure :	Champaign	Date:	05-Mar-19	
		Basin :	Illinois			
Location						
Surface Elev.			Surface Coordinate Elevation			
PROGRAM		ACTUAL		PROGRAM		ACTUAL
Spud Date		Rig Days	60			
Compl Date		Total Depth	6350			
In Service		Well Cost \$/Ft	\$0.00			
Drilling Days		Well Cost \$/Day	\$0.00			
Close Out Date:		Completion Type:	Open Hole	Well Status:	Pre Permit	
Description	Dry Hole Budget	Completed Budget	Total Budget	Actual Expenditure	Actual Over/Under	% Over/Under
1 TANGIBLE COSTS						
2 Casing	472,550	0	472,550	\$0	472,550	100%
3 Casing Accessories; Float Equip & Liners	70,785	0	70,785	\$0	70,785	100%
4 Tubing		102,500	102,500	\$0	102,500	100%
5 Well Equipment - Surface	23,000	34,500	57,500	\$0	57,500	100%
6 Well Equipment - Subsurface	0	237,500	237,500	\$0	237,500	100%
7 Other Tangible Costs	0	20,000	20,000	\$0	20,000	100%
8 Contingency	42,475	29,588	72,063	\$0	72,063	100%
9 Total Tangible Costs	\$608,810	\$424,088	\$1,032,898	\$0	1,032,898	100%
10 INTANGIBLE COSTS						
11 PREPARATION & TERMINATION						
12 Surveys	6,000	0	6,000	\$0	6,000	100%
13 Location Staking & Positioning	2,500	0	2,500	\$0	2,500	100%
14 Wellsite & Access Road Preparation	84,000	0	84,000	\$0	84,000	100%
15 Service Lines & Communications	57,000	0	57,000	\$0	57,000	100%
16 Water Systems	6,000	0	6,000	\$0	6,000	100%
17 Rigging Up/Rigging Down/ Mob/Demob	130,000	0	130,000	\$0	130,000	100%
19 Total Preparations/MOB	\$285,500	\$0	\$285,500	\$0	285,500	100%
20 DRILLING - W/O OPERATIONS						
21 Contract Rig	893,760	104,000	997,760	\$0	997,760	100%
22 Drig Rig Crew/Contract Rig Crew/Catering	0	0	0	\$0	0	
23 Mud, Chem & Engineering Servs	178,250	10,000	188,250	\$0	188,250	100%
24 Water	37,000	2,000	39,000	\$0	39,000	100%
25 Bits, Reamers & Coreheads	85,000	0	85,000	\$0	85,000	100%
26 Equipment Rentals	88,364	0	88,364	\$0	88,364	100%
27 Directional Drig & Surveys	0	0	0	\$0	0	
28 Diving Services	0	0	0	\$0	0	
29 Casing & Wellhead Installation & Inspection	58,500	3,000	61,500	\$0	61,500	100%
30 Cement, Cementing & Pump Fees	273,000	0	273,000	\$0	273,000	100%
31 Misc. H2S Services	0	0	0	\$0	0	
32 Total Drilling Operations	\$1,613,874	\$119,000	\$1,732,874	\$0	1,732,874	100%
33 FORMATION EVALUATION						
34 Coring	0	0	0	\$0	0	
35 Mud Logging Services	132,500	0	132,500	\$0	132,500	100%
36 Drillstem Tests	0	0	0	\$0	0	
37 Open Hole Elec Logging Services	200,000	0	200,000	\$0	200,000	100%
39 Total Formation Evaluation	\$332,500	\$0	\$332,500	\$0	332,500	100%
40 COMPLETION						
41 Casing, Liner, Wellhead & Tubing Installation	0	10,000	10,000	\$0	10,000	100%
42 Remedial Cementing and Fees	0	0	0	\$0	0	
43 Cased Hole Elec Logging Services	25,000	30,000	55,000	\$0	55,000	100%
44 Perforating & Wireline Services	0	60,000	60,000	\$0	60,000	100%
45 Stimulation Treatment	0	0	0	\$0	0	
46 Production Tests	0	50,000	50,000	\$0	50,000	100%
48 Total Completion Costs	\$25,000	\$150,000	\$175,000	\$0	175,000	100%
49 GENERAL						
50 Supervision	194,250	40,000	234,250	\$0	234,250	100%
51 Insurance	0	0	0	\$0	0	
52 Permits & Fees	5,000	0	5,000	\$0	5,000	100%
53 Marine Rental & Charters	0	0	0	\$0	0	
54 Helicopter & Aviation Charges	0	0	0	\$0	0	
55 Land Transportation	16,000	0	16,000	\$0	16,000	100%
56 Other Transportation	0	0	0	\$0	0	
57 Fuel & Lubricants Non Rig	6,000	0	6,000	\$0	6,000	100%
58 Camp Facilities	40,500	0	40,500	\$0	40,500	100%
59 Allocated Overhead - Field Office	0	0	0	\$0	0	
60 Allocated Overhead - Main Office	240,600	41,000	281,600	\$0	281,600	100%
61 Allocated Overhead - Overseas	0	0	0	\$0	0	
62 Contingency Intangible Costs	137,961	17,500	155,461	\$0	155,461	100%
64 Total General Costs	\$640,311	\$98,500	\$738,811	\$0	738,811	100%
65 TOTAL INTANGIBLE COSTS	\$2,897,185	\$367,500	\$3,264,685	\$0	3,264,685	100%
TOTAL TANGIBLE COSTS	\$608,810	\$424,088	\$1,032,898	\$0	1,032,898	100%
66 TOTAL WELL COST	\$3,505,995	\$791,588	\$4,297,583	\$0	4,297,583	100%
67 Timed Phased Expenditures						
68 This Year						
69 Future Years						
70 Total						

Injection Well

The well diagram for the injection well is shown below in Figure C1.2.

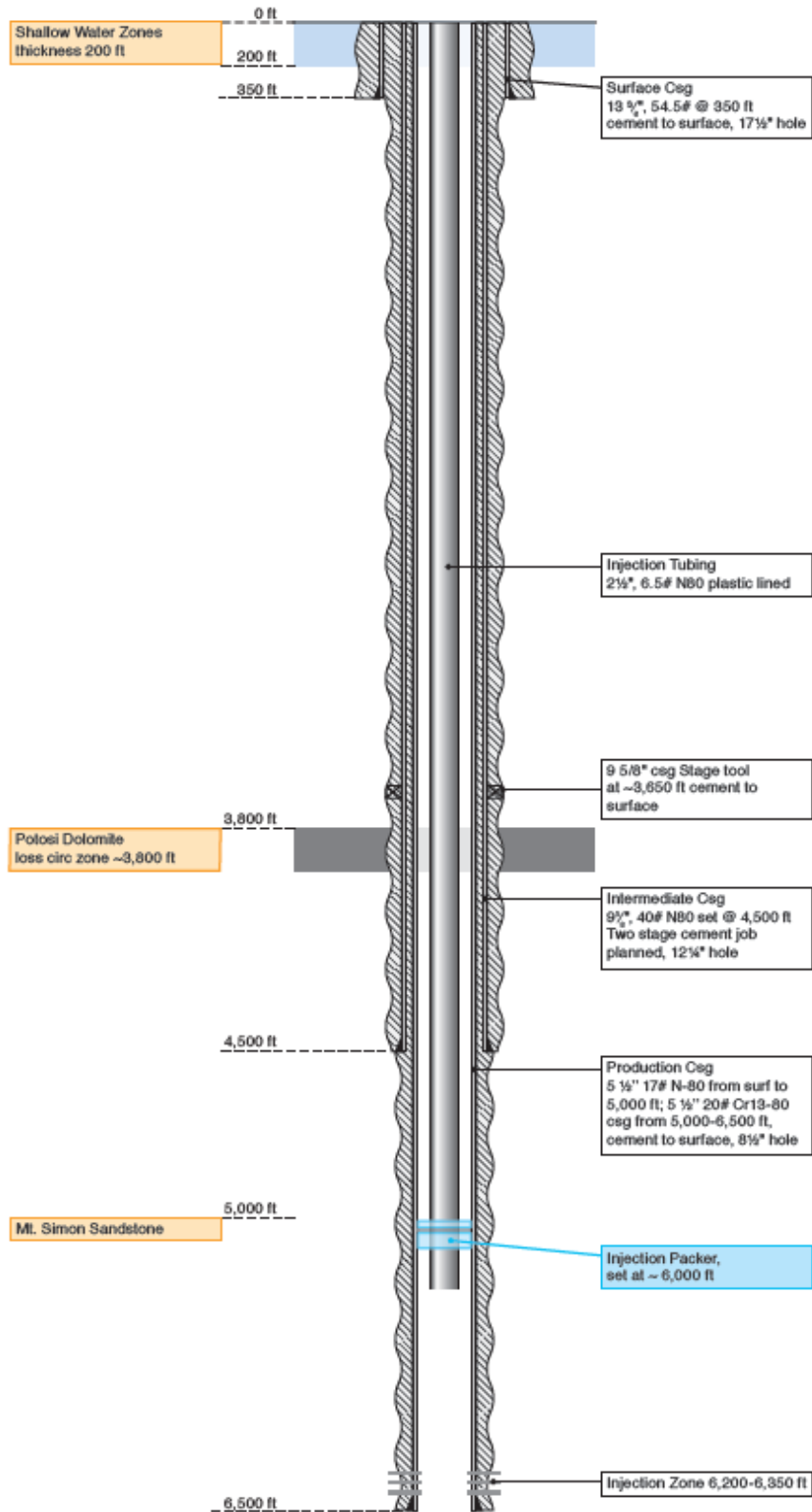


Figure C1.2. Injection Well Diagram

Injection Well Details

The DDU project injection well will be used to return the extracted brine to the lower Mt. Simon formation at a depth of approximately 6,500 ft. The well will be drilled to approximately 6,500 ft allowing room for additional injection zones to be opened if needed. The drilling should take approximately 50 days. The well will be used for the injection of heavy ($\pm 200,000$ TDS) brines and as such is regulated by the IEPA with guidance from the USEPA. There has been discussion that the well might be drilled under a Class V experimental permit, but this would have no bearing on well construction as the well would still have to be constructed to Class I standards. Class I standards state that all casing strings must be cemented to surface and that all components must be compatible with the injected fluid.

The casing and the corresponding borehole are presented below in Table C1.4.

Table C1.4. Casing and Wellbore detail Injection Well

String-Depth	Size in	Hole size in	Inner Dia.	Weight #/ft	Grade
Surface 0-350 ft	13 3/8	17 1/2	12.615	54.5	J-55
Int. 0-4500 ft	9 5/8	12 1/4	8.835	40	J-55 HC
Inj 0-5000 ft	5 1/2	8 1/2	4.892	17	N-80
Inj 5000-6500 ft	5 1/2	8 1/2	4.778	20	Cr13-80

As per regulations all casing strings will be cemented to surface. Cement types and properties are shown below in Table C1.5.

Table C1.5. Injection Well Cementing Detail

Drill String Depth	Type	Density (ppg)	Yield (Cu ft/sk)	K (Btu/hr·ft·°F)
Surface 0–300 ft	Class A	15.6	1.18	0.73
Int Lead 3,650–0 ft	Cmt/poz	12.5	1.85	0.54
Int Tail 4,500–3,650 ft	Class A	15.6	1.18	0.73
Inj Lead 4,500–0 ft	Cmt/poz	12.5	1.85	0.30
Int Tail 6,500–4,500 ft	Class A	15.6	1.18	0.73

The intermediate casing will be cemented in two stages using a packer type cementing stage collar. The chrome alloy casing across the injection zone is per regulation. The injection string will be cemented in one stage unless well conditions dictate a two-stage cementing operation is required.

The well will be drilled with a freshwater drilling mud. Lost circulation is expected in the Potosi section of the Knox formation at approximately 3,500–3,800 ft. The loss of returns will require mitigation with cement plugs or drilling to intermediate casing point with partial or no returns.

After the well is cased and cemented a section of approximately 150 ft of the LMSS will be perforated using tubing conveyed perforating technique. Injection testing including a step rate test

will be conducted to determine adequate injectivity and formation fracturing pressure. Other tests might be performed to acquire additional reservoir information.

An injection packer would then be run into the well on 2 $\frac{7}{8}$ -inch 6.5#/ft N-80 tubing which is to be plastic lined. The wet surfaces of the packer will be constructed of a chrome alloy material. The tubing-casing annulus will be filled with a weighted brine containing corrosion control additives. The surface facility will consist of an injection pump, pressure and temperature measurement recording equipment as well as flow meters to measure the volume of injected fluid. A small tank will be required. No downhole gauge is planned unless the injection permit specifically requires one as injection pressure should be well below fracturing pressure.

Injection Well Cost

The estimated cost of drilling and completing the DDU injection well is \$3.82 million. A detailed Cost Estimate is presented below in Table C1.6.

The injection well cost of \$3.62 million is reasonable for a Class I injection well to this depth. There are very few opportunities to lower the cost; however, there are possibilities that could cause the cost to increase. The intervention to control the severe loss circulation zone is included in the estimate. If the lost circulation zone is especially severe then the cost of intervention could exceed the amount budgeted. The use of the plastic lined injection string saves about \$150,000 over the use of a chrome alloy injection string. If the injection permit requires frequent surveillance logging runs to be made in the well, then the plastic-coated tubing might not be appropriate or may have to be replaced every few years. It may still be cheaper in the long run to have a planned replacement of the lower cost material than the larger cost of the alloy tubing. Another item that could raise the cost would be if the permit requires a down hole pressure monitoring. If so then the cost would increase by \$75,000-100,000. There might be enough contingency built into the AFE to cover that but if so, it would require the other components to come in at estimated cost or below. As previously mentioned, the cost presented are today's cost. Market conditions could raise or lower the overall cost of the injection well.

An estimate of \$25,000 is included for the surface facilities. The well cost includes a contingency of 7.5% for tangible costs and a 5% contingency for intangible costs. An overhead cost of 7.5% is also included for project management.

Extraction and Injection Rate Cost Matrix

The final step of the well design task was to develop a matrix so that the costs of both the extraction and injection and wells could be estimated for different flow rates. Injection is assumed to be into the same horizon as extraction is from. Four ranges of flow with the associated well costs are presented below in Table C1.6.

Table C1.6. Injection Well Cost Detail

Illinois DDU Geothermal Mt. Simon Injection Well AUTHORIZATION FOR EXPENDITURES - Est Cost							
In US \$							
Operator:	TBD	Project Type :	DDU Geothermal				
Contract Area:		Well Name :	Mt. Simon DDU Injector # 1				
Contract Area #:		Well Type :	Brine injector				
Prepared by	JMK	Platform/Tripod :		AFE #:	1		
		Field/Structure :	Champaign	Date:	04-Mar-19		
		Basin :	Illinois				
Location		Surface Coordinate					
Surface Elev.		Elevation					
PROGRAM		ACTUAL		PROGRAM		ACTUAL	
Spud Date		Rig Days	60				
Compl Date		Total Depth	6300				
In Service		Well Cost \$/Ft.	\$0.00				
Drilling Days		Well Cost \$/Da	\$0.00				
Close Out Date:		Completion Type:	Open Hole		Well Status:	Pre Permit	
Description	Dry Hole Budget	Completed Budget	Total Budget	Actual Expenditure	Actual Over/Under	%	
1 TANGIBLE COSTS							
2 Casing	399,400	0	399,400	\$0	399,400	100%	
3 Casing Accessories; Float Equip & Liners	62,850	0	62,850	\$0	62,850	100%	
4 Tubing		89,500	89,500	\$0	89,500	100%	
5 Well Equipment - Surface	20,000	48,000	68,000	\$0	68,000	100%	
6 Well Equipment - Subsurface	0	25,500	25,500	\$0	25,500	100%	
7 Other Tangible Costs	0	0	0	\$0	0	100%	
8 Contingency	38,544	11,344	49,888	\$0	49,888	100%	
9 Total Tangible Costs	\$520,794	\$174,344	\$695,138	\$0	695,138	100%	
10 INTANGIBLE COSTS							
11 PREPARATION & TERMINATION							
12 Sunveys	6,000	0	6,000	\$0	6,000	100%	
13 Location Staking & Positioning	2,000	0	2,000	\$0	2,000	100%	
14 Wellsite & Access Road Preparation	84,000	0	84,000	\$0	84,000	100%	
15 Service Lines & Communications	50,000	0	50,000	\$0	50,000	100%	
16 Water Systems	5,500	0	5,500	\$0	5,500	100%	
17 Rigging Up/Rigging Down/ Mob/Demob	130,000	0	130,000	\$0	130,000	100%	
19 Total Preparations/MOB	\$277,500	\$0	\$277,500	\$0	277,500	100%	
20 DRILLING - W/O OPERATIONS							
21 Contract Rig	813,960	125,000	938,960	\$0	938,960	100%	
22 Drig Rig Crew/Contract Rig Crew/Catering	0	0	0	\$0	0	100%	
23 Mud, Chem & Engineering Servs	164,250	5,000	169,250	\$0	169,250	100%	
24 Water	30,000	2,000	32,000	\$0	32,000	100%	
25 Bits, Reamers & Coreheads	77,500	0	77,500	\$0	77,500	100%	
26 Equipment Rentals	87,614	0	87,614	\$0	87,614	100%	
27 Directional Drig & Sunveys	0	0	0	\$0	0	100%	
28 Diving Services	0	0	0	\$0	0	100%	
29 Casing & Wellhead Installation & Inspection	46,000	3,000	49,000	\$0	49,000	100%	
30 Cement, Cementing & Pump Fees	258,000	0	258,000	\$0	258,000	100%	
31 Misc. H2S Services	0	0	0	\$0	0	100%	
32 Total Drilling Operations	\$1,477,324	\$135,000	\$1,612,324	\$0	1,612,324	100%	
33 FORMATION EVALUATION							
34 Coring	0	0	0	\$0	0	100%	
35 Mud Logging Services	120,000	0	120,000	\$0	120,000	100%	
36 Drillstem Tests	0	0	0	\$0	0	100%	
37 Open Hole Elec Logging Services	155,000	0	155,000	\$0	155,000	100%	
39 Total Formation Evaluation	\$275,000	\$0	\$275,000	\$0	275,000	100%	
40 COMPLETION							
41 Casing, Liner, Wellhead & Tubing Installation	0	6,000	6,000	\$0	6,000	100%	
42 Remedial Cementing and Fees	0	0	0	\$0	0	100%	
43 Cased Hole Elec Logging Services	27,000	35,000	62,000	\$0	62,000	100%	
44 Perforating & Wireline Services	0	60,000	60,000	\$0	60,000	100%	
45 Stimulation Treatment	0	0	0	\$0	0	100%	
46 Production Tests	0	70,000	70,000	\$0	70,000	100%	
48 Total Completion Costs	\$27,000	\$171,000	\$198,000	\$0	198,000	100%	
49 GENERAL							
50 Supervision	201,500	60,000	261,500	\$0	261,500	100%	
51 Insurance	0	0	0	\$0	0	100%	
52 Permits & Fees	0	20,000	20,000	\$0	20,000	100%	
53 Marine Rental & Charters	0	0	0	\$0	0	100%	
54 Helicopter & Aviation Charges	0	0	0	\$0	0	100%	
55 Land Transportation	12,900	0	12,900	\$0	12,900	100%	
56 Other Transportation	0	0	0	\$0	0	100%	
57 Fuel & Lubricants Non Rig	5,500	0	5,500	\$0	5,500	100%	
58 Camp Facilities	39,500	0	39,500	\$0	39,500	100%	
59 Allocated Overhead - Field Office	0	0	0	\$0	0	100%	
60 Allocated Overhead - Main Office	210,000	47,000	257,000	\$0	257,000	100%	
61 Allocated Overhead - Overseas	0	0	0	\$0	0	100%	
62 Contingency Intangible Costs	132,353	34,155	166,508	\$0	166,508	100%	
64 Total General Costs	\$601,753	\$161,155	\$762,908	\$0	762,908	100%	
65 TOTAL INTANGIBLE COSTS	\$2,658,577	\$467,155	\$3,125,732	\$0	3,125,732	100%	
65 TOTAL TANGIBLE COSTS	\$520,794	\$174,344	\$695,138	\$0	695,138	100%	
66 TOTAL WELL COST			\$3,820,870	\$0	3,820,870	100%	
67 Timed Phased Expenditures							
68 This Year							
69 Future Years							
70 Total							

Table C1.7. Well Costs for Different Flow Rates

Flow Rate bbl/day	Extract well \$M	Inject Well \$M	Total Cost \$M
2000-4000	3.90	3.30	7.20
4000-7200	4.30	3.82	8.12
7500-10000	4.40	4.32	8.72
10000-12000	5.10	4.45	9.65

The costs presented in Table C1.7. are estimates and not based on a line by line analysis as the costs presented for the Well AFE's were; however, they are representative for the purpose of illustrating how costs change with flow rates. The well geometries for each type of well changed as flow rates increased so that the matrix above has three different wellbore geometries for each type of well.

C2. Assessment of Water Chemistry Impacts on Equipment Design and Costs

From Trimeric Corporation LLC

April 5, 2019

Assessment of Water Chemistry Impacts

The objective of this task was to review available water characterization data for the different reservoirs under consideration, and then make calculations to predict the potential for scaling and precipitation of different minerals that could occur based on expected changes in temperature, pressure, or exposure to air or other materials as the brine is handled. Trimeric examined several dozen well reports from laboratory testing of water samples from the MSS and SPS in July 2018 to get an initial characterization of the water chemistry from these two reservoirs.

In December 2018 the project team decided to focus the evaluation on the water from the MSS. A representative composition for water from the MSS was selected from the BEST project (Okwen et al., 2017) for more detailed evaluation and this composition is provided in the following table.

Table C2.1. Major Constituents of MSS Geothermal Fluid

Constituent	Concentration (mg/L)
HCO₃⁻ (CaCO₃-equiv.)	21
Al	3
B	18
Ba	3
Br	650
Ca	20,800
Cl	120,000
F	<25
Fe	69
K	1,930
Li	14
Mg	1,980
Mn	54
Na	45,300
NH₃	8
Rb	3
NO₃	<2
Si	15
SO₄	290
Sr	781
Zn	3
Total TDS	~230,000

The water composition from Table C2.1 was evaluated using the following methods:

- Examined solubility product constants as an indication of scale potential
- Calculated relative saturation of various minerals using aqueous chemical equilibria calculations
- Submitted water samples to a vendor of water treatment chemicals for their evaluation using their software programs

Based on an initial examination of solubility products at 77°F (25°C), several compounds are potentially near their solubility limits including calcium carbonate, calcium sulfate, barium sulfate, and ferrous carbonate. Whether or not these compounds will precipitate depends to varying extents on the pH, temperature, and quantity of dissolved CO₂ in the water. Calcium carbonate generally becomes more soluble as the temperature drops, so in that regard the scale potential may decrease as heat is removed from the brine in the geothermal facility. However, as the brine is returned to the reservoir the temperature will increase again, which leads to increased scale potential as the water is warmed up. Barium sulfate solubility decreases as the temperature drops, so the potential for barium sulfate scaling will increase as heat is removed from the water.

Additional calculations were made using a different method to estimate the relative saturation of several minerals over a range of temperatures from 90–110 °F. These calculations also indicated that calcium carbonate was likely have the potential for scaling depending on the pH, temperature, and amounts of dissolved carbon dioxide in the water. Similar calculations were made as a courtesy by a representative from a leading international water-treating company that yielded similar results. To summarize, the following materials are highly likely to form scale in the system based on the water composition used for the analysis:

- Calcium carbonate
- Barium sulfate

Additional compounds that might have some potential for scale are:

- Calcium sulfate dihydrate (gypsum)
- Calcium sulfate (as anhydrite)
- Ferrous carbonate
- Silica

In addition to the precipitation of these minerals, if the water is exposed to oxygen there is also the potential to form insoluble oxides of iron and manganese based on the amounts of these metals in the water. These oxides, if formed, would also likely form scale in the system.

Treatment Concepts

The objective of this task was to identify and develop treatment concepts for managing or mitigating the potential for scaling and precipitation and estimate treatment costs. Given the relatively large flow rate of brine and high levels of dissolved solids, the treatment concepts that were considered were limited toward minimizing the amount of bulk chemicals used and any

volumes of waste sludge that might be produced. For example, processes to remove dissolved solids were excluded from consideration. The only treatment method considered was the addition of scale inhibitors to slow or eliminate the formation of scale in the system.

Determination of the specific scale inhibitor and required dosage would require conducting laboratory tests on the water. However, based on discussions with chemical suppliers of scale inhibitors, a phosphonate-based scale inhibitor would likely be effective. An example of a commonly used class of phosphonate scale inhibitor would be derivatives of diethylenetriamine penta-(methylenephosphonic acid). For this class of inhibitor, a typical dose might be about 10 ppmw. At a brine flow rate of 6,000 bbl/day, this corresponds to about 2.5 gallons/day of inhibitor. Based on a typical cost of about \$30/gallon, this would be about \$75 per day. Based on the design space heating rate of 2 MMBtu/hr, this corresponds to approximately \$1.60/MMBtu toward the total cost of heat. Compared to other high cost items such as the extraction and injection wells, the cost of inhibitor is not expected to be a major contributor to the total cost of heat in this DDU application, but this task has provided an initial accounting for the impact of brine treatment on total cost of heat.

In addition to the addition of scale inhibitors, simple filtration to removed suspended solids may also be needed. Data collected for the MSS water in a previous study (Kaplan et al., 2017) showed high levels of solids (about 2,800 mg/L). At this level, the quantity of solids associated with a 6,000 bbl/day stream would be about 3 metric tons per day on a dry basis. Assuming these data are accurate, the removal of 2,800 mg/L per day of solids would most likely not be economical. If the actual TSS levels are lower, as evidenced by some of the water analyses for the MSS that showed little or no suspended solids, it may be practical to provide some filtration of the water prior to feeding the water to the pumps used for reinjection into the formation.

Materials of Construction

The MSS water is relatively corrosive to metal due to the high levels of dissolved solids in the water. The water can be transported in plastic pipes (e.g. PVC, CPVC, or fiberglass). For contact with metal components such as heat exchangers and pumps, carbon steel would not be acceptable. Stainless steel alloys may also not be suitable due to the high chloride concentration in the water. A higher-grade alloy such as Hastelloy® or titanium may be required

Impact of Water Characteristics on Heat Exchanger Sizes

Compared to pure water, the MSS brine will not transfer heat as well and as a result there will be an impact on the size of the required heat exchangers. Trimeric conducted an evaluation of these impacts with regard to the expected differences in viscosity, density, heat capacity, and thermal conductivity. For turbulent flow, the variation in heat transfer coefficient (and the required size of the heat exchanger) can be related to changes in the physical properties using a typical heat transfer correlation such as the Colburn equation:

$$Nu = 0.023Re^{0.8}Pr^{1/3}$$

The use of this equation is described in most standard textbooks on heat transfer and is not described further in this report. It can be shown that for a given flow velocity and tube diameter, the heat transfer coefficient is proportional to the following parameters:

- Thermal conductivity raised to the 0.67 power
- Viscosity raised to the negative (0.467) power
- Density raised to the 0.8 power
- Heat capacity raised to the 0.33 power

The estimated relative properties of the Mt. Simon water compared to pure water are shown in the following table, which was developed using data from ASHRAE (2017) for 20 wt. % sodium chloride solution at temperatures of 80–100°F.

Table C2.2. Estimated physical and thermal properties of fluids (from ASHRAE, 2017)

	Pure Water	MSS Water
Thermal conductivity	1	0.78
Viscosity	1	1.60
Density	1	1.15
Heat Capacity	1	0.82

Based on the above relative properties, the brine-side heat transfer coefficient might be about 30% lower for the MSS water than for pure water under the same flow conditions. For a heat exchanger transferring heat from brine to water, about half of the resistance to heat transfer might be on the brine side. This would suggest that the overall heat transfer coefficient might be about 20% lower for the brine/water exchanger. This would result in a heat exchanger that is roughly 20% larger for transferring the same amount of heat from brine to water as compared to a heat exchanger transferring heat between two pure water streams.

C3. DDU GES Infrastructure Design

ISGS Geothermal Heat Recovery Complex

Assessment of Energy Use, GES Configurations, and Piping Routes

Report Date – October 18, 2019

Prepared by

Illinois State Geological Survey

and

Trimeric Corporation

P.O. Box 826

Buda, TX 78610

512-295-8118

www.trimeric.com

Authors: Yongqi Lu, Hafiz Salih, Wenfeng Fu – Illinois State Geological Survey
Ray McKaskle, Austyn Vance, Kevin Fisher – Trimeric Corporation

Table of Contents

<u>1. Analysis of Energy End-Use Demands in ACES Legacy Corridor</u>	140
<u>1.1 Energy end-users</u>	140
<u>1.2 End-use heat demands</u>	142
<u>1.3 Hourly heat load and design basis</u>	146
<u>1.3.1 Hourly heat load</u>	146
<u>1.3.2 Peak load</u>	148
<u>1.3.3 DDU design load</u>	149
<u>2. Assessment of Geothermal Energy Systems</u>	150
<u>2.1 GES scenarios</u>	151
<u>2.1.1 Case I: Baseline GES</u>	151
<u>2.1.2 Case II: GES with supplementary heat sources</u>	154
<u>2.2 GES Piping System</u>	158
<u>2.3.1 Brine/water piping routes</u>	158
<u>2.3.2 Pipe and trench sizing and costs</u>	160
<u>References</u>	162

1. Analysis of Energy End-Use Demands in ACES Legacy Corridor

1.1 Energy end-users

Exploitation of DDU geothermal energy as an alternative heating option for heating and cascading energy usage is investigated for the area of the College of Agricultural, Consumer, and Environmental Sciences' (ACES) Legacy Corridor (abbreviated as ACES Corridor hereafter). Recommendations regarding the extension and development of this new ACES Corridor along an extended and improved Lincoln Avenue in southeast of the campus have been provided in the recent Campus Master Plan of the University of Illinois.^[1] Accordingly, strategic relocation and consolidation of agricultural research and services facilities to ACES Corridor are expected in the foreseeable years to come.

In this study, six agricultural facilities are considered as potential end users of DDU geothermal energy in ACES Corridor. Three of them, including the Energy Farm, Poultry Farm, and Beef/Sheep Research Field Laboratory, are existing facilities, while the Feed Technology Center, ISRL, and Dairy Farm, will be relocated to ACES Corridor in the near future (e.g., 3–5 years). These facilities represent a variety of animal farms, laboratories, and other units configured to support teaching, basic discovery, and applied production research. A map of these existing and planned facilities is shown in Figure 1. A brief description of these facilities is provided as below.^[2]

- Energy Farm occupies 320-acre research plots as a “living laboratory” for field research and production needs for university researchers working on biofuel sources. The Farm has a 12,000 ft² building that includes office space, sample processing labs, and equipment storage. It also owns several facilities tailored to grow and work with tall biofuel crops including a 20-ft tall, 2,100 ft² biofuel crop breeding greenhouse and two matching growth chambers that allow for breeding efforts utilizing crops that require daylength control to initiate flowering in Illinois. These facilities require thermal heat for space heating and crop growth needs.
- Beef/Sheep Research Field Laboratory is a state-of-the-art 10-acre facility, which is the largest livestock research operation in the US. The primary research emphasis of the Beef/Sheep Lab has been on applied nutrition in both feedlot and breeding cattle. The Lab has 8 cattle barns and 1 sheep barn with the capacity of holding 1,000 beef cattle and 100 sheep on slotted floors. Outside of calving season the cow herd is located at 180 acres of intensively grazed mixed grass pastures located in north-west of the Lab. The Lab also hosts a metabolism barn capable of housing maximum 12 individual stalls. Both the metabolism barn as well as the office building are heated and cooled. In addition, two working facilities for cattle handling are heated, and cattle barns are heated only when the temperature is below 25 °F.
- Poultry Research Farm is utilized to conduct research in poultry nutrition, gut health, production and environmental management, immunology, and ovarian cancer. The Farm has six buildings providing ~25,000 ft² of space, which includes a breeder bird facility, a growing bird facility, a cage-laying house, a hatchery/brooder facility, and a building for specialized, more intensive research. There are about 12,000 chickens currently raised in the farm. Most building space are maintained at about 75 °F, while others may desire various temperatures depending on their functions. For examples, the feed mixture room is

kept at ~70 °F, battery cages for chicks at 90F (with electric heaters), walk-in egg incubators at 99.5 °F for 3-week hatchery, and the growing bird facility operating at 90 °F from April thru September.

- The ISRL is planned for relocation to the ACES Legacy Corridor, which is currently located on the southern part of the U of IL campus. ISRL is a full process-based facility comprising breeding, gestation, farrowing, nursing, growing and finishing rooms with total capacity for 120 sows. Current research at ISRL has focused on bio-medical sciences using pigs as a model for human health and medicine. Most ISRL space is kept at 73–75 °F, heated with NG-fired heaters in winter and cooled with air-water evaporative cooling cells in summer, except that the nursing temperature at 90 °F for the 1st week and decreasing at 0.5 °F/day to 75 °F afterwards.
- Dairy Cattle Research Unit (abbreviated as Dairy Farm hereafter) is presently located south of the main campus and may be relocated to ACES Legacy Corridor in the longer term. The Dairy Farm provides animals and infrastructure to conduct research in genetics, nutrition, physiology, immunology and management. The farm is considered a confinement facility with the exception that developing heifers have access to dirt exercise lots. There are ~180 mature lactating cows and 150 replacement heifers. The cows are milked in a double 12 parallel parlor. The milking parlor is the major energy user, equipped with two refrigeration units for providing milk tank refrigeration at 38 °F and indoor cooling for cows and staffers, a NG-fired heater and a supplementary NG boiler for supplying hot water (170 °F at 400 gallons/day) for hydronic space heating in winter and wash water in daily operation. Tap water is used in a plate & frame cooler to cool hot milk from 102 to 60 °F. Except for calf barns that employ NG-fired heaters for heating, other barns for cow housing don't require heaters in winter as the heat released from cow bodies can maintain the desired room temperature at 40 °F. Cow housing barns use tunnel ventilation for cooling in summer.
- The Feed Mill produces custom research and production diets for all livestock and poultry on the campus. The mill will be relocated to the ACES Legacy Corridor in 2020 and then be known as the Feed Technology Center. The Feed Mill produces ~3,500 tons of feed annually, and is essential to the research conducted on the campus that requires high-quality ingredients and custom diet formulations manufactured at small quantities. The Mill's production factory is equipped with an electric hammer mill operating on a daily basis to make herd diets or mix custom research diets. A pellet mill uses steam from a NG-fired water-tube boiler (20 psig) for grain pelletizing. An outdoor grain dryer with heat capacity of 4 MMBtu/hr is installed outdoor, applying 140 °F hot air generated from a NG burner as a heating medium for batch drying operation. After relocation, the Feed Technology Center will include high-throughput storage, processing, mixing, extruding, bagging, and delivery systems, will be expanded to deliver ~8,000 tons of specialized small-batch research diets per year.

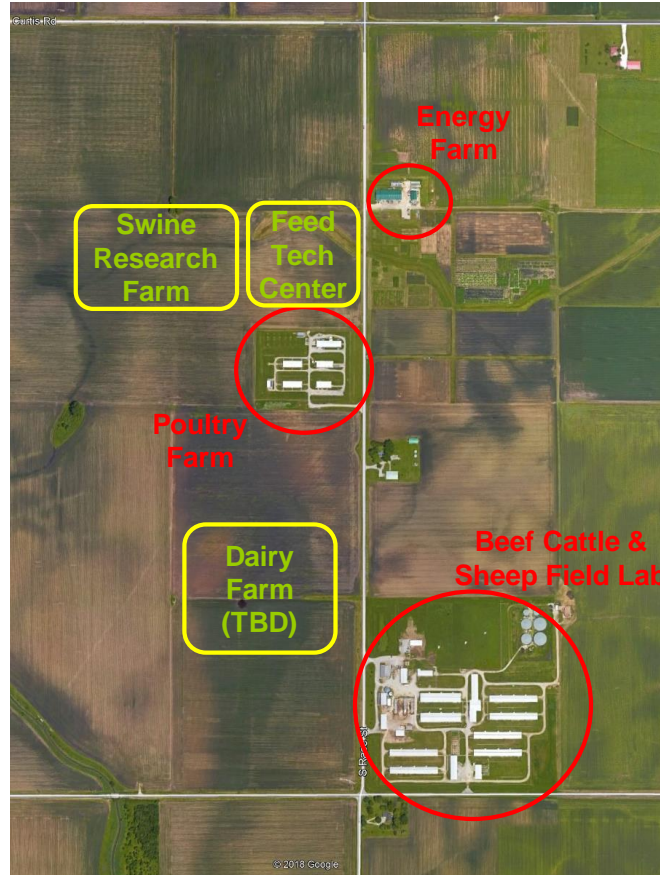


Figure C3.1. Existing and planned agricultural research & field facilities in ACES Legacy Corridor (red circles indicate the existing facilities and yellow frames the planned facilities).

1.2 End-use heat demands

Site visits were made to each of the six facilities and the visits indicate that space heating prevails over cooling needs. Cooling for most existing barns housing cattle, poultry or swine is either not required or provided by simple ventilation or air-water evaporative cooling cells in the summertime. Therefore, DDU geothermal energy is considered to only provide heating use in the Corridor area.

To understand heat demands in ACES Corridor, the historical data of fuel consumption for each facility in recent three years from fiscal years (FY) 2015 to 2017 were retrieved from the University of Illinois' Energy Billing System (EBS).^[3] Table 1 gives the monthly fuel consumption by each facility. The Energy Farm uses propane for space heating and hot water production. The Swine Farm uses both natural gas (NG) and propane fuels, but propane use is minor (<10% in total fuel use). All the other farms use natural gas as a sole fuel source. Note that the monthly data reported in EBS represents that in the previous month, thus a correction to the time mismatch has been made in Table C3.1.

Table C3.1. Monthly fuel consumption by six agricultural facilities from FY2015 to FY2017
(Data collected from EBS database)

Fuel consumption (MMBtu)		Energy Farm (LPG)	Beef/Sheep Res. Field Lab. (NG)	Poultry Farm (NG)	ISRL (NG & LPG)	Dairy Farm (NG)	Feed Mill (NG)	Total
FY2017 (July 2016 - June 2017)	Jul	0.00	3.89	16.68	20.60	16.90	18.40	76.46
	Aug	0.00	3.91	12.23	15.50	16.10	73.40	121.14
	Sep	478.24	4.55	20.01	62.66	17.40	70.60	653.46
	Oct	0.00	6.77	17.79	79.40	19.80	20.60	144.36
	Nov	172.65	26.93	31.13	230.80	87.90	109.50	658.91
	Dec	359.59	158.51	173.09	769.82	282.30	196.50	1,939.80
	Jan	379.09	135.11	111.56	718.41	198.40	179.90	1,722.46
	Feb	210.15	225.22	96.50	524.64	144.70	156.50	1,357.70
	Mar	168.55	321.56	133.90	551.13	122.00	159.20	1,456.33
	Apr	0.00	91.80	102.10	200.10	41.60	127.60	563.20
FY2016 (July 2015 - June 2016)	May	104.13	23.04	50.80	148.60	42.70	12.60	381.87
	Jun	159.39	4.49	13.40	38.60	32.50	4.70	253.07
	Jul	0.00	4.66	11.12	27.90	21.70	106.60	171.98
	Aug	0.00	5.11	27.80	22.40	21.70	104.40	181.41
	Sep	63.93	3.99	11.12	138.32	16.70	95.80	329.86
	Oct	102.76	22.09	17.79	125.60	28.40	87.30	383.93
	Nov	102.76	76.93	121.20	371.70	104.90	128.70	906.18
	Dec	0.00	111.99	162.34	579.30	150.50	180.50	1,184.63
	Jan	-29.69	153.31	112.30	786.20	178.40	186.60	1,387.12
	Feb	0.00	397.98	117.86	663.30	139.20	148.90	1,467.24
FY2015 (July 2014 - June 2015)	Mar	952.52	161.56	50.04	656.26	82.40	143.00	2,045.78
	Apr	0.00	59.83	73.39	298.50	75.10	194.40	701.22
	May	97.14	18.38	88.95	336.07	32.70	102.80	676.03
	Jun	0.00	4.61	25.57	26.40	19.30	33.00	108.88
	Jul	0.00	3.67	24.46	35.80	20.40	71.00	155.33
	Aug	331.54	3.11	28.91	31.80	18.80	75.20	489.36
	Sep	0.00	3.63	30.02	72.40	23.90	54.40	184.35
	Oct	91.59	11.65	22.24	229.05	49.80	98.60	502.93
	Nov	0.00	115.62	96.74	489.50	136.20	128.10	966.15
	Dec	414.97	114.71	133.43	689.20	174.50	167.90	1,694.71
FY2015 (July 2014 - June 2015)	Jan	54.59	186.64	132.32	733.60	186.10	121.40	1,414.65
	Feb	406.72	551.24	132.32	728.87	174.40	71.50	2,065.04
	Mar	503.45	436.88	105.63	634.88	128.10	175.90	1,984.84
	Apr	0.00	136.44	90.06	350.00	65.80	134.10	776.41
	May	308.30	18.75	35.58	102.10	28.80	118.00	611.53
	Jun	160.84	7.69	23.35	46.93	19.50	103.90	362.20

It should be noted that for the Energy Farm, the data shown in Table 1 represents the monthly amount of propane refilled into storage tanks, which doesn't reflect the actual use of propane in that month. Thus, the propane refilling data in Table 1 needs to be converted to energy consumption data. For this purpose, the values of daily degree day, which is closely correlated to heating (and cooling) demands, were used to predict heat consumption. The daily degree day (D) on a specific date can be calculated as:

$$D_i = 65 - \frac{t_{max}^i + t_{min}^i}{2} \quad (1)$$

Where D_i is the degree day on the i -th day and t_{max}^i and t_{min}^i are the highest and lowest ambient temperatures, respectively, on that day. The larger D_i indicates the colder weather requiring more heat use. When the value of D_i is less than 0, heating supply is assumed to be no longer needed.

Based on the degree days, the monthly heat consumption in the j -th month of a fiscal year (Q_j^e) is estimated as:

$$Q_j^e = \left(\sum_{j=1}^{12} Q_j^e \right) \times \frac{\sum_{i=1}^{\text{days in } j \text{ month}} d_i}{\sum_{i=1}^{\text{days in FY}} d_i} \quad (2)$$

Where $d_i = \begin{cases} D_i & (\text{if } D_i > 0) \\ 0 & (\text{if } D_i \leq 0) \end{cases} \quad (3)$

Using the above approximation approach, the monthly fuel consumption data for the Energy Farm was predicted as shown in Table C3.2.

Table C3.2. Monthly fuel consumption from FY2015 to 2017 with corrected energy use data for Energy Farm

Fuel consumption (MMBtu)	Energy Farm (LPG)	Beef/Sheep Res. Field Lab. (NG)	Poultry Farm (NG)	ISRL (NG & LPG)	Dairy Farm (NG)	Feed Mill (NG)	Total	
FY2017 (July 2016 - June 2017)	Jul	4.15	3.89	16.68	20.60	16.90	18.40	80.61
	Aug	0.00	3.91	12.23	15.50	16.10	73.40	121.14
	Sep	7.21	4.55	20.01	62.66	17.40	70.60	182.43
	Oct	79.95	6.77	17.79	79.40	19.80	20.60	224.31
	Nov	236.80	26.93	31.13	230.80	87.90	109.50	723.06
	Dec	486.70	158.51	173.09	769.82	282.30	196.50	2,066.91
	Jan	442.79	135.11	111.56	718.41	198.40	179.90	1,786.17
	Feb	297.09	225.22	96.50	524.64	144.70	156.50	1,444.64
	Mar	298.18	321.56	133.90	551.13	122.00	159.20	1,585.97
	Apr	107.69	91.80	102.10	200.10	41.60	127.60	670.90
May	68.59	23.04	50.80	148.60	42.70	12.60	346.33	
Jun	2.62	4.49	13.40	38.60	32.50	4.70	96.31	
FY2016 (July 2015 - June 2016)	Jul	0.67	4.66	11.12	27.90	21.70	106.60	172.65
	Aug	1.33	5.11	27.80	22.40	21.70	104.40	182.74
	Sep	7.20	3.99	11.12	138.32	16.70	95.80	273.13
	Oct	73.86	22.09	17.79	125.60	28.40	87.30	355.03
	Nov	152.78	76.93	121.20	371.70	104.90	128.70	956.20
	Dec	199.97	111.99	162.34	579.30	150.50	180.50	1,384.60
	Jan	313.29	153.31	112.30	786.20	178.40	186.60	1,730.10
	Feb	247.16	397.98	117.86	663.30	139.20	148.90	1,714.40
	Mar	145.58	161.56	50.04	656.26	82.40	143.00	1,238.84
	Apr	104.52	59.83	73.39	298.50	75.10	194.40	805.74
May	42.39	18.38	88.95	336.07	32.70	102.80	621.29	
Jun	0.67	4.61	25.57	26.40	19.30	33.00	109.55	
FY2015 (July 2014 - June 2015)	Jul	3.45	3.67	24.46	35.80	20.40	71.00	158.79
	Aug	0.91	3.11	28.91	31.80	18.80	75.20	158.73
	Sep	38.18	3.63	30.02	72.40	23.90	54.40	222.53
	Oct	129.82	11.65	22.24	229.05	49.80	98.60	541.16
	Nov	332.36	115.62	96.74	489.50	136.20	128.10	1,298.51
	Dec	362.00	114.71	133.43	689.20	174.50	167.90	1,641.73
	Jan	451.64	186.64	132.32	733.60	186.10	121.40	1,811.69
	Feb	476.00	551.24	132.32	728.87	174.40	71.50	2,134.32
	Mar	316.91	436.88	105.63	634.88	128.10	175.90	1,798.30
	Apr	122.73	136.44	90.06	350.00	65.80	134.10	899.13
May	35.27	18.75	35.58	102.10	28.80	118.00	338.50	
Jun	2.73	7.69	23.35	46.93	19.50	103.90	204.09	

Table C3.3 gives a summary of monthly NG and propane consumption for each facility averaged over a 3-year period (FY2015 to FY2017). As can be seen from the table, the Swine Farm was the

largest energy consumer compared with the others, accounting for ~38% of total fuel consumption by all the six facilities. The Poultry Farm and Dairy Farm used the least amounts of energy, contributing <10% of total energy use as the Poultry Farm is relatively small and dairy cows desire low temperatures and thus have few heat demands.

The changes of monthly fuel consumption over time at each of these facilities are also displayed in Figure C3.2. The NG or propane consumption, which is mainly used for space heating, is highly correlated to the seasonal weather conditions. For each facility, the NG or propane consumption became high from October until next May, peaked within December to March, and became minimal in the summertime from June until September.

Table C3.3. Average fuel consumption over three years from FY2015 to FY2017

Fuel consumption (MMBtu)	Energy Farm (LPG)	Beef/Sheep Res. Field Lab. (NG)	Poultry Farm (NG)	ISRL (NG & LPG)	Dairy Farm (NG)	Feed Mill (NG)	Total
Jul	2.76	4.07	17.42	28.10	19.67	65.33	137.35
Aug	0.75	4.04	22.98	23.23	18.87	84.33	154.20
Sep	17.53	4.05	20.38	91.13	19.33	73.60	226.03
Oct	94.54	13.50	19.27	144.68	32.67	68.83	373.50
Nov	240.65	73.16	83.02	364.00	109.67	122.10	992.59
Dec	349.56	128.40	156.28	679.44	202.43	181.63	1,697.75
Jan	402.57	158.35	118.73	746.07	187.63	162.63	1,775.99
Feb	340.08	391.48	115.56	638.94	152.77	125.63	1,764.45
Mar	253.56	306.67	96.52	614.09	110.83	159.37	1,541.03
Apr	111.65	96.03	88.52	282.87	60.83	152.03	791.92
May	48.75	20.06	58.44	195.59	34.73	77.80	435.38
Jun	2.01	5.60	20.77	37.31	23.77	47.20	136.65
Yearly total	1,864.39	1,205.40	817.90	3,845.44	973.20	1,320.50	10,026.84
Fuel use during non-heating season (4 months - June to September)							
Average Monthly Consumption (MMBtu)	5.76	4.44	20.39	44.94	20.41	67.62	163.56
Average Hourly Consumption (MMBtu)	0.01	0.01	0.03	0.06	0.03	0.09	0.22
Fuel use during heating season (8 months - Oct to May)							
Average Monthly Consumption (MMBtu)	230.17	148.45	92.04	458.21	111.45	131.25	1,171.58
Average Hourly Consumption (MMBtu)	0.32	0.20	0.13	0.63	0.15	0.18	1.60

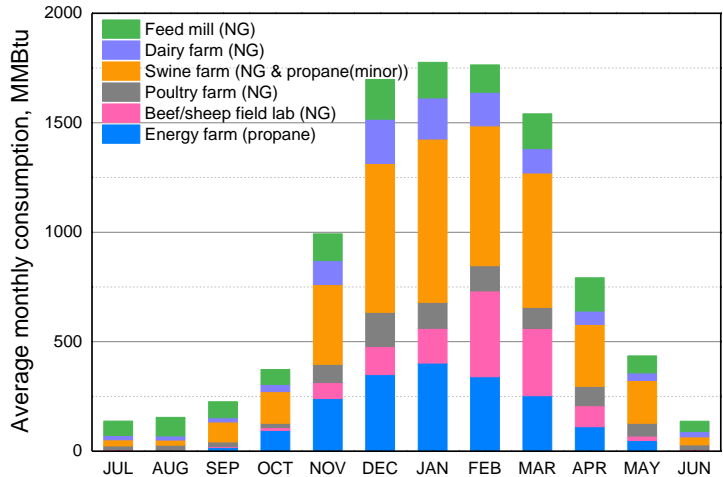


Figure C3.2. Average monthly fuel consumption by six agricultural facilities.

1.3 Hourly heat load and design basis

The profile of hourly heat load is necessary to determine the peak load of heat use and a design load desirable for the DDU geothermal energy system (GES). Because the hourly energy use data is not available, the monthly data as well as hourly weather information were used to predict the hourly heat load in this study.

1.3.1 Hourly heat load

Based on the climate data of Champaign county, the degree days over FY2015 to FY2017 were estimated [Eq.(1)] and used to assess the local ambient temperature condition. As afore mentioned, degree days are typical indicators of energy consumption for space heating and cooling. A nominal temperature of 65°F (18 °C) is generally adopted in estimating degree days. If the ambient temperature is below 65°F, then heating is deemed as necessary. The sum of degree days over periods such as a month, a season or an entire heating season can be used in estimating the periodical amount of heating required for a building.

As shown in Figure C3.3, most of the degree days from June to September are negative, indicating few heat demands during this period. Thus, these four summer months are assumed to cover the non-heating season. Positive degree days occur from October until May with peaks within January and February, which is consistent to the temporal change of monthly fuel use (Figure C3.2). Accordingly, the heating season is considered to start from October through next May (8 months).

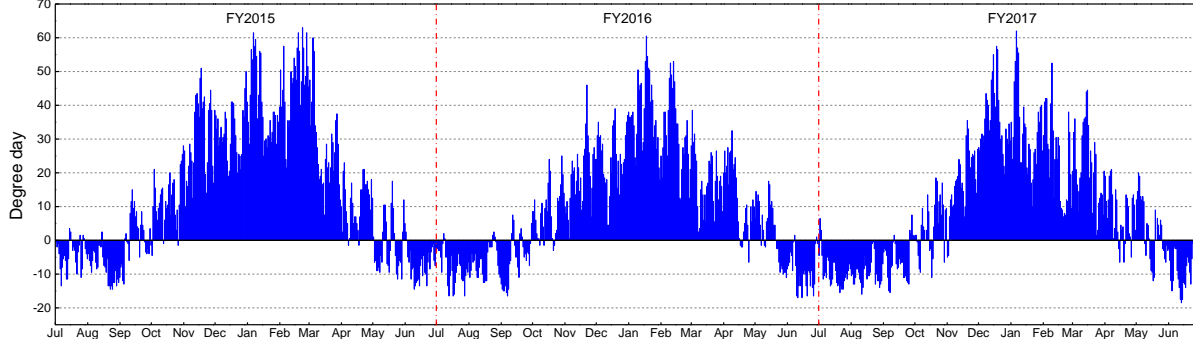


Figure C3.3. Estimated degree days in Champaign county from FY2015 through FY2017.

During the non-heating season, NG or propane is mostly consumed to provide the daily needs of domestic water. Monthly and hourly base demands for domestic water use over the entire year are assumed to be the same as those in the summertime (i.e., June to September):

$$Q_b^m = \frac{1}{4}(Q_6^m + Q_7^m + Q_8^m + Q_9^m) \quad (\text{MMBtu/month}) \quad (4)$$

$$Q_b^h = \frac{Q_b^m}{732} \quad (\text{MMBtu/hr}) \quad (5)$$

Where Q_b^m and Q_b^h are the monthly and hourly base heat load for domestic water use, respectively, for the entire year and the value of 732 is the monthly hours averaged over June to September.

Heat usage in the heating season includes both domestic water production and space heating. Thus, the amount of fuel used for space heating can be obtained by subtracting the above-determined base energy use (i.e., domestic water) from the total energy use. The hourly load for space heating highly depends on the ambient temperature, and a linear relationship between hourly heat load and approach of the ambient to the nominal temperature is assumed in the calculation. As aforementioned, a nominal temperature of 65°F is adopted as an approximate cutoff temperature, below which heating is demanded. Thus, the hourly heat load ($Q_{i,j}^h$) at i -th hour in j -th month over the entire year is estimated as follows:

$$Q_{i,j}^h = \begin{cases} Q_b^h & (\text{if } j = 6, 7, 8, 9) \\ \frac{D_{i,j}^h}{\sum_{i=1}^{\text{hours in } j \text{ month}} D_{i,j}^h} \times (Q_j^m - Q_b^m) + Q_b^h & (\text{if } j = 1, 2, 3, 4, 5, 10, 11, 12) \end{cases} \quad (6)$$

$$\text{Where } D_{i,j}^h = \begin{cases} 65 - t_{i,j} & (\text{if } t_{i,j} < 65) \\ 0 & (\text{if } t_{i,j} \geq 65) \end{cases} \quad (7)$$

and $t_{i,j}$ is the hourly ambient temperature of i -th hour in j -th month.

Hourly heat loads for the six agricultural facilities were estimated based on the approach describe above. The results are displayed in Figure C3.4 and sorted from large to small values in Figure C3.5. Overall, to greater or lesser extents, heating is required for 5,832 hours annually on a three-year average. Higher heat load demands appear often in colder months such as January and February.

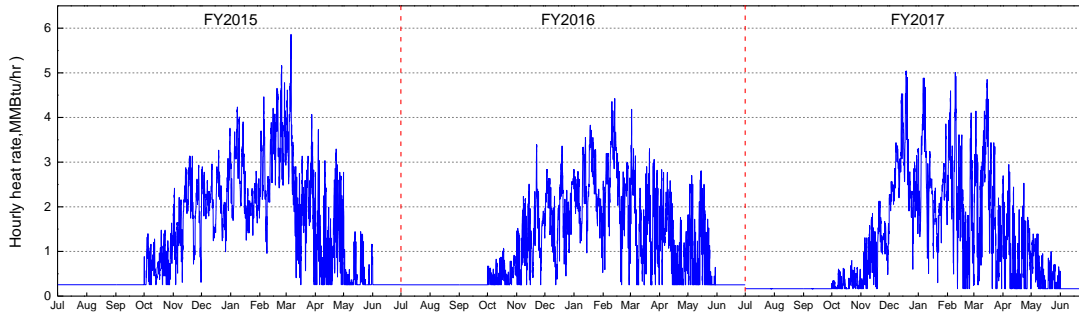


Figure C3.4. Hourly heat load demands for six agricultural facilities from FY2015 through FY2017.

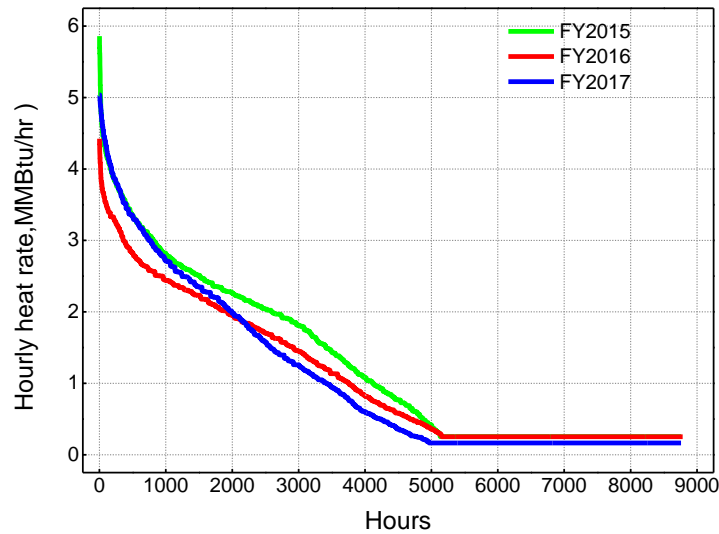


Figure C3.5. Hourly heat load demands of six agricultural facilities sorted from high to low levels.

1.3.2 Peak load

As shown in Figure C3.5, the hourly peak load reached 5.86 MMBtu/hr in FY2015, 4.42 MMBtu/hr in FY2016 and 5.04 MMBtu/hr in FY2017, with a 3-year average at 5.68 MMBtu/hr. However, high heat loads only last for a short accumulative duration (e.g., <200 hours for heat load demands >4 MMBtu/hr).

The peak load demand is an important design parameter for the GES system. To ensure the peak load is not underestimated, another approach based on the data of degree days is also used to estimate the peak load. In this approach, the peak load is approximately estimated as follows: ^[4]

$$Q_{max}^h = \frac{D_{max}}{D_{ave}} \times \frac{Q^y}{h^y} \quad (8)$$

Where D_{max} and D_{ave} are the highest and average degree day temperatures, respectively, through a year; Q^y is the total heat demand of a year; and h^y is the total hours of a year. On the basis of the degree day-based approach as well as the energy and climate data afore described (Table C3.2 and Figure C3.3), the peak loads in FY2015, FY2016 and FY2017 are obtained (Table C3.4). For the comparison purpose, the peak loads obtained from the hourly load analysis above are also listed in the table.

Table 25. Peak load demands calculated with degree day approach and hourly load analysis.

Year		Max degree day, °F	Average degree day, °F	Yearly average load, MMBtu/hr	Peak load based on Eq.(8), MMBtu/hr	Peak load from Fig.C3.5, MMBtu/hr
FY2017		62.0	9.42	1.06	7.01	5.86
FY2016		60.5	10.44	1.09	6.30	4.42
FY2015		63.0	14.79	1.28	5.45	5.04

As seen from Table C3.4, the results of peak load obtained according to the two different methods differ to some extent. The average peak load over the three years and between the two estimation methods amounts to 5.68 MMBtu/hr. Thus, as a conservative estimate, a peak load of 6 MM Btu/hr is adopted for the GES analysis in this study.

1.3.3 DDU design load

As shown in Figure C3.4, extremely high heat loads only occurs for a short period of time. For example, the occurrence of heat load demands above 5 MMBtu/hr only has an accumulated duration of 16 hours through a year. It is obvious that a GES design based on the peak load demand is not necessary because there are other ways obtain heat to address the heating load differential (e.g., heat pumps and NG heater).

An economical approach would consider satisfying a portion of total heat load demand with geothermal energy while leaving the balance of total heat load supplied by other sources such as NG-fired boilers. In particular for existing buildings, the balance of the total heating load can be satisfied by using the existing heating systems. As a result, the size of GES equipment can be reduced significantly to avoid expensive costs otherwise required for providing the peak load that only occurs for a short period of time through a year. The GES for meeting the baseload demand can also operate at a relatively steady rate instead of high turndown. In this regard, the desired GES system will use a combination of geothermal energy for baseload and supplementary heat sources for peak load.

In order to determine a suitable baseload provided with geothermal energy, the accumulative total heat load demand is plotted versus GES capacity in Figure C3.6. As seen from the figure, the relationship between the % accumulative heat load demand and heat supply capacity is not linear. The results show that a heat supply capacity of 2 MMBtu/hr can satisfy at least 80% of annual total heat load demand compared with the peak load requirement as high as ~6 MMBtu/hr. Therefore, a design load of 2 MMBtu/hr is deemed ideal and used for the analysis of DDU GES system discussed below.

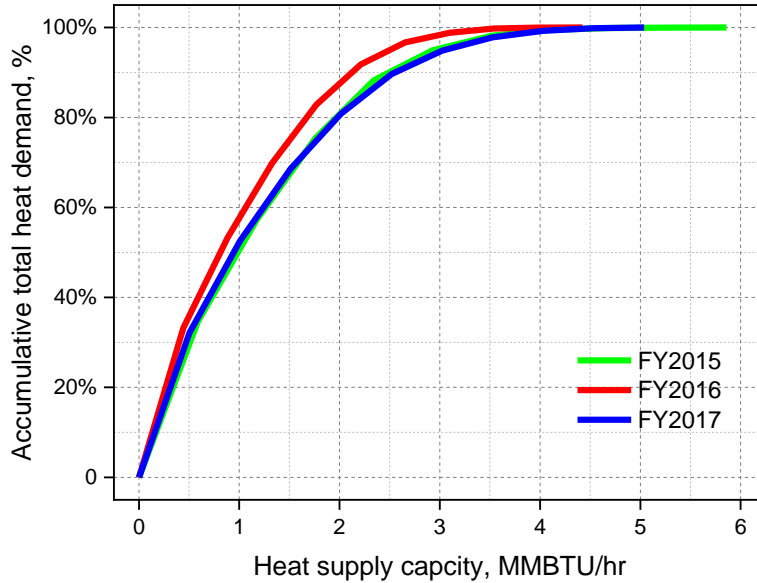


Figure C3.6. Accumulative heating load demand vs. heat supply capacity.

2. Assessment of Geothermal Energy Systems

A heat pump-based GES was initially proposed to extract heat from geothermal fluid to water circulating for heating buildings as shown in the Heating Mode in Figure C3.7. Under heating mode, the geothermal fluid provides heat to the refrigerant in the evaporator of the heat pump and then the refrigerant provides heat to the hot water return in the condenser. The heat pump may also operate under cooling mode (Figure C3.7): the geothermal fluid removes heat from the refrigerant in the condenser and the refrigerant then chill the cooling water return in the evaporator. In some cases, the heat pump can be operated to meet some cooling and some heating demands at the same time (Combined Heating and Cooling Modes, Figure C3.7). Considering the annual total heat load is much greater than the annual cooling load, heating mode would be dominant in this application. A heat pump-based system is commonly regarded to be efficient and cost effective and was thus proposed for the DDU GES application.

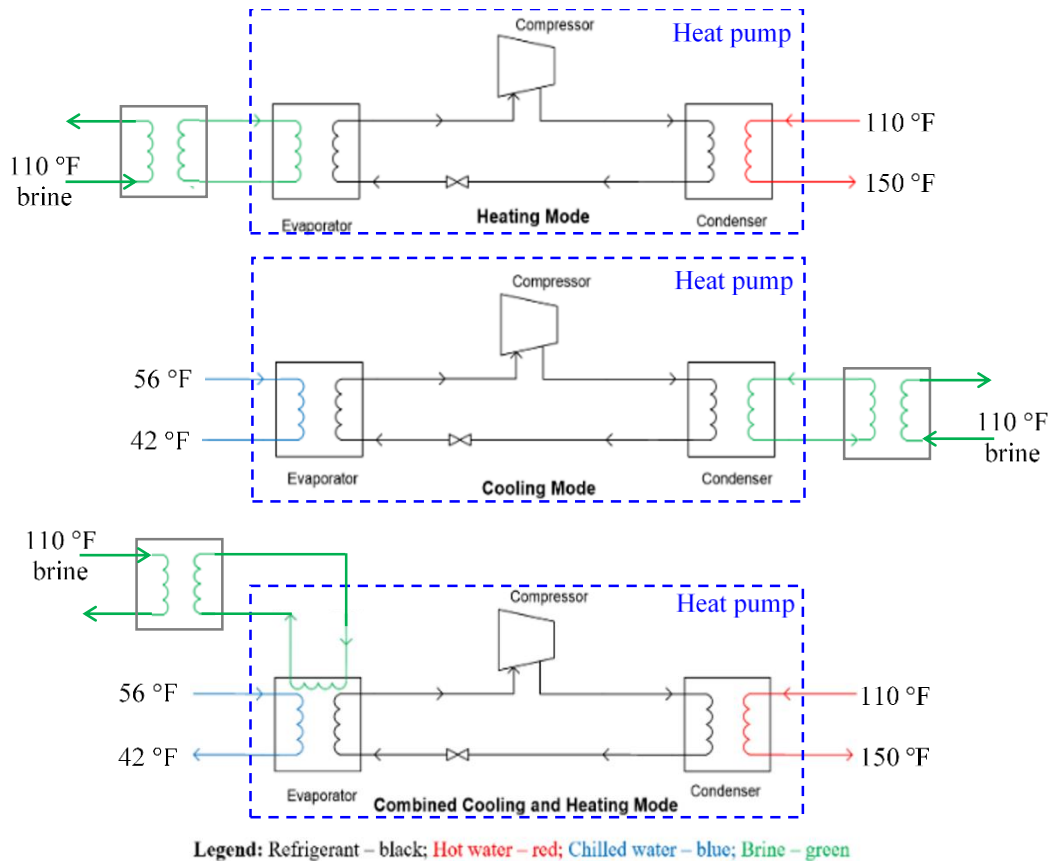


Figure C3.7. Concept diagram of the heat pump-based GES.

However, the heat pump-based GES concept had been considered as *non-direct* use of deep geothermal energy during the project. To meet the “*direct*” deep use requirement, alternative GES cases that directly use geothermal energy have been developed and assessed.

2.1 GES scenarios

Two DDU-based GES cases have been configured to utilize St Simon brine for supply heat use to ACES Corridor.

2.1.1 Case I: Baseline GES

Case 1 is the baseline GES case where MSS geothermal fluid directly transfers its heat to hot water via a heat exchanger to meet the design heat load (i.e., 2 MMBtu/hr). All heat use is provided by St Simon brine without other supplementary heat sources. At this design capacity, the GES can provide 80% of annual total heat demand in ACES Corridor. The general arrangement for the baseline process is displayed in Figure C3.8.

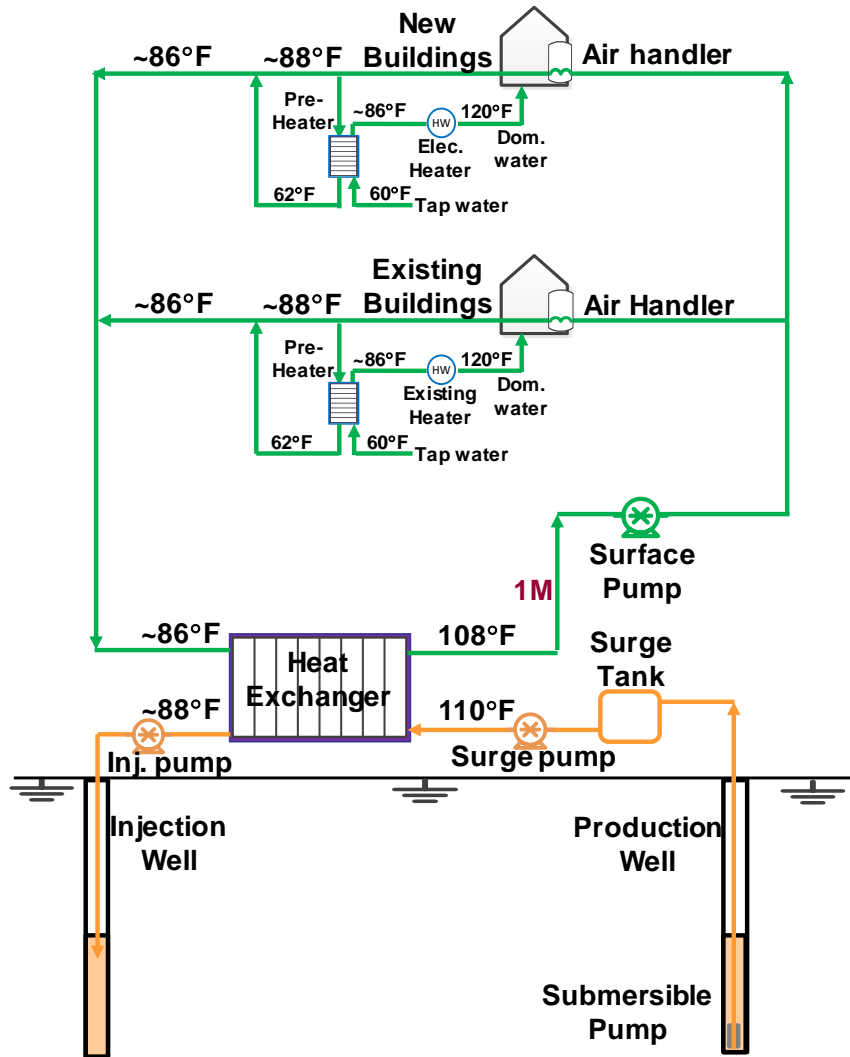


Figure C3.833. Conceptual diagram of baseline GES case with design DDU heat supply capacity of 2 MMBtu/hr.

The GES utilizes two separate water circulating loops to aid geothermal heat transfer from Mt Simon reservoir. One is an open loop for brine fluid (in orange color). In the brine loop, the hot brine is pumped from the extraction well with an electric submersible pump (ESP) into a surge tank. Stored brine is pumped with a surge pump through a plate & frame heat exchanger. The cooled brine is then injected into the geothermal reservoir through the injection well, aided by an injection pump to overcome the flow resistance through the well casings and static pressure in the reservoir. The other is a close loop for clean water (in green color). In the clean water loop, the water absorbs heat from the brine via the heat exchanger, then is pumped with a surface pump to overcome the flow resistance through the piping and building heating components. In each building, the hot water transfers heat to air via an air handler, and the heated air circulates through the building's heating, ventilation & air conditioning (HVAC) system for space heating. A small portion of the water cooled after the air handler is employed to preheat tap water entering a domestic water heater. After such cascading heat use, this portion of the cold water is mixed with the main cold water and then returns to the plate & flame heat exchanger to continue the cyclic

process. The brine and clean water loops are interfaced with the plate & flame heat exchanger that transfers the heat from the brine to the water directly. The separate brine and water loops are necessary because Mt Simon brine fluid contains a high concentration of total dissolved solids that can precipitate and form scaling in the pipes and equipment components subject to pressure and/or temperature changes.

Heat and mass balances for the baseline GES case were modelled to obtain process performance information. The major parameters assumed in the modeling are listed in Table C3.5. The results of heat & mass balances are displayed in Figure C3.9.

Table C3.5. Major assumptions used in Case 1 heat & mass balance modeling

Parameters	Value
Brine density (kg/cm ³)	1,170
Brine specific heat (kJ/kg·K)	3.43
Brine temperature from extraction well (°F)	110
Brine pressure of extraction well (bar)	1.3
Brine temperature after heat exchange (°F)	88
Brine surge pump pressure (bar)	7.8
Brine-water temperature approach at heat exchange terminal (°F)	1.8
Water temperature at air handler inlet (°F)	108
Water temperature at air handler outlet (°F)	87
Air temperature at air handler inlet (°F)	75
Air temperature at air handler outlet (°F)	95
Air-water temperature approach at air handler terminals (°F)	12
Tap water temperature at preheater inlet	60
Tap water preheated temperature at preheater outlet	86
Heat load demands between new and existing facilities	58:42
Design heat load (MMBtu/hr)	2

The modeling results show that to provide 2 MMBtu/hr design heat load, the required flow rate of brine amounts to 54.4 ton/hr (i.e., 6,375 bbl/day), which is consistent to the design of wells based on 6,000 bbl/day (4,000-7200 bbl/day) flow capacity. The temperature of the spent brine return is reduced from 110 °F in the surge tank to 88 °F before it is pumped by an injection pump back to the injection well. A circulating water flow rate at 46.0 ton/hr is required to carry over the heat load demand (2 MMBtu/hr) by heat exchange to air. The cold return water after used for space heating further provides 0.08 MMBtu/hr heat for preheating tap water from 60 to 85 °F before it enters the water heaters. The heat use demand in this case includes 1.12 MM Btu/hr for heating the new facilities, 0.81 MM Btu/hr for heating the existing facilities, and 0.08 MM Btu/hr for preheating domestic water production.

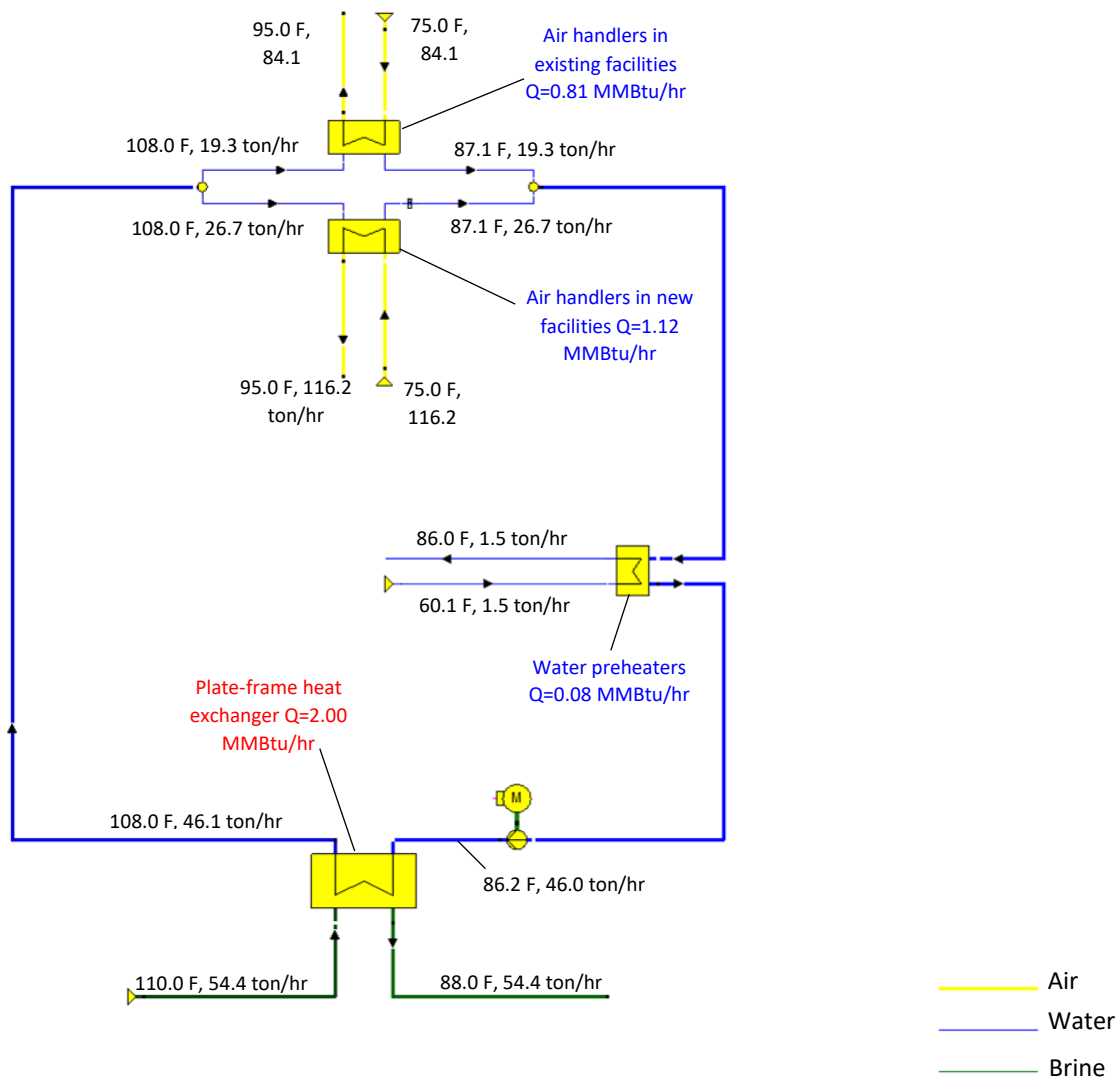


Figure C3.9. Heat and mass balances of Case 1 GES system (heat supply indicated in red and heat uses in blue).

2.1.2 Case II: GES with supplementary heat sources

Case II is a combination of Case 1 (DDU of geothermal for baseload) and supplementary heat supply using a heat pump and existing NG heating facilities to meet the peak load demand. When the heat load demand is ≤ 2 MMBtu/hr, all heat is supplied from the brine fluid. Only when the heat load demand is > 2 MMBtu/hr, the supplementary heat sources (i.e., heat pump and NG facilities) will be operated. Case II can satisfy the leak load demand (i.e., 6 MMBtu/hr) and provide 100% of annual total heat demand. The general arrangement of Case II process is displayed in Figure C3.10.

In case II process, either the brine or the clean water loop is similar to that in baseline Case 1. When the heat load demand is above the DDU design capacity, a new heat pump is used to partially supplement the hot water requirement (108 °F). The supplementary hot water produced by the heat

pump joins that from the plate & frame heat exchanger, and the mixture stream is then pumped by a surface pump to the air handlers in individual buildings. At the same time, existing NG heating facilities in the current farms are also utilized to supplement the heat supply in addition the heat pump. In individual building facilities, either air handlers or domestic water preheaters are operated under the process conditions same as Case I. After the heat exchange with air, a portion of the cold water is fed to the condenser of the heat pump for being reheated to 108 °F. The rest of the cold water returns to the main plate & frame heat exchanger, among which a slipstream is sent to the evaporator of the heat pump as a low-temperature heat source and after being cooled, flows back to the main cold return.

Modeling of heat and mass balances for Case II GES system were also conducted to assess the process performance. The assumptions used for the modeling of heat pump, such as the compressor pressure, throttle pressure, evaporation and condensation temperatures, are provided in Table C3.6. Other major assumptions adopted in the modeling are referred to Case I.

The results of heat and mass balance modeling for Case II are displayed in Figure C3.11. The brine flow rate remains at 54.4 ton/hr. The brine return is injected at 67 °F, indicating that with the aid of the heat pump, more geothermal heat (3.91 MMBtu/hr) is extracted from the brine fluid compared with that in Case I (2.00 MMBtu/hr). To satisfy the peak load demand, a total of 101.5 ton/hr hot water is required to be produced through the water-brine heat exchanger and the heat pump, providing 4.29 MMBtu/hr of total heat supply. Additional 1.68 MMBtu/hr of heat is supplemented by existing NG heating facilities in the farms currently residing in ACES Corridor, providing supplementary heat directly to the buildings through existing HVAC systems. The heat pump adds 0.42 MMBtu/hr of heat to the system because of the electric power use (112 kW_e net) for the compressor. Under the current design conditions, the heat pump can achieve a high Coefficient of Performance (COP = 4.98). The design conditions were selected based on the modeling analysis. For example, the cold-water return used as the low-temperature heat source for the heat pump evaporator is tuned to be at 71 °F by circulating a portion of the produced chilled water (~51 °F) back to the cold return feed entering the evaporator (Figure C3.10).

As displayed in Figure C3.11, the peak heat demand reaches 6.00 MMBtu/hr, including 0.81 + 1.68 MM/hr required for heating the existing facilities, 3.44 MM Btu/hr for heating the new facilities, and 0.08 MM Btu /hr for preheating domestic water production. The peak load is fully satisfied by multiple heat sources, including 3.91 MM Btu/hr from the brine fluid, 0.42 MMBtu/hr through the electric compressor motor of the heat pump, and 1.68 MMBtu/hr from NG heaters.

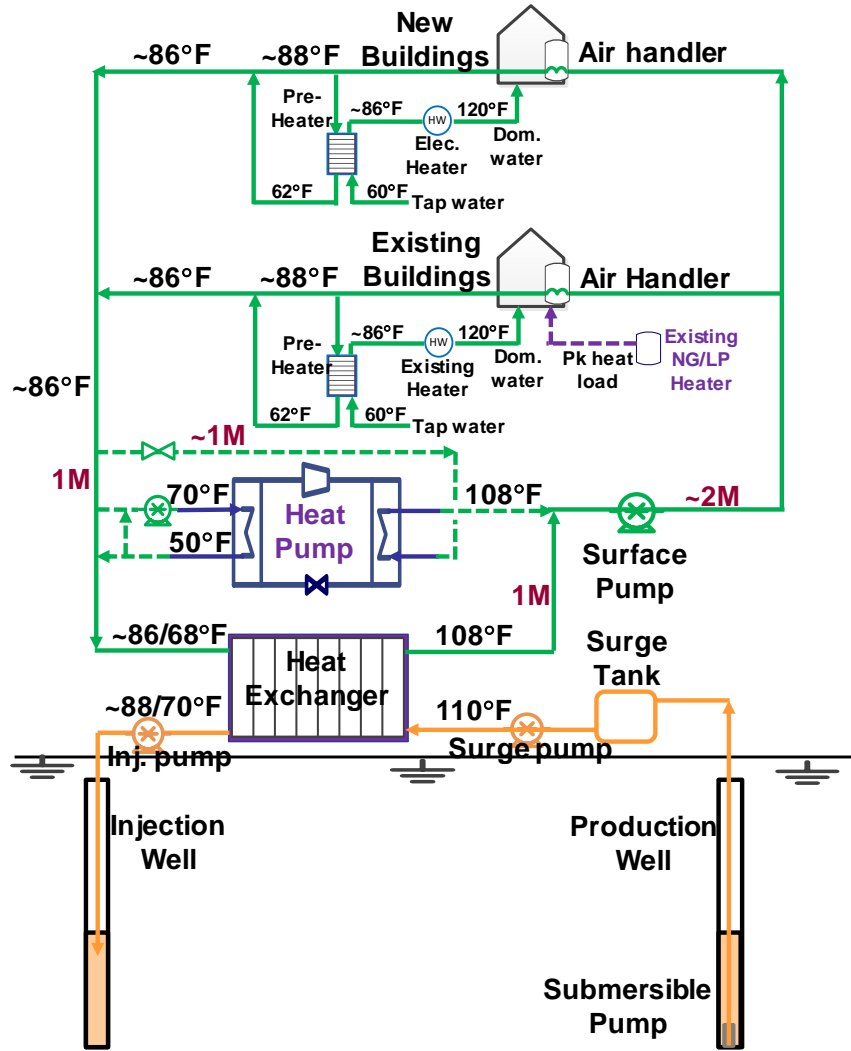


Figure C3.10. Conceptual diagram of the GES system with supplementary heat pump and existing NG heating facilities for meeting leak load demands.

Table C3.6. Major assumptions used in Case II heat & mass balance modeling

Parameters	Value
Brine density (kg/cm ³)	1,170
Brine specific heat (kJ/kg·K)	3.43
Brine temperature from extraction well (°F)	110
Brine pressure of extraction well (bar)	1.3
Brine temperature after heat exchange (°F)	88
Brine surge pump pressure (bar)	7.8
Brine-water temperature approach at heat exchange terminal (°F)	1.8
Water temperature at air handler inlet (°F)	108
Water temperature at air handler outlet (°F)	87
Air temperature at air handler inlet (°F)	75
Air temperature at air handler outlet (°F)	95
Air-water temperature approach at air handler terminals (°F)	12
Tap water temperature at preheater inlet	60
Tap water preheated temperature at preheater outlet	86
Heat load demands between new and existing facilities	58:42
Design heat load (MMBtu/hr)	2
Heat pump working medium	R410A
Heat pump compressor outlet pressure (bar)	26.0
Heat pump compressor isentropic efficiency (%)	85
Heat pump compressor throttle pressure (bar)	9.2
Heat pump condenser outlet water temperature (°F)	108

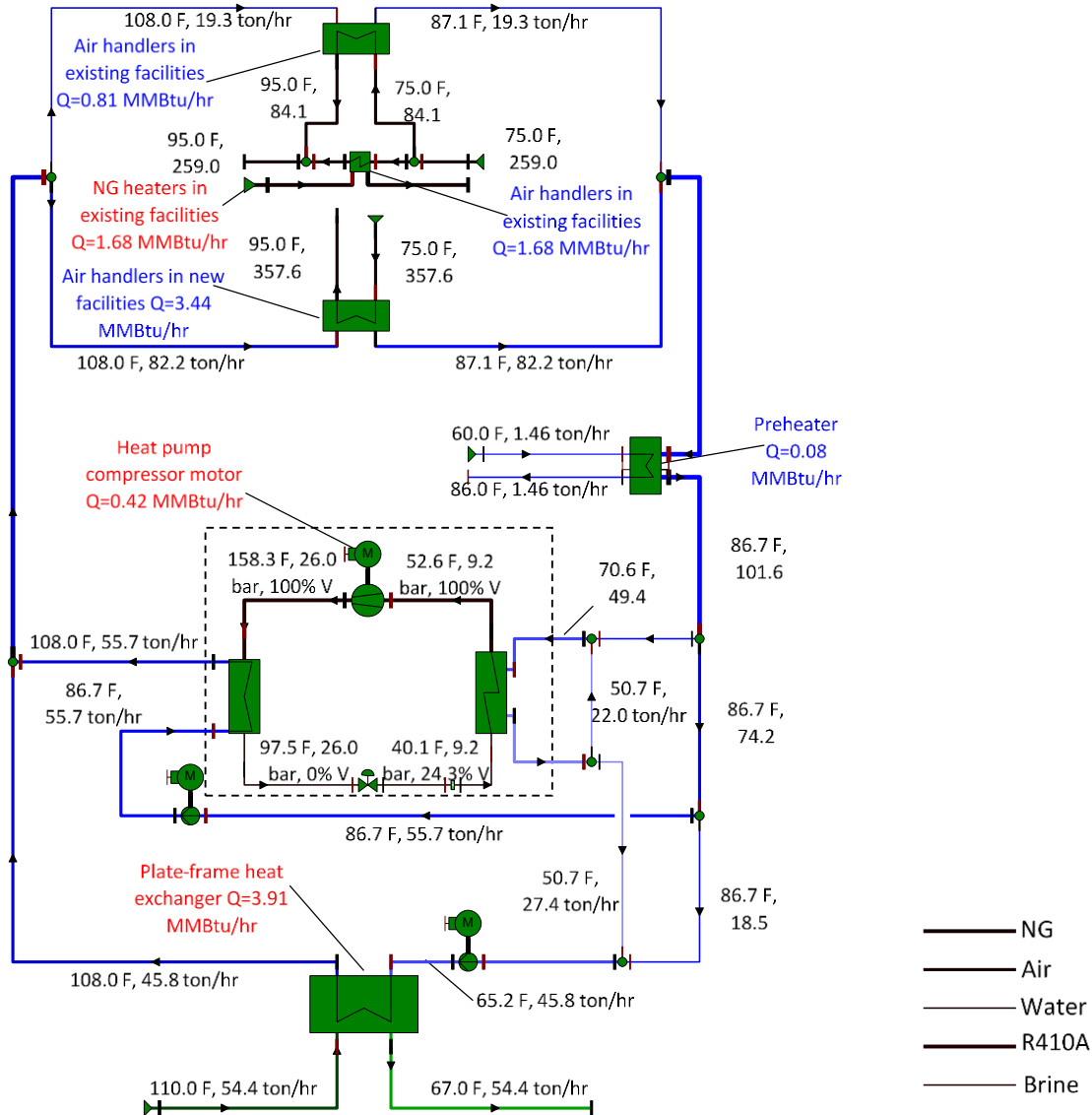


Figure C3.11. Heat and mass balances of Case II GES system with a heat pump and NG heating facilities as supplementary heat sources (heat supplies indicated in red and heat uses in blue).

2.2 GES Piping System

2.3.1 Brine/water piping routes

The “virtual” routes of the brine and clean water piping systems are illustrated in Figure C3.12. All pipes will be insulated and buried underground. According to the current plot plan, the extraction well (southeast of the map) sits on the East Old Church Road about $\frac{1}{4}$ mile east of the Race street and the injection well (northwest of the map) on the Curtis Road about $\frac{3}{4}$ miles west of the Race street. The two wells are 1.4 miles in distance, which according to reservoir simulations conducted in Task 3, would incur no interference of reservoir temperature profile within 50 years as a result of brine withdrawal and injection. Both wells are close to existing buildings, which allows for convenient access to electric power feed. A small building structure near the production well is necessary to house the process and control facilities (e.g., the plate & frame heat exchanger, surge and storage tanks, pumps, heat pump (for peak loads), power breaker, instrumentation &

control). This will also allow for immediate transfer of heat from the brine to the clean water loop when the plate-flame heat exchanger is near the production well. Another small building structure near the injection well is needed to house the injection pump and other instrumentation & control components.

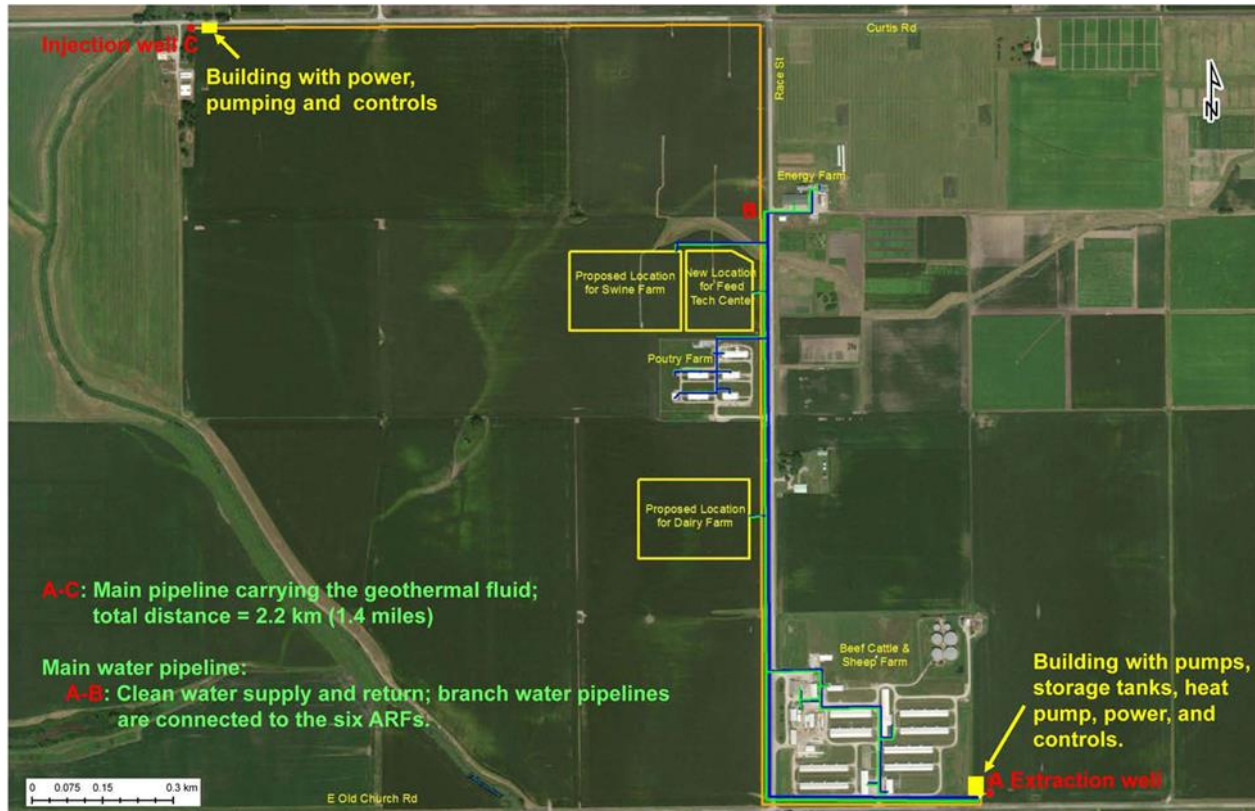


Figure C3.12. “Virtual” routes for brine and water piping lines.

Three main pipes will be constructed for the piping system to deliver the brine, clean water supply, and clean water return. The main brine pipe will be 2 miles in total length, starting from the production well (A) towards the west along the Old Church Road, towards north along the Race Street, and then towards the west along the Curtis Street to reach the injection well (C). Either the main water supply or return pipe is 1 mile in length, from the plate & flame heat exchanger exit near the extraction well towards the end of the pipe on the Race Street near the Energy Farm.

Multiple branch pipes will be built to withdraw the water from the main supply and return the water to the main return for each agricultural facility. All the six facilities, including the three to be relocated to this area, reside on either side of the Race Street, allowing for easy access to the main pipes for water supply and return. For the Poultry Farm and Beef/Sheep Lab, their water piping routes were determined in reference to the existing NG piping routes because their heat use is presently produced by NG firing. For the Energy Farm, no NG pipes are available (tanked propane is currently used instead) and thus the water piping route was arranged to allow for access to the two main heat users, i.e., the office building and greenhouses. For the three new facilities that are not yet built in AECS Corridor, their natural gas piping routes were assumed to be

approximate to those on their current locations. A description of the main and branch pipelines is presented in Table C3.7.

Table C3.7. Length and sizing information of main and branch hydronic piping systems

		Pipe length, ft	Case I Pipe size, inch	Case II Pipe size, inch
Main pipes	Brine pipe	10,560	6	6
	Clean water supply	5,280	6	6
	Clean water return	5,280	6	6
Branch pipes (water supply & return)	Energy Farm	603 (×2)	2	3
	Beef/Sheep Res. Field Lab.	2,160 (×2)	2	3
	Poultry Farm	1579 (×2)	2	2
	ISRL	675 (×2)	3	4
	Dairy Farm	2,377 (×2)	2	3
	Feed Mill	299 (×2)	2	2

2.3.2 Pipe and trench sizing and costs

Brine and water pipes are sized based on the typical fluid velocity not greater than 5 ft/s to avoid any excess pressure drop. The pressure drop for either main line is kept < ~50 psi over the entire distribution distance. The main brine line is a 6-inch pipe to handle ~6,000 bbl/day of brine fluid with a total pressure drop of 29 psi over 2 miles of distribution distance. The main water loop employs a 6-inch pipe to deliver ~6,000 bbl/day of water with a total pressure drop of 28 psi over 2 miles of distance (1 mile for supply pipe and 1 mile for return pipe) in Case I and to deliver 12,000 bbl/hr of water with a total pressure drop of 52 psi in Case II. In comparison, the sizes of branch pipes for each facility are smaller as their flow rates are lower than the main lines. The estimated pipe sizes for Case 1 and Case 2 are also included in Table C3.7.

High-density polyethylene (HDPE) pipes are chosen over Polyvinyl chloride (PVC) pipes. Both are durable and strong for water piping applications, but HDPE is more resistant to salt, corrosive fluids and abrasion from dust and precipitates and thus regarded more suitable for delivery of high-salinity brine. All pipes buried underground are insulated and bonded with jacketing. Two insulation materials, Foamglas and Gilsulate, were assessed and compared. Foamglas insulation (e.g., \$21.51/ft at 2" thickness for 6" pipe based on a quotation received) is selected in the current study because it is less expensive than Gilsulate (estimated \$500 /yard³). Based on heat transfer calculations, a thickness of 2" insulation is required to ensure the temperature loss within 1 °F through a mile of piping distance.

Total piping cost comprises the expenses of piping material, insulation material, fittings and valves, and pipe laying. The prices (\$/ft) of HDPE pipes with varying sizes and pressure ratings were obtained from vendors. The prices (\$/ft) of various Foamglas pipes with all-service jacketing were also quoted by vendors. The cost associated with fittings & valves was assumed to be 5% of total materials costs. The cost of pipe laying was estimated based on the rates reported in the literature with correction for inflation and reference year.^[5] The results of estimated piping costs are shown in Table C3.8.

Table C3.8. Costs of main and branch hydronic piping systems

		Pipe length, ft	Case I, \$	Case II, \$
Main pipes	Brine pipe	10,560	297,790	297,790
	Clean water supply	5,280	148,895	148,895
	Clean water return	5,280	148,895	148,895
Branch pipes (supply & return)	Energy Farm	603 (×2)	15,840	18,958
	Beef/Sheep Res. Field Lab.	2,160 (×2)	56,755	67,928
	Poultry Farm	1579 (×2)	41,488	41,488
	ISRL	675 (×2)	21,225	26,147
	Dairy Farm	2,377 (×2)	62,442	74,735
	Feed Mill	299 (×2)	7,847	7,847
Total			801,179	832,685

The piping will need be buried in trenches. According to University of Illinois’ Facilities & Services (F&S), a 5-foot depth from the bottom of pipe is required for trenching. For either main or branch hydronic lines, pipes running for the same route will share the same trench where possible. The maximum allowable slope for an excavation is adopted as 1:1 based on the local soil property. For a trench accommodating multiple pipes, a horizontal arrangement instead of vertical stacking is preferred for convenience of repair & maintenance. F&S also requested that the pipes in the same trench should be distant for 2 feet.

Based on the above assumptions, the trenching requirement for the main and branch lines were preliminarily estimated. Three types of trenches are configured. Trench 1 buries the main brine, water supply and water return lines starting from the extraction well (A) to the water pipe end (B, near the Energy Farm). Trench 2 houses only the brine main line from B location to the injection well (C). Trench 3 accommodates the branch lines of water supply and return for each agricultural facility. The conceptual diagrams of these types of trenches are displayed in Figure C3.13 for the illustrative purpose.

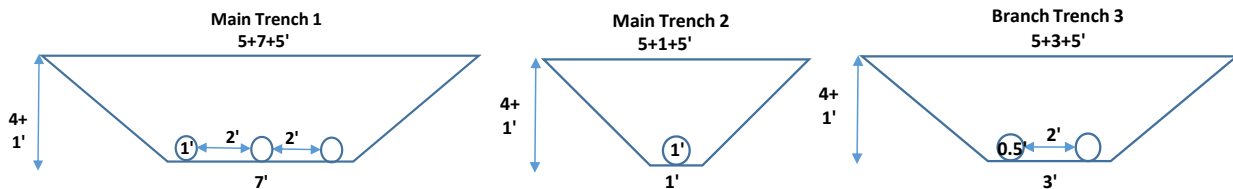


Figure C3.13. Conceptual diagrams of three types of trenches (Note that the marked pipe diameters include insulation, and are not exact but approximate values for illustrative purpose).

High-level trenching cost estimates including excavation and backfilling were obtained for each of these trenches. According to the estimates from F&S, the trenching cost could reach \$125/ft, \$60/ft and \$75/ft for Trenches 1, 2 and 3, respectively. In comparison, the costs based on a literature approach [5] were much lower: excavation estimated at ~\$10/yard³, backfilling to top of the pipe at \$14/yard³ and backfilling to top of the trench at \$4/yard³ (after correction for inflation and reference year), which is equivalent to be only 1/4 to 1/3 of the F&S estimates. Due to the large sizes required for these trenches, the Horizontal Directional Drilling (HDD) technical option was also discussed with a civil & environmental engineering company, and the costs of trenching through agricultural fields were estimated at \$55/ft for Trench 1, 30/ft for Trench 2 and \$40/ft for Trench 3. On the basis of these three cost sources, the respective medium-level rates, \$63/ft, 30/ft

and \$38/ft, were adopted in calculating the trenching costs associated with excavation and backfilling. The results of trenching costs are summarized in Table C3.9. Note that as approximate cost estimates, there are no differences of the trench sizing and costs assumed between Case 1 and Case 2 in the current study.

Table C3.9. Costs of trench excavation and backfilling

	Description	Length, ft	Excavation & backfilling cost, \$
Trench 1	Main pipes (brine, water supply & return)	5,280	330,000
Trench 2	Main brine pipe	5,280	158,400
Trench 3 (branch water supply & return)	Energy Farm	603	22,609
	Beef/Sheep Res. Field Lab.	2,160	81,007
	Poultry Farm	1,579	59,217
	ISRL	675	25,312
	Dairy Farm	2,377	89,125
	Feed Mill	299	11,200
Total		18,253	776,870

References:

1. The Impact of Place: University of Illinois at Urbana-Champaign Campus Master Plan, November 2017.
2. <https://ansc.illinois.edu/research-outreach/farm-facilities>, as of October 15, 2019.
3. <https://www.fs.illinois.edu/services/utilities-energy/business-operations/energy-billing-system>, as of October 15, 2019.
4. Andrew D. Althouse, Carl H. Turnquist, Alfred F. Bracciano, Daniel C. Bracciano, Gloria M. Bracciano. Modern Refrigeration and Air Conditioning (20th Ed.), Goodheart-Willcox Publisher, July 18, 2016.
5. NRCS/USDA, Irrigation Pipe Cost Estimator (Version 3), June 2007.

C4. Assessment of Water Chemistry, Heat Distribution Losses, and DDU System Sizing & Costs

ISGS Geothermal Heat Recovery Complex

Assessment of Water Chemistry, Heat Distribution Losses, and DDU System Sizing & Costs

Report Date – October 18, 2019

Prepared by

Illinois State Geological Survey

and

Trimeric Corporation

P.O. Box 826

Buda, TX 78610

512-295-8118

www.trimeric.com

Authors: Austyn Vance, Ray McKaskle, Kevin Fisher – Trimeric Corporation
Yongqi Lu – Illinois State Geological Survey

Disclaimer

This report was prepared as an account of work sponsored by an agency of the United States Government. Neither the United States Government nor any agency thereof, nor any of their employees, makes any warranty, express or implied, or assumes any legal liability or responsibility for the accuracy, completeness, or usefulness of any information, apparatus, product, or process disclosed, or represents that its use would not infringe privately owned rights. Reference therein to any specific commercial product, process, or service by trade name, trademark, manufacturer, or otherwise does not necessarily constitute or imply its endorsement, recommendation, or favoring by the United States Government or any agency thereof. The views and opinions of authors expressed therein do not necessarily state or reflect those of the United States Government or any agency thereof. The findings, opinions, and recommendations expressed are those of the author and not necessarily those of the University or its Project Director.

Contents

1.0	Introduction	166
2.0	Project Objectives	166
3.0	Water Chemistry Impacts on Equipment Design and Costs	167
3.1	Potential for scaling, fouling, corrosion, blockage, and precipitation	167
3.2	Concepts and costs for managing scaling/precipitation	167
3.3	Materials of construction based on water chemistry	168
3.4	Impact of water properties on heat exchanger size and pump requirements	168
4.0	Heat Losses in Surface Equipment	169
5.0	Deep Direct Use Heating and Cooling Systems	170
5.1	Review of cases and end use heating requirements	170
5.2	Preliminary estimates of equipment sizes and costs and operating costs	174
5.3	Sensitivity of the levelized cost of heat vs. the total heat demand	176
6.0	Conclusions and Recommendations	178
7.0	References	179

Introduction

The U.S. Department of Energy (DOE) Office of Energy Efficiency & Renewable Energy (EERE) is interested in assessing the potential for use of energy from fluids in low temperature sedimentary basins and similar basins. Target applications include space heating for buildings at universities and similar sites such as military installations. DOE EERE is also interested in cascading applications such as using fluids cooled after providing energy for space heating further for pre-heating domestic hot water before the fluids are discharged from the facilities. The University of Illinois led a project to assess the feasibility and cost of using fluids from Illinois Basin (ILB) reservoirs for Deep Direct Use (DDU) heating applications focused on providing space heating for existing and new campus facilities and related cascading applications.

Trimeric Corporation was part of the Infrastructure Team on this project. The Infrastructure Team was charged with assessing the feasibility and estimating costs for several options to make use of the energy contained in fluids stored in ILB reservoirs. Infrastructure items in this assessment included brine extraction wells, brine injection wells, surface facilities such as tanks, piping, fluid pumps, insulation, heat exchangers, systems for peak heating demands including heat pumps and LPG and natural gas-fired heaters, air handlers, domestic hot water systems, and related items. Unique challenges associated with utilization of relatively low temperature (78°F to 114°F) ILB reservoir fluids, coupled with the project requirement that DDU be used as the primary heating method for space heating were addressed during the work summarized in this report. Comparisons with conventional heating options are provided as are recommendations for improving DDU options and areas for further study to that end.

Project Objectives

The overall project objective for the University of Illinois Geothermal Heat Recovery Complex: Large-Scale, Deep Direct-Use System in a Low-Temperature Sedimentary Basin project was to determine the feasibility of designing a Geothermal District Heating and Cooling (GDHC) system for the University of Illinois at Urbana-Champaign (U OF IL) campus utilizing Geothermal DDU. Supporting objectives included assessing the technical and economic potential of DDU and project feasibility. Options were to be compared using the Levelized Cost of Heat as calculated by the formula specified by U.S. DOE for this project.

Trimeric Corporation worked with ISGS and other participants in the Task 4.0 Infrastructure team to determine the impact of infrastructure considerations on the project objectives. This report covers the following key items related to the infrastructure required for DDU:

- Assessment of water (brine) chemistry impacts on equipment design and costs
- Estimated heat losses in surface equipment
- Options for water and brine pumping
- Technical and economic evaluation of DDU heating systems

Project objectives with respect to infrastructure included minimizing system capital and operating costs as well as increasing system reliability by using components proven in similar

applications whenever possible. The low temperature of the St. Peter basin fluid (~ 78 oF) was considered and due to the low temperature of this fluid, the team ultimately decided that it was necessary to pursue use of the warmer Mt. Simon fluid (~ 114 oF) even though the Mt. Simon fluid is expected to have significantly higher concentrations of chlorides and other total dissolved solids (TDS). Additional treatment consideration to manage scaling, precipitation, fouling, and corrosion with the higher TDS Mt. Simon fluid are included in the evaluation summarized in this report. Mr. Jeff Urlaub of MEP Associates provided valuable insight and guidance to the other Infrastructure Team members based on his experience with commercial geothermal applications for similar office and university buildings, even though these applications use hotter geothermal fluids and/or heat pumps as opposed to DDU as the primary method for space heating.

Water Chemistry Impacts on Equipment Design and Costs

The objective of this Subtask was to review available brine chemistry data for the Mt. Simon Sandstone in the Illinois Basin and make calculations to predict the potential for mineral scaling and precipitation that could occur based on expected changes in temperature, pressure, and/or exposure to air or other materials as brine is extracted and injected.

Potential for scaling, fouling, corrosion, blockage, and precipitation

A representative composition of brine chemistry was selected for evaluation from data compiled for the BEST project (Okwen et al., 2017). An initial calculation of solubility and relative saturation of various minerals at 77°F (25 °C) indicated that several compounds are nearing their solubility limits, including calcium carbonate, calcium sulfate, barium sulfate, and ferrous carbonate. The likelihood of precipitation depends on variation in the pH, temperature, and quantity of dissolved CO₂ in the brine.

The relative saturation of several minerals was further calculated using a different method over a range of temperatures (90–110°F). Calcium carbonate and barium sulfate show high scaling potential. Calcium sulfate dihydrate (gypsum), calcium sulfate (as anhydrite), ferrous carbonate, and silica show some precipitation potential. In addition, insoluble iron and manganese oxides may be formed and cause scaling if exposed to air.

Concepts and costs for managing scaling/precipitation

The objective of this part of the assessment was to identify, develop, and estimate the costs for brine treatment procedures for managing and mitigating scaling and precipitation. Given the relatively high flow rate through the piping system and elevated level of dissolved solids in the brine, removal of dissolved solids was excluded and the addition of scale inhibitors to slow or eliminate the formation of scale in the system was considered.

Using a phosphonate-based scale inhibitor, such as a derivative of diethylenetriamine penta-(methylenephosphonic acid), could eliminate scale formation. A typical application would require ~10 ppmw of inhibitor in water. At a flow rate of 6,000 bbl/day, ~2.5 gallons/day of inhibitor would be required. This would add ~\$75/day to overall operating costs. Based on the baseload

heating rate of 2 MMBtu/hr, the addition of inhibitor accounts for ~\$1.60/MMBtu, an insignificant increase compared to the total cost of heat.

In addition to scale inhibitors, filtration may be needed to remove total suspended solids (TSS) before injection. Based on data collected from a previous study of the Mt. Simon Sandstone (Kaplan et al., 2017), a significant amount of TSS (~2,800 mg/L) could accumulate during injection. Circulating 6,000 bbl/day would create ~3 metric tons/day (dry weight), which would most likely make filtration costly. Filtration for lower TSS levels as evidenced by some of the water analyses for the Mt. Simon Sandstone may be more practical.

Materials of construction based on water chemistry

Brine from the Mt. Simon Sandstone is relatively corrosive to metal due to high levels of dissolved solids. Therefore, the brine should be transported in high density composite pipes manufactured using various materials, such as HDPE, PVC, CPVC, or fiberglass. Brine contact with heat exchangers and pumps manufactured from carbon steel must be avoided. Furthermore, stainless steel alloys may be unsuitable due to the high chloride concentration. A higher-grade alloy, such as Hastelloy® or titanium, might be required depending on the outcome of corrosion test results and the philosophy of the detailed design team. Typically, a titanium pipe is five times the cost of stainless steel. Cost estimates for both options (stainless steel tubes and titanium tubes for the brine / clean water heat exchanger) are provided later in this report.

Impact of water properties on heat exchanger size and pump requirements

Compared to fresh water, brine from the Mt. Simon Sandstone has both a higher viscosity and a lower thermal diffusivity and will consequently require larger heat exchangers. The impacts on heat exchangers regarding the expected differences in brine viscosity, density, heat capacity, and thermal properties were evaluated. For turbulent flow, variations in the heat transfer coefficient (and the required size of the heat exchanger) can be calculated while also evaluating changes to the physical properties of brine using the Colburn equation heat transfer correlation:

$$Nu = 0.023Re^{0.8}Pr^{1/3}$$

Where Nu is the Nusselt number (the ratio of convective to conductive heat transfer), Re is the Reynolds number for fluid flow, and Pr is the Prandtl number (ratio of momentum diffusivity to thermal diffusivity).

Changes in flow rate or pipe diameter lead to variations in the heat transfer coefficient that are in the following proportions with these parameters:

- Thermal conductivity changes by $\lambda^{2/3}$
- Viscosity changes by $\eta^{-0.467}$
- Density changes by $\rho^{0.8}$
- Heat capacity changes by $c^{0.33}$

The estimated relative properties of the brine and fresh water are shown in Table C4.1. In this example, the brine contains 20 wt. % sodium chloride and has a temperature between 80–100°F.

Table C4.1. Estimated physical and thermal properties of fluids (from ASHRAE, 2017)

Property	Fresh Water	Brine
Thermal conductivity	1	0.78
Viscosity	1	1.60
Density	1	1.15
Heat Capacity	1	0.82

Based on these values, the heat transfer coefficient of brine from the Mt. Simon Sandstone could be ~30% lower than for fresh water under identical flow conditions. For heat exchange between the brine and fresh water loop, about half of the resistance in heat transfer might be on the brine stream side. This translates to a 20% decrease in the heat transfer coefficient or a 20% increase in the required heat exchanger area compared with heat transfer between two pure water streams.

Heat Losses in Surface Equipment

An important consideration in the design of geothermal systems is the heat loss that occurs as warm fluids are transported and handled in the system prior to the extraction of the useful heat. Trimeric performed an analysis of heat losses in the surface equipment to understand the magnitude of the losses and what would be required to manage these losses to an acceptable level. Several variables impact the rate at which heat is lost from the system, including the pipe size, piping material, insulation characteristics, and temperature of the surroundings. The analysis included both the brine surface piping from the extraction well to the injection well and the main clean water lines. Part of this analysis involved a sensitivity study on heat losses in above ground piping compared with buried piping and insulated above and below ground piping.

The heat loss sensitivity analysis showed that the temperature loss over a mile for above ground uninsulated pipe was 13°F, for above ground insulated pipe it was 3.6°F, for buried uninsulated pipe it was 2.1°F, and for buried insulated pipe it was 1.4°F. The analysis was conducted using representative values of 60 gpm for the water flow, a hot water temperatures of 130°F, an ambient air temperature of 32°F, a pipe length of 1 mile, and a 2.875” pipe outer diameter. The thermal conductivity of the soil was assumed to be 0.4 W/m·°C), and the insulation was assumed to be 2” calcium silicate. The buried pipe depth was assumed to be 3 feet for the sensitivity. Since minimizing heat losses in this application is of high importance, it was decided that the design would incorporate lines that were buried and insulated.

Later in the study as the design concept was refined, and the design flowrate was established to be 6,000 bpd, the hot brine temperature would be 110°F, the pipe distances may be up to two miles, the pipe size for the main lines would be 6”, the insulation would be 2” Fiberglass, and the buried piping depth would be 5 feet. Surface facility equipment such as the brine surge tank and clean hot water storage tank should also be insulated to prevent heat loss.

PVC (polyvinyl chloride) and HDPE (high-density polyethylene) piping materials could both be used for all of the surface piping in this application. The surface piping operating pressure is less

than 100 psig, which makes it suitable for PVC pipe. HDPE piping can accommodate higher pressure surges than PVC pipe. HDPE has more expensive fittings and higher installation costs than PVC piping. ISGS chose to move forward with HDPE piping material for the purpose of this study.

Trimeric determined the pipe size based on pressure drop and velocity in the lines. The pressure drop and velocity were determined in process modeling software VMGSim version 10. The guideline that Trimeric used for liquid velocity in the pipe is 5 ft/s or less. Trimeric decided that the pressure drop for 6,000 bpd of water over 2 miles of piping should not exceed 50 psi. With these guidelines, it was determined that the brine and main clean water piping should have an inner diameter of ~6 inches.

Deep Direct Use Heating and Cooling Systems

Review of cases and end use heating requirements

ISGS decided to consider two different cases for preliminary design and cost estimation. In Case 1, the DDU system provides 2 MMBtu/hr of heat or around 80% of the total annual heating load. In Case 2, the DDU system provides 2 MMBtu/hr of heat, and during peak heating periods, a heat pump provides an additional 2.3 MMBtu/hr, and existing LPG / natural gas-fired heaters provide an additional 1.7 MMBtu/hr (the heat pump and the heaters combined provide the remaining 20% of the total annual heating load).

There are six users or facilities that will be utilizing the DDU heat in this study, and multiple buildings per facility. Three of the facilities are existing facilities with existing heaters that provide heat to the buildings. Three of the facilities in the study are new buildings that do not yet exist, and therefore have no existing heating equipment. A DDU system that is capable of providing 2 MM BTU/hr will be sufficient to provide 80% of the heat to all six facilities on an annual basis. During peak loads, a total of 6 MMBtu/hr is required. Case 1 does not include additional heat from any heat source other than the DDU system. Therefore Case 1 does not provide enough heat for the facilities during peak loads.

C4.1 and C4.2 show process flow diagrams of Cases 1 and 2 respectively.

For both cases the hot brine is extracted from the well with a submersible pump. The hot brine enters the brine surge tank, which has a residence time of about 10 minutes, and operates near atmospheric pressure. The surge tank pump is a stainless-steel centrifugal pump that increases the pressure to 100 psig before entering the brine / clean water heat exchanger. The heat exchanger uses the brine to heat clean water via non-contact heat transfer. The clean water is then circulated to the facilities to provide heating. The brine travels 2 miles in underground piping to the injection well pump. This line does not need to be insulated since the heat it can provide has already been transferred to the clean water. The injection well pump is a stainless-steel Triplex pump that increases the pressure to 1,166 psig for injection.

The clean water that has been heated by the brine in the heat exchanger enters the clean water surge tank. The clean water surge tank provides up to 12 hours of storage for the hot water in a

carbon steel tank. Then the surface pump, which is a carbon steel centrifugal pump, pumps the clean water to around 100 psig to keep the clean water circulating from the heat exchanger to the facilities and back. The hot clean water branches off to each facility and each building within the facilities. At each building, the hot clean water exchanges heat with air in an air handler. The air handler provides warm air to the buildings. The clean water is then used further to provide preheating for domestic hot water use before recirculating to the brine heat exchanger.

For Case 2 during peak loads, the heat pump and existing heaters are turned on to provide additional heating to the buildings. The heat pump removes heat from a slip stream of the cooled clean water and uses it to heat up the clean water circulating to the facilities by means of a refrigeration loop. When the heat pump is running, the clean water temperature entering the brine / clean water heat exchanger drops to 68°F and the brine temperature leaving the heat exchanger drops to 70°F. Process modeling in VMGSim was used to confirm the temperatures shown in the process flow diagrams.

The Case 1 heating system is designed to provide 2 MMBtu/hr of heat and the Case 2 heating system is designed to provide up to 6 MMBtu/hr of heat. The system is most efficient at full design loads; however most of the time the heating requirement will be less than full design. This applies for both Case 1 and Case 2. In order to increase efficiency, VFDs (variable frequency drives) are to be installed on all pumps and fans to increase the turndown capacity of equipment. Equipment will be turned off when possible to reduce energy use. The submersible pump manufacturer recommends turning off the submersible pump in the brine extraction well no more than once or twice per day with a minimum shutdown time of one hour. Shutting down the submersible pump might allow solids (scale, fines) to fall back into the pump and lead to premature failure. Trimeric assumed this pump could be shut down once a day for up to 12 hours. This allows the pump to operate at full loads even when partial heating loads are required, while storing hot clean water that is not needed yet in the clean water surge tank.

Preliminary piping and instrumentation diagrams (P&IDs) for both cases can be found in the attachments. The preliminary P&IDs show example controls, pipe sizes and materials, and where insulation is required.

Figure C4.1. Case 1 Process Flow Diagram

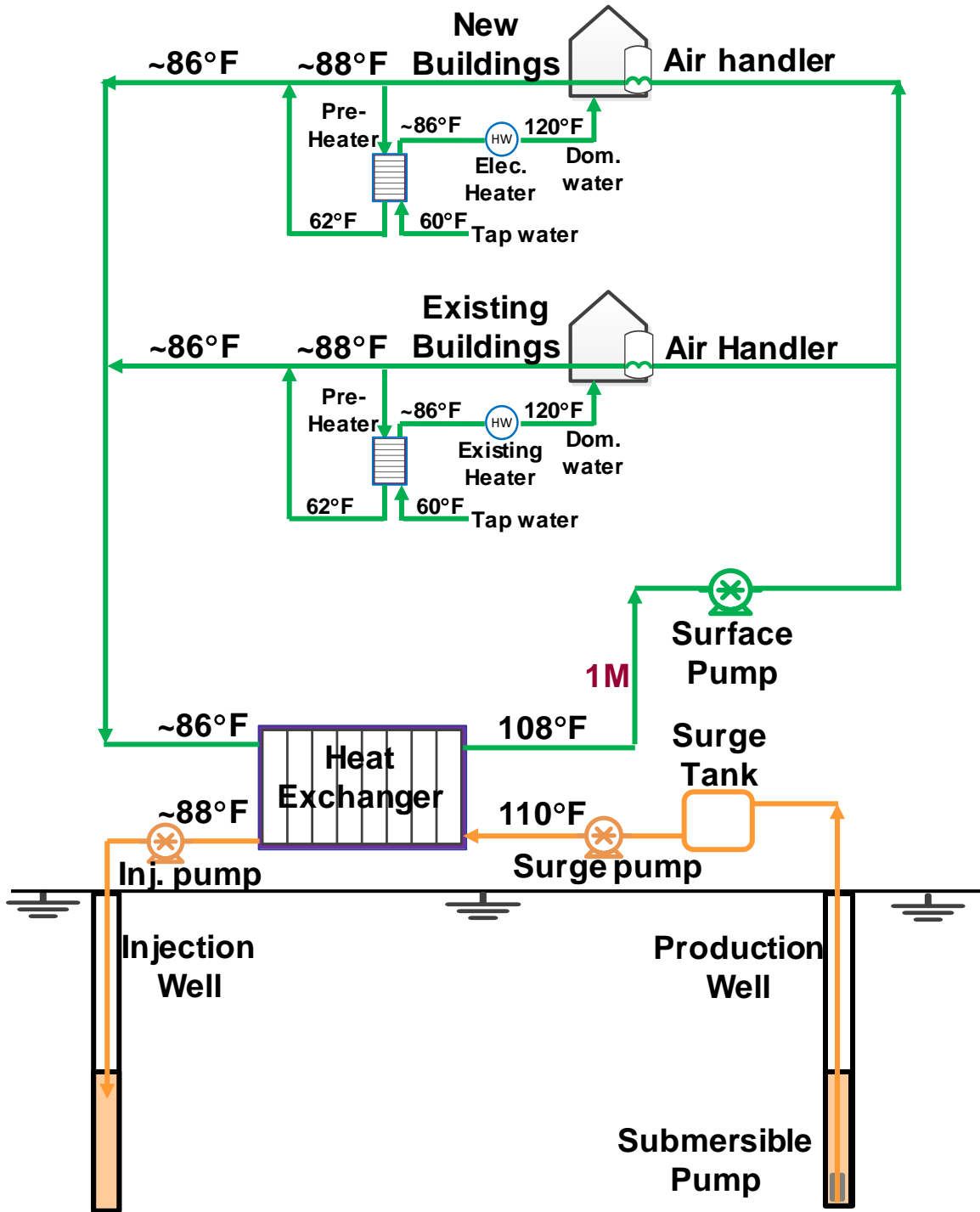
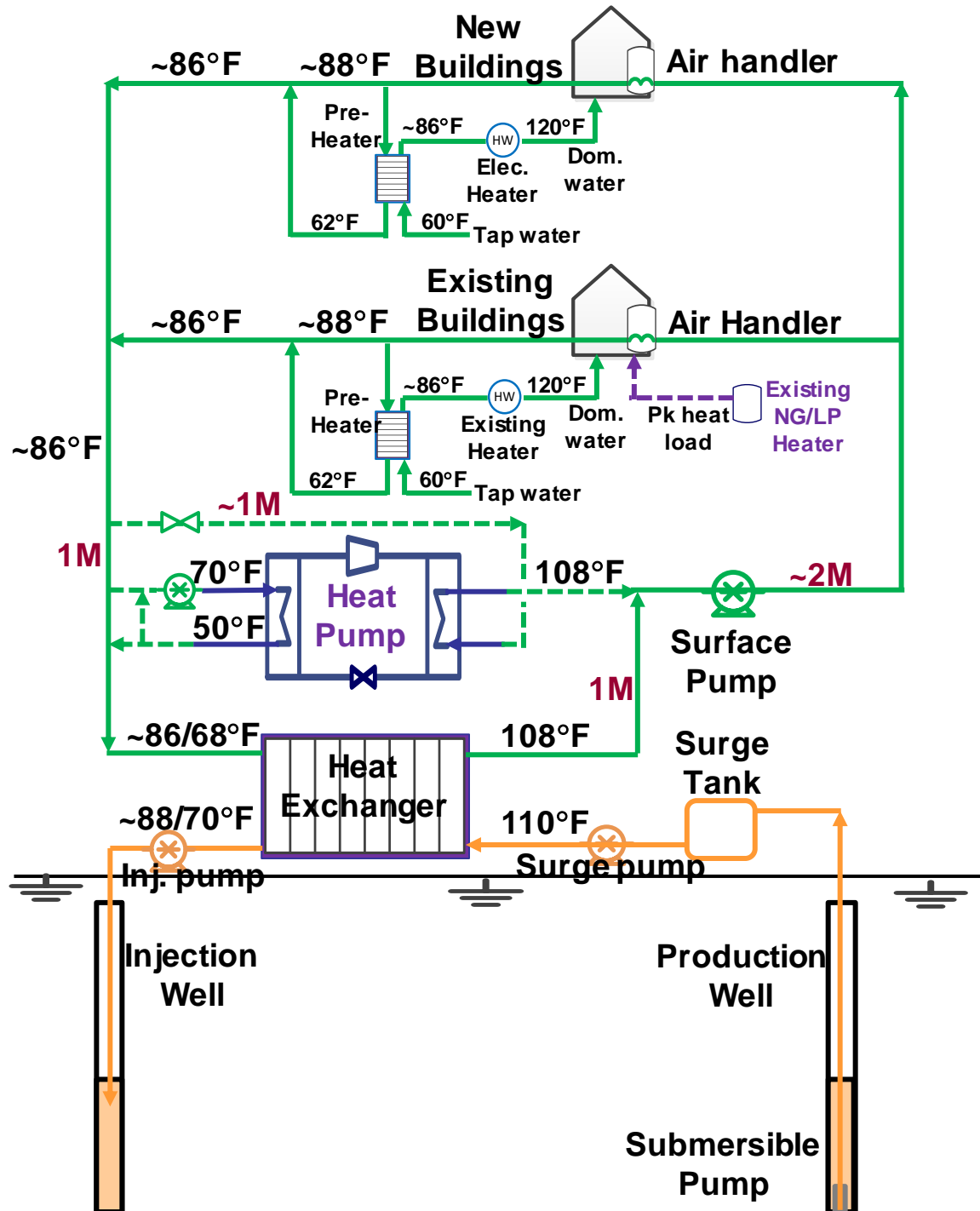


Figure C4.2. Case 2 Process Flow Diagram



Preliminary estimates of equipment sizes and costs and operating costs

Trimeric estimated equipment sizes, costs, and operating costs for the surface equipment. Equipment costs were determined in a variety of ways. The heat exchanger, clean water surge tank, surge tank pump, and surface pump costs were estimated in Aspen Capital Cost Estimator version 10. For the brine surge tank, injection well inlet pump, and heat pump cost estimates, Trimeric reached out to vendors for budgetary quotes. The air handler, domestic water preheater, and smaller horsepower pump VFD costs were scaled from catalog pricing for “off-the-shelf” equipment from a leading national supplier of this type of mechanical equipment. There is no spare equipment included in the costs. The estimates for surface facility equipment specifications, purchased equipment costs, and total installed costs are shown in Table C4.2. An installation factor of 2 was used to estimate the total installed surface facility capital cost from the total purchased equipment cost. The total installed cost for the Case 1 surface facility is \$1,484,000. The total installed cost for the Case 2 surface facility is \$2,048,000. The table also includes the piping and trenching costs rounded to the nearest thousandth. The piping and trenching costs are added to the total installed cost for the surface facility to come up with the total installed capital cost for each case.

Most of the cost difference between Cases 1 and 2 is from the cost of the brine/clean water heat exchanger (which has a significantly higher duty in Case 2), air handler, and heat pump. The base heat exchanger cost estimates are for 316 stainless steel tubes, which will be in contact with the brine. Trimeric also estimated the cost of the heat exchanger with titanium tubes and came up with purchased equipment cost estimates of \$428,700 for Case 1 and \$753,300 for Case 2, which is about three times more expensive than the cost used with stainless steel tubes. It was previously stated that the cost of titanium can be up to five times more expensive than the cost of stainless steel. In addition to the tube bundle(s), the cost of the exchanger also includes the cost of the exchanger shell, which is carbon steel regardless of the tube material since Trimeric specified that clean water will go on the shell side. The heat exchanger was sized for a 2°F difference in temperature between the brine exiting the exchanger and the clean water entering the exchanger. This small approach was chosen to heat the clean water as much as possible, but it also means that the heat exchanger size will be larger than it would be without such a tight temperature approach. The heat exchanger for Case 1 and Case 2 have a significant cost difference due to the different temperature differential across the exchanger.

Figures C4.3 and C4.4 show that for the base case the clean water temperature entering the heat exchanger is around 86°F, and the brine temperature leaving the exchanger is around 88°F. When the heat pump is running on Case 2, the clean water temperature entering the heat exchanger is around 68°F and the brine temperature leaving the exchanger is around 70°F. The larger temperature increase for Case 2 requires a larger heat exchanger size.

The air handlers for Case 1 were sized based on the baseload heating requirement for all buildings in all the facilities (2 MMBtu/hr total). It is assumed that existing air handlers at the existing buildings are not used for this case. The air handlers for Case 2 were sized for the baseload for existing buildings and for the peak load for new buildings. For Case 2 during peak loads, the existing building heaters turn on to provide additional heat through the existing air handlers, while the baseload requirements are met with the clean water air handlers. The new buildings would

have new air handlers sized for the peak load requirement where all of the heat in Case 2 is provided by a combination of the hot clean water from DDU and from the heat pump.

Table C4.2. Surface Facility Capital Cost Estimates

Surface facilities equipment	Specifications			Capital cost	
	General Specs	Case 1	Case 2	Case 1	Case2
Heat Exchanger	316SS tube/CS shell, max 100 psig	HX area = 7,018 ft ²	HX area= 12,759 ft ²	\$149,500	\$251,000
Surface Pump	Centrifugal, CS, 25/100 psig in/outlet	182 gpm flow / 11 hp	390 gpm flow / 23 hp	\$9,200	\$11,400
Air Handler	Total 20 handlers for 6 facilities, 70/95F air inlet/outlet	Total capacity= 2.0 MMBtu/hr (all for baseload)	Total capacity= 4.6 MMBtu/hr (peak for new & base for old buildings)	\$61,600	\$124,000
Domestic Water Preheater	Total 21 preheaters, 60 to 86F preheating			\$37,700	\$37,700
Heat Pump	Heat duty = 2.3 MMBtu/hr, 86/108 F inlet/outlet			n/a	\$116,000
Brine Surge Tank	520 ft ³ FRP tank, near atm pressure			\$17,600	\$17,600
Clean Water Surge Tank	160,000-gallon CS tank, near atm pressure			\$168,000	\$168,000
Injection Well Inlet Pump	Triplex (piston), 316SS, 50/1166 psig inlet/outlet, 169 hp			\$285,800	\$285,800
Surge Tank Pump	Centrifugal, 316SS casing, 5/100 psig inlet/outlet, 14 hp			\$12,400	\$12,400
Total Surface Facility Purchased Equipment Cost (PEC), \$				\$742,000	\$1,024,000
Total Surface Facility Installed Capital Cost, \$				\$1,484,000	\$2,048,000
Piping Cost (Including Materials, Insulation, and Installation), \$				\$801,000	\$833,000
Trenching, Excavation, and Backfilling Cost, \$				\$777,000	\$777,000
Total Installed Capital Cost, \$				\$3,062,000	\$3,658,000

The estimated total annual operating costs are shown in Table C4.2. The costs are broken down into electricity usage and electricity cost per equipment, chemical injection cost, the cost of natural gas usage (for existing LPG/NG peak heaters in existing buildings) for Case 2 during peak heating loads, and the maintenance cost. The unit cost of electricity used in this study was \$0.08/kWh based on direction from ISGS. The chemical used for injection into the brine costs \$30/gallon. The cost of natural gas was estimated to be \$5/MMBtu. The annual maintenance cost for the surface facilities was estimated to be 4% of the surface facility installed capital cost.

The maintenance cost in the table also includes the maintenance cost for the submersible pump. The submersible pump maintenance cost was estimated to be \$2,100 per month based on a pump life of 3–5 years before replacement or a major rebuild may be necessary. The total annual operating cost for Case 1 is \$239,732. The total annual operating cost for Case 2 is \$272,868. The majority of the operating cost comes from the electricity usage for the pumps. Variable frequency drives have been included for the pumps to reduce the electricity usage as much as possible and this has been accounted for in the operating cost estimates. The maintenance costs are also a significant portion of the operating costs.

Table C4.3. Annual OPEX

	<i>Electric power use, kW</i>		<i>Electricity cost, \$/year</i>	
	<i>Case 1</i>	<i>Case 2</i>	<i>Case 1</i>	<i>Case 2</i>
<i>Electric submersible pump</i>	254	254	81,267	81,267
<i>Injection well inlet pump</i>	126	126	40,300	40,300
<i>Surge tank pump</i>	11	11	3,431	3,431
<i>Surface pump</i>	8	17	2,527	2,687
<i>Electric hot water heaters</i>	22	22	3,336	3,336
<i>Air handler power requirement</i>	37	86	11,842	13,545
<i>Heat pump</i>	0	112	0	4,476
<i>Total electricity</i>	<i>458</i>	<i>628</i>	<i>142,703</i>	<i>149,042</i>
<i>Chemical injection cost</i>			12,490	12,490
	<i>Supplementary NG use, MMBtu</i>		<i>Cost, \$/year</i>	
	<i>Case 1</i>	<i>Case 2</i>	<i>Case 1</i>	<i>Case 2</i>
<i>Supplementary NG facilities</i>	0	849	0	4247
	<i>Surface capital cost</i>		<i>Maintenance cost, \$/year</i>	
	<i>Case 1</i>	<i>Case 2</i>	<i>Case 1</i>	<i>Case 2</i>
<i>Maintenance cost</i>	1,483,471	2,047,252	84,539	107,090
Total Annual OPEX, \$/year			239,732	272,868

Sensitivity of the levelized cost of heat vs. the total heat demand

Trimeric was asked to perform a sensitivity analysis on the levelized cost of heat versus the total heat demand. Four brine flowrates were considered. The starting point was the 6,000 bbl/day brine flowrate used for Cases 1 and 2 with costs shown in the tables above. Trimeric scaled the surface facility and piping costs calculated for 6,000 bbl/day of brine in order to estimate costs for sensitivity cases with brine flowrates of 12,000 bbl/day, 18,000 bbl/day, and 24,000 bbl/day.

The 18,000 bbl/day sensitivity assumes one 6,000 bpd extraction well and one 12,000 bpd extraction well and correspondingly one 6,000 bpd injection well and one 12,000 bpd injection well. The 24,000 bbl/day sensitivity assumes two 12,000 bpd extraction wells and two 12,000 bpd injection wells. As per estimates from Jim Kirksey of the Infrastructure Task team, the maximum practical rate for a single well is 12,000 bpd (Kirksey, 2019). Beyond 12,000 bpd, additional wells

need to be drilled. In Table C4.4 and C4.5, the estimated surface equipment total purchased cost and installed cost, the cost of the extraction well(s) and injection well(s), the piping cost, the total capital and operating costs, and the heat load for each sensitivity case.

The levelized cost of heat in \$/MMBtu is also included in these tables. This cost does not consider the time value of money. The equipment cost is not discounted over time. Per ISGS, the life of the project is 50 years for this sensitivity analysis. To calculate the cost of heat, the total capital cost was divided by 50 years to annualize the capital costs. The annual capital cost was added to the annual operating cost and divided by the annual heat load to calculate the levelized cost of heat for each case.

The Case 2 well costs are the same as the Case 1 well costs, because the brine flowrate does not change between cases. Case 2 obtains additional heat from a heat pump and existing LPG / natural gas heaters; therefore, the cost differences between Case 1 and Case 2 are in the surface equipment and piping costs. There is a step change in the capital cost from one to two extraction wells and from one to two injection wells, which can be seen clearly in Figure C4.3 and Figure C4.4. Note that there is more uncertainty in the cost estimates for brine flow rates greater than 6,000 bpd in the following tables and figures as they are estimated using scaling factors from the more detailed estimates for the 6,000 bpd cases as described earlier in this report.

Table C4.4. Case 1 Sensitivity of Capital and Operating Cost of Heat vs. Total Heat Demand

Brine Flow Rate bbl/day	Surface Equipment Total Purchased Cost	Surface Equipment Total Installed Cost	Extraction Well Cost	Injection Well Cost	Water Pipelines Cost	Total Capital Cost	Operating Cost, \$/year	Heat Load, MMBtu/yr	\$/MMBtu
6,000	\$742,000	\$1,484,000	\$4,300,000	\$3,820,000	\$1,578,000	\$11,182,000	\$239,732	7,994	58.0
12,000	\$1,125,000	\$2,250,000	\$5,100,000	\$4,450,000	\$2,392,000	\$14,192,000	\$479,463	15,988	47.7
18,000	\$1,434,000	\$2,868,000	\$9,400,000	\$8,270,000	\$3,051,000	\$23,589,000	\$719,195	23,982	49.7
24,000	\$1,705,000	\$3,410,000	\$10,200,000	\$8,900,000	\$3,625,000	\$26,135,000	\$958,926	31,976	46.3

Table C4.5. Case 2 Sensitivity of Capital and Operating Cost vs. Total Heat Demand

Brine Flow Rate bbl/day	Surface Equipment Total Purchased Cost	Surface Equipment Total Installed Cost	Extraction Well Cost	Injection Well Cost	Water Pipelines Cost	Total Capital Cost	Operating Cost, \$/year	Heat Load, MMBtu/yr	\$/MMBtu
6,000	\$1,024,000	\$2,048,000	\$4,300,000	\$3,820,000	\$1,610,000	\$11,778,000	\$272,868	9,992	50.9
12,000	\$1,552,000	\$3,104,000	\$5,100,000	\$4,450,000	\$2,440,000	\$15,094,000	\$545,737	19,984	42.4
18,000	\$1,980,000	\$3,960,000	\$9,400,000	\$8,270,000	\$3,112,000	\$24,742,000	\$818,605	29,976	43.8
24,000	\$2,353,000	\$4,706,000	\$10,200,000	\$8,900,000	\$3,699,000	\$27,505,000	\$1,091,473	39,968	41.1

Figure C4.3. Case 1 Sensitivity of Capital Cost vs. Total Heat Demand

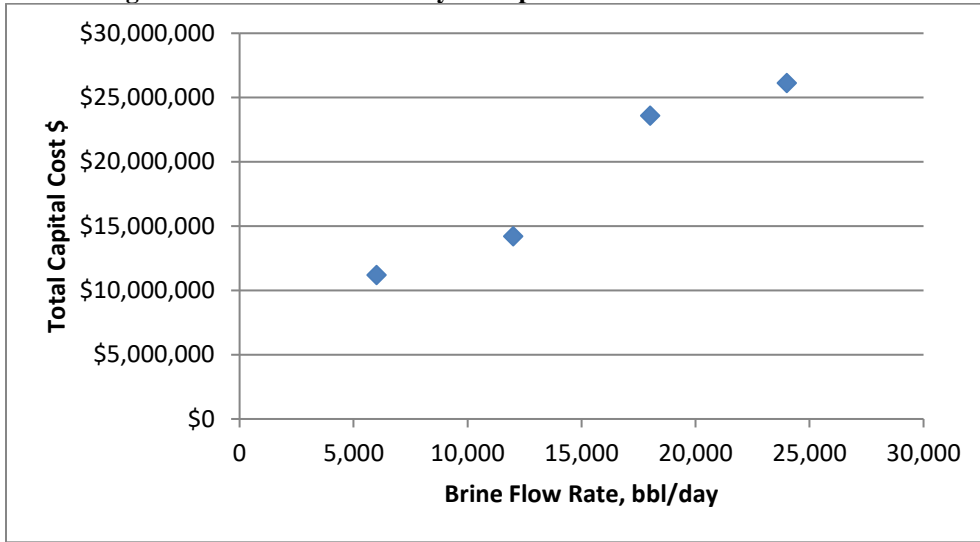
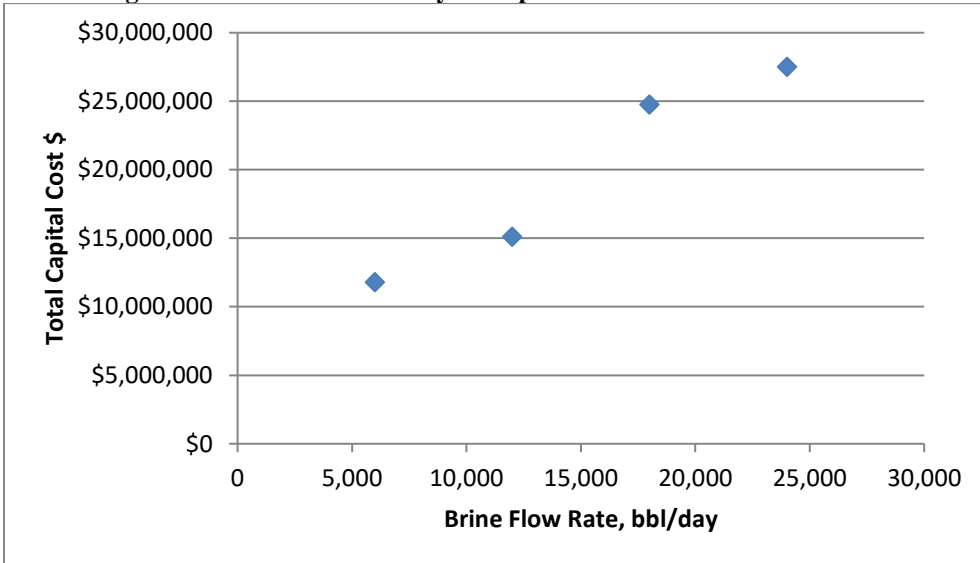


Figure C4.4. Case 2 Sensitivity of Capital Cost vs. Total Heat Demand



Conclusions and Recommendations

Key conclusions from this work with respect to the Infrastructure aspects of the GeoHRC DDU project are as follows:

- DDU of low-temperature (~ 114 °F) Mt. Simon formation brine results in low generation of geothermal heat due to the low amount heat that can be extracted from the fluid using DDU ($\Delta T = \sim 20$ °F);
- Costs of heat for DDU in the current scenarios are high compared to conventional sources of heat (\$50-100/MMBtu for DDU vs. \$5-10/MMBtu for natural gas and ~\$19/MMBtu for steam on the U OF IL campus);

- Well costs and electrical power requirements are major contributors to the DDU Levelized Cost of Heat (LCOH);
- Adding a heat pump for peak heating needs improved LCOH by ~10% in current scenario;
- Cascading application of spent brine for preheating domestic hot water is insignificant compared to overall DDU economics, because heat demands are dominated by space heating.

Recommendations for further study are as follows:

- Investigate any additional options to reduce extraction well and injection well costs as these costs dominate the capital cost aspects of DDU LCOH, even when they are amortized over 50 years.
- Investigate any additional options to reduce the cost of electricity and the electrical power requirements as these dominate operating costs.
- Perform a sensitivity analysis on brine temperature vs. the LCOH.
- Study the effect of brine salinity, composition, etc. on pumping costs, the heat transfer coefficient in heat exchangers, and the LCOH
- Drill a test well to collect samples of the Mt. Simon fluid near the U OF IL campus in order to experimentally measure and confirm the temperature profile vs. depth, actual salinity, actual composition, and corrosivity to stainless steel and higher alloys.
- Once actual fluid data are available, reassess scaling, precipitation, fouling, and corrosion and their potential impacts on the LCOH.

This evaluation demonstrated that DDU in the cases selected for this evaluation is likely to be technically feasible based on commercial availability of suitable equipment from similar convention processes. However, capital and operating costs for DDU are significantly higher than conventional approaches at this time. The reasons for this and recommendations for improving the economics of DDU in the cases studied (and similar applications) are noted above.

References

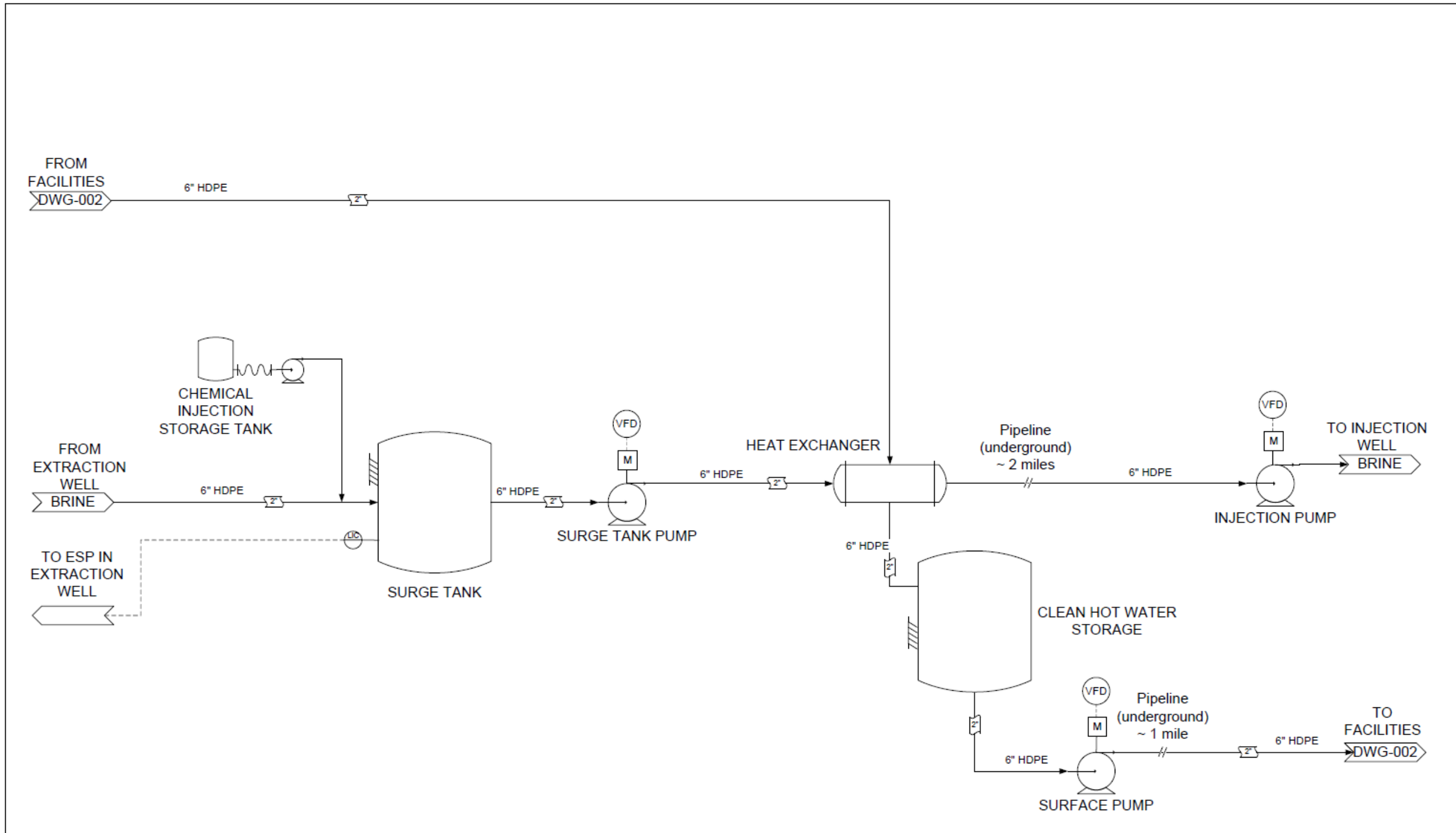
American Society of Heating, Refrigerating and Air-Conditioning Engineers (ASHRAE) (2017). “ASHRAE Handbook”. American Society of Heating, Refrigerating and Air Conditioning Engineers Atlanta, GA, 1088 p.

Kaplan R, Mamrosh D, Salih HH, Dastgheib SA. (2017). “Assessment of desalination technologies for treatment of a highly saline brine from a potential CO₂ storage site”. *Desalination*, 404, 87-101. <http://dx.doi.org/10.1016/j.desal.2016.11.018>

Kirksey, J. (2019). “GeoHRC: Large-Scale, Deep Direct-Use System in a Low-Temperature Sedimentary Basin Well Design Report v1.3”. Aug. 5, 2019. Loudon Technical Services LLC.

Okwen R, Frailey S, Dastgheib S. (2017). “Brine Extraction and Treatment Strategies to Enhance Pressure Management and Control of CO₂ Plumes in Deep Geologic Formations”. U.S. Department of Energy, Office of Scientific and Technical Information (OSTI), 349 p. <http://dx.doi.org/10.2172/1363792>

Piping and Instrumentation
Diagram (P&ID)
U of IL DDU GES (Case 1)
from Trimeric Corporation
2019-10-08



LEGEND

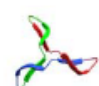
2" = Insulation, thickness in inches

FILENAME: BGS GEO HRC PSDS CASE 1 10019 VSD

DATE:

DRAWN BY: Austyn Vance

REVISIONS						
REV.	DATE	DESCRIPTION	BY	CHECKED	APPROVED	APPROVED
0			AEV			

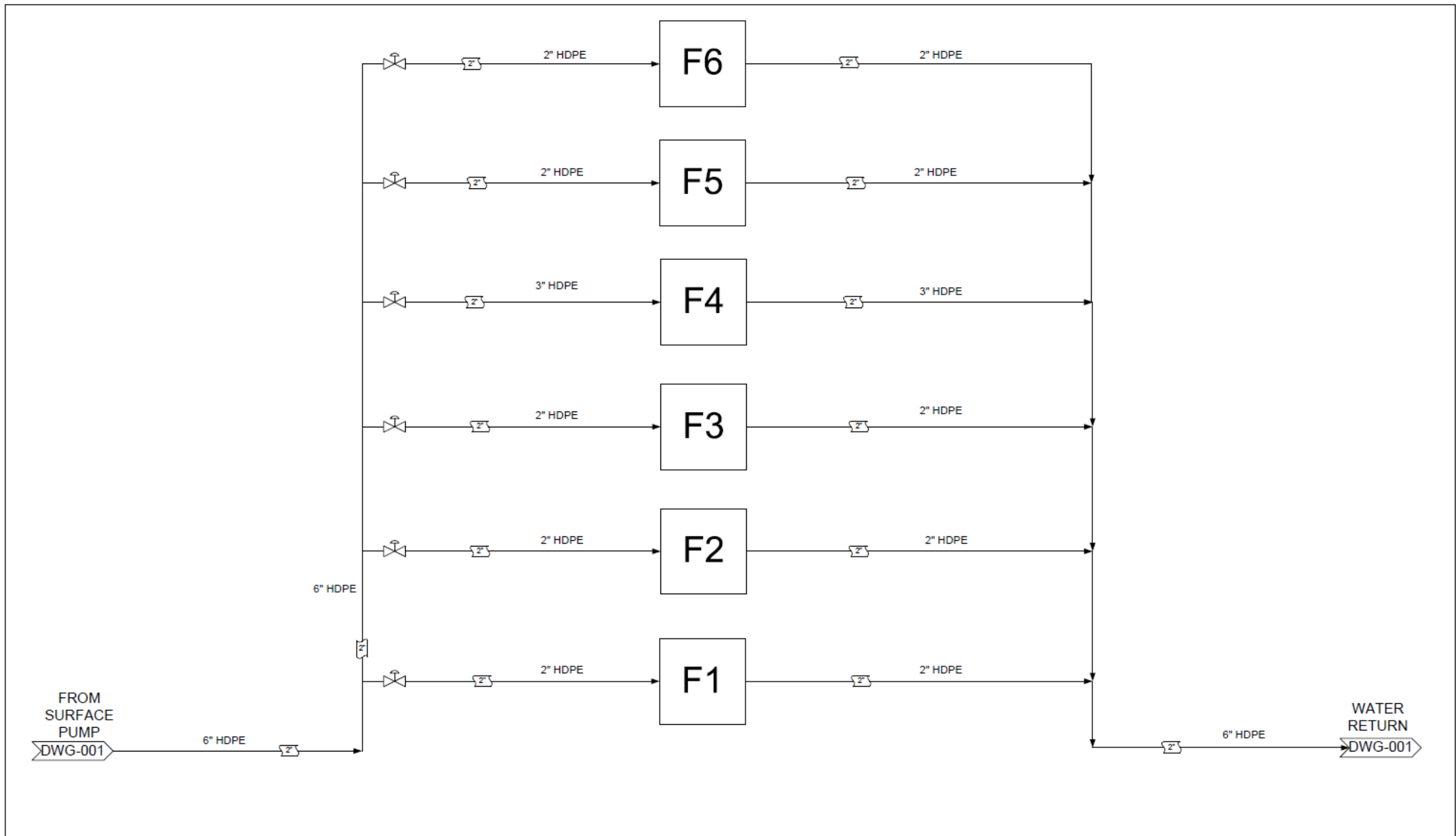


TRIMERIC CORPORATION
P.O. Box 826
Buda, Texas 78610

**CASE 1
HEAT SOURCE**

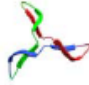
CLIENT/SITE: _____ JOB NUMBER: X0000.XXX

DRAWING NUMBER: DWG-001 SCALE: NONE



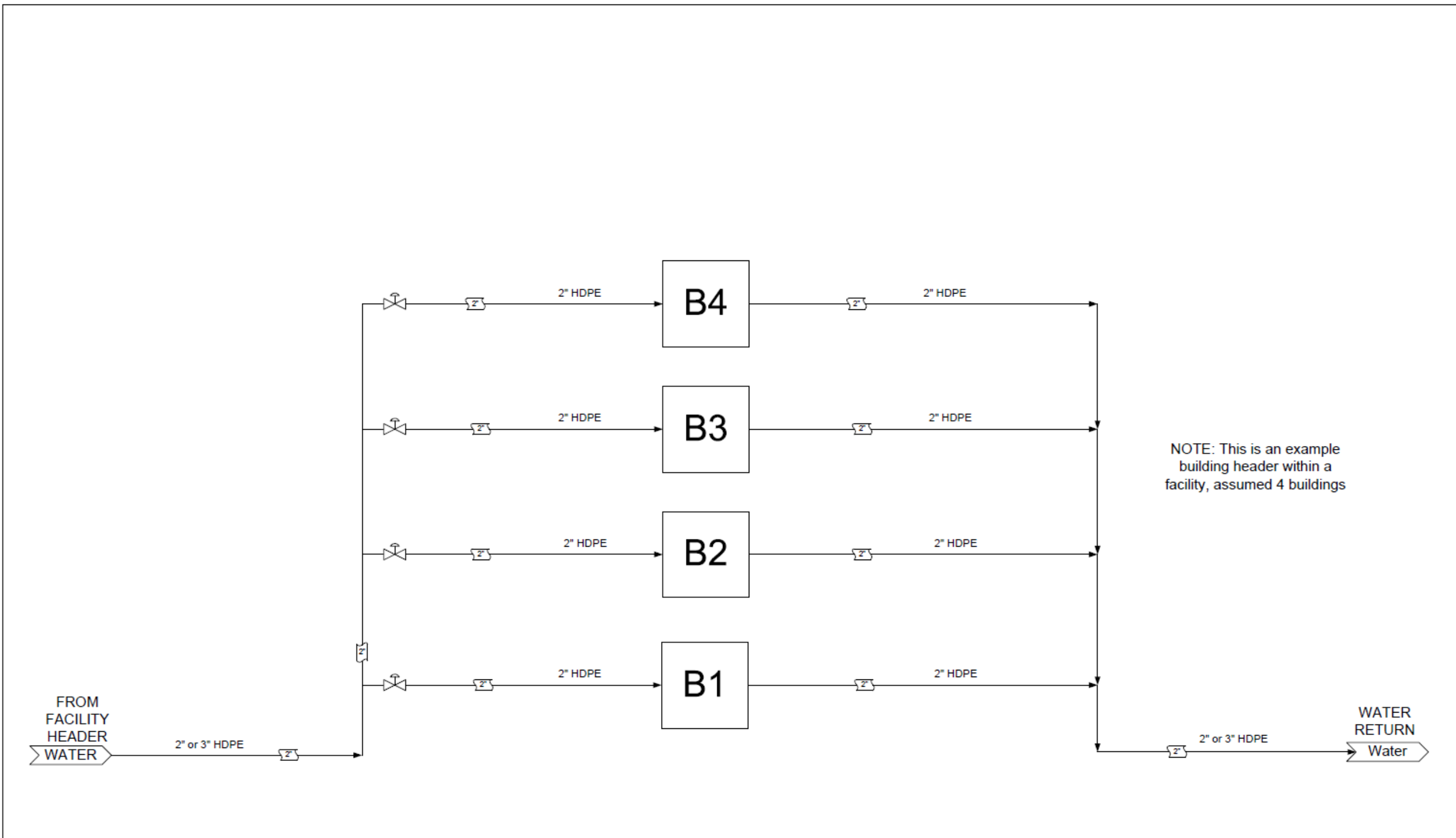
FILENAME	DATE	DRAWN BY
ISGS GEO HRC P&IDS CASE 1 100819 VSD		Austyn Vance

REVISIONS						
REV.	DATE	DESCRIPTION	BY	CHECKED	APPROVED	APPROVED
0			AV			



TRIMERIC CORPORATION
P.O. Box 826
Buda, Texas 78610

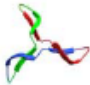
CASE 1 FACILITY HEADER	
CLIENT/SITE	JOB NUMBER
DRAWING NUMBER	SCALE
DWG-002	NONE



NOTE: This is an example building header within a facility, assumed 4 buildings

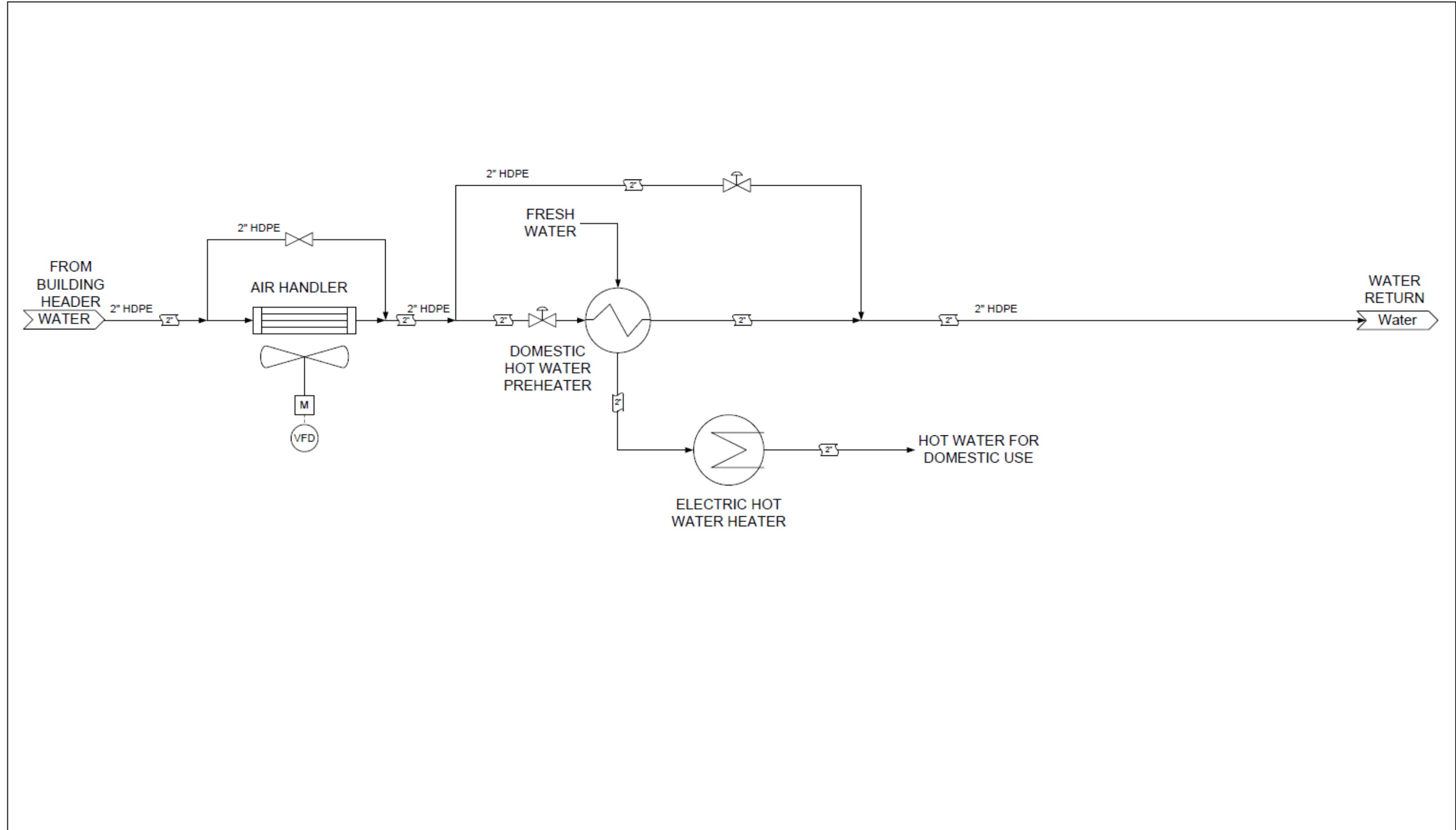
FILENAME	DATE	DRAWN BY
1808 GEO HRC P&DS CASE 1 100819 VSD		Austyn Vance

REVISIONS						
REV	DATE	DESCRIPTION	BY	CHECKED	APPROVED	APPROVED
0			AEV			



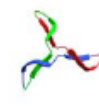
TRIMERIC CORPORATION
P.O. Box 826
Buda, Texas 78610

CASE 1 BUILDING HEADER	
CLIENT/SITE	JOB NUMBER
DRAWING NUMBER	SCALE
DWG-003	NONE



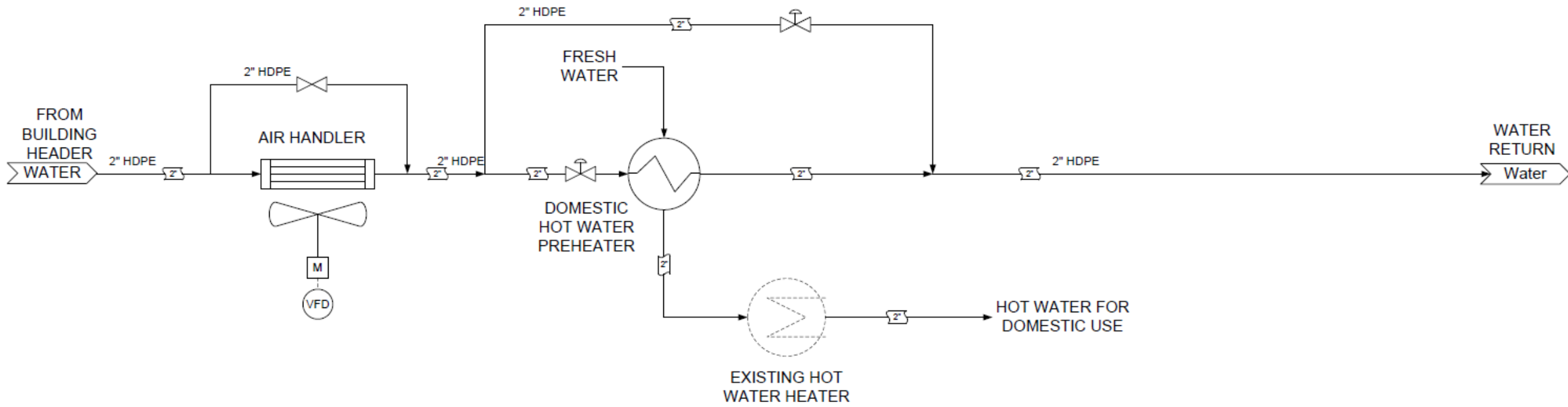
FILENAME: 1908 GEO HRC P&ID CASE 1 100819 VSD
 DATE:
 DRAWN BY: Austyn Vance

REVISIONS						
REV.	DATE	DESCRIPTION	BY	CHECKED	APPROVED	APPROVED
0			AEV			

 **TRIMERIC CORPORATION**
 P.O. Box 826
 Buda, Texas 78610

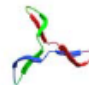
CASE 1
NEW BUILDING EXAMPLE
DRAWING

CLIENT/SITE	JOB NUMBER
DRAWING NUMBER	SCALE
DWG-004	NONE



FILENAME: ISGS GEO HRC P&IDS CASE 1 100819.VSD
 DATE:
 DRAWN BY: Austyn Vance

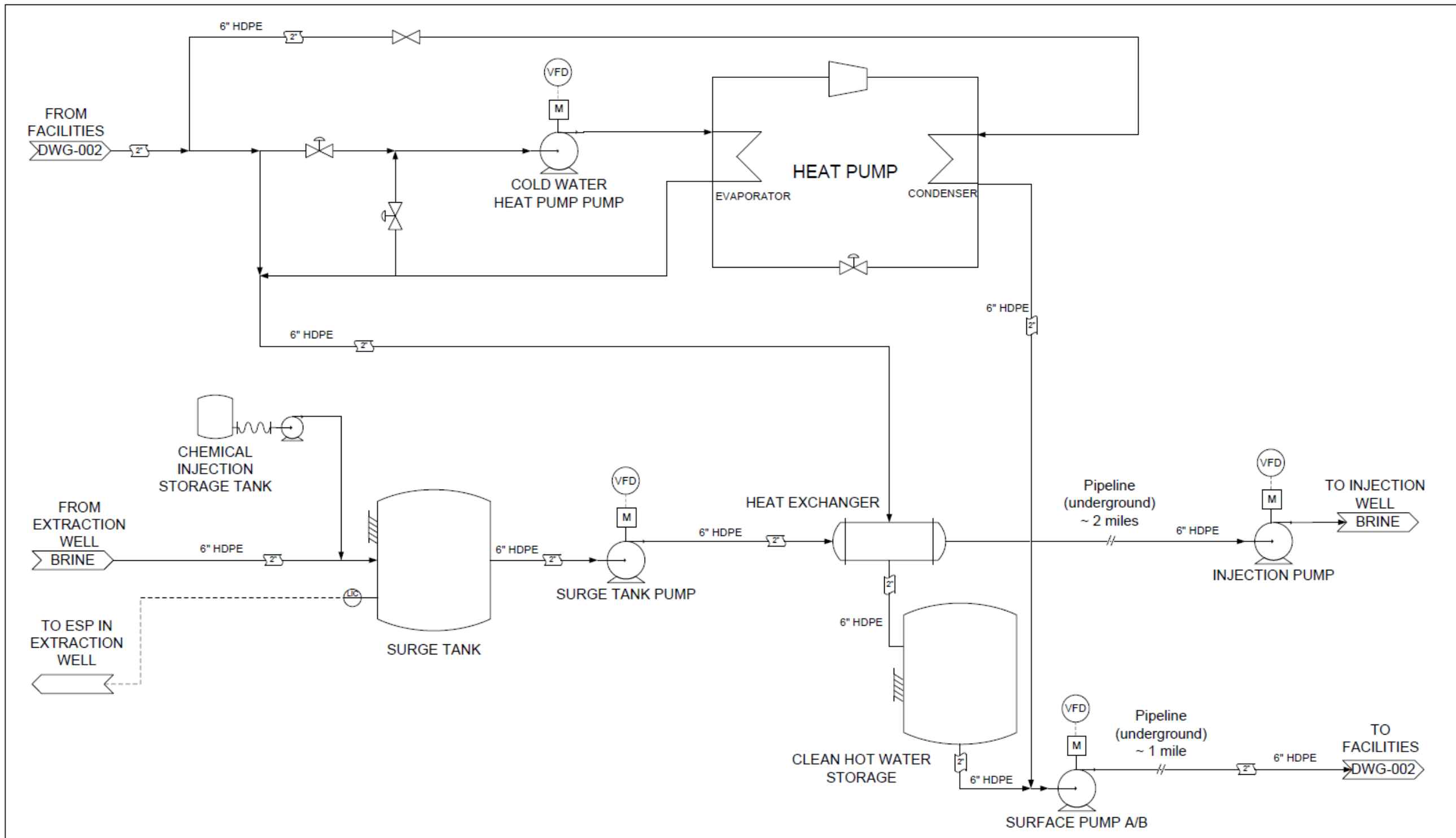
REVISIONS						
REV.	DATE	DESCRIPTION	BY	CHECKED	APPROVED	APPROVED
0			AEV			

 **TRIMERIC CORPORATION**
 P.O. Box 826
 Buda, Texas 78610

CASE 1
EXISTING BUILDING EXAMPLE
DRAWING

CLIENT/SITE: Xxxxxx,xx
 JOB NUMBER: Xxxxx,xx
 DRAWING NUMBER: DWG-005
 SCALE: NONE

Piping and Instrumentation
Diagram (P&ID)
U of IL DDU GES (Case 2)
from Trimeric Corporation
2019-10-08



LEGEND
 [Symbol] - Insulation, thickness in inches

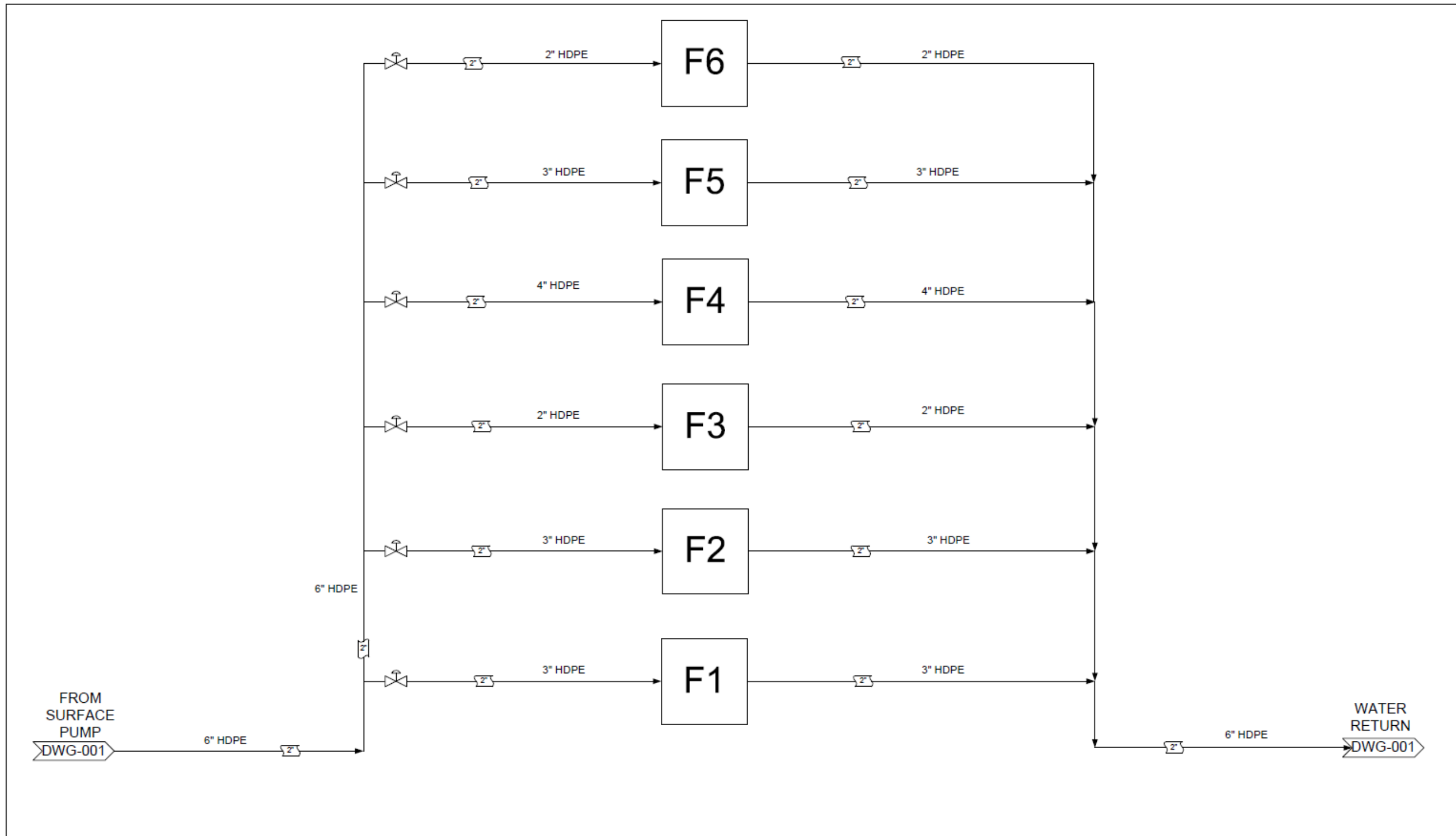
FILENAME: 1926 GEO HRC P&IDS CASE 2 10062019 VSD
 DATE: _____
 DRAWN BY: Austyn Vance

REVISIONS						
REV.	DATE	DESCRIPTION	BY	CHECKED	APPROVED	APPROVED
0			AV			

TRIMERIC CORPORATION
 P.O. Box 826
 Buda, Texas 78610


**CASE 2
 HEAT SOURCE**

CLIENT/SITE: _____ JOB NUMBER: Xxxxx.xx
 DRAWING NUMBER: DWG-001 SCALE: NONE



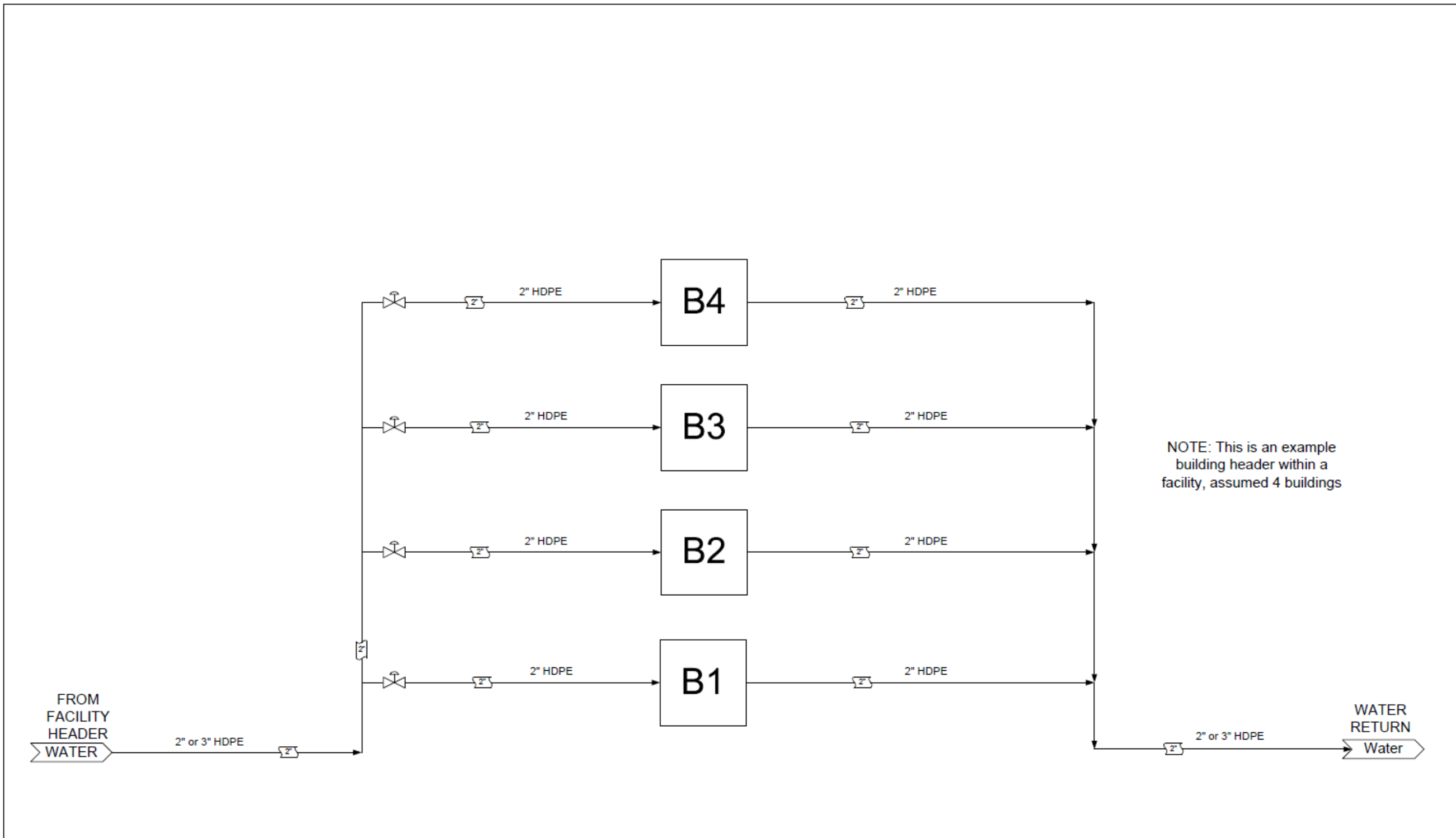
FILENAME	DATE	DRAWN BY
1808 GEO HRC P&IDS CASE 2 10082019 VSD		Austyn Vance

REVISIONS						
REV.	DATE	DESCRIPTION	BY	CHECKED	APPROVED	APPROVED
0			AEV			



TRIMERIC CORPORATION
P.O. Box 826
Buda, Texas 78610

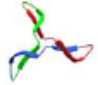
CASE 2 FACILITY HEADER	
CLIENT/SITE	JOB NUMBER
DRAWING NUMBER	SCALE
DWG-002	NONE



NOTE: This is an example building header within a facility, assumed 4 buildings

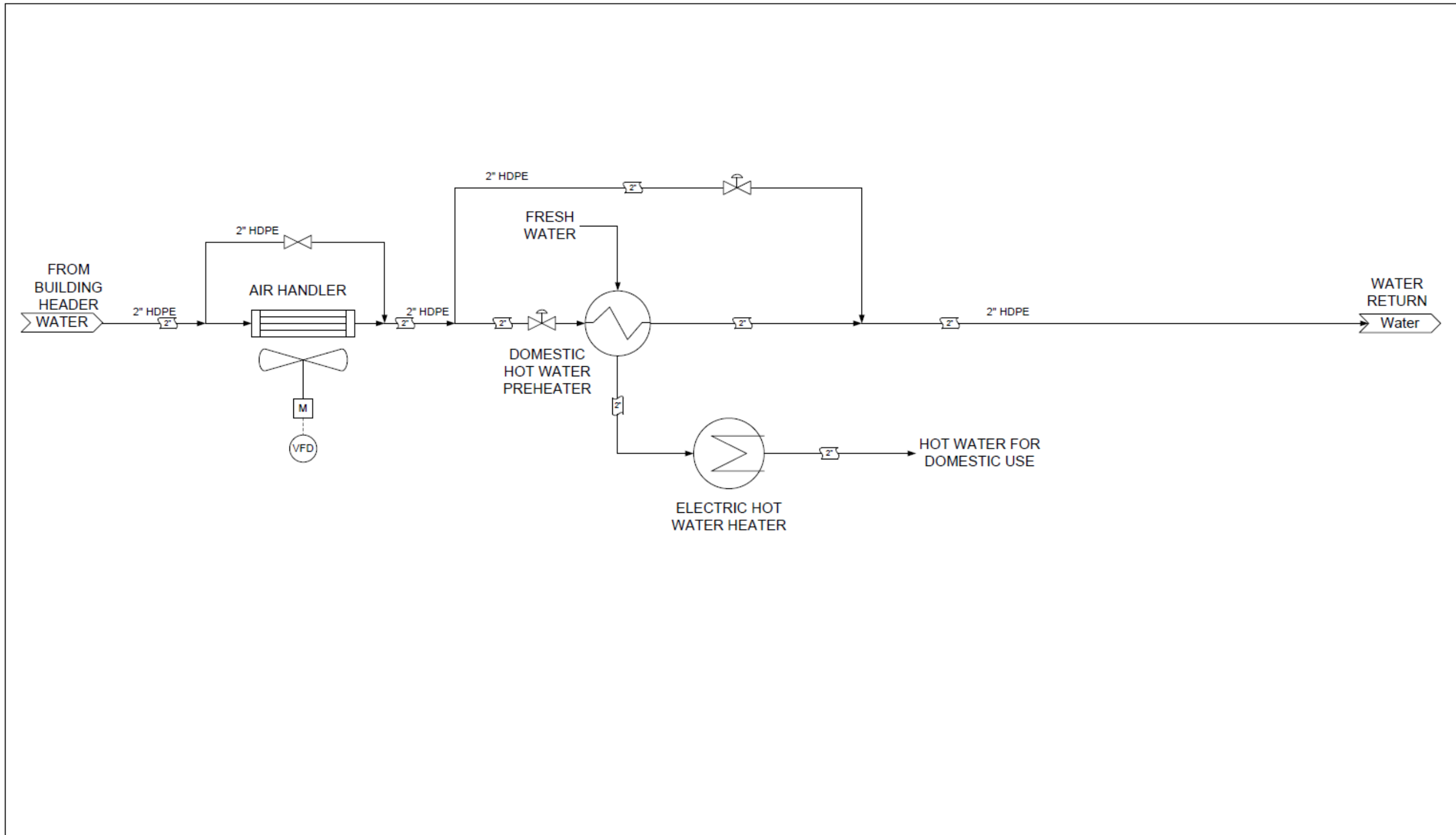
FILENAME	DATE	DRAWN BY
ISGS GEO HRC PWDG CASE 2 10062018 VSD		Austyn Vance

REVISIONS						
REV.	DATE	DESCRIPTION	BY	CHECKED	APPROVED	APPROVED
0			AEV			



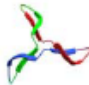
TRIMERIC CORPORATION
P.O. Box 826
Buda, Texas 78610

CASE 2 BUILDING HEADER	
CLIENT/SITE	JOB NUMBER
DRAWING NUMBER	SCALE
DWG-003	NONE



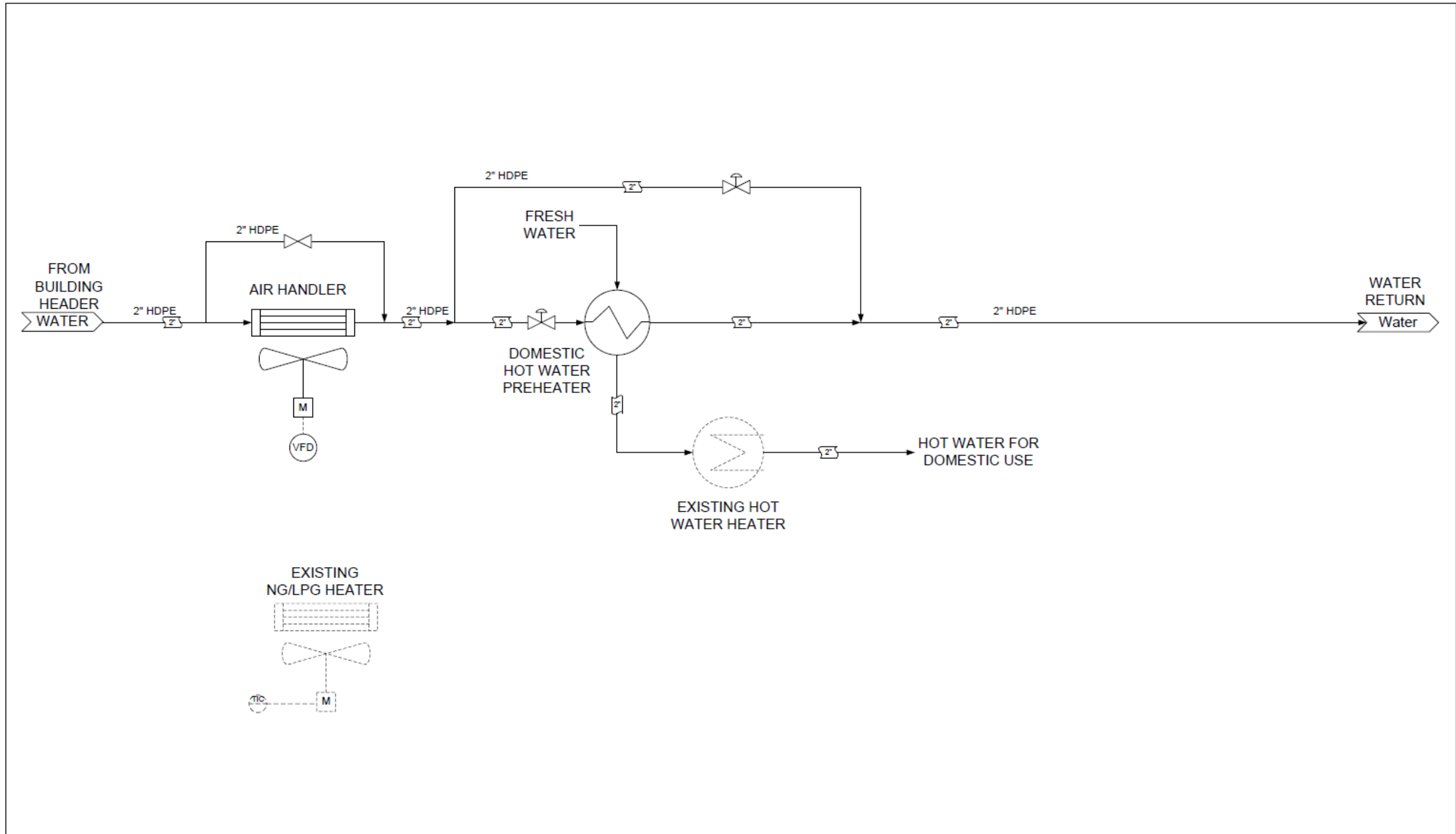
FILENAME: 1908 GEO HRC P&IDS CASE 2 10082019.VSD
 DATE:
 DRAWN BY: Austyn Vance

REVISIONS						
REV.	DATE	DESCRIPTION	BY	CHECKED	APPROVED	APPROVED
0			AEV			

 **TRIMERIC CORPORATION**
 P.O. Box 826
 Buda, Texas 78610

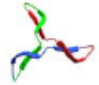
**CASE 2
 NEW BUILDING EXAMPLE
 DRAWING**

CLIENT/SITE	JOB NUMBER
DRAWING NUMBER	SCALE
DWG-004	NONE



FILENAME: 1808 GEO HRC P&ID CASE 2 10/6/2019 VSD
 DATE: _____
 DRAWN BY: Austyn Vance

REVISIONS						
REV.	DATE	DESCRIPTION	BY	CHECKED	APPROVED	APPROVED
0			AEV			

 **TRIMERIC CORPORATION**
 P.O. Box 826
 Buda, Texas 78610

CASE 2
EXISTING BUILDING EXAMPLE
DRAWING

CLIENT/SITE: _____ JOB NUMBER: X0000.XX
 DRAWING NUMBER: DWG-005 SCALE: NONE

**Conceptual Overview
of the Department of Defense (DoD's)
Potential Utilization of Deep Direct-Use (DDU)
Geothermal Energy in the Illinois Basin**

**Created as a Supplement to the Investigation by the
University of Illinois Urbana-Champaign's (UIUC)
DDU Study of the Illinois Basin region for the
Department of Energy (DOE)
under EERE Contract #DE-EE0008106.0000**



**Prepared by
Andrews Hammock & Powell, Inc.
250 Charter Lane Suite 100
Macon, GA 31210**

September 25th, 2019

Contents

<u>1.</u>	<u>Executive Summary</u>	194
<u>2.</u>	<u>Background</u>	194
<u>3.</u>	<u>Potential DoD Opportunities for DDU</u>	195
<u>4.</u>	<u>Potential Benefits of DDU</u>	202
<u>5.</u>	<u>Barriers</u>	204
<u>6.</u>	<u>Solutions</u>	206
<u>7.</u>	<u>Appendix A. Brochure for “Heat Amplifier”</u>	207

Executive Summary

Andrews, Hammock and Powell, Inc. (AH&P) was tasked by faculty and personnel at the University of Illinois at Urbana-Champaign (U OF IL), under their PO# P1745178, to perform a conceptual investigation to examine potential opportunities, benefits, utilization barriers (and potential solutions to overcome said barriers) associated with the deployment of Deep Direct-Use (DDU) of geothermal resources in the Illinois Basin. While the potential opportunities listed herein are often applicable beyond just one geographic area, this report is focused on the “Illinois Basin” described in previous U of IL feasibility studies for the Department of Energy. Furthermore, this report is generally focused on potential DoD applications or considerations. The Statement of Work (SOW) also requested some “quantitative estimates”, which was difficult to provide given this project’s 12-hour labor budget, though herein is an attempt to quantify the equivalent annual natural gas consumption (thermal load) that might need to be present/eliminated to justify the construction of a DDU system. The potential “opportunities” are described herein by end-use and include applications like the pre-heating of domestic or process feedwater, radiant heating systems and even novel applications like the use of low grade geothermal DDU heat as source energy for a (compressor-less) Absorption Heat Pump which is sometimes alternately described as a “Heat Amplifier” or “Heat Transformer” in some manufacturer’s literature. The potential DDU heat is described herein as “Very Low Temperature” (VLT) when it refers to heated water obtained from the St. Peter Sandstones, typically at 23.1 to 25.9 °C (73.6 to 78.6°F) per previous U of IL research and “Low Temperature” (LT) when it refers to heated water obtained from the Mt. Simon Sandstones at around 36.9 to 49.8°C (98.4 to 121.6°F). For the sample equipment selections herein, as suggested by U of IL, 112°F supply water, from approximately 6700 ft. below the surface was utilized as a possible geothermal supply water design condition. This resources then creates, via an aggressive (2°F approach) plate and frame Heat Exchanger (PFE), 110°F “closed loop” space-heating water serving a building’s (or an industrial process’s) lower temperature (110 °F or less) needs/loads. The applications for the DDU of VLT water are very limited while the DDU of LT water is broader. This report makes no attempt to determine if the utilization of VLT or LT water obtained by DDU in the Illinois Basin can truly be done within certain economic parameters and no engineering evaluations or “engineering” of any kind is offered whatsoever under this PO, only general observations, system descriptions and some manufacturers information and selection data. This report is limited to an overview of potential DoD applications/opportunities for DDU, the mapped-out location of many of the DoD Bases, Garrisons, National Guard facilities, etc. within, or just beyond (within 100 miles), the generally recognized perimeter of the Illinois Basin, and some potentially relevant DoD policies and directives that might encourage DoD’s consideration of DDU for new or retrofit work in the Illinois Basin, and perhaps beyond.

Background

The University of Illinois at Urbana-Champaign (U of IL) is performing a feasibility study for the U.S. Department of Energy (DOE) to investigate the development of Deep Direct-Use (DDU) geothermal systems that extract energy from the strata in the Illinois Basin, and then integrate this resource with the heating and cooling infrastructure of existing and new agricultural research facilities at U of IL. That study and report will address challenges to DDU’s deployment (engineering, regulatory, commercialization, economics) at U of IL and, deployment for other end-users (e.g., universities, DoD installations, etc.) in the Illinois Basin,

and in similar sedimentary basins. This sub-report is strictly focused on limited DoD considerations.

Potential DoD Opportunities for DDU

Geothermal heating and cooling systems have gained interest with military installations over the last several decades. The current “geothermal architecture” for military installations typically includes relatively shallow (typically less than 600’ deep) vertical boreholes with HDPE u-bends inserted and grouted therein, to reject/absorb heat to and from the geologic formation. These are “closed” (recirculating) systems that typically utilize ground source heat pumps to heat and cool various buildings. Rarely (only four known DoD examples in the US), these closed loop systems will also include a true thermal storage component known as BTES (Borehole Thermal Energy Storage). Another “geothermal” system architecture *occasionally* utilized by military installations are “open loop” geothermal heat pump systems (possibly with an energy storage aspect like ATES (Aquifer Thermal Energy Storage). These systems utilize the water bearing formation to provide moderate temperature (typically below 75F) cooling water and heating source water (native groundwater) supplied to ground source heat pump equipment which then, via a refrigeration cycle, provides chilled or elevated temperature air or fluids for thermal purposes, albeit via energy-intensive compressors, in a standard vapor-compression refrigeration cycle.

Alternately, DDU geothermal systems *directly* utilize warmer (typically above 75F) water from deeper underground formations to heat and cool (only if an absorption cycle is utilized) buildings and/or processes. The major difference between DDU and other types of geothermal systems like “geothermal heat pumps”, is that DDU systems do not require the use of a refrigeration compressor to harvest usable heat from the groundwater. According to previous feasibility studies of DDU at or near the University of Illinois (U of IL), deeper formations in the area known as the Illinois Basin can potentially contain water with temperatures as warm as 49.8 °C (121.6°F). The previous study states *“The temperature of formation water in the St Peter Sandstone (634 M (2080 Ft.) Deep) within the area of research is estimated to range from 23.1 to 25.9 °C (73.6 to 78.6°F) based on bottom hole temperatures from well logs and the temperature profile of a wireline log from the Illinois Basin-Decatur project in nearby Macon County. Temperature estimates of the formation water in the deeper Mt. Simon Sandstone 1,280 meters (4199 Ft. Deep) range from 36.9 to 49.8 °C (98.4 to 121.6°F).”*

For discussions in this report, the St Peter Sandstone formation will be described as containing water at **“Very Low Temperatures (VLT)”**, and the Mt. Simon Sandstone described as containing water at **“Low Temperatures (LT)”**. Water at these temperatures (especially VLT) are typically not preferred for heating purposes due to their low “quality” (aka usefulness, or essentially, its temperature); however, both the St. Peter Sandstone formation, and the Mt. Simon Sandstone formations contain water that can *potentially* be utilized for DDU heating purposes, if the applications are carefully chosen, the design of the systems implemented correctly and the scale of the application sufficiently large to recover the considerable expense of drilling and equipping geothermal DDU wells that must pierce deeply into the formation to retrieve this resource and deliver it to a useful application.

Figure C6.1 that follows illustrates the military installations either “in” (atop), or near (i.e. within a 100 miles of its perimeter) the “Illinois Basin” that have been identified and located

(mapped in Figure C6.1) as of the date of this report. The size of each the military installation has not been investigated, but, overall, DDU geothermal is expected to be more feasible at larger installations due to economies of scale with this type of technology (i.e. VLT or LT DDU).

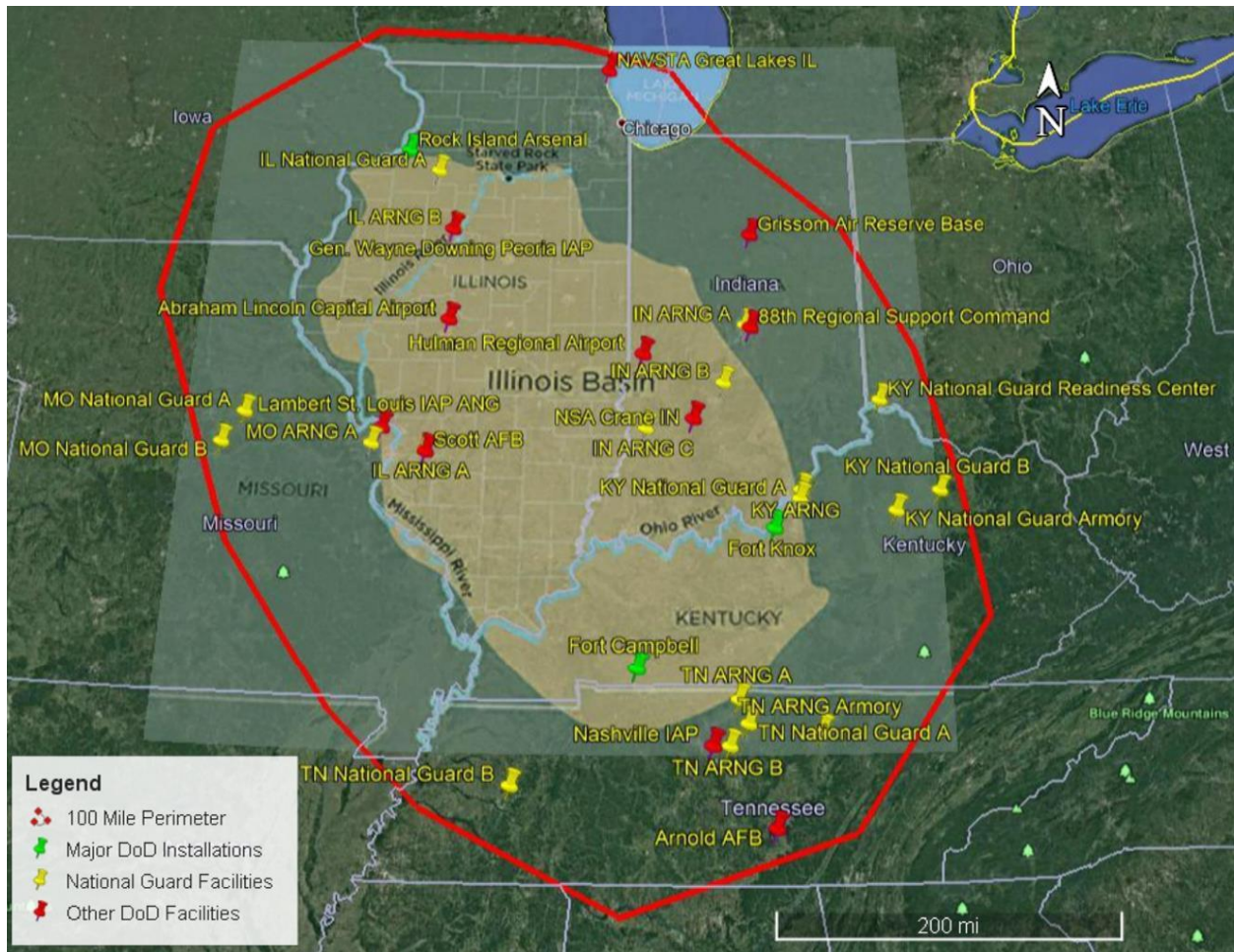


Figure C6.1. Military Installations located within the “Illinois Basin” (indicated by color coded push pins atop the tan shading) or near the Basin. The red oval-like shape represents an imaginary border that is approximately 100 miles outside the generally accepted perimeter of the Illinois Basin that forms the area of interest in the original U of IL DDU study for DOE.

a. Low Temperature (LT) 98.4 to 121.6°F (Mt. Simon Sandstone) DDU Opportunities

i. Hot Water Coils for Space Heating

For most DDU applications, LT water (or warmer) is preferred over VLT water. Water at the upper end of the anticipated LT temperature range can easily be used to heat commercial buildings by utilizing “deeper” (more rows) hot water coils inside of (for instance) variable air volume (VAV) boxes vs. shallower (less rows) coils that might be selected when “standard” (140F-180F) is present. Both design water temperatures can be used to provide (typically) 90°F + air to the space for space heating or reheating purposes. Air Handling Unit (AHU) preheat coils can also be supplied with water from

DDU systems to preheat return or outside air utilized by a VAV AHU. The AHU would need to be equipped with a deeper preheat coil than normal to utilize the DDU water to supply the typically required moderate temperature leaving the AHU, typically 52-55°F. In this application, the DDU water would be isolated from the building's heating water via a plate and frame stainless steel heat exchanger to eliminate any chance of fouling hot water piping within the building, and/or hot water coils to equipment. Plate and frame heat exchangers (PFEs) can have approaches as small as 2°F (See Figure C6.2). With U of IL advising the assumed LT water from the formation is at 112°F, and, utilizing a 2°F approach at the plate and frame heat exchanger, the water entering the hot water coils is approximately 110°F. Using a deeper (e.g. 4 row) hot water coils in a VAV reheat box, the primary air can typically be heated from 55°F to 95°F +. Please note that in this sample equipment selection, the moderate 22°F (119-70=22°F) was utilized as requested by U of IL, but it might be possible to reduce the cost of the very expensive DDU pumps and wells (i.e. the higher the Delta T the lower the GPM needed for a given amount of heat transfer) if that is feasible geothermally. That doesn't mean you can always buy a commercial HW coil (especially a small one in unitary equipment) that can produce high Delta T's, but it is often possible. In the example herein (See Figure C6.3), the manufacturers selection software would not provide a selection quite to the PFE's 22°F Delta T, but at 21.5°F (110-88.5°F), it is very close. Higher coil waterside Delta Ts of (for example) 25°F or higher, can sometimes be achieved with larger or custom coils and/or applications with colder inlet air temperature as might be found on a 100% outside air unit.

Summary			
Detail			
Nozzles/Dimension			
Match Requirement			
Model	AP31	No Of Plates	157
Dry Weight	1,100.37	Flooded Weight	1,495.88 lb
Uc	1,126.74 Btu/hr,ft2, °F	Ud	1,126.74 Btu/hr,ft2, °F
U Service	990.70 Btu/hr,ft2, °F		
Effective Area	550.5740 ft2	Total Area	557.588 ft2
Fouling	0.0001 hr,ft2, °F/Btu		
Excess Surface	13.73%	Heat Load	1,094,103.94 Btu/h
Hot T. In/Out(°F)	112.0/90.0	Cold T. In/Out(°F)	88.0/110.0
Volume Flow Rate Hot(GPM)	100.00	Volume Flow Rate Cold(GPM)	100.00
Plate Material	304	Plate Thickness	0.4 mm

Figure C6.2. Example Plate and Frame Heat Exchanger Performance



#	1
Qty	1
Model	SDV5
Unit Size	12
Max Primary (CFM)	1000
Min Primary (CFM)	300
Min Oper PD (in. w.g.)	0.52
Max Dis NC	--
Max Rad NC	--
Min Rad Lw	36, --, --, --, --
Max Dis Lw	56, 48, 44, 42, 39, 36
Reheat (CFM)	500
WC Capacity (MBH)	21.40
EAT (°F)	55.00
LAT (°F)	94.40
Fluid Flow (GPM)	2.00
FPD (ft. w.g.)	0.41
Rows	4L
EWT (°F)	110.00
LWT (°F)	88.50

Figure C6.3. Example VAV Box Coil Performance

ii. Pre-Heating of Domestic Water Applications:

Domestic water used in most commercial buildings needs to be maintained at 140°F or higher to drastically reduce the growth of legionella. This means that LT water cannot typically be utilized alone to provide domestic water heating for a building. However, pre-heating domestic water is a very common practice and can reduce domestic water heating costs by as much as 50%. The architecture for a DDU domestic water pre-heating system would include a submersible pump to pump the warm DDU ground water through one side of a plate and frame heat exchanger with a low temperature approach design. The load side of the plate and frame heat exchanger would be connected to the cold-water feed to the domestic hot water system. When domestic hot water is demanded, the incoming cold water to the water heater flows through the heat exchanger before entering the water heater. Typical domestic incoming cold-water temperatures can range from 40°F to 70°F depending on ground temperatures and the quantity/proximity of elevated storage tanks.

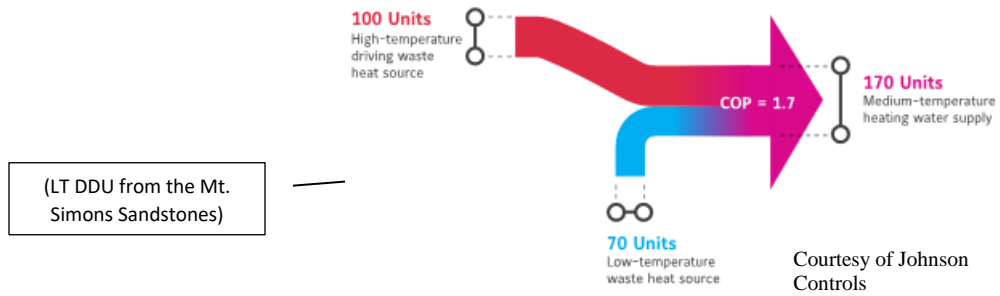
iii. Process Heating Applications

Water temperatures for process applications on military bases can vary greatly depending on the process taking place. For most processes, water temperatures needed will be higher than water temperatures acquired from the DDU resources considered herein. In this case, pre-heating of the incoming water for process uses can be considered. Pre-heating of process water can be achieved typically by utilizing a plate and frame heat exchanger to capture heat from the DDU water and transfer it to the process water.

iv. Absorption Heat Pump (Heat Amplifier) Applications: A novel type of absorption unit is considered for this project as some DoD installations have utilized “standard” absorption chillers in the past to make chilled water from waste heat, pre-existing steam sources, natural gas, etc. and might be inclined to consider them again in conjunction with DDU geothermal systems. York, a division of Johnson Controls, offers a unique absorption machine that can be configured into what they classify as two types of “heat pumps” although that phrase can be very confusing to the general public and even engineers as it evokes an image of a “compressorized” unit, which is not a component this machine ever utilizes (Figure C6.4). Typically, they are described as being available in either a “Type 1” (Heat Amplifier) or “Type 2” (Heat Transformer) configuration, but this narrative and its illustrations will stick with the former as it is the configuration most applicable to this study/report. A compressor-less Absorption Heat Pump (or Heat Transformer) would allow DoD or another end-user to capture a Low Temperature (LT) resource from the Illinois basin (say with temperatures above 100F and up to 122F) and even a Very Low Temperature (VLT) resource from the Basin (as long as it is at or above 86F) and then “combine” it indirectly with a high temperature stream of heat (typically 275F or higher), and create a combined medium heat (typically in the 200F region) energy stream that is useful in a wide variety of applications.

For example, at a large DoD base where there is fossil fuel electrical generation on-site, (CHPs, recip. Engines, etc.), that equipment’s heat stream’s total energy flow can be increased by as much as 70% when combined with LT DDU. This architecture can yield a quality (temperature) of heat that is significantly higher (e.g. 200F) than that natively found in the Illinois Basin at depths of 6,700 ft. or less, *without the use of electricity-consuming refrigeration compressors*. Alternately, if steam is already plentiful on a Base, and economically priced (e.g. lower cost natural gas), a “Heat Amplifier” (Absorption Heat Pump) can *enable* the production of a valuable (e.g. 200F) energy stream where, although 1 unit of energy may be coming from a fossil fuel source (unless it is a bio-fuel), approximately 0.7 units of renewable energy can be harvested from the Illinois Formation. In this example, approximately 0.7/1.7 or 41% of this high quality (200F) heat stream would be coming from “renewable” energy. This process, and an example “Heat Amplifier”, is shown in Figure C6.4 on the next page.

v. Radiant Floor Heating Systems and Thermally Active Buildings (TAB) Applications with a LT DDU resource: With the Mt. Simon formation capable of producing supply water temperatures up to up to 122F, it is possible to design Radiant Floor Heating systems that can effectively utilize this resource for a variety of space heating applications (Figure C6.5). Though fairly rare in the US, radiant piping (both for heating and cooling) can be routed throughout the entire building’s structure (e.g. ceiling slabs, interior walls, floor slabs, etc.) can serve as heat transfer systems and as a “TAB”, can have significantly improved energy efficiency due to economies of transporting hot and “cold” via a fluid rather than via the less efficient (but ubiquitous) “forced air” system.



Basic Heat Flow Schematic of a “Heat Amplifier” or a Compressor-Less Absorption Heat Pump



York YHAP-C (Compressor-less) Absorption Heat Pump
i.e. “Heat Amplifier”

Innovative Absorption Heat Pump (Type I) Application Heating COP 1.7

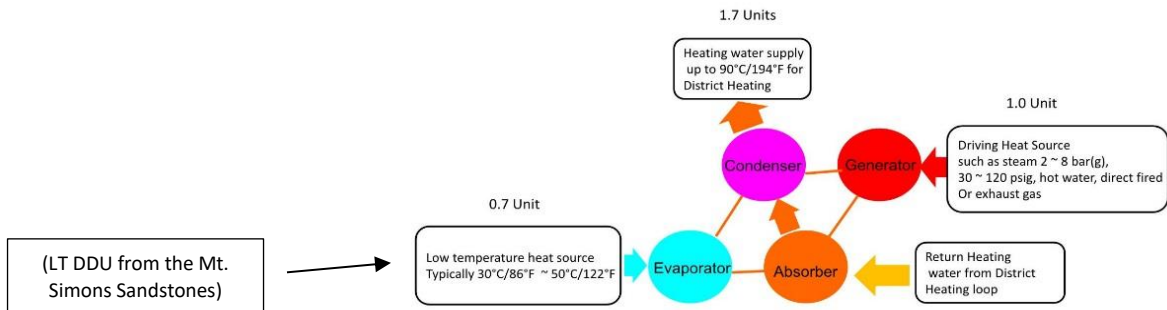


Figure C6.4. Absorption Heat Pump or “Heat Amplifier” that utilizes a Low Temperature Heat source (e.g. LT DDU Geothermal Energy at 30-50°C) and a High Temperature Heat Source (e.g. 134-175°C steam) and combines their total energy input into a single stream of Medium Temperature (up to 90°C) Heat



Figure C6.5. Commercial Radiant Floor Heating System (Before installation of upper slab).

b. Very Low Temperature (VLT) 73.6 to 78.6°F (St. Peter Sandstone) DDU Opportunities

There are, at least conceptually, possibly opportunities for utilizations of the very low temperature DDU resources typical of the temperatures found in the St Peter Sandstone (23.1 to 25.9 °C (73.6 to 78.6 °F) formation, although the applications appear limited and marginally economically viable due to their near “room temperature” properties.

i. Pre-Heating of Domestic and Makeup Water in Cold Climates

According to the Pacific Northwest National Laboratory (PNNL), in cold climates the incoming domestic cold water in the US can become as cold as 39°F (Anchorage, Alaska), and in Chicago, Illinois incoming domestic cold-water temperatures can drop as low as 54°F. DDU water with temperature ranges similar to the VLT water found in the St. Peter Sandstone can be utilized for pre-heating of incoming domestic water to water heaters, and makeup water to hydronic heating boilers. The architecture for this application would typically utilize a submersible pump to extract the DDU ground water from the formation and pass it through a plate and frame heat exchanger. The load side of the heat exchanger would be connected to the domestic incoming cold water with a storage tank and recirculating pump. This would allow the water to be (very moderately) pre-heated and stored during times of low/no demand and then this preheated (60’s F) water would enter the actual domestic or process water heating systems as pre-heated feed water when demand arose.

ii. Absorption Heat Pump (Heat Amplification) of a VLT Resource: As previously described in section 3.a.iv, it is possible to adapt this technology to a VLT resource if it reaches at least 86F when delivered to the Absorption Heat Pump. See the verbiage in that section for a complete description of this process and the lower most illustration

in Figure C6.4 for the arrangement and minimum temperature of the “low temperature heat source” that enters the evaporator of the absorption unit.

- iii. **VLT Radiant Floor Systems:** It is conceivable, if DoD has warehouse spaces or other spaces, where it is desired to just keep a well-insulated space (with limited infiltration) at room temperatures just above freezing (say 35-40F), it might be possible to utilize VLT DDU supply water at approximately 75F to keep these spaces above freezing.

Potential Benefits of DDU

The benefits of DDU for end users such as the military, universities, and others are numerous. Utilizing DDU geothermal has a huge potential to reduce carbon emissions and increase energy security and energy resiliency.

c. Reduction of Carbon Emissions

In 2017, 11.6 percent of 2017 greenhouse gas emissions came from businesses and homes primarily from fossil fuels burned for heat, the use of certain products that contain greenhouse gases, and the handling of waste. The International Scientific Consensus suggests that the United States will need to reduce economy-wide Greenhouse Gas emissions by 80% by mid-century. Utilizing DDU for space heating, and heating/preheating water for processes and domestic use can greatly assist in meeting this goal. DDU can eliminate the need for gas heating, and/or heat pumps in some applications by reducing or eliminating the need to burn fossil fuels to heat spaces, and/or water.

d. Increase Resiliency and Energy Security “Inside the Fence”

Recently DoD has shown an increasing interest in improving resiliency and energy security “Inside the Fence” of military facilities. It is very important that military bases have a high level of resiliency and security to bounce back from natural disasters such as tornadoes, hurricanes, floods, fires, etc., manmade disasters and even acts of terrorism. Energy independence (“Inside the Fence”) helps military bases withstand power outages, water/sewer interruptions, and gas interruptions.

According to the DoD Annual Energy Management and Resilience Report (AEMRR) Fiscal Year 2017, 22% of the utility outages were caused by “acts of nature” and other causes and were not due to Planned Maintenance or Equipment Failure. The use of DDU water for military bases greatly increases resiliency and security by sourcing heating energy from beneath the ground at the Base, not via a pipe or powerline entering the property from offsite. The DDU architecture can withstand even the most brutal of natural disasters such as hurricanes/tornados, and floods and man-made calamities and terroristic activities. Utilizing DDU for space/water heating is a huge step in the right direction toward increasing energy resiliency and security.

Figure C6.6 below serves as evidence of how resilient and secure geothermal systems are. The Marine Corps Logistics Base located in Albany, GA suffered more than \$88 million in damages in 2017 when an EF3 tornado ripped through the industrial sector

of the base. The Borehole Thermal Energy Storage (BTES) geothermal system below however was completely unharmed. DDU systems would also enjoy the security of being installed underground and protected from many forms harm.



Figure C6.6. MCLB Albany Tornado Aftermath & Untouched Underground Geothermal BTES System

e. DoD Economic Benefits through Energy Savings:

Though difficult to estimate the specific economic impact to DoD in terms of energy savings in the Illinois Basin, it is estimated that, including National Guard units that are at least partially funded through DoD, there are at least 29 military installations in the region. (See Figure C6.1). To accomplish the energy savings necessary to make DDU geothermal a viable option for capital projects it is obvious that DDU geothermal will need to be implemented on large scale heating loads. While a detailed economic analysis is beyond the scope of this report, a rough DDU Geothermal Economic Analysis is shown in Figure C6.7 as an example of the loads needed to recover the cost of a hypothetical DDU well doublet competing with an existing natural gas system.

f. Increase Compliance with DoD Directives, Policies and Goals

Many Executive Orders, Policies, Industry Standards, Mandates and Regulations are pushing all DoD entities to lower energy and/or water consumption. DDU geothermal has the potential to increase compliance with DoD Directives, Policies, and Goals.

Some examples are:

- EO 13514, “Federal Leadership in Environmental, Energy and Economic Performance” stresses Sustainable Buildings, greenhouse gas reduction, water efficiency and most of the aspects of EO 13423.
- EO 13423, “Strengthening Federal Environmental, Energy and Transportation Management” mandates reducing energy intensity and water intensity and increasing renewable energy consumption.
- Energy Policy Act of 2005 mandates an increase in the use of renewables and the procurement of energy efficient products.
- The Federal Leadership in High Performance and Sustainable Buildings MOU 2006 brought together 16 Federal Agencies to commit to design, construct and operate their facilities in an efficient and sustainable manner.

Barriers

DDU has many benefits for military bases in the Illinois Basin when water warm can be obtained in sufficient quantities and temperatures to handle or supplement the pre-existing heating loads; however, as with any technology, there are barriers that should be addressed. Some of the barriers identified related to DDU heating are: environmental considerations, high drilling cost/limited number of available-economical drillers, and reduced cost of a primary “competitor” natural gas, due to advanced techniques such as fracking. Each of these barriers can potentially be overcome.

g. Environmental Considerations

The environmental aspect of DDU should be considered before pursuing. In many areas of military bases, landfills and other contaminated areas should be located before drilling is planned or commences. Drilling through a contaminated site could result in contaminating drinking water aquifers. Some states will require environmental permits before extracting, or injecting (typically a Class V Underground Injection Control-UIC permit is required) groundwater. In some areas water quality testing may even be required for a period of time after construction of the wells to ensure no contaminants are being introduced by the water injected into the formation.

h. Construction Economic Barriers (High System Costs/Limited-Expensive Drillers)

Drilling can be a major cost in traditional geothermal systems where well depths rarely exceed 500’. DDU geothermal wells that contain water warm enough to utilize are generally much deeper. For example, the St. Peter Sandstone is approximately 2,080 Ft. deep, while the Mt. Simon Sandstone is approximately 4,200 Ft. deep. Drilling to these depths requires special drilling skills that most (inexpensive) water well drillers are not experienced at. Typically for depths such as those required for DDU, a driller that is experienced in oil/mineral well drilling and exploration is required. While there are oil/mineral well drillers available, an oil well driller may not be willing to take the risk of

drilling a deep geothermal well with a low rate of return vs. an oil well with a potential high rate of return.

An example rudimentary economic analysis for a DDU geothermal system to tap into the Mt. Simon Sandstone is illustrated below. Depths shown in columns 1&2 are taken from information in the previous study. The U of IL provided the cost for drilling wells (\$400 per foot), and serves as a starting point for discussions. The total system installed cost is simply illustrated/assumed at 1.5 X the drilling/well cost. Natural gas is assumed to cost \$0.495 per therm per information form U of IL and the gas savings needed over 10 years, as shown in Column 7 is intended to provide an example illustration of how big of a load might be need for a project. The 10 years shown in the next column was utilized under the assumption that it would be desired to recover the entire capital cost (using simple payback with no escalation, inflation, time value of money, etc.) of the DDU in that period. The last column is simply the annual natural gas consumption needed to be eliminated by the “free” heat the DDU to recover the capital cost. This is considered by most any measure, a substantial amount of annual gas load/consumption that would need to be present in the near vicinity of the DDU well.

Extraction Well Depth (Ft)	Injection Well Depth (Ft)	Est. Drilling Cost (\$/Ft)	Estimated Drilling Cost (\$)	Estimated Total System Cost	Estimated Gas Cost/Therm	Gas Needed to Save for Payback (Therms)	Payback Period Desired (Yrs)	Therms/Yr Savings for Desired Payback
6,700	6,700	\$ 400.00	\$ 5,360,000	\$ 8,040,000	\$ 0.50	16,242,424	10	1,624,242.42

Figure C6.7. Example DDU Geothermal Economic Analysis

i. Alternate Fuel Economic Barriers (Low Alternative Fuel cost)

In recent years natural gas costs have been reduced due to unconventional methods of gas extraction such as Fracking. Fracking is pumping a fluid into a well in order to break up the rock that bears oil or gas to release the hydrocarbons trapped inside. The current price of natural gas often makes it difficult for “renewable” alternative to compete on a purely short-term economic basis. Fracking is contributor to low natural gas prices as it expands the available supply. Natural gas that was previously not extractable is now extractable and cheap due to Fracking. Continued reduced natural gas prices are a legitimate barrier to using DDU water for heating spaces, domestic water, and process water.

j. Limited Design Experience

Most new technologies have a gap between the early market and the mainstream market. This gap is largely due to the limited experience in the market with designing and implementing the new technology. DDU geothermal is subject to this market gap since design guidelines for these systems have not been established and the number of practitioners is limited. Even though design of the system components (pumps, piping, coils, wells, HXs, etc.) are reasonably established and are understood by some engineers, end users may be hesitant to utilize DDU geothermal due to the lack their “normal design community” having experience, readily available guidelines or training in DDU implementation.

Solutions

The barriers of DDU geothermal (even though not numerous) can be seen as project-ending obstacles. However, solutions to the barriers can be developed.

k. Environmental Considerations

The water well drilling industry has environmental guidelines that must be followed to minimize chances of water supply contamination. In addition to water well drilling, environmental guidelines for construction of oil and gas wells, that are typically constructed more similarly and drilled at the depths needed for DDU geothermal should be followed. Strategic planning of DDU well locations should be performed before selecting a well location to eliminate the possibility the well may be located in an area of contamination. Contaminated sites could include landfills, underground storage tanks for hazardous waste, etc. Other sites to consider avoiding are where activities have taken place in the past such as mining, industry, chemical and oil spills, and waste disposal.

l. Tax Incentives/Tax Credits:

While there are typically tax incentives/credits available for DDU projects in the private sector, DoD itself cannot typically take advantage of these vehicles to reduce the net cost of a DDU system. However, if DoD agrees to partnering with a private entity that could own and operate the DDU system, that is located on or adjacent to DoD property, with an appropriately sized thermal load, and then (for example), DoD buys the hot water thermal resource under a Purchased “Power” (Thermal) Agreement (PPA), then it might be possible to take advantage of these incentives/credits.

m. Cost Solutions

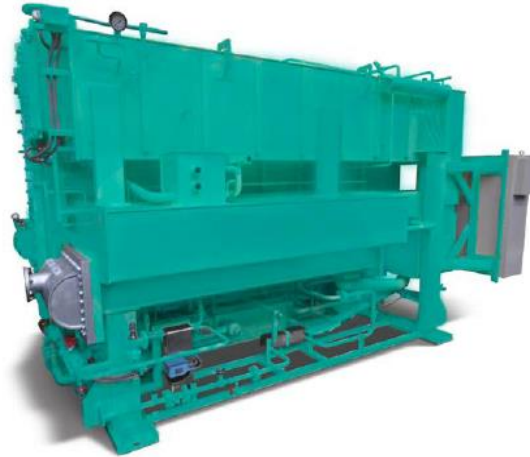
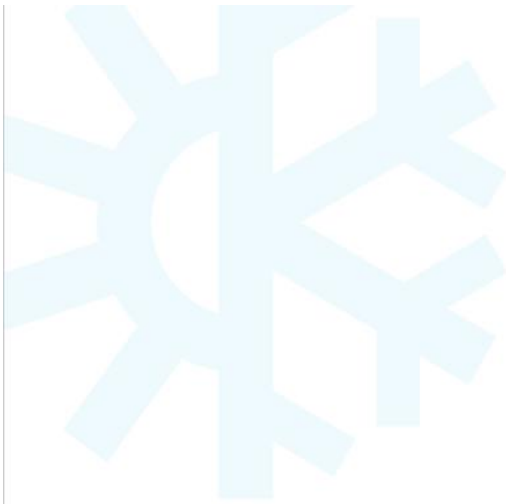
Reducing the drilling cost of DDU geothermal wells is likely to create the biggest impact to overcoming barriers to wider scale DDU implementation. Obviously though, locating with near certainty, the hottest geology, at the shallowest possible depth, beneath large scale heating loads/needs, is the fundamental pre-requisite to cost effective DDU projects. Though plentiful, “drinking water well” drillers, who also often participate in the semi-related “geothermal heat pump” groundloop heat exchanger (GHX) market, are typically disinterested in the DDU market due to inadequate equipment, training, experience, fear of the unknown, risk and many factors. Accordingly, even if the DDU market expands significantly, it is doubtful they will enter this market and put downward pressure on construction cost. Constructing DDU geothermal wells in areas of the country where oil and gas production is taking place may help insure a more plentiful supply of interested/capable drillers for DDU well construction, which could therefore keep downward pressure on DDU drilling cost.

Appendix A. Brochure for “Heat Amplifier”



**YORK® YHAP-C
ABSORPTION HEAT PUMPS**





YORK® YHAP-C Absorption Heat Pumps

ACHIEVES HIGHEST ENERGY AND WATER SAVINGS WHILE HELPING REDUCE CO₂ EMISSIONS.

The YORK® YHAP-C absorption heat pump saves energy by transferring heat (energy) from waste heat sources to increase the temperature of supplied hot water. The additional heat (energy) required by a heat pump system is far less than needed by a boiler.

YHAP-C absorption heat pumps are ideal for district heating and industrial process heating applications, because they take advantage of waste heat energy found in industrial facilities and deliver high-temperature hot water.

Maximizing performance by design

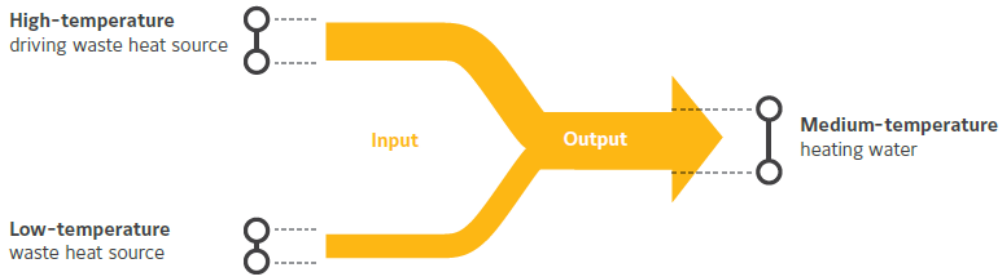
Driving heat sources: YORK® absorption heat pumps use a variety of driving heat sources, such as jacket water from a gas engine, low to high pressure steam, direct fired or even exhaust gas. As a result, the unit helps reduce primary energy consumption, water and carbon dioxide emissions. The YHAP-C design is also more efficient and reliable than conventional designs, because it employs innovative, 2-step evaporation and absorption technology.

To meet the needs of different heating applications, two types of YHAP-C absorption heat pumps are available:

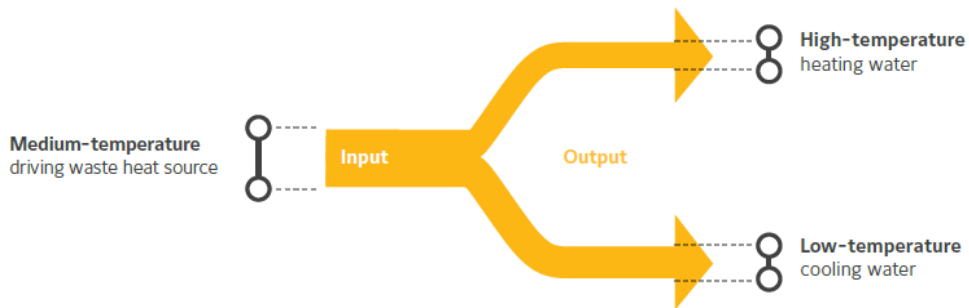
- **Type I** heat pump, also referred to as a heat amplifier, is driven by a high-temperature driving heat source in the generator section.
- **Type II** heat pump, also referred to as the heat transformer, is driven by a medium-temperature driving heat source in the generator and evaporator sections.

Two Types of YHAP-C Heat Pumps

Type I: Driven by high-temperature driving heat source in generator



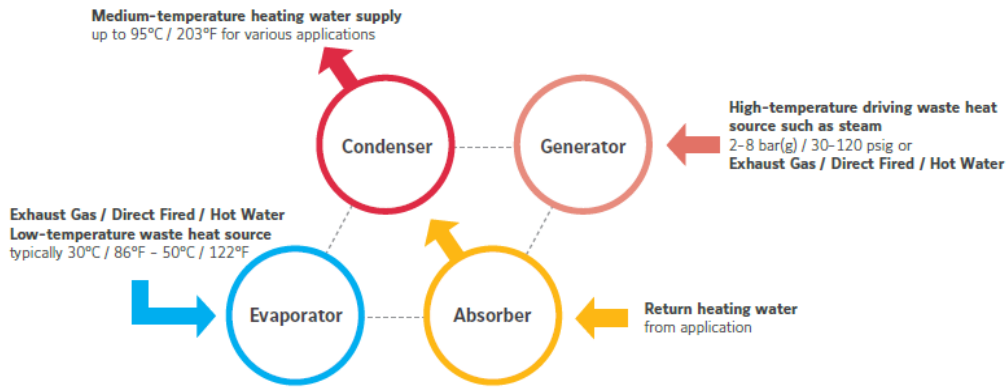
Type II: Driven by medium-temperature driving heat source in generator and evaporator



Type I Flexible Operating Envelope

The Type I heat pump, also referred to as a heat amplifier, is driven by a high-temperature waste heat source in the generator section. The low-temperature waste heat source is fed into the evaporator section. With these two heat sources, the Type I heat pump amplifies and provides useful medium temperature heat from the absorber and condenser section.

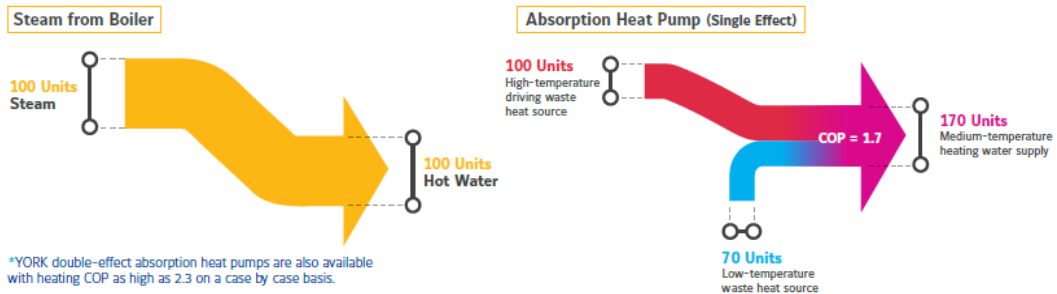
How it Works



Heat Balance

Compared to the typical steam boiler's 0.93 Coefficient of Performance (COP), the Type I unit provides a COP as high as 1.7*, delivering up to 95°C (203°F) hot water for various heating applications. This unit also provides a good turndown over a range of heating loads.

Performance of Boiler Compared to Absorption Heat Pump



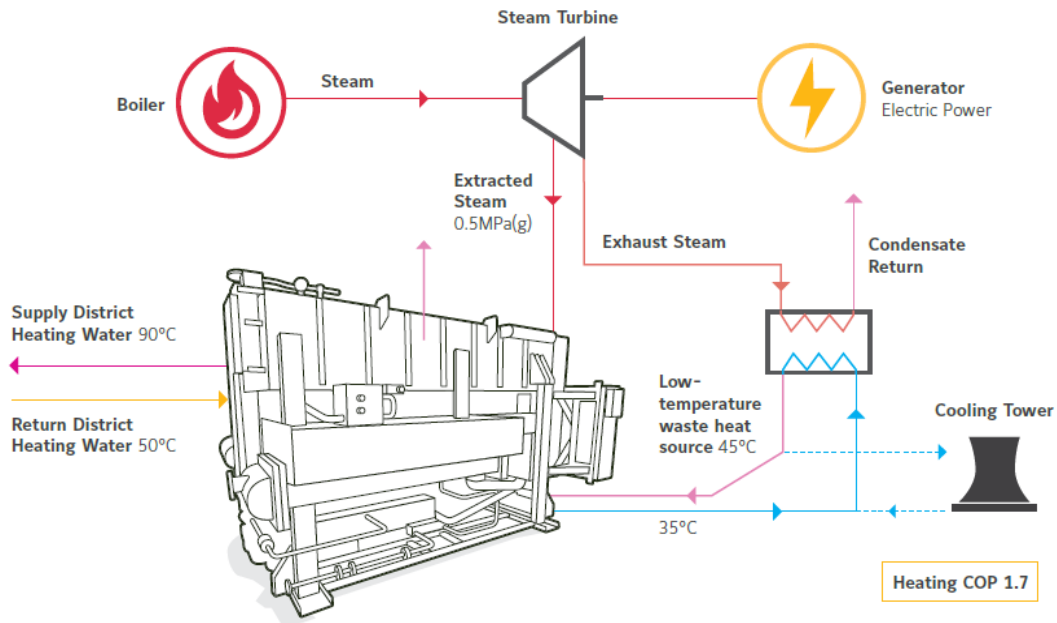
Type I Industrial Application

The Type I unit produces a high amount of medium-temperature heat from the absorber and condenser section based on a relatively smaller amount of high-temperature waste heat in the generator section and low-temperature waste heat in the evaporator section.

In this Type I application, the extracted steam at 0.5 MPa(g) from the power steam turbine is the driving heat source in the generator section. The water diverted from the cooling tower is the low-temperature waste heat source that is fed into the evaporator section. The heat pump delivers 90°C (194°F) from

the absorber and condenser section, which can be used for district heating or boiler feed water pre-heating. This application saves primary energy, reduces steam and water consumption and helps cut emissions.

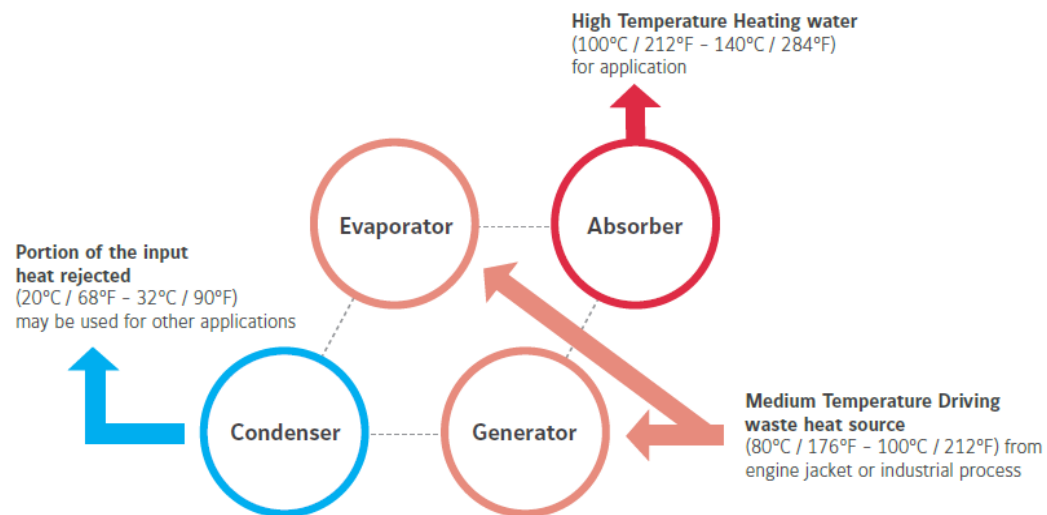
With a Type I absorption heat pump, it is typical to have a heating COP of 1.7, meaning 1.7 units of heat is obtained from the absorber and condenser with a 1.0 unit of driving heat source in the generator and .7 units being in the evaporator section.



Type II Flexible Operating Envelope

The Type II heat pump, also referred to as a heat transformer, is driven by a medium-temperature waste heat source in the generator and evaporator sections. This unit transforms and provides small, useful high-temperature heat from the absorber section. The rejected heat from the condenser can be used as the cooling water for other applications.

How it Works



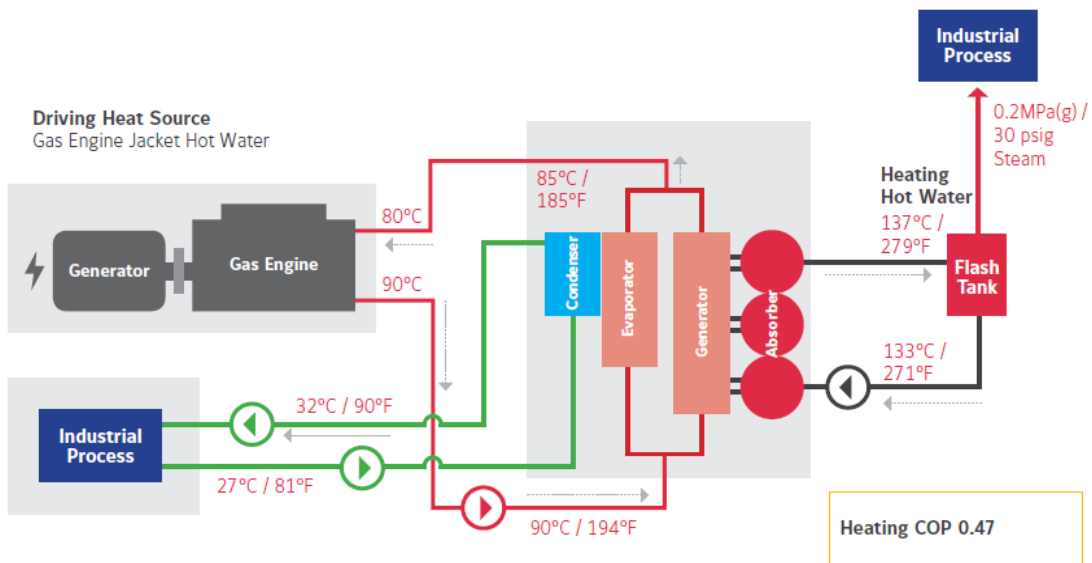
Heat Balance

The Type II heat pump with a COP of 0.47 can deliver high-temperature hot water up to 140°C (284°F), which is ideal for industrial processes. This unit also provides a good turndown over a range of heating loads.

Type II Industry Application Process Heating Application

With a Type II absorption heat pump, it is typical to have a heating COP of 0.47, meaning 0.47 units of heat is obtained from the absorber with a 1.0 unit of driving heat source in the evaporator and generator. The 0.53 units of heat rejected in the condenser can be used for other process applications.

In this Type II absorption heat pump application, the jacket water of the gas engine at 90°C (194°F) is the driving heat source. The heat pump delivers 137°C (279°F) from the absorber section that can be flashed in a tank to produce low-pressure steam at 0.2 MPa(g) for process heating. A portion of the input heat is rejected through the condenser section and is used for other purposes in the facility.





Why install anything but YORK®?

You want high performance. You expect efficiency. And you need a chiller that gives you confidence.

When your reputation is at stake, it's smart to demand nothing less than YORK® technology and service. That's because we provide local service and parts to keep your equipment operating at peak performance year after year. Enjoy the peace of mind knowing that trained service experts and Original Equipment Manufacturer parts are available from Johnson Controls – the largest HVAC service and preventative maintenance organization in the world.



Johnson Controls, the Johnson Controls logo, YORK and Metasys are registered trademarks of Johnson Controls, Inc. in the United States of America and other countries. Other trademarks used herein may be trademarks or registered trademarks of other companies. © 2017 Johnson Controls, Inc. P.O. Box 423, Milwaukee, WI 53201. All rights reserved worldwide. Printed in USA PUBL-8196ZH-B-0817. Supersedes: PUBL-8196ZH-A-0816.

FOR MORE INFORMATION VISIT JOHNSONCONTROLS.COM



Appendix D – Products Developed Under Award and Submissions to the Geothermal Data Repository (GDR)

D1. Products Developed Under Award

Publications, conference papers, or other public releases of results:

1. Thomas, L.K. 2019. “District-Scale Geothermal System Performance Evaluation using Thermodynamic and Environmental Analysis.” Master of Science Thesis, University of Wisconsin-Madison, 117 p. <http://digital.library.wisc.edu/1793/79313>.
2. Stumpf, A., J. Damico, R. Okwen, T. Stark, S. Elrick, W.J. Nelson, Y. Lu, F. Holcomb, J. Tinjum, F. Yang, S. Frailey, and Y-F. Lin. 2018. “Feasibility of a Deep Direct-Use Geothermal System at the University of Illinois at Urbana-Champaign. Geothermal Resources Council Transactions 42: 227–248. <https://www.osti.gov/servlets/purl/1462352>.
3. ISGS Receives \$720,000 Award from DOE for Geothermal Research <https://isgs.illinois.edu/achievements/october/isgs-receives-720000-award-doe-geothermal-research>

Web site or other Internet sites that reflect the results of this project:

1. Geothermal at the Energy Farm <https://icap.sustainability.illinois.edu/project/geothermal-energy-farm>

Networks or collaborations fostered:

1. (Great Lakes SedHeat Network (GLSN): <https://igws.indiana.edu/glsn/overview>)

Technologies/Techniques:

N/A

Inventions/Patent Applications, licensing agreements:

N/A

Other products, such as data or databases, physical collections, audio or video, software or netware, models, educational aid or curricula, instruments or equipment:

N/A

D2. Submissions to the Geothermal Data Repository (GDR)

University of Illinois Campus Deep Direct-Use Feasibility Study - Energy Farm Propane

Use Logs

This submission includes an excel workbook containing propane energy logs for the U of IL Energy Farm from March 2013 to March 2016. It also includes heating degree day information for the region from the period October 1 to March 31, for the years 2008 to 2013.

The propane logs are for use in parameterizing the demand and life-cycle assessments associated with the project. This data provides information about energy loads for the buildings being included in the DDU applications.

Lin, Y. University of Illinois

Dec 18, 2017

University of Illinois Campus Deep Direct-Use Feasibility Study - Bedrock Geology ArcGIS

Layers

Bedrock Geology of Champaign County, Illinois, map layers (shapefiles).

Layers included:

- 1) Champaign County bedrock units.
- 2) Champaign County bedrock surface contours. Contour interval of 25 feet.
- 3) Colchester coal surface contours. Contour interval of 50 feet.
- 4) Kimmswick Limestone top contours, in the Mahomet dome area. Contour interval of 20 feet.
- 5) New Albany shale base contour. Contour interval of 100 feet.

Nelson, W. University of Illinois

Mar 20, 2018

University of Illinois Campus Deep Direct-Use Feasibility Study - Geological Characterization of the Mt. Simon Sandstone

These studies undertook detailed analyses of the Mt. Simon Sandstone in the Illinois Basin for geological storage and sequestration, and brine extraction.

Lin, Y. et al University of Illinois

Mar 30, 2018

University of Illinois Campus Deep Direct-Use Feasibility Study - Design of Injection Well #1 (CCS1)

Includes specification sheet, wellbore geometry, and drilling fluids at section target depth associated with the design of Injection Well #1 (CCS1) for the Illinois Basin Decatur Project (IBDP).

Greenberg, S. University of Illinois

Mar 30, 2018

University of Illinois Campus Deep Direct-Use Feasibility Study - Designs for Deep Injection and Monitoring Wells

The following information is provided about the design of deep wells constructed in the Illinois Basin to store, sequester, or dispose of CO₂, natural gas, and industrial wastes.

Lin, Y. et al University of Illinois

Mar 30, 2018

University of Illinois Campus Deep Direct-Use Feasibility Study - Regional Geology

Links to papers and reports describing the structure and character of the Illinois Basin geology. Included are descriptions of the two reservoirs that are being modeled for the DDU feasibility project at University of Illinois, the St. Peter and Mt. Simon Sandstones.

Lin, Y. et al University of Illinois

Mar 30, 2018

University of Illinois Campus Deep Direct-Use Feasibility Study - Geological Characterization of the St. Peter Sandstone

These studies undertook detailed analyses of the formations within the Cambro-Ordovician strata above the Mt. Simon Sandstone in the Illinois Basin, including the St. Peter Sandstone, for geological storage and mineral potential.

Lin, Y. et al University of Illinois

Mar 30, 2018

University of Illinois Campus Deep Direct-Use Feasibility Study - Thermal Properties of Geologic Formations in Illinois Basin

Thermal property data for rocks and minerals and unconsolidated (glacial) sediments units from within and outside the Illinois Basin were compiled for modeling heat transport in the subsurface.

Lin, Y. et al University of Illinois

Mar 30, 2018

University of Illinois Campus Deep Direct-Use Feasibility Study - Porosity and Permeability of Rock Formations

Porosity and permeability data from published and unpublished sources for the St. Peter and Mt. Simon Sandstones in the Illinois Basin.

Damico, J. et al University of Illinois

Mar 30, 2018

University of Illinois Campus Deep Direct-Use Feasibility Study - Long-Term Meteorological Data

This submission includes meteorological data recorded by National Weather Service at University of Illinois Willard Airport, Savoy IL for period 1972 to 2018. This data is for use in parameterizing the demand and life-cycle assessments associated with the project and provides information about energy loads for the buildings being included in the DDU applications. This includes how energy demand fluctuates with seasonal changes in climate, which is used to model expected demand for the DDU system.

Lin, Y. et al University of Illinois

Mar 30, 2018

University of Illinois Campus Deep Direct-Use Feasibility Study - Geology Log and Drilling Prospectus

Geology log and drilling prospectus for University of Illinois at Urbana-Champaign (U of IL) Energy Farm.

Nelson, W. University of Illinois

Apr 16, 2018

University of Illinois Campus Deep Direct-Use Feasibility Study - Chemistry of Formation Waters

Studies of chemical composition of natural brines from rock formations in the Illinois Basin as part of the University of Illinois deep direct-use feasibility study.

Lin, Y. et al University of Illinois

Apr 23, 2018

University of Illinois Campus Deep Direct-Use Feasibility Study - Revised Campus Master Plan Map

Revised master plan for the University of Illinois Urbana-Champaign campus. Note, the corridor where the U of IL Energy Farm is located will expand with the relocation of the ISRL and Feed Technology Center.

Lin, Y. University of Illinois

Apr 26, 2018

University of Illinois Campus Deep Direct-Use Feasibility Study - Geocellular Modeling

This submission includes 3-D geocellular model files with formation top and formation thickness data for the St. Peter and Mt. Simon Sandstones in University of Illinois Deep Direct-Use project area. An input parameters file is also included for the St. Peter Sandstone.

Damico, J. University of Illinois

May 07, 2018

University of Illinois Campus Deep Direct-Use Feasibility Study - Subsurface Temperature Profile

High resolution fiber-optic distributed temperature sensing logs from the Illinois Basin Decatur Project (IBDP) in Decatur, IL were used to model the thermal profile in the Illinois Basin.

Lin, Y. et al University of Illinois

Jun 13, 2018

Feasibility of a Deep Direct-Use Geothermal System at the University of Illinois Urbana-Champaign

Paper authored by Stumpf et al. for the 2018 Geothermal Resources Council Annual Meeting held in Reno, NV USA. Included with the paper is the Microsoft PowerPoint presentation made at the GRC meeting and data tables associated with some of the figures.

Stumpf, A. et al University of Illinois

Dec 31, 2018

Geocellular model of St. Peter Sandstone for University of Illinois at Urbana-Champaign DDU Feasibility Study

The geocellular model of the St. Peter Sandstone was constructed for the University of Illinois at Urbana-Champaign DDU feasibility study. Starting with the initial area of review (18.0 km by 18.1 km [11.2 miles by 11.3 miles]) the boundaries of the model were trimmed down to 9.7 km by 9.7 km (6 miles by 6 miles) to ensure that the model enclosed a large enough volume so that the cones of depression of both the extraction and injection wells would not interact with each other, while at the same time minimizing the number of cells to model to reduce computational time. The grid-cell size was set to 61.0 m by 61.0 m (200 feet by 200 feet) for 160 nodes in the X and Y directions.
Damico, J. University of Illinois
Dec 31, 2018

Geocellular Model of Mt. Simon Sandstone for University of Illinois at Urbana-Champaign DDU feasibility study

The geocellular model of the Mt. Simon Sandstone was constructed for the University of Illinois at Urbana-Champaign DDU feasibility study. Starting with the initial area of review (18.0 km by 18.1 km [11.2 miles by 11.3 miles]) the boundaries of the model were trimmed down to 9.7 km by 9.7 km (6 miles by 6 miles) to ensure that the model enclosed a large enough volume so that the cones of depression of both the extraction and injection wells would not interact with each other, while at the same time minimizing the number of cells to model to reduce computational time. The grid-cell size was set to 61.0 m by 61.0 m (200 feet by 200 feet) for 160 nodes in the X and Y directions. Within the model, 67 layers are represented that are parameterized with their sediment/rock properties and petrophysical data.
Damico, J. University of Illinois
Dec 31, 2018

Extraction/Injection Well Design for Deep Direct Use at University of Illinois at Urbana-Champaign

The large scale Deep Direct Use (DDU) geothermal project in the low temperature environment of the Illinois Basin requires drilling and completing two wells. One well would be the extraction (extraction) well and would be built to deliver a flow rate of approximately 6000 barrels per day (bbl/d) of brine from the lower part of the Mt. Simon Sandstone at a depth of approximately 6300 feet bgs (below ground surface). The injection well would be constructed to return the extracted brine into the upper part of the Mt. Simon Sandstone at a depth of approximately 5250 feet bgs.
Kirksey, J. and Lu, Y. University of Illinois
Mar 31, 2019

Mt. Simon Sandstone Brine Chemistry for DDU Technology at the U of IL Campus

A review of brine chemistry data for the Mt. Simon Sandstone in the Illinois Basin is provided for calculations to predict the potential for mineral scaling and precipitation. The assessment includes expected changes in temperature, pressure, and/or exposure to air or other materials as brine is extracted and injected.
Lu, Y. and McKaskle, R. University of Illinois
Mar 31, 2019

Appendix E – F&S and U of IL Campus Support

Strong support for the DDU feasibility study and future development of geothermal energy on the U of IL campus came from the University leadership, Office of the Vice Chancellor for Research, Office of Capital Programs and Real Estate Services, Prairie Research Institute (PRI), College of Agricultural, Consumer and Environmental Sciences (ACES), Institute for Sustainability, Energy, and Environment (iSEE), and F&S. During this study, the following members have been contributing their expertise and support:

Matthew Tomaszewski: Associate Provost for Capital Planning

Harley Johnson: former Faculty Fellow at the Office of the Vice Chancellor for Research; current Associate Dean for Research in The Grainger College of Engineering

Mark Ryan: Executive Director, PRI

Steve Whittaker: Director of Energy Research and Development, ISGS, PRI

Kimberly Kidwell: Dean and Robert A. Easter Chair, ACES

Germán Bollero: Associate Dean for Research, ACES

Douglas Wolters: Director of Operations - Facilities Planning and Management, ACES

Timothy Mies: Director, Energy Farm Operations, ACES

Miles Redden: Manager, Beef & Sheep Field Research Laboratory, ACES

Katie Grott: Manager, Poultry Farm, ACES

Madhu Khanna: Associate Director for Research, iSEE

Ximing Cai: Associate Director for Campus Sustainability, iSEE

Mohamed Attalla, Executive Director, F&S

Kent Reifsteck: Director of Utilities and Energy Services, F&S

Keith Erickson: Associate Director of Utility Distribution, F&S

Michael Larson: Director of Utilities Production, F&S

Betsy Liggett: Capital Projects, F&S

Morgan White: Associate Director of Sustainability, F&S